PREFACE

I would like to introduce the report on the scientific activity of the Frank Laboratory of Neutron Physics (FLNP) of the Joint Institute for Nuclear Research (JINR) in 1997. The report consists of two parts. The first is a brief review of the result of experimental and theoretical investigations in condensed matter physics, nuclear physics and applied research. The second contains experimental reports that provide more detailed information on the conducted research. The list of 1997 publications completes the picture.

The 1997 year was a difficult one for FLNP. The February cycle of the IBR-2 pulsed reactor was cancelled because of financial difficulties. From June to November, IBR-2 was shut down due to malfunctioning of the fast alarm system.

Further development of User Policy aimed at attracting a larger number of physicists, chemists, biologists, and specialists in materials science to carry out experiments at IBR-2 was one of the main objectives in the reported year. As a result, 152 proposals for experiments were received in 1997 and the total amount of experiments conducted with IBR-2 from 1995, the year of the launch of IBR-2 user policy, to 1997 is over 460. Proposals came from 25 countries, including JINR nonmember states. On the average, the requested beam time was 2.5 time larger than available.

The financial situation in FLNP remains unstable. A lot of works on the project for IBR-2 modernization have been suspended. The IREN projected has practically been frozen up.

At the same time, in the reported year, FLNP managed to put into operation the new spectrometer SKAT, include into user policy the REFLEX spectrometer and continue the construction of the KOLHIDA spectrometer for neutron nuclear physics and the FSD instrument for strain measurements.

In spite of the difficult economical situation in its host country, FLNP JINR retains the position of one of the leading neutron centers in Europe thanks to continued effort aimed at development of new and improvement of the existing experimental and theoretical facilities.

V.L.Aksenov
Director

28 February 1998

1.1. CONDENSED MATTER PHYSICS

In accordance with theme -0864- neutron scattering investigations in the field of condensed matter physics are conducted at IBR-2 using four main experimental techniques: diffraction, small-angle scattering, inelastic scattering, and polarized neutron optics. Beam time is allocated according to experts recommendations based on submitted proposals and the existing long-term agreements for co-operation.

Spectrometers for investigations in condensed matter physics. To the experimental halls of the IBR-2 reactor 14 neutron beams are extracted and physical instruments are arranged on them. At present, 12 spectrometers are for condensed matter investigations. In 1997, nine of them were operating in the user mode: HRFD, DN-2, NSVR, YuMO, SPN, REFLEX-P, KDSOG, NERA, and DIN. The DN-12 spectrometer had undergone radical modernization completed by the summer of 1997. Following PAC recommendations the SNIM spectrometer was excluded from the user program for 1997. The DIFRAN spectrometer operated in the frame of a special program.

For the most part, the main parameters of spectrometers included in the IBR-2 working schedule have been formed and on the whole, they are on the world level. At the same time, work to expand the possibilities of several instruments was conducted in 1997.

The parameters of the DN-12 diffractometer for experiments with high pressure cells based on sapphire or diamond anvils were essentially improved by introducing a new neutron guide. This curved 20 m supermirror neutron guide gave a double increase in the total thermal neutron flux and at the same time, a several times increase in the flux of neutrons with $\lambda>2$ E (Fig. 1) and a sharp decrease in the background (see Sec. Experimental Reports).

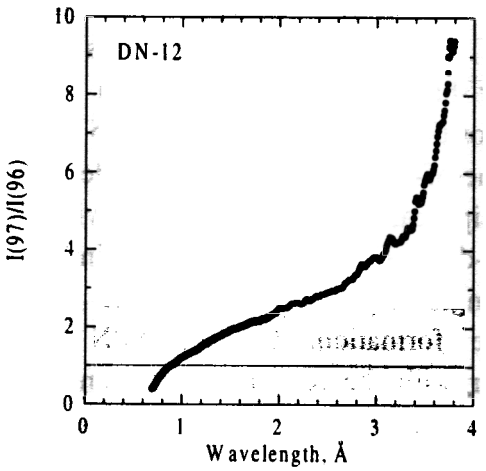

Fig.1. An increase of the neutron flux on the sample after installation of the supermirror neutron guide in the DN-12 diffractometer.

Another event of equal importance was putting into operation of the SKAT spectrometer in place of the NSVR spectrometer that had operated over 10 years at IBR-2. The detector system for SKAT arranged in the vertical plane made it possible to optimize essentially the registration of pole figures in investigations of bulk sample textures, have shorter measuring times as well as improve the quality of measurements.

On the high resolution Fourier diffractometer (HRFD) a second detector at $2\theta=-152°$ was put into operation. This reduced the time of structure experiments two times. Final adjustment of the detector elements decreased the geometrical component of the resolution function. This reduced the relative width of the resolution function to 0.12% for d=1.5 E and the rotation velocity of the chopper 8000 rpm. In Figure 2 diffraction spectra measured with HRFD and the TOF-diffractometer HRPD at ISIS with the flight path 100 m are compared. One can see that in

spite of the fact that HRFD has an approximately 5 times shorter flight path the resolutions of these spectrometers are about equal.

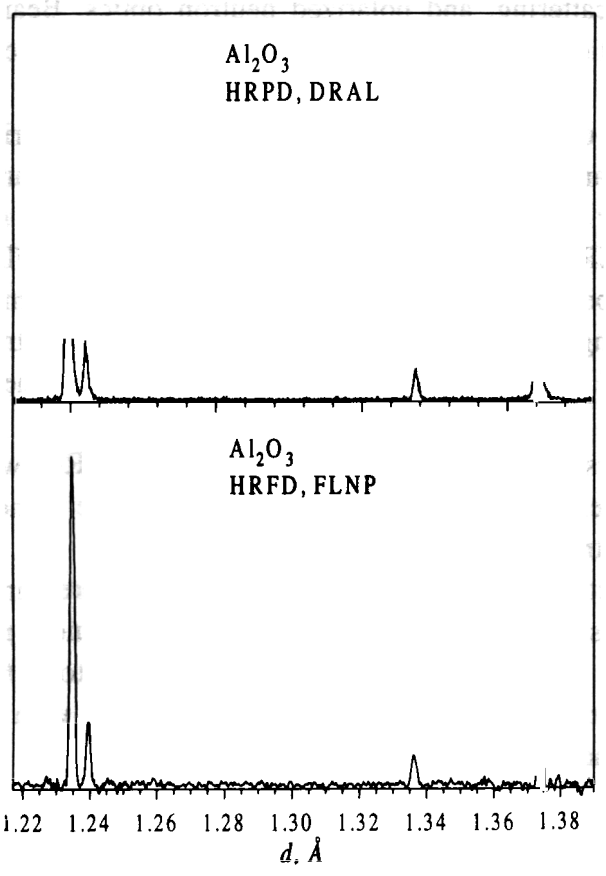

Fig.2. The part of the diffraction spectrum from one Al_2O_3 sample measured with HRPD (ISIS) and HRFD (IBR-2) diffractometers .

In 1997, work to improve position-sensitive detectors was carried out. The possibilities of the DN-2 diffractometer have noticeably increased after a two-dimensional detector (320x280 mm^2) with the position resolution about 2.5 mm in two coordinates started operation. In addition to time-of-flight analysis, this detector allows registering the three-dimensional scattering in the reciprocal space of the crystal without rotating the sample or the detector. Figure 3 illustrates a tow-dimensional distribution of intensity in one of the reciprocal lattice sites in a La_2CuO_4 single crystal following the tetragonal to orthorhombic phase transition and twin structure formation. On the SPN spectrometer experiments using a linear position-sensitive detector with the resolution 1.5 mm started. This detector registers the reflected neutron distributions in the SPN reflectometric mode and can be also used to realize the SPN small-angle mode.

Execution of the scientific program. From 1995 the scientific program for investigations with the IBR-2 spectrometers is formed, in the main, on the basis of proposals submitted to experts commissions by users from JINR member states (10% from other countries). About one half of proposals is for investigations under auspices of long-term agreements for cooperation between FLNP and other laboratories or institutes in investigation of particular problems of condensed matter physics.

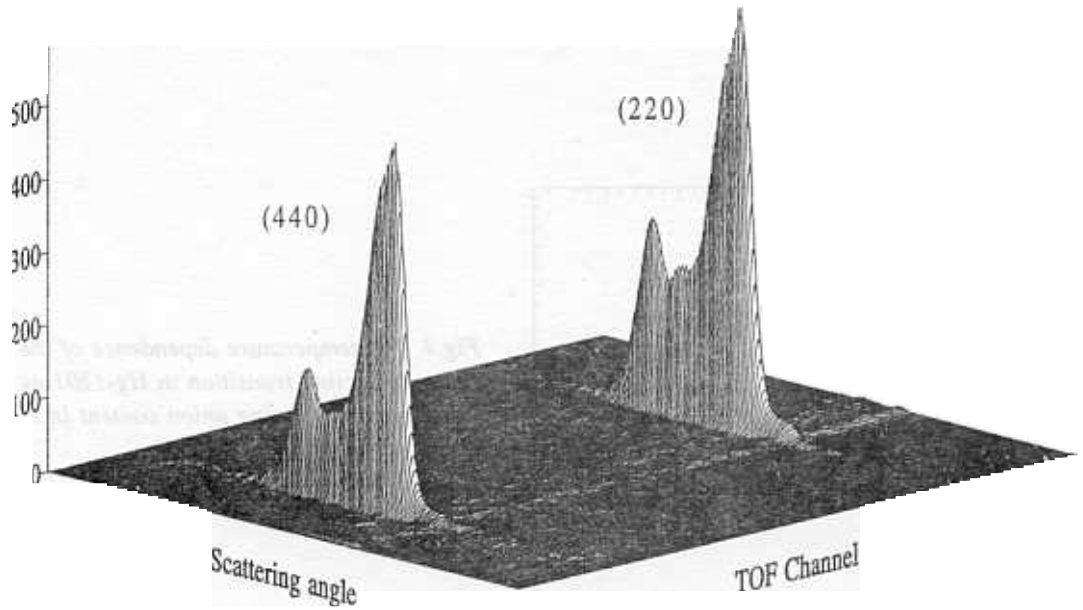

Fig.3. Neutron diffraction pattern along of (hh0) direction of a La_2CuO_4 crystal (in the ferroelastic phase), measured with a two-dimensional PSD and summed over vertical coordinate of the detector.

Diffraction experiments. The program for investigations of mercury based high temperature superconductors carried out in collaboration with the Department of Chemistry of Moscow State University (MSU) continued and extended to studies of the atomic structure of the compound $HgBa_2CuO_4F_\delta$ i.e., the compound with extra oxygen replaced by fluorine atoms. The idea of the experiment is to replace a bivalent doping element by a monovalent element. In this case, the conservation of the charge balance and the ionic nature of carriers formation require doubling the amount of doping atoms to have an equivalent superconducting transition temperature. The *Hg-1201* initial phase with T_c=61 was successfully fluorinated with XeF_2 in MSU (E.V.Antipov's laboratory). As a result, T_c increased initially to 97 K and then decreased which was followed by suppression of superconducting properties as the fluorine content in the sample increased. A neutron diffraction analysis of two $HgBa_2CuO_4F_\delta$ compositions (experiments with HRFD at IBR-2 in May 1997) confirmed the implantation of fluorine in the charge reservoir (*Hg*-plane) and really showed the doubling of the fluorine content in the structure in comparison to *HG-1201* oxygen phases with close T_c (Fig. 4). This is a strong argument in favor of the ionic model of electric charge carriers (holes) formation in *Hg*-1201 in the process of doping (see Sec. Experimental Reports).

To investigate the phenomenon of macroscopic phase separation in superconducting crystals, a series of experiments to study the transformation twinning in $La_2CuO_{4+\delta}$ crystals were conducted with the DN-2 diffractometer. Concurrently, experiments with the *X*-ray diffractometer of ISSP (Chernogolovka) were carried out. In the DN-2 experiments the new position-sensitive detector was used. The measurements demonstrated that the domain (twin) structure in such crystals is noticeably different from the classical scheme realized at a loss of an axis of the 4th order and observed in KDP crystals or *Y-123*. It appears that the boundaries between domains are mainly coherent (the portion of domains with incoherent boundaries is not large). Moreover, in crystals where macroscopic phase separation takes place this portion is not

larger than a few percent. This, possibly, leads to extra oxygen diffusion and, as a result, to separation.

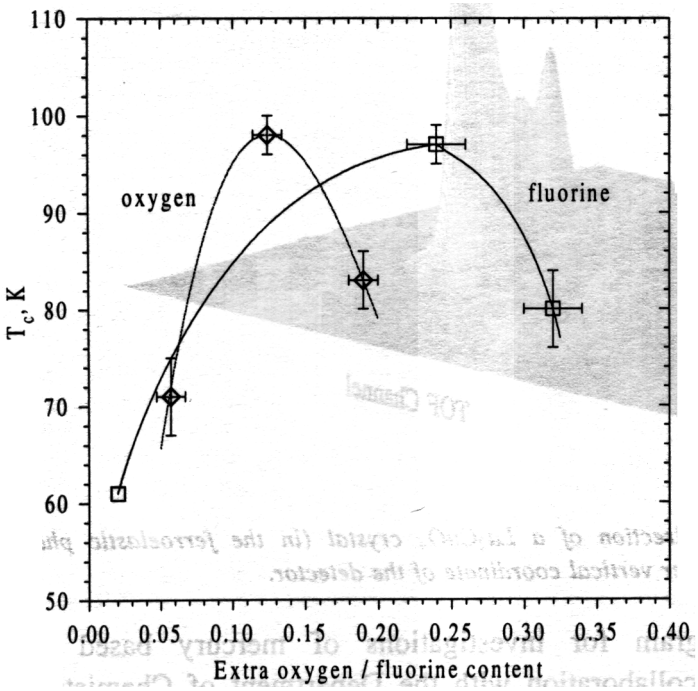

Fig.4. The temperature dependence of the superconducting transition in Hg-1201 as a function of the doping anion content in the cases of oxygen or fluorine doping.

Studies of the magnetic state of crystals in both neutron and μSR experiments yield interesting results. During 1997, a number of such investigations were performed using the μSR spectrometers in the Meson Factory in PSI (Villigen, Switzerland). One of the compositions of the system $U(Pd_{1-x}Fe_x)_2Ge_2$ studied earlier in detail by means of neutron diffraction was investigated on the GPD spectrometer over a wide temperature interval. It is discovered that muon spin precession takes place at not only one but two and even more frequencies (Fig. 5). An analysis proves that this is connected with the existence in an elementary cell of the compound of equivalent crystallographic positions which are nonequivalent from the point of view of the magnetic surrounding (see Sec. Experimental Reports).

Another example of analysis of combined neutron and μSR data is the results obtained for $La_2CuO_{4+\delta}$ single crystals with the doping level δ=0.02-0.03, i.e., lying inside the miscibility gap but having a reduced coefficient of oxygen diffusion. According to neutron data the long-range order with the coherent length large enough to observe the magnetic diffraction peaks is established either in a small volume portion (~10%) of the crystal or is not established at all. At the same time, μSR data are evidence of the fact that in the superconducting phase transition point or its vicinity there arises the magnetic order sufficient to observe muon spin precession. These results can be interpreted as the appearance of separation into the superconducting and antiferromagnetic phases that occurs on the electron level in regions small in size and is induced by the superconducting state transition (see Sec. Experimental Reports).

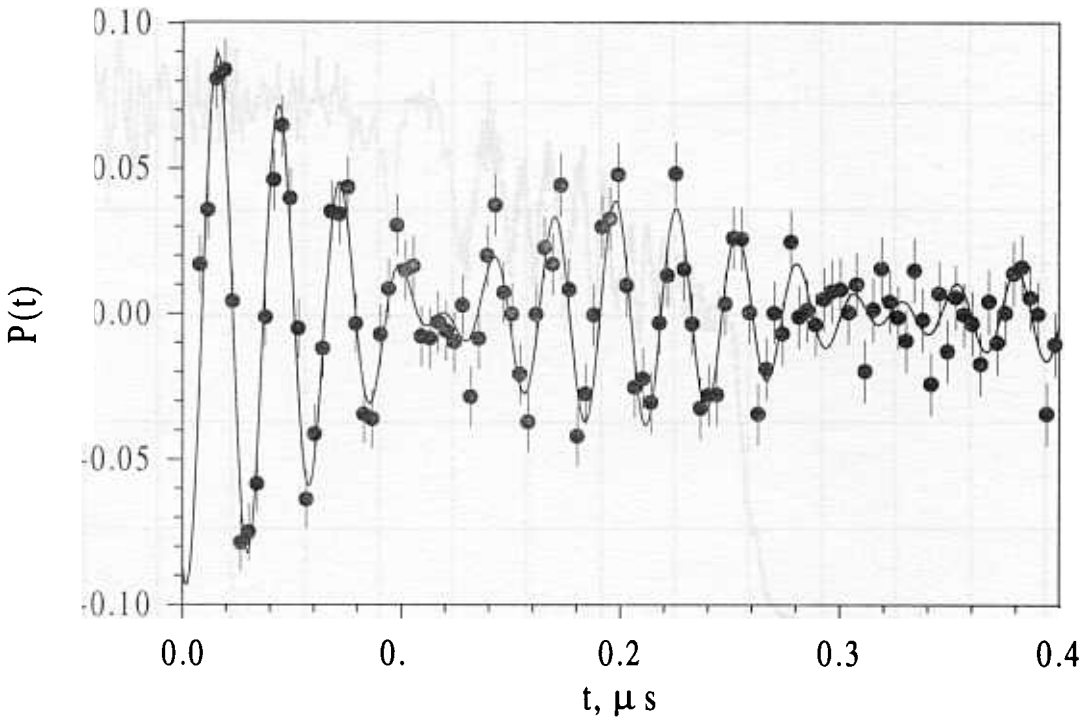

Fig.5. *The time dependence of the muon spin polarization function in the $U(Pd_{0.99}Fe_{0.01})_2Ge_2$ at 13K measured by μSR-spectroscopy. The polarization reflects the muon spin precession around internal magnetic fields in the sample. The presence of characteristic beats is due to the existence of two or more precession frequencies.*

FLNP in collaboration with IBC (Moscow), ISSP (Budapest) and LURE (Orsay) investigated the vesicle transition in the system phospholipin/sodium cholate/water with the YuMO spectrometer. Morphological and structural changes following changes in the temperature or the detergent concentration were studied. In a dimyristylphospatydilcholine-based system the transition from the multilamellar structure to the unilamellar structure formed through the stage of elongated rod-like micelles formation was observed. Also, an analysis of SANS data allowed determination of the geometrical characteristics of the formed micelles.

The first experiments of generating and registration of neutron standing waves were carried out on the SPN spectrometer. Developing the method may prompt the solution of the problem of the determination of the structural positions of atoms in the near-surface region of matter. In the experiment the dependence of the intensity of γ-quanta emitted following neutron capture in a thin gadolinium layer (~50 E) deposited on a magnetized Fe layer (~1000 E) on the incident neutron beam polarization was registered. The preliminary analysis of the measured dependence allows us to speak about an observation of a standing neutron wave with about 90% probability (see Sec. Experimental Reports).

Concurrent with detailed certification, on the new polarized neutron reflectometer REFLEX experiments to study the properties of some neutron-optical systems, such as multilayer mirrors produced by PINP (Gatchina) and CIFI (Budapest), the interference filter for the UCN spectrometer (Dubna-Grenoble-Melbourne collaboration), etc. were carried out. A high resolution of the reflectometer which is probably the record one today makes it possible to obtain information about fine details of surface layers (Fig. 6).

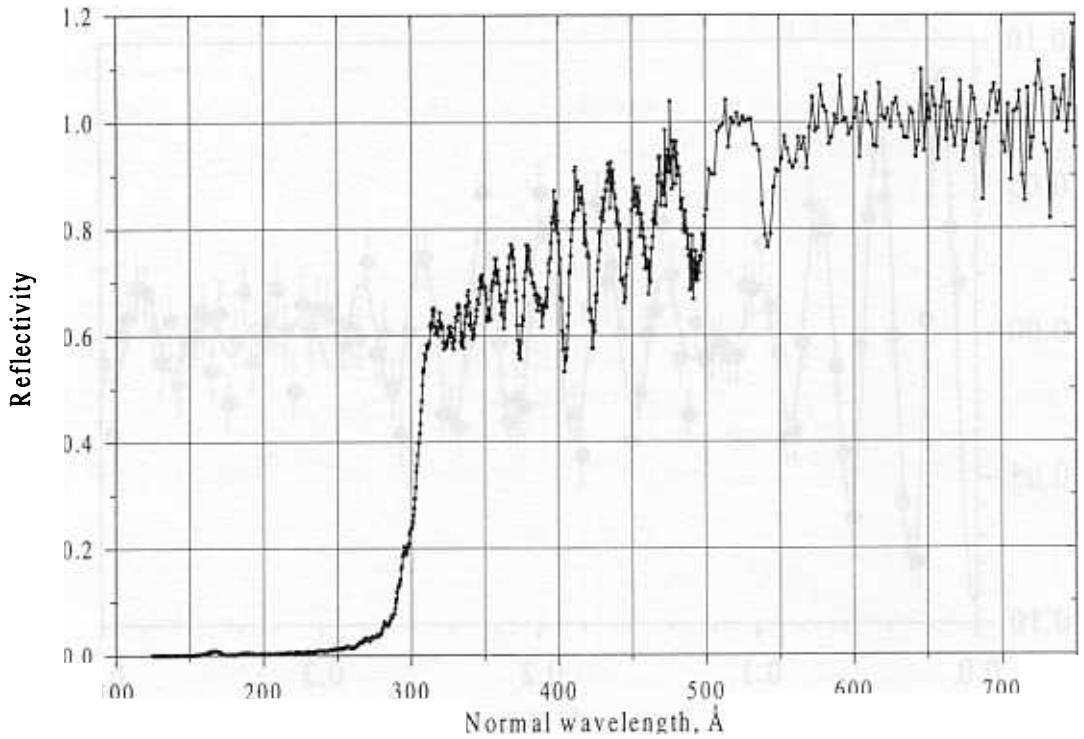

Fig.6. *The reflection coefficient of neutrons from multilayer mirrors. The modulation of the reflection coefficient is due to fine details of the surface layer.*

The main research direction on the NERA spectrometer was the study of the dynamics of ammonium and methyl groups at phase transitions in stoichiometric compounds of the type $(NH_4)_2SO_4$ and solid solutions of the type $(NH_4)_{2-x}Rb_xSO_4$. Replacing ammonium ions by Rb with about equal ionic radius leads to some disorder in the system of hydrogen bonds and allows investigation of the influence of disorder on the dynamics of ammonium. The system $(NH_4)_{2-x}Rb_xSO_4$ was investigated over the entire concentration interval ($0 \le x \le 2$) for a wide temperature range ($10 \le T \le 300$ K) by neutron diffraction, inelastic and quasielastic scattering. This has made it possible to complete the determination of the phase diagram of the compound on which the critical transition point to the ferroelectric phase was found. The registered inelastic scattering spectra were used to verify the macroscopic model of the dynamics of such crystals. The model yields a satisfactory explanation for the mechanism of the observed phase transitions and the role of ammonium dynamics in the formation of the ferroelectric properties of crystals (see Sec. Experimental Reports).

In 1997, on the KDSOG spectrometer largely increased the number of external users and consequently, the number of solved problems, including, in particular, the measurement of crystalline fields in HTSC and CMR materials, determination of phonon spectra in ferroelectrics, Ni_3Al-based intermetallic compounds, isotope substituted amorphous alloys in the system *Zr-Ni* and nitrous steels, and the study of hydrogen vibrations in nonequilibrium ω-*Ti* and *Zr*, the intermetallic compound *FeTi*, and complex carbo- and nitrohydrates. One of the interesting results obtained is the discovery of a change in the magnetic response following the doping of the compound $AlSr_2Er_{1-x}Ca_xCu_2O_7$ (1212). This allowed constructing the model of charge redistribution in the CuO_2 planes. There are plans for carrying out experiments to verify the model over a wide doping range.

On the DIN spectrometer investigations in traditional directions, such as the atomic dynamics of liquid metal systems with gas admixtures, relaxation characteristics of liquid

helium, hydrogen dynamics in triple implantation systems based on transitional metals of the V-group, continued and were aimed at refining and systematization of the earlier obtained data.

Applied research was actively conducted on the HRFD diffractometer (investigations of internal stresses in bulk samples, determination of the structure of activated catalysts) and the NSVR diffractometer (textures of geological materials).

In particular, Al_2O_3/Al composites with a ceramic matrix were studied with HRFD. The development of the technology of production of new materials has led to the new method of manufacturing composite materials by infiltrating metals into a porous ceramic matrix by means of gas pressure and formation of a deep grid microstructure. In this case, fragile ceramic materials are strengthened by introducing the elastic phase using metals, as a rule. This makes it possible to improve the mechanic characteristics of composites. Usually, a metal is infiltrated into the matrix at temperatures a little higher than the melting temperature of the metal. The typical materials of that kind are Al_2O_3/Al composites where the metallic Al phase is infiltrated in the porous ceramic α-Al_2O_3 matrix. Residual stresses in Al_2O_3/Al composites arise as a consequence of an essential difference between the coefficients of thermal expansion of two phases (for Al_2O_3 - $\alpha=8.3\times10^{-6}$ $°C^{-1}$, for Al - $\alpha=22.5\times10^{-6}$ $°C^{-1}$). On HRFD two series of Al_2O_3/Al composites with the average size of metallic implants 0.1 μm or 1 μm were investigated. In each series the porosity of the matrix and correspondingly, the volume portion of Al is 15%, 25%, or 35%. An intensity analysis of Al reflexes demonstrates the existence of a strong texture in the metallic phase and the absence of a preferred orientation in the Al_2O_3 phase (see Sec. Experimental Reports).

Scientific program of the Condensed Matter Physics Division in 1997 was performed in cooperation with the following institutes and organizations:

Bulgaria	University; Institute for Nuclear Research and Nuclear Energy (Sofia)
Czech Republic	Polytechnical Institute (Prague)
Egypt	Atomic Energy Authority of Egypt (Cairo)
Finland	Technical Center (Espoo)
France	Laboratoire Leon Brillouin (Saclay); Institut Laue-Langevin (Grenoble)
Georgia	University (Tbilisi)
Germany	Hahn-Meitner Institute (Berlin); Research Center (Rossendorf); University (Bayreuth); Technical University (Kemnitz); Research Center (Darmstadt); GKSS (Geesthacht); Fraunhofer Institute for Nondestructive Testing (Dresden-Saarbruecken)
Hungary	Research Institute for Solid State Physics (Budapest)
D.P. Republic of Korea	University (Pyongyang)
Poland	Institute of Nuclear Physics (Cracow); University (Poznan)
Romania	Atomic Physics Institute (Bucharest)
Russia	Kurchatov Institute; Institute of Solid State Physics; Institute of Theoretical and Experimental Physics; Petersburg Nuclear Physics Institute; Institute of Physics of Metals; Moscow State University; Institute of Crystallography; Physical Energetical Institute (Obninsk)
Slovakia	University (Bratislava)
Sweden	University (Goteborg)
Switzerland	Paul Scherrer Institute (Villigen)
U.K.	Rutherford Appleton Laboratory (Abingdon)
Uzbekistan	Institute of Nuclear Physics (Tashkent)
Vietnam	Institute of Physics (Hanoi)

1.2. NUCLEAR PHYSICS WITH NEUTRONS

In 1997, nuclear physics investigations with slow neutrons were carried out on seven beams of the IBR-30 + LUE-40 neutron source, on beam 11 of the IBR-2 reactor and on neutron beams of other sources in Russia, Germany, France, USA, and China. In the reported year, the research program at IBR-30 was formed accounting for the working schedule of creation of the new JINR neutron source for nuclear physics investigations, IREN. A very extensive program of studies in resonance neutron induced fission was, in the main, completed. At the same time traditional investigations of the properties of highly excited states of heavy nuclei, parity violation effects, and reactions with emission of charged particles were successfully carried out. Very interesting and promising results were obtained with UCN in ILL.

1.2.1. EXPERIMENTAL

Parity Violation and Time Non-Invariance Effects in the Interaction of Resonance Neutrons with Nuclei

TRIPLE collaboration. Recent results

In the framework of a TRIPLE collaboration, the investigation of the mass dependence of the mean-square matrix element M_W of the weak neutron-nucleus interaction continued on the polarised neutron beam of LANSCE, Los-Alamos. The $(\sigma_n k_n)$ correlation measurements were conducted by the transmission method for natural Pa and the capture gamma-ray registration method for the ^{106}Pa and ^{108}Pa isotope targets. For the neutron energies $E_n < 1000$ eV, there are observed 6 p-wave neutron resonances with meaningful P-odd effects. It was established that most of the resonances represent the compound states of ^{105}Pa nuclei. Analysis of replicated experiments with ^{232}Th and ^{238}U targets in the energy region up to 300 eV is completed. The results for the mean-square matrix elements M are: $M(^{238}U)$ = 0.68+0.25-0.16 meV, $M(^{232}Th)$ = 1.28+0.33-0.24 meV. In them, the main uncertainty is due to the limited number of resonances. For uranium, 3 P-odd effects with a plus and 3 with a minus sign are found while for thorium, the existence of the so-called "sign effect" (all effects (10) have plus signs) is confirmed.

Nuclear fission

Angular correlations of fission fragments in the resonance neutron induced fission of the ^{235}U nucleus

Investigations of the angular anisotropy of fission fragments $A_2(E_n)$ with respect to the target spin orientation continued on beam 5 of IBR-30. The total measurement time at low sample temperature ($T \sim 0.1$ K) for measuring the angular anisotropy of fission fragments $A_2(E_n)$ with respect to the target spin orientation increased up to 1100 hours. Thus, the experimental data for $A_2(E_n)$ are now available in energy bins of 0.05 eV with an accuracy of 3 – 5 %, up to $E_n < 30$ eV. With the aid of an original code for multilevel, many-channel R-matrix analysis as well as a specially modified standard code SAMMY, the $A_2(E_n)$ data are fitted together with spin separated and total fission cross-sections, neutron capture and total cross-sections. It is established that to describe the experimental data adequately, one has to assume that fission channels with K=0, K=1 and K=2 are open for resonances with spin J=3 and channels with K=1, K=2 - for resonances with spin J=4. In this case, the relative contribution to $A_2(E_n)$ from different K-channels appears to be 18%, 63% and 19% for K=0, 1 and 2, respectively. It is also found that the interference of resonances with different spins appears to be significant and contributes approximately 16% to $A_2(E_n)$. It becomes evident that the old approach in which

definite A_2 values were assigned to definite resonances does not work because of a high level density and strong interference between resonances.. Progress in the description of the fission process is achieved thanks to the new theoretical approach developed by Barabanov- Furman. The results of measurements and the theoretical description are presented in Figure 1.

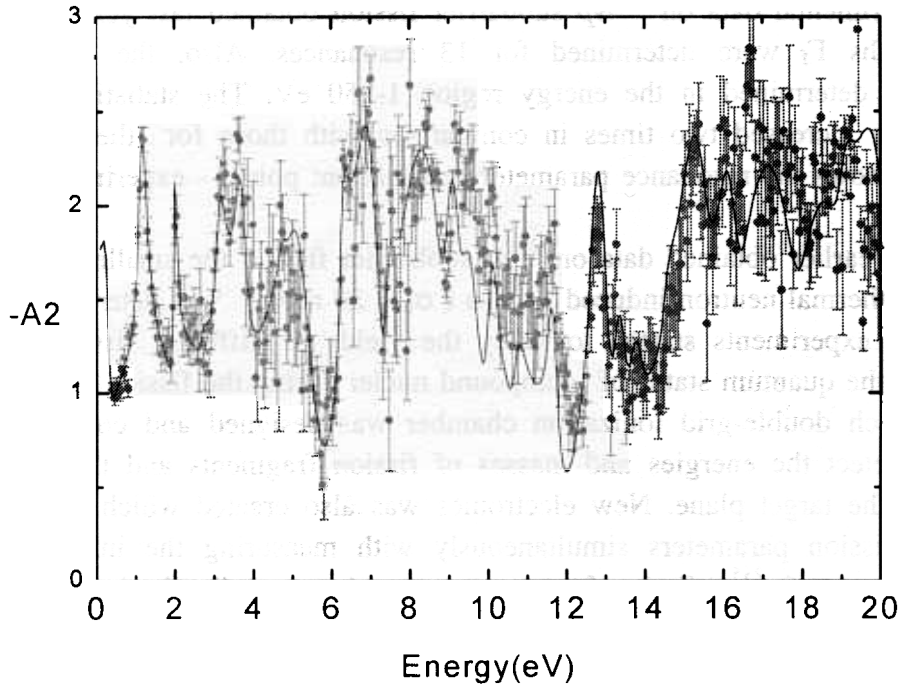

Figure 1

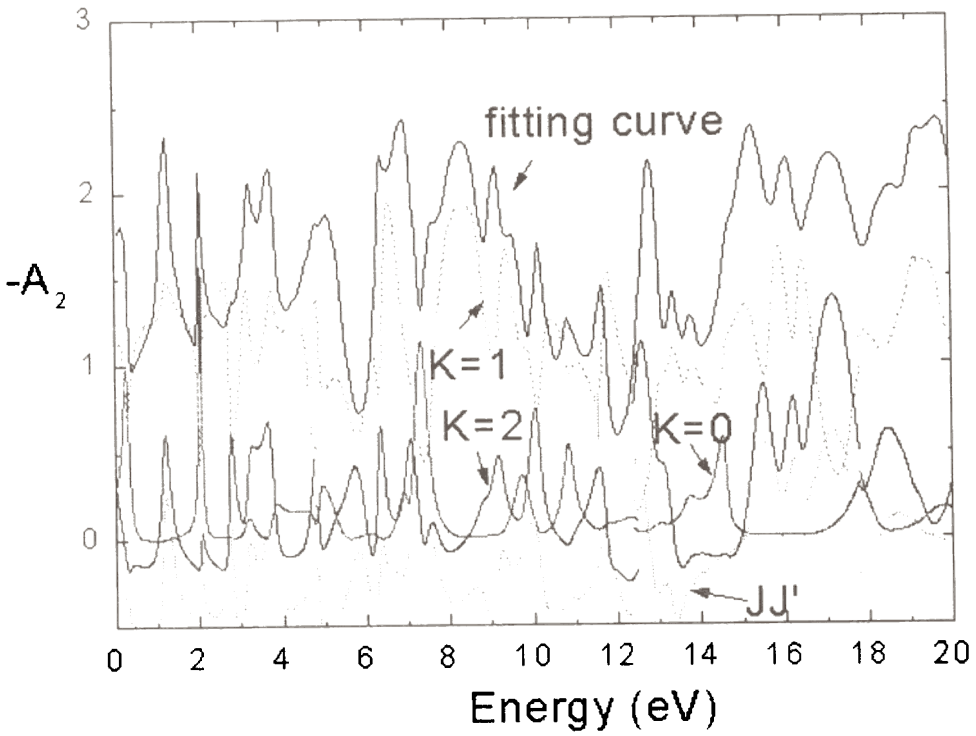

Figure 2

Solid points are the experimental data. The solid curve is the theoretical curve with parameters correlating well with total cross section and fission cross section data (total and spin separated). Figure 2 illustrates the influence of separate K-channels and spin interference.

Subthreshold fission and delayed neutron yields

The experimental data on ^{237}Np subbarrier fission obtained last year were improved and the fission widths Γ_f were determined for 13 resonances. Also, the cross section energy dependence was determined in the energy region 1- 50 eV. The statistical accuracy and the energy resolution increased two times in comparison with those for the data set obtained in 1993. Figure 3 shows the resonance parameters evaluation: points - experimental data, solid line - fitting curve.

From the earlier obtained data on ^{234}U subbarrier fission the smallest upper limit for the cross-section of thermal neutron induced fission ($\sigma_{nf} \leq 20$ mbn) was determined.

The first experiments started to study the yields of different fission modes and their correlation with the quantum states of compound nuclei during the fission induced by resonance neutrons. A Frisch double-grid ionization chamber was designed and constructed in 1997. It allows one to detect the energies and masses of fission fragments and the emission direction with respect to the target plane. New electronics was also created which makes it possible to measure these fission parameters simultaneously with measuring the initial neutron time of flight. Measurements of ^{235}U fission fragment mass and energy distributions were performed up to 25 eV. About 50 million fission events were registered and data analysis started.

For the first time neutron resonances in the $^{243}Am(n,f)$ reactions were measured using a fast ionization chamber which makes it possible to register fission fragments against a high background of α-particles ($N_f / N_\alpha \sim 10^{-10}$). This opens good possibilities for measuring earlier unknown fission cross-sections for minor actinides in the resonance region.

High resolution prompt γ- spectroscopy of fission fragments

To refine the earlier experimental data on independent fission fragment yields and obtain new information with the aid of fast γ-γ coincidences for two fission fragments, measurements of the γ-spectrum of ^{239}Pu fission fragments were performed on the 57 m flight path of beam 5 at IBR-30. There were registered $6 \cdot 10^8$ fission events. Data processing is in progress.

Highly excited states of nuclei

Cascade gamma decay of compound states after thermal neutron capture

Investigations of highly excited nuclear states in energy regions not properly studied so far, continued. To this end, coincidence gamma spectra of 2γ-cascades were studied for ^{140}La and $^{188,90}Os$ target nuclei. The energy of the final levels lies below 0.8 MeV. Analogously to the earlier studied spherical nuclei, the cascade γ-decay of their compound states demonstrates typical features. Namely, the probability of excitation and γ-decay of low lying (E<2-3 MeV) states enhances in comparison with model calculations based on standard assumptions concerning the level density and radiative strength functions. At the same time, these probabilities are relatively depressed at high excitation energies. So, the situation is quite opposite to that observed in deformed nuclei where most 2γ-cascades are connected with the excitation of levels lying above 3-4 MeV.

A combined analysis of experimental results for 40 nuclei studied up to now gives good reason to believe that the coupling nucleon interaction at excitation energies in the 1-5 Mev

energy region produces much stronger influence on the levels structure than predicted by modern nuclear models.

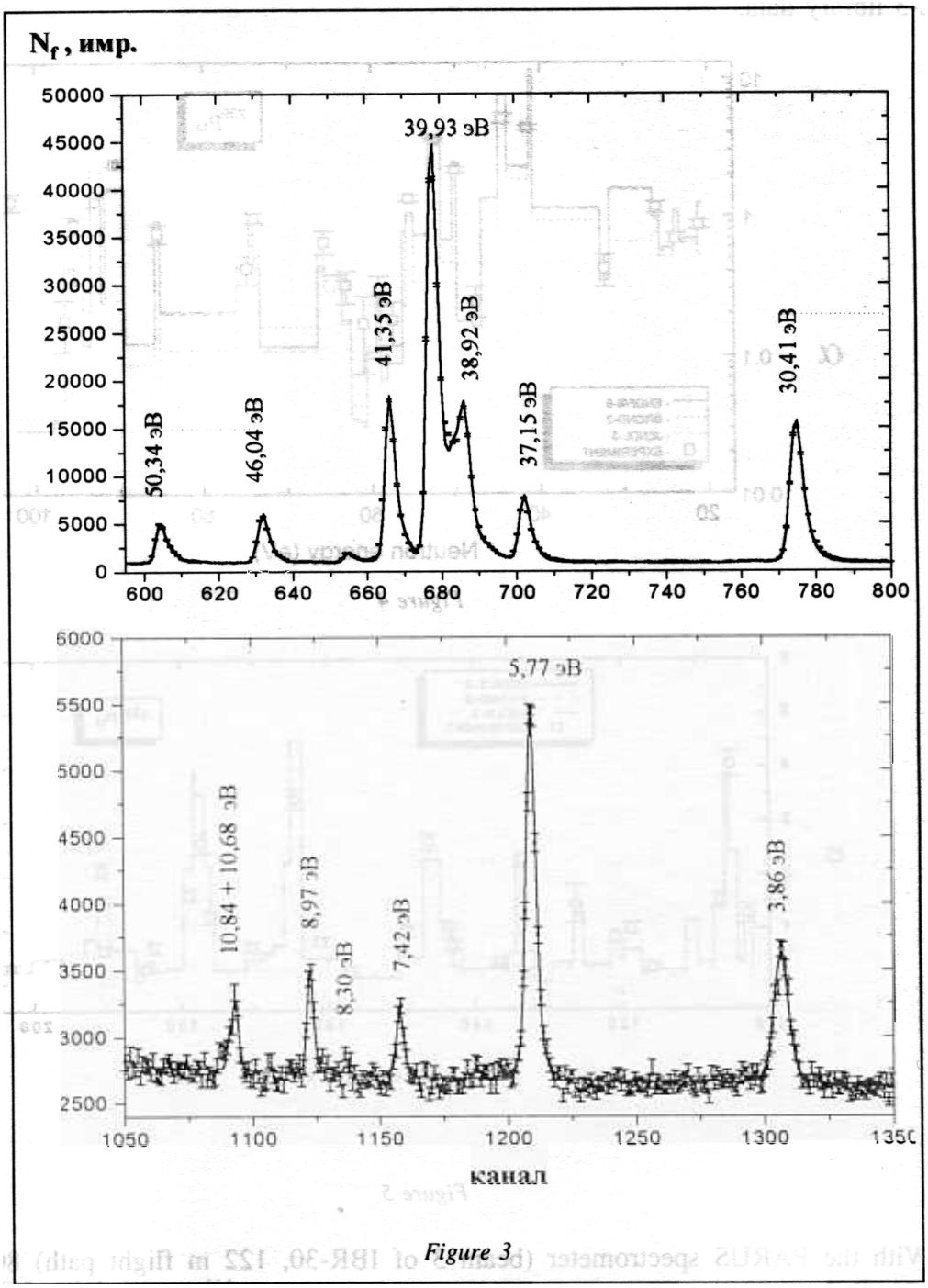

Figure 3

Radiative resonance neutron capture. ROMASHKA & PARUS spectrometers

Pioneering experiments to measure the effects of resonance self-shielding and the value of $\alpha = \sigma_\gamma / \sigma_f$ for ^{235}U target nuclei in the 20-2000 eV energy region were performed. Multiplicity spectra were also measured for the ^{239}Pu target to refine the α value for ^{239}Pu in the 0.007-20 keV energy region. As a result, α values were obtained for 80 resonances and several energy groups.

Figure 4 and 5 show the experimental α values for ^{239}Pu (points) in comparison with the evaluated by the GRUCON computer program on the basis of BROND-2, ENDF/B-6, and JENDL-3 library data.

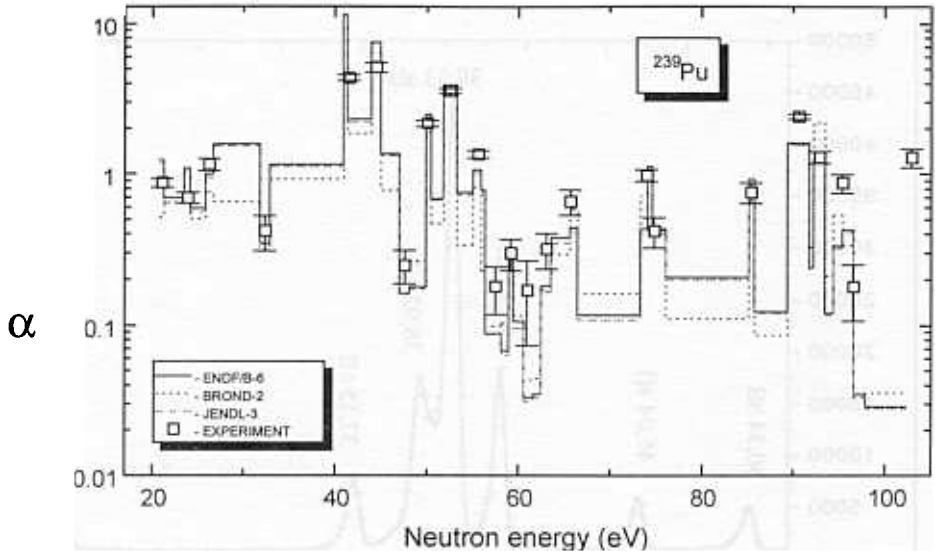

Figure 4

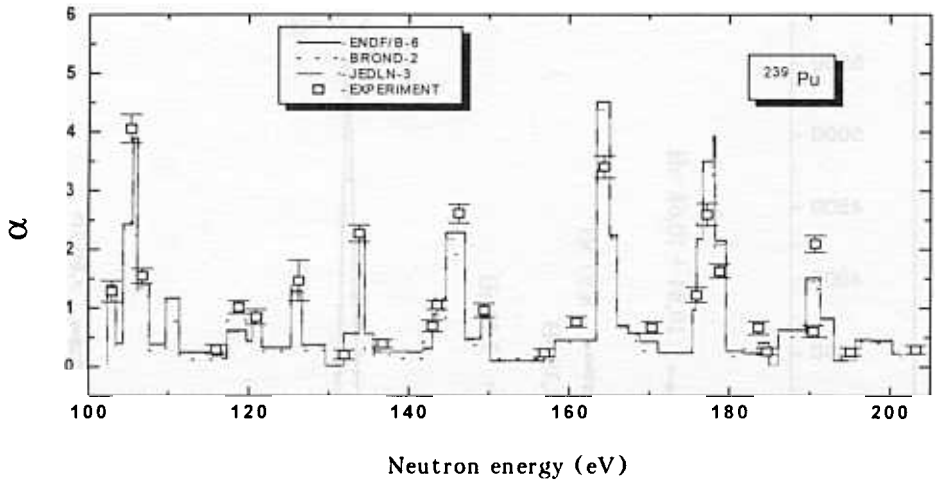

Figure 5

With the PARUS spectrometer (beam 3 of IBR-30, 122 m flight path) 80-litre volume multisectional detector multiplicity spectra were measured for ^{232}Th, $^{235, 238}U$, ^{239}Pu and *Pb* to determine α values and radiative capture cross sections.

Neutron induced reactions with charged particle emission

The $^{26}Al(n,\alpha)$ and $^{26}Al(n,p)$ nuclear reactions may form the basis of the main mechanism of *Al* destruction in nature. Precise measurements of their cross sections are important for the understanding of γ-spectra of "live" ^{26}Al in our Galaxy and " dead" ^{26}Al in meteorites.

In collaboration with Los-Alamos physicists investigations of the $^{26}Al(n, \alpha)^{23}Mg$ and $^{26}Al(n, p)^{26}Mg^{*}$ reactions in the energy region from thermal to 10 keV and 70 keV, respectively, were performed. The results are illustrated in Figure 6 and 7.

These very reactions are mainly responsible for *Al* destruction in the nucleosynthesis and the determination of their cross sections is therefore very important.

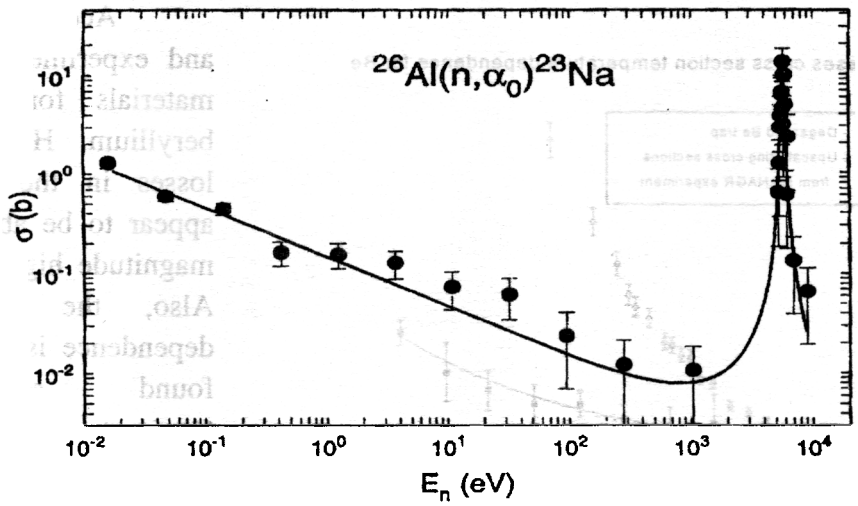

Figure 6

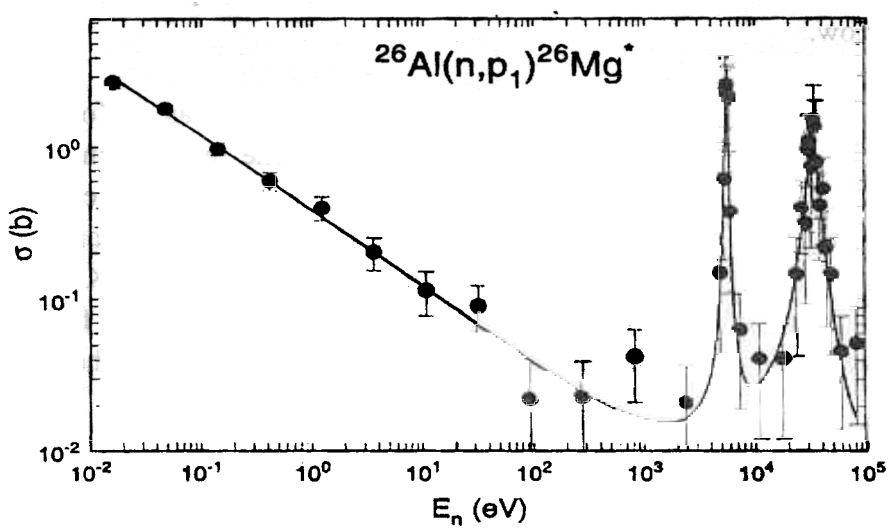

Figure 7

(n, γ) reactions for astrophysics

The investigation of the $^{48}Ca(n, \gamma)$ reaction completed in 1997. The results were obtained and processed for a Maxwellian neutron spectrum with kT = 25 keV. The $^{50}Ti(n, \gamma)$ reaction was studied with neutrons from a Maxwellian spectrum with kT = 25 keV as well as with 29 keV and 145 keV monoenergy neutrons. The results are being processed.

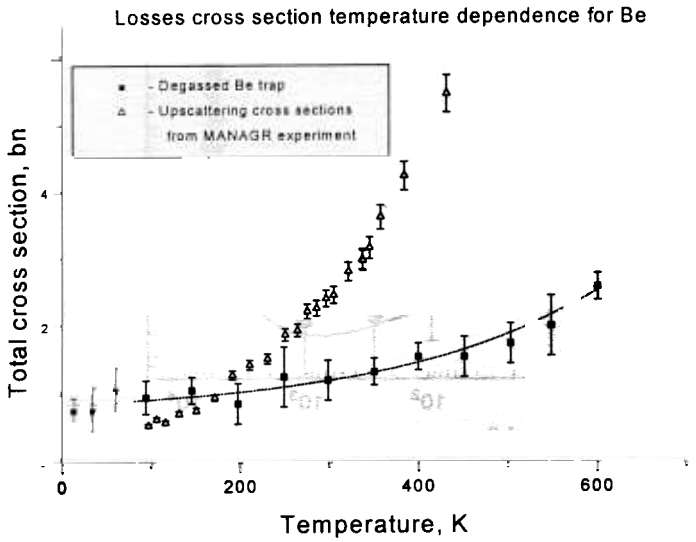

Figure 8

According to both theory and experiment, one of the best materials for UCN storage is beryllium. However, total UCN losses in the walls of a trap appear to be about two orders of magnitude higher than predicted. Also, the UCN temperature dependence is surprising: there is found some additional temperature-independent mechanism of losses with a high cross section of 0.9 bn corresponding to the loss probability $3 \cdot 10^{-5}$ per bounce (solid curve in Figure 8). Also, in the same experiment it was determined that no additional losses in the walls material take place. Thus, the losses can be attributed to the surface. This experiment has no reasonable explanation up to now.

An experiment to study the upscattering of UCN on Be was performed in May-April 1997 on the High Flux Reactor in Grenoble, France. The experimental count rates of upscattered neutrons were transformed into upscattering cross-sections. One can see the results in Figure (uppper triangles). Introducing capture cross-sections obtained in different experiments one can explain the anomaly of UCN losses for temperatures down to 90 K. It should be noted that further investigations of UCN upscattering in the temperature interval from 90 K to liquid helium temperatures are essential for the verification of the hypothesis of anomalous upscattering.

Precise experimental test of the UCN dispersion law

In the frame of a FLNP-Kurchatov Institute-ILL-Melbourne University collaboration, a precision experiment to verify the neutron wave dispersion law was performed using an original method. It is based on a search for the resonance line shift in an interference filter, the Fabri-Perrot interferometer, accompanied with a change in the neutron velocity component parallel to the filter surface. It is found that when the filter moves parallel to its surface with the velocity 35 m/s, the effective neutron spectrum goes through the resonance shifted by $+0.100 \pm 0.016$ neV for the initial UCN energy 107 neV. In the test experiment it was shown that when the initial spectrum is narrow and the transmission line of the filter broadens, monochromatic neutrons do not change their energy during tunnelling through the moving filter. The observed effect may be interpreted as a very serious evidence of the fact that some deviation from the commonly accepted dispersion law really exists.

1.2.2. THEORETICAL

The effect of electromagnetic interactions on the strangeness-conserving β-decay of baryons, neutron (**n**) and Σ-hyperon (**Σ**), is demonstrated. The modifications of the total decay probability, $\delta W_n \approx 8\%$, $\delta W_\Sigma \approx 0.5\%$, the $e^{\pm}$ spectrum and the angular distribution with respect to the polarization vector ξ of the initial baryon, $\delta A_n \approx -1.9\%$, $\delta A_\Sigma \approx 1.8\%$, were obtained. The dependence of the results on the value of the ultraviolet cut-off parameter Λ is elucidated. The spectrum and the yield of γ-radiation accompanying β-decay are calculated and special attention is paid to infrared (soft-photon) radiation. The photon radiation of pions constituting the baryon's ``pion cloud" is investigated. Radiative corrections to the total β-decay probability, the electron energy and the angular distributions found in this work prove to be of pivotal importance for obtaining the main characteristics of weak interaction by experimental data processing.

It is shown that applying the multiple wave scattering technique to the problem of the interaction of slow neutrons with a substance with simple crystalline structure does not reveal any anomalies in the slow neutron dispersion law and cannot explain excessive UCN losses during storage in material traps.

A possible alternative explanation of anomalous UCN losses is investigated theoretically. The ground for this hypothesis is the de Broglie description of the wave function. The results of experiments are analyzed under this assumption.

Due to high densities, some intermediate products of the *pp*-cycle in stars can emerge not only from two-body but also three-body initial states. Their role is not properly estimated yet. Moreover, three-body states have different selection rules and may significantly change the entire picture of the nucleosynthesis. We performed (for the first time) a microscopic analysis of several nuclear reactions not included in the standard model of the *pp*-chain. The fate of ^7Be in this chain is of special interest. The fact is that a combined analysis of all experiments measuring the neutrino flux from the sun leads to a paradox conclusion: the production of ^7Be nuclei (more precisely, the flux of neutrinos due to ^{7}Be) must be strongly suppressed or even negative. This means that something is wrong either in the standard model or in the experimental data.

The problem of possible *T*-invariance violation in the "backward" elastic scattering of neutrons by a spinless nucleus was investigated. It is shown that under *T*-invariance the amplitude and the cross-section of "backward" scattering do not depend on the neutron spin. An observation of such dependence will unambigously point to T-invariance violation. However, the fulfilled estimates of the possible spin asymmetry of "backward" scattering demonstrate that the corresponding effect is very weak (about 10^{-8} - 10^{-7}) and can hardly be observed experimentally in the nearest future.

1.2.3. METHODOLOGY

KaTRIn project status

In the frame of the KaTRIn project (see a separate article below) aimed at studying time–non invariant (*T*-odd) effects in resonance neutron induced reactions, work to create a ^{3}He based neutron polarizer - analyzer was carried out during 1997 in collaboration with Lebedev institute (Moscow).

A ^3He based neutron polarizer with laser pumping is attractive for many tasks in neutron physics. It does not require cooling and strong magnetic fields. The polarization that can be

achieved for 1 eV neutrons is about 75% with the transmission about 20%. This allows such a polarizer to be compact with a small weight.

During 1997, the prototype of the *Rb* - ^3He polarizer, a two-chamber aligned aluminosilicate glass cell filled with ^3He at 10 atm, was created. Two Helmholtz ∅ 1400 mm coils to produce the leading field about 20 G with the homogeneity not worse than 5×10^{-4} in the center and a pair of RF ∅ 600 mm coils perpendicular to the leading one were built and will operate at 80 kHz. The pick - up coils are incorporated with a cell holding platform. The setup is a multifunctional stand for the investigation and adjustment of the design and working regime of the cell.

Neutron induced reactions with emission of charged particles

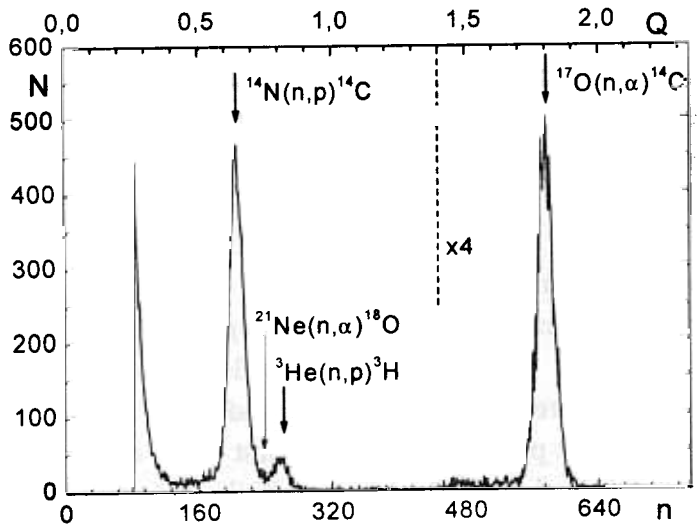

Figure 9

Using the created unique ionization chamber (IC) with a gas target a number of reactions were measured, including: $^{17}O(n, \alpha)^{14}C$, $^{36}Ar(n, \alpha)^{33}S$ and $^{21}Ne(n, \alpha)^{18}O$. The new method for measuring *(n, α)* and *(n, p)* was developed and tested on the thermal neutron beam at the IBR-2 reactor. Figure 9 shows the pulse-height spectra form the IC collector.

The thermal neutron cross sections obtained from these measurements are in good agreement with earlier ones for ^{17}O and ^{36}Ar while for ^{21}Ne, our result is significantly smaller.

Further development of this technique will make it possible to use resonance neutrons in the investigation, particularly, of *(n, α)* reactions using ^{37}Ar and ^{39}Ar targets. These processes are of crucial importance for the understanding of the origin of ^{36}S rare isotopes.

Modernization of the ISOMER installation

The new system for automatic alternating the background and physical measurements was created.

The new fast electronics was created to decrease sufficiently the dead time in the whole delayed neutron registration module.

After the modernization rather precise data on delayed neutron yields from the ^{237}Np fission induced by thermal neutrons were obtained.

Neutron spectra analysis in the 2-100 keV region with the aid of a (n, γ) converter.

The new method of neutron spectrometry based on shape analysis of γ lines was tested at the electrostatic generator EG-5. The preliminary results show high efficiency of the method for the purposes of spectrometry with stationary and pulsed neutron sources.

The anticompton gamma spectrometer HPGe-BGO for nuclear physics experiments at pulsed neutron sources

The HPGe detector with the efficiency 9% and the resolution 2.0 keV at the energy 1332.5 keV is used as the main part of the spectrometer. The detector is 78 mm in diameter and 120 mm in length. The choice of the design is determined by its simplicity and cost as well as the results of computer modelling. The schematic view of the spectrometer including the passive shielding is presented in Figure 10. The BGO surrounding consists of 32 rectangular crystals with maximum dimensions 40 mm × 40 mm × 80 mm and the total volume 3 litres. A simplified system with 10 photomultipliers is used for photon registration. The employed module scheme of the design allows the transformation of the shielding to make the spectrometer suitable for studying γ-ray multiplicities in neutron-nuclear interactions. Figure 11 demonstrates the unsuppressed (1) and suppressed (2) experimental spectra together with the experimental (3) and calculated (4) suppression coefficients for the standard ^{60}Co source. The use of the CSS for the investigation of the peculiarities of the resonance neutron induced fission of ^{239}Pu has reduced the background of the measured prompt γ-spectra 2 - 3 times and improved the accuracy of fission fragment yields by a factor of 1.5.

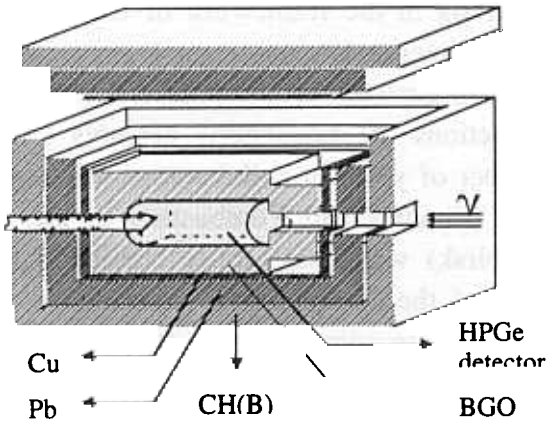

Figure 10

Test of the UGRA installation

The first test of the UGRA instrument shows that it is necessary to modernize old neutron detectors to adjust them for operation in vacuum conditions. This work was carried out at the end of 1997. However, without IBR-30 neutron beams it turned out to be impossible to test the new detectors.

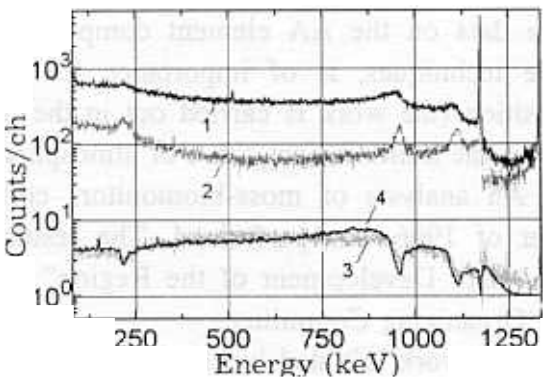

Figure 11

Construction of the KOLHIDA instrument

The new set-up KOLHIDA shipped from Georgia in 1996 is and mounted and adjusted on beam 1 of the IBR-2. This installation allows one to use the intense beam of polarized neutrons to study nuclear pseudomagnetism and some new parity violating effects in neutron optics.

1.3. APPLIED RESEARCH

A series of multielement NAA studies of ecological samples from the Kola peninsula to investigate technogenic transformation of podzolic *Al-Fe*-soil as a result of air pollution by copper-nickel production were completed. These studies were conducted in cooperation with the Institute of Industrial Ecology of the North of the Kola Scientific Center from 1992.

The first stage of the International Program for the study of atmospheric deposition of heavy metals on the territory of Romania was completed. Moss-biomonitors were collected in the Eastern Carpathians in 1995. The obtained results are represented as maps made using the GIS (geographic information systems) technologies (GIS-INTEGRO) in collaboration with the Department of Mathematics of the International University of Nature, Society and Man in Dubna.

Work to analyze peat samples from peat cores in Arctic Norway was fulfilled. A comparison was conducted of the results of the paleoclimatic reconstruction of the atmospheric deposition in the North with the new data obtained by the sector for neutron activation analysis and radiation research (NAA&RR) for peat cores from Switzerland and Indonesia in the framework of the collaboration with the Institute of Geology of the University in Bern, Switzerland.

One of the important directions of investigations in ecology by the NAA&RR sector is the study of the multielement composition of different fractions of atmospheric aerosols (AA) from West and East Siberia. This work carried out for a number of years in collaboration with specialists in atmospheric ecology from the Institute of Chemical Kinetics and Combustion of the Siberian Branch of the Russian Academy of Sciences (Novosibirsk) was successfully continued in 1997. Several hundreds of AA samples from different areas of the Novosibirsk, Krasnoyarsk, Tumen, Irkutsk, and Baikal regions have been analyzed using NAA. In some of them (the Tumen, Irkutsk and Baikal regions), a high content of a number of technogenic, including toxic elements – *Ni, Co, As, Cd, Mo, Ag, W,* is observed in AA. This is an alarming signal and is of interest for ecologists.

The data obtained for a large number of elements (45-65) were submitted to ecologists of the Institute of Chemical Kinetics and Combustion of the Siberian Branch of RAS and at present, are used to reveal the most significant sources and factors of technogenic pollution of the atmosphere over these Siberian regions as well as to study regional and local peculiarities and yearly and seasonal dynamics of changes in the AA element composition. A large amount of reliable data on the AA element composition obtained by NAA, one of the most sensitive and suitable techniques, is of importance for the formation of the data bank on the AA element composition (the work is carried out in the Siberian Branch of RAS). Several papers covering the results of the multielement NAA of atmospheric aerosols are to be published.

An analysis of moss-biomonitors collected near the Baikal paper producing plant in the summer of 1996 was performed. The results of this investigation presented at the International Forum "Safe Development of the Region" (July 2-6, 1997, Irkutsk) won the Second Prize of the Forum Organizing Committee.

The work initiated by the Department of Geography of Moscow State University and aimed at studying the microelement composition of ferro-manganese nodeles from one of the regions in the Pacific Ocean was completed.

Analytical studies of the NAA&RR sector to analyze rocks, soil, sediments and water contributed to the development of the experimental interrepublican system of ecological monitoring of the Terek basin.

The paper devoted to studies of the halogen distribution from the coast of the Arctic Ocean deep into the continent carried out in collaboration with the Norwegian University of Science and Technology (Trondheim), is prepared for publication.

At the NATO Conference "Ecological Problems of Industrial Regions of the Urals" held on May 25-30, 1997, three reports on the use of the biomonitoring technique to study atmospheric deposition of heavy metals were presented. This gained the appraisal of specialists from the Academy of Metallurgy in Magnitogorsk and the Institute of Biophysics in the town of Ozersk of the Chelyabinsk region (MAYAK Industrial Enterprise) and led to the development of a project for studying atmospheric deposition of heavy metals and radionuclides in the Chelyabinsk region by nuclear physics methods. The proposal for the project was submitted to the IAEA and has successfully developed into a co-ordinated research program on biomonitoring air pollution through trace element analysis.

Part of industrial monitoring work under the auspices of the other IAEA grant connected with monitoring of the plant for production of phosphorous fertilizers in the town of Voskresensk in the Moscow Region was completed and the the results were submitted to the IAEA as a yearly report.

In the framework of a special course "Neutron activation analysis as a nuclear physics method for the determination of the element composition of matter, its application to ecological studies" by M.V.Frontasyeva, four-year students of the Department of Ecology of "Dubna" University do practicals in the NAA&RR sector.

In 1997, investigations of semiconducting crystals of the A^3B^6-$A^3B^3C^6_2$ type with a highly anisotropic crystalline lattice structure continued. The electric and photoelectric properties of the heterojunction (HJ) in a *TlSe* - $TlInSe_2$ system obtained by the liquid-phase epitaxy method from a *TlSe* melt on the surface (110) of $TlInSe_2$ are described in the framework of the model of an isotypical HJ without local states on the interface. The main parameters of HJ – the boundaries of free and valence zones, equal to E_c=0.69 eV and E_v=0.05 eV, respectively, were estimated. The peculiarities observed in the HJ photoresponse spectra were explained using the Dember effect. The results are to be published in "Physics and Technology of Semiconductors" and "Nuclear Instruments and Methods".

Studies of defect structures in crystals with specific physical properties which are of interest for applied research, continued.

Defect formation in nonstoichiometric crystals in solid zirconium oxide and yttrium oxide solutions with different concentrations (the monocrystals were grown by E.E.Lomonova and V.V.Osiko) was investigted using two diffraction methods: (1) diffusion scattering to determine short-range order and (2) Bragg diffraction to determine the middle structure. The experiments were carried out with participation of Bente Lebech in the Riso National Laboratory, Denmark, and Arthur Schulz in the Argonne National Laboratory, USA. It is shown that in the cubic structure the main peculiarities of the diffuse scattering pattern are connected with the existence of implanted oxygen atoms and the fact that the population of their positions changes little as the concentration of yttrium oxide changes. At the same time, an increase in Laue diffuse scattering as the concentration of yttrium oxide increases is probably connected with an increase in statistical

isotropic displacements in the *Zr/Y* averaged position. It is established that in the tetragonal phase, the observed strong hardening of crystals is connected with the coexistence of coherently linked cubic and tetragonal phases with a low yttrium oxide concentration. Most recent results are obtained with the high resolution Fourier diffractometer in FLNP.

The cycle of neutron diffraction measurements to investigate the defect structure of a *C60* fullerene crystal (grown by R.K.Nikolaev in ISSP in Chernogolovka) was conducted by the same group of people in Riso and ANL at room temperature, 200 K and 20 K.

The data processing and a symmetry analysis of the reciprocal space geometry of fullerenes are under way. As a preliminary result, it is established that several twinning systems exist in the fullerene crystal and its symmetry in the low temperature phase is not P a-3, as it is accepted in the literature, and is sooner lower than that.

The main tasks of the NAA&RR sector for 1998. In accordance with traditional research themes the main objectives of the sector in 1998 are the investigations in the field of ecology and environmental protection. In the framework of the European Program "Atmospheric Heavy Metal Deposition in Northern Europe 1995" monitoring of several regions in the Arctic, Norway, Finland, and Rome as well as studies of the multielement composition of atmospheric aerosols in West and East Siberia (the "Aerosols of Siberia" and "Aerosols of Baikal" projects) will be continued. Several research projects and programs are under preparation in collaboration with the Institute of Limnology of SB RAS (Study of atmospheric aerosols and sediments of Lake Baikal); Swiss Institute of Geology (Study of element composition of peat cores from different regions of the world for paleoclimatic reconstruction); Institute of Radioecological Problems, Minsk (Study of the effect of the Chernobyl accident on the health of children); Institute of Geology, RAS and V.I.Vernadsky Institute of Geology and Chemistry (Estimation and prediction of a balance in the distribution of toxic elements in technologic flows from the Astrakhan gas-refining complex), a number of the Urals Institutes and the IAEA (biomonitoring of atmospheric deposition in the Urals regions with a high technogenic impact).

In the field of condensed matter physics, the mechanisms of electric conductivity in heterojunctions (volt-ampere and volt-capacitive characteristics) in crystals with a highly anisotropic crystalline structure will be investigated. For this purpose, a *p-p-TlSe-TlInSe$_2$* heterojunction will be produced for which the material for epitaxial *TlSe* plating will be preliminarily purified by the zone recrystallization method up to the concentration of acceptors $N_{a1} \sim 10^{15}$-10^{16} cm^{-3}, and the substrate material *TlInSe$_2$* will be alloyed with *Se* up to the concentration of acceptors $N_{a2} \sim 10^{14}$-10^{15} cm^{-3}. This will make it possible to improve the HJ detector characteristics, i.e., increase the current sensitivity to g-n radiation, extend the range of spectral sensitivity to include the long-wave region, decrease the response time, etc.

2. NEUTRON SOURCES

2.1. THE IBR-2 PULSED REACTOR

In 1997, the reactor operation for physical experiments on extracted neutron beams was continued. Detailed information on the operation of the reactor is presented in Tables 1 and 2.

On June 12, 1997, the reactor was shut down to repair a malfunction in the prompt emergency shutdown (PES) system (the system could not be set in the operative position, connected with a decrease in the travel range).

In accordance with the characteristics of the control and emergency system (CES) and methods of providing safety accepted for the IBR-2 reactor, in response to the alarm signal the 1PES and 2PES systems shut down the reactor (efficiency – 0.36 ± 0.02 β_{eff} and 0.49 ± 0.03 β_{eff}, respectively) for less than 0.02 s.

The measurement of the efficiency and speed of response of 1,2PES with the decreased working strokes of the PES units on July 11-16, 1997 demonstrated that on retention of the speed of response less than 0.02 s the efficiency of CES units was 0.21 β_{eff} for 1PES and 0.35 β_{eff} for 2PES, respectively.

In places accessible to observation (using a remotely controlled tool and photographing and filming) the elements which can affect the technology of setting PES system in the operative position were examined by stages. This made it possible to detect a worn spot on the upper front surface of the 1PES unit. This spot is direct evidence that the 1PES unit in the operative position came in contact with the case of the stationary reflector.

So, the provided clearance disappeared, and this prevented the setting of the 1PES unit in the operative position. A visual inspection of the 1PES unit and the places of the construction of the 1PES channel accessible to observation testified that all elements are intact (see Fig.1 and 2). When examining the mechanism of the rod of 1PES, the vertical backlash of the lower end of the rod was detected, which is a result of the wear while in service.

Taking into account that the efficiency of the PES units is practically independent of (within the travel range) the location of the point of the operative position of units, and depends on the travel range itself, it was decided to move the construction of 1PES 12mm away from the active zone and to fix it in that position, as well as to replace the water moderator by a newly manufactured one with geometry which ensures the absence of contact between 1PES and water moderator within the full travel range.

The results of the repairs are illustrated in Table 3.

The repairs, which proceeded under difficult radiation conditions, were completed in October 1997, and on November 11, 1997, the reactor was put into operation.

Positive experience in operating two movable reflectors of the IBR-2 reactor, which have worked out their service life: the first one – 13000 hrs. and the second – 20000 hrs, made it possible to redetermine the limit values for the levels of vibration for the third generation reflector (PO-2R) now in service. These levels are used as a basis to control the operation of the reflector. In addition, vibration diagnostics is carried out to detect malfunctions of the movable reflector early in their development using different algorithms of static analysis of vibration signals, which make it possible to identify the origin of changes in this or that parameter of vibration signals.

Table 1

IBR-2 reactor operation characteristics for 1997

№ cycle	Start and completion dates of cycles	Operation time for physical experiments, $T_{ph.e.}$	MR operation time, T_{MR}	Number of emergency shutdowns, N_{ES}	Causes of emergency shutdowns (malfunction classification according to RD-04-10-94)						Number of operating beams
					Voltage drops (MR8)	Equipment breakdowns (MR7)	Electronic equipment breakdowns (MR7)	Personnel errors (MR5)	Scheduled emergency shutdowns	Malfunctions of safety systems (MR4)	
1	20.01 - 01.02	250	284	2	1	0	1	0	0	0	12
2	10.02 - 21.02	cancelled by order of the FLNP Directorate									
3	10.03 - 25.03	263	328	5	3	0	0	0	0	2	12
4	07.04 - 18.04	252	273	2	0	1	0	0	1	0	12
5	19.05 - 30.05	242	273	4	1	2	1	0	0	0	12
6	9.06 - 12.06*	54	92	2	0	0	0	0	0	2	12
7	10.11 - 26.11	367	441	5	1	0	2	1	1	0	12
8	8.12 - 26.12	403	427	6	0	1	5	0	0	0	12
	Total:	**1831**	**2118**	**26**	**6**	**4**	**9**	**1**	**2**	**4**	

* the reactor was shut down because of a malfunction in the prompt emergency shutdown systems (1,2PES)

Table 2

IBR-2 operational parameters as on November 1, 1997

№	Parameter	Achieved	Allowed
1	Total operation time for physical experiments, hrs.	32143	
2	Total generated energy, MW/hrs.	60970	85000
3	PO-2R total operation time, hrs.	6392	18000
4	Maximum fluence on the reactor jacket at the centre of the active core (10^{22} n/cm^2), for $E_n > 0.1$ MeV	2.68	3.72
5	Maximum fuel burning, (%)	~ 4.9	6.5
6	Total number of emergency shutdowns	380	550

Table 3

Efficiency, speed of response and full travel range of 1,2PES units in the previous and new working positions

Characteristics	Previous value	Value in a new working position
Full efficiency of 1PES, β_{eff}	0.36±0.02	0.37±0.02
Full efficiency of 2PES, β_{eff}	0.49±0.03	0.37±0.02
Speed of response of 1PES, s	less than 0.02	less than 0.02
Speed of response of 2PES, s	less than 0.02	less than 0.02
Full travel range of 1PES, mm	23.5	24
Full travel range of 2PES, mm	23.5	17.5

The diagnostics of the current state of PO-2R is performed using the vibration monitoring program, the basis for which is the construction of base spectrum "mask" from data of vibration measurements in i-th cycle (operation time of the reflector in one cycle is ~ 280 hrs). This cycle is chosen as stationary from the viewpoint of constancy of characteristics of vibration signals picked up from the bearing supports of PO-2R following its running-in. The allowable limit values of vibration levels are established for each subrange of spectrum characteristics (low-frequency, medium and high-frequency). The position of current spectra relative to the base mask characterizes the current state of the movable reflector. The analysis of the trend curve, constructed from the results of measurements of vibration-acceleration as a function of the number of operation cycles taking the statistical spread of readings into account, allows us to evaluate the residual service lifetime of PO-2R.

In addition, to evaluate the degree of wear of rubbing parts of the movable reflector—radial and radial thrust bearings, spur and cone gears, journals of the shaft of the reflector—and to establish a correlation with the parameters of vibration signals, the method of neutron activation analysis of samples of oil of the lubrication system of PO-2R was proposed. This method makes it possible to determine the content of the wear products on the basis of analysis of spectral presentation of nuclides of activated metal impurities. The nuclide content in oil samples, radiation energy in keV, and pulse area following the operation of PO-2R for 21 cycles (6000 hrs) are presented in Table 4.

Table 4

Spectral content of metal impurities in oil samples following the operation of PO-2R for 6000 hrs.

Element No.	Energy, keV	Pulse area	Resolution in keV	Nuclide
1	135.95	350	1.84	Se-75
2	192.45	174	1.88	Fe-59
3	264.51	386	3.73	Se-75
4	279.36	208	1.66	Hg-203, Se-75, Pb-203
5	320.02	789	2.38	Cr-51
6	336.14	264	2.57	In-115m
7	411.95	165	2.77	Au-198
8	528.20	156	1.91	Cd-115
9	563.74	146	4.75	Cs-134, Sb-122
10	602.73	789	2.08	Cs-134, Sb-124
11	646.33	115	4.80	Sb-124
12	723.27	163	2.83	Sb-124
13	765.14	140	2.76	Nb-95
14	834.61	220	6.51	Mn-54, Ga-72
15	1099.17	770	2.69	Fe-59
16	1115.44	4757	3.26	Zn-65
17	1173.06	1373	3.13	Co-60
18	1291.18	481	2.78	Fe-59
19	1332.23	1267	4.37	Co-60
20	1460.27	275	4.19	K-40
21	1689.75	99	1.45	Sb-124

Qualitative and quantitative changes in mass of the wear products in oil in the further stages of the operation of PO-2R together with the results of vibration diagnostics will allow us to detect more precisely the starting moment of the progressing wear of the rubbing parts under study.

The experimental investigations into the dynamic properties of the IBR-2 reactor have been carried out. The main result of these studies is as follows: after the second reloading (1996) the reactor operates steadily over a whole range of power (up to 2 MW) and at a sodium flow rate of 80-120 m^3/h.

Work to manufacture a cryogenic moderator (CM) has been completed in the main. However, the factory endurance tests have revealed that significant modifications in the construction are required to ensure reliability of CM, which will delay the ultimate date of manufacture until the middle of 1998.

Work to modernize the circulating water supply system has been performed. This makes it possible to set a more economical regime of water supply when the reactor does not operate.

The reserve power supply of IBR-2 from the Ivankovskaya hydroelectric power station in case of emergencies at the GPP-2 reserve control desk has been improved.

The financing of theme 0851 was low and unstable as before. For eleven months the contract payment amounted to 806 million rubbles (~140 k$) as compared to the annual plan of 1620 k$. For this reason, work on the projects for the modernization of IBR-2 and the production of TVELs has not been carried out. The debts for work executed in 1996 have not been redeemed either.

Table 5

Financing of theme 0851 (IBR-2) in 1997 (in k$) (as on November 1, 1997)

	STE	CM	MR-3	TVEL	Main Equipment	Total
January	–	–	–	–	–	–
February	–	–	–		–	–
March	–	9	–	–	–	9
April	8.5	6	–	–	7	21.5
May	8.3	13.1	–	–	–	21.4
June	–	–	–	–	–	–
July	2.6	–	–	–	–	2.6
August	24.5	3.7	–	30.1	–	58.3
September	1.0	–	–	–	2.6	3.6
October	2.7	–	20.6	–	–	23.3
TOTAL:	**47.6**	**31.8**	**20.6**	**30.1**	**9.6**	**139.7**

2.2. THE IREN PROJECT

The project status. Following the recommendations of the JINR Plenipotentiary Committee (March 1993) the JINR Directorate adopted the decision, approved at the 76th Session of the JINR Scientific Council June 1994), to construct the new modern source of resonance neutrons for investigations in fundamental and applied nuclear physics. The completion date (physical startup date) was the end of 1997. The IBR-30 analogous scheme, i.e., the combination of a powerful linear electron accelerator and a subcritical multiplying target, was chosen for the new neutron source. The new IREN facility will permit the neutron energy resolution to be increased an order of magnitude at a double increase in luminosity.

In 1997 financing of the work on the IREN project became lower than in 1996 (30 K$ per year) and only extraordinary efforts of the project management allowed to preserve validity of the key contracts ensuring construction of the main IREN systems. So to the initial completing date of the IREN project established at the official beginning of the project in 1994 we have at least two years delay. To the end of 1997 in the frame of the project implementation it was invested 870 K$ and the total cost of the signed contract achieved 2700 K$. In spite of lack of financing minor progress took place in design and construction of the electron gun (at LHE and LPP), the RF system of the LUE-200 and the full scale stand for testing the accelerating systems of the linac (at FLNP). The first variant of the control system for the IREN was created and will be tested during 1998 at the IBR-30.

The situation with implementation of the IREN project was considered by the special expert committee formed by the JINR Directorate and by the 7th session of the Program Advisory Committee for nuclear physics. Both committees strongly recommended the JINR Directorate to seek possibilities for completing the project in 1999-2000.

3. MEASUREMENT AND COMPUTATION COMPLEX

Work within the theme was focused on two main activities:

- operation and modernization of equipment and software of the spectrometer measurement and control systems, as well as design of new data acquisition systems based on electronics in VME standard;
- development of local computing network.

Data acquisition systems. In 1997, trouble-free operation of the experiment automation systems on the spectrometers of the Scientific Department of Nuclear Physics (SD NP) at the IBR-30+LUE-40 complex and of the Scientific Department of Condensed Matter Physics (SD CMP) at the IBR-2 reactor was afforded. In addition, at the majority of spectrometers, work to modernize specific subsystems (detector electronics – DN-12, NERA-PR, SPN, UGRA, the setup with polarized nuclei, etc.; control over executive mechanisms – HRFD, SKAT, SPN, KOLHIDA; temperature regulators – HRFD, NERA-PR; data acquisition and accumulation – PARUS, ROMASHKA, EPSILON, etc.) was completed.

The studies of the annular PSD at the YuMO spectrometer have been completed. The amplitude and position spectra were measured with new detector electronics. A set of electronic blocks for all 8 wires of the detector was manufactured and is to be adjusted.

In 1997, experience in using VME-based data acquisition systems at the NSVR, SKAT and NERA-PR spectrometers was gained. The debugging of the software for the VME-system at HRFD is nearing completion. All blocks of the unified electronics for the DN-2 spectrometer were constructed (block for receiving data from PSD; processor block and histogram memory block). The analogous electronics is being constructed for the SPN, DN-12 and YuMO spectrometers.

Network and computer infrastructure. In 1997, new communication equipment of the CISCO firm was installed and put into operation in the FLNP local computing network (LCN). This made it possible to switch over to data-transfer rates of up to 100 Mbits/s in the FLNP network. The proposed LCN structure for 1997-2000 is presented in Fig.1. It is based on the Switch technology, which allows different LCN standards to be used in one network.

The Workgroup Switch Catalyst 5000 is the central element of the network. For connections inside the central segment (computer center (CC)) the 10/100TX commutated ports with the data transfer via twisted pairs are used, and for connections between the segments (buildings) up to twelve 100FX (Fast Ethernet) ports with the data transfer via fibre-optic communication lines are employed. The Catalyst 2800 commutator, which has one 100FX port and sixteen 10TX ports, has been chosen as a peripheral communication node in the segments. The end users are connected to the network via HUBs using mainly the 10XT standard.

At present, two Catalyst 2800 commutators (for the experimental setups of IBR-2 and offices of the Scientific Department of Nuclear Physics) are available. In the near future two more commutators (for IBR-2 and offices of the Scientific Department of Condensed Matter Physics) will be purchased.

A separate workstation with the SUN Net Manager software and the CiscoWorks package integrated with it, is used to control LCN and computers of the SUN-cluster. These means allow one to promptly change the network configuration and its load, to obtain dynamic and statistical

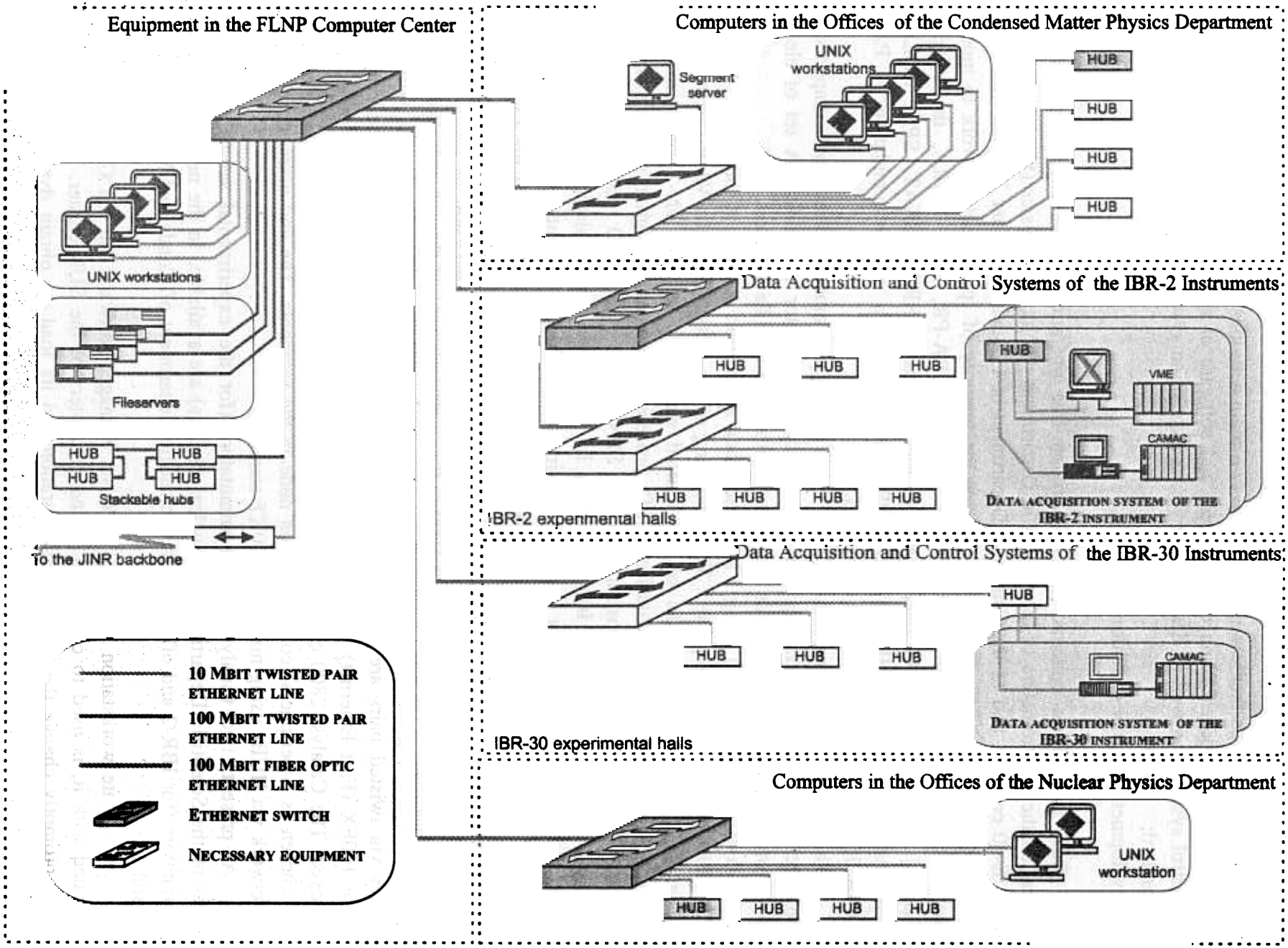
Equipment in the FLNP Computer Center
Computers in the Offices of the Condensed Matter Physics Department
UNIX workstations
Segment server
HUB
HUB
HUB
HUB
UNIX workstations
Fileservers
HUB
HUB
HUB
HUB
Stackable hubs
To the JINR backbone
Data Acquisition and Control Systems of the IBR-2 Instruments
HUB
HUB
HUB
HUB
HUB
HUB
HUB
HUB
VME
CAMAC
DATA ACQUISITION SYSTEM OF THE IBR-2 INSTRUMENT
IBR-2 experimental halls
Data Acquisition and Control Systems of the IBR-30 Instruments
HUB
HUB
HUB
HUB
CAMAC
DATA ACQUISITION SYSTEM OF THE IBR-30 INSTRUMENT
IBR-30 experimental halls
10 MBIT TWISTED PAIR ETHERNET LINE
100 MBIT TWISTED PAIR ETHERNET LINE
100 MBIT FIBER OPTIC ETHERNET LINE
ETHERNET SWITCH
NECESSARY EQUIPMENT
Computers in the Offices of the Nuclear Physics Department
UNIX workstation
HUB
HUB
HUB
HUB

analysis of the traffic for the commutator ports, to block access to certain ports for all users except for the specified ones, to limit unauthorized access to the network, etc.

The installation of new network equipment and software has made it possible to sharply reduce the number of collisions in the network and the load onto the Backbone when exchanging large data arrays.

In 1997, the optic communication line between the buildings of CC and IBR-2 was assembled and put into service. The technical project for switching over the network in the Laboratory and SD CMP buildings to twisted pairs was worked out.

The radical reconstruction of the network provides new possibilities in the development of information service. An example is the information system for the users of the IBR-2 reactor. This system allows the users (including external users) to obtain information in real time on the current state of the reactor and its most important parameters from the FLNP Web-server. The data are presented in the form of tables and graphs. The system provides for automatic renewal of information and generation of HTML-pages as the data coming from the measuring complex located at the reactor are updated. The core of the system is the data processing server, which operates on the basis of the PV-Wave commercial package intended for analysis and visualization of data. The programs of the server are written in the built-in programming language of the mentioned package. The server provides for reading, coping and processing of data, as well as for generation of HTML-pages and graphic files to present information to the users on request from the program-clients. The use of the WWW technology results from the desire to make information available for as many users as possible, and to avoid designing applications on a large number of platforms used in the Laboratory.

In the near future the outdated file-servers, SUN SPARCstation 10 and 2 will be replaced by Enterprise 3000, and all machines of the SUN-cluster will be changed to the Solaris 2.6 operating system. The fast commutator by the New Bridge firm is to be installed to connect FLNP LCN with the JINR backbone network. This will provide access to the centralized resources of the Institute at the rate of 100 Mbits/s. On completion of this work, in the Laboratory a new network infrastructure will be created, which will meet modern requirements as to reliability, transfer rate, potentialities and computational resources.

The controllability of the network and the possibility to dynamically distribute resources and priorities create optimum conditions for using LCN in carrying out experiments on the Laboratory base installations.

In 1997, the International Workshop on Data Acquisition Systems for Neutron Experimental Facilities (DANEF'97, June 2-4, 1997, Dubna) was held, twenty five papers were published and one dissertation thesis was defended.

4. EXPERIMENTAL REPORTS

4.1. CONDENSED MATTER PHYSICS

Diffraction

Effect of Fluorination on the Structure and Superconducting Properties of the *HG-1201* Phase
A.M.Abakumov, V.L.Aksenov, V.A.Alyoshin, E.V.Antipov, A.M.Balagurov, D.A.Mikhailova, S.N.Putilin, M.G.Rozova

Development of the DN-12 Diffractometer: New Parameters
V.L.Aksenov, A.M.Balagurov, D.P.Kozlenko, S.L.Platonov, B.N.Savenko, V.P.Glazkov, V.A.Somenkov, A.P.Bulkin, V.A.Kudryashev, V.A.Trounov

Neutron Diffraction Study of the CMR Compound $La_{0.35}Pr_{0.35}Ca_{0.30}MnO_3$
A.M.Balagurov, V.Yu.Pomjakushin, V.L.Aksenov, N.A.Babushkina, L.M.Belova, O.Yu.Gorbenko, A.R.Kaul, N.M.Plakida, P.Fischer, M.Gutmann, L.Keller

The Structure of $HgBa_2CuO_{4+\delta}$ at Ambient and High Pressure at $0.06 \leq \delta \leq 0.19$
A.M.Balagurov, V.L.Aksenov, D.V.Sheptyakov, E.V.Antipov, S.N.Putilin, P.G.Radaelli

Advanced Material Studies of the HRFD Diffractometer
G.D.Bokuchava, J.Rodel, J.Schreiber, N.R.Shamsutdinov, S.Skirl, M.Stalder

Residual Stress Investigation in a Welded FE510D Plate
G.D.Bokuchava, G.Bruno, F.Fiori, J.Schreiber, N.R.Shamsutdinov, Yu.V.Taran

Effects Induced in Nickel Foils by High-Current Pulsed Electron Beam Irradiation
G.D.Bokuchava, V.V.Sikolenko, A.V.Kalmikov, S.A.Korenev

Investigation of Rock Anisotropy by Neutron Diffraction and Acoustic Sounding
T.I.Ivankina, K.Klima, T.Lokajicek, A.N.Nikitin, Z.Pros, K.Ullemeyer

Microscopic Phase Separation in La_2CuO_{4+x} Induced by the Superconducting Transition
V.Yu.Pomjakushin, A.A.Zakharov, A.M.Balagurov, A.Schenck, F.N.Gygax, A.Amato, D.Herlach, A.I.Beskrovny, V.N.Duginov, Yu.V.Obukhov, A.V.Pole, V.G.Simkin, A.N.Ponomarev, S.N.Barilo

Small-Angle Scattering

Non-Lamellar Phases in Ternary Systems $POPC/C_{12}E_2/H_2O$
T.Gutberlet, G.Klose, A.Islamov

Distribution of Surfactant $C_{12}E_n$ in Phospholid Membranes
T.Gutberlet, G.Klose, M.Kiselev

Temperature-Induced Micelle to Vesicle Transition in the DMPC/NaC System: a Small-Angle Scattering Study
M.A.Kiselev, P.Lesieur, A.M.Kisselev, S.Borbely, T.N.Simonova, L.I.Barsukov

Structural Model of the 30S Subunit of a Ribosome Thermus Thermophilis by Small-Angle Scattering
Lixin Fan, I.N.Serdyuk, D.I.Svergun, V.V.Volkov, R.Giles, A.Wiedenmann, R.May

SANS Study of Three-Layer Micelles of an ABC Block Copolymer
J.Plestil, H.Pospisil, M.Steinhart, J.Kriz, B.Masar

Joint Use of X-Ray Diffraction in Crystals and Small-Angle Scattering in Solutions to Determine the Three-Dimensional Structure of the 70S Ribosome
I.V.Shcherbakova, S.Ch.Agalarov, O.M.Selivanova, A.S.Spirin, V.L.Aksenov, L.Fan, I.N.Serdyuk, D.I.Svergun, V.V.Volkov, V.Lyamzin, M.Koch, K.Wilson, R.May

Inelastic Scattering

Study of the Phonon-Maxon Region in the Liquid Helium Excitation Spectrum
K.H.Andersen, I.V.Bogoyavlenskii, V.G.Kolobrodov, A.V.Puchkov, A.N.Skomorokhov

Neutron Scattering Study of Pyridinium Salts
L.Bobrowicz-Sarga, P.Gzarnecki, J.Wasicki, T.Sarga, I.Natkaniec

Neutron Scattering Study of Phase Transitions in Cyclohexanone
L.Bobrowicz-Sarga, W.Nawrocik, A.Wurflinger, T.Sarga, S.I.Bragin

Partial Dynamic Structure Factors for Amorphous Isotopic *Ni-B* Alloys
S.N.Ishmaev, I.Natkaniec, E.Svab, L.S.Smirnov

Neutron Scattering Study of Heavy Water and Ice under Hydrostatic *Ar* Pressure
G.G.Malenkov, A.A.Averkiev, L.Bobrowicz-Sarga, S.I.Bragin, I.Natkaniec, L.S.Smirnov

Neutron Scattering Investigations of Ammonium Dynamics in $(NH_4)_{2-x}Rb_xSO_4$ Mixed Salts
I.Natkaniec, M.L.Martinez Sarrion, L.Mestres, L.S.Smirnov, L.A.Shuvalov

Investigation of Hydrophobic Hydration Effects by Inelastic Neutron Scattering
A.G.Novikov, M.N.Rodnikova

X-Ray and Neutron Scattering Study of the Nb-O Solid Solutions
H.Wipf, S.Danilkin, E.Jadrowski, H.Fuess, T.Wieder

Polarized Neutrons

Observation of Spatial Splitting of a Polarized Neutron Beam as it is Refracted on the Interface of Two Magnetically Non-Collinear Media

V.L.Aksenov, H.Fredrikze, S.V.Kozhevnikov, Yu.V.Nikitenko, M.Th.Rekveldt, J.Schreiber

Determination of the Magnetic Field Penetration Depth in *Nb* and $Yba_2Cu_3O_7$ Superconducting Films by Polarized Neutron Reflectometry

V.Lauter-Pasyuk, H.J.Lauter, V.L.Aksenov, E.I.Kornilov, A.V.Petrenko, P.Leiderer

Profile Analysis

Migration of *Ta* into *Si* under the Influence of the Fast Heavy Ion Irradiation

A.P.Kobzev, O.A.Nikonov, A.Ju.Didyk, V.A.Skuratov

Neutron Activation Analysis

A Survey of Heavy Metal Deposition in Romania Using Mosses as Biomonitors

M.V.Frontasyeva, C.Oprea, A.Lucaciu, E.Steinnes

4.2. NEUTRON NUCLEAR PHYSICS

Neutron Properties

Measurements of the Thermal Neutron Cross Section of the $^{17}O(n,\alpha)^{14}C$, $^{21}Ne(n,\alpha)^{18}O$, and $^{36}Ar(n,p)^{33}S$ Reactions for Gaseous Samples

Yu.M.Gledenov, V.I.Salatski, P.V.Sedyshev, P.J.Szalanski, J.Andrzejewski, A.Zak

Direct Experimental Estimation of the Level Density in Heavy Nuclei at E_{ex} < 3-5 MeV Excitation Energy

V.A.Khitrov, A.M.Sukhovoj

Fission

Measurement of the Gamma-Ray Multiplicity Spectra and the Alpha Value for ^{239}Pu in the Energy Region 2-2150 eV

H.Faikov-Stanczyk, Hyon Sung Ho, Yu.V.Grigoriev, V.Ya.Kitaev, V.V.Sinitsa

Effect of fluorination on the structure and superconducting properties of the Hg-1201 phase

A.M.Abakumov[1], V.L.Aksenov[2], V.A.Alyoshin[1], E.V.Antipov[1], A.M.Balagurov[2], D.A.Mikhailova[1], S.N.Putilin[1], M.G.Rozova[1]

[1]*Department of Chemistry, Moscow State University, 119899 Moscow, Russia*
[2]*Frank Laboratory of Neutron Physics, JINR, 141980 Dubna, Russia*

$HgBa_2CuO_{4+\delta}$ (Hg-1201) is one of the most attractive compounds for investigating the relationship between structure and superconducting properties owing to its simple structure, wide range of superconducting compositions (from underdoped to highly overdoped states), small number of structural parameters, and an absence of stacking faults, cation intermixing, large static atomic displacements, etc. In general, there is good agreement in the published structural parameters of Hg-1201 and their variations caused by changes in the concentration of the extra oxygen located in the Hg-layer. There are severe discrepancies, however, among different papers concerning the occupancies of the Hg and extra oxygen sites, though these parameters are extremely important for understanding the doping mechanism in Hg-based superconductors. The high extra oxygen content (up to δ=0.18 for the optimally doped Hg-1201 [1]) determined in several studies is in obvious contradiction with the optimal hole number, p_{opt}, per conduction CuO_2 layer, which is assumed to be $p_{opt}\approx 0.16$ (see [2] and refs. therein) and the δ_{opt}=0.08–0.09 determined by iodometric titration [3,4]. As a result, the most natural and simplest ionic model of Hg-1201 doping (two holes per inserted extra oxygen atom) is presently under discussion and the reduced doping efficiency of oxygen in Hg-1201 has been assumed [1, 5, 6].

To verify the different hypotheses, we decided to exchange the extra oxygen in the Hg-1201 structure with extra fluorine atoms. Oxygen and fluorine anions have close crystallochemical behaviors, while their formal charges differ significantly: –2 and –1, respectively. Therefore, assuming a simple charge transfer model, we would expect the extra fluorine concentration to be twice as high for the fluorinated phase for the same doping level. It would also be interesting to determine the dependence of T_c and the structural parameters vs. the extra fluorine content.

Single-phase samples of $HgBa_2CuO_{4+\delta}$ were synthesized from a mixture of $Ba_2CuO_{3+\delta}$ and HgO according to the procedure described in [7], then reduced in a dynamic vacuum to the composition $HgBa_2CuO_{4.01}$ determined by iodometric titration. The samples were monophase and exhibited superconductivity with T_c=61 K. The reduced Hg-1201 samples were subsequently fluorinated by XeF_2 under different conditions. All operations were made in a glove box in a dried N_2 atmosphere that excluded the presence of O_2. The conditions of the treatments, lattice constants (determined using a FR-552 Guinier camera, Ge internal standard) and the superconducting properties of the initial and six fluorinated samples are summarized in Table I.

The neutron diffraction measurements of samples #3 and #5 were performed at room temperature with the high-resolution RTOF Fourier diffractometer (HRFD) at the IBR-2 pulsed reactor in Dubna. A cylindrical, 5-mm diam, Ti-Zr can was used to hold the Hg-1201 powder (m≈1 g).

TABLE I. Fluorination conditions, T_c values and lattice parameters of $HgBa_2CuO_4F_\delta$. M is the molar ratio of XeF_2 to Hg-1201.

N	Conditions	$T_{c,onset}$ / T_c, K	*a*, Å	*c*, Å
1	reduced Hg-1201	61 / 61	3.8915(5)	9.529(2)
2	M=0.1, 150°C, 15 h	97 / 97	3.8828(4)	9.523(1)
3	M=0.3, 200°C, 15 h	97 / 97	3.8825(3)	9.510(1)
4	M=0.5, 200°C, 15 h	96 / 96	3.8788(5)	9.498(1)
5	M=0.4, 200°C, 20 h	90 / 80	3.8742(4)	9.493(2)
6	M=0.3, 200°C, 30 h	88 / 80	3.8721(5)	9.482(2)
7	M=1.0, 200°C, 50 h	78 / –	3.8679(7)	9.459(2)

The high d_{hkl} resolution of the diffraction patterns helped us calculate the difference scattering density map for the basal plane of the unit cell. This map, calculated excluding the F atom (Fig.1), revealed an extra anion only in the middle of the mesh (1/2,1/2,0) and no anion near the middle of the edge was found. Therefore, we can conclude that the fluorinated Hg-1201 samples have a stoichiometric cation composition with only one site for the oxidizing extra anion.

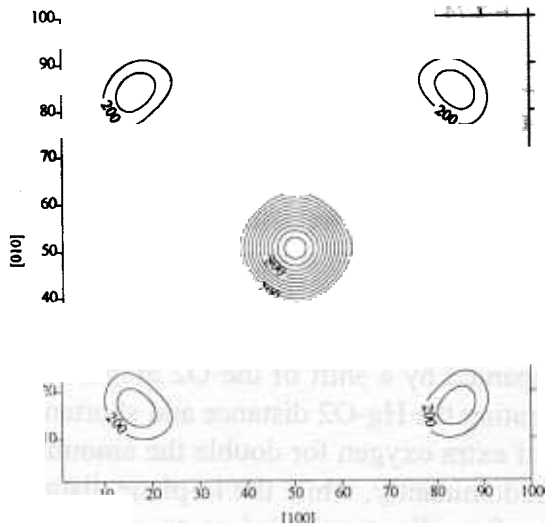

Fig.1. *The difference scattering-density map for the basal plane for sample #3 calculated with the difference of the experimental and calculated structure factors. The fluorine atom was excluded from the calculation. The extra anion is seen only in the middle of the mesh. The amplitude of its peak is ~5 times larger than the most intensive background maxima.*

The occupancy of the fluorine position was refined with a fixed thermal parameter of 1 $Å^2$. The values of n(F)=0.24(2) and n(F)=0.32(2) were obtained for samples #3 and #5, respectively. Thus, the n(F) values are significantly larger than the values of 0.124(9) and 0.19(1) obtained for the oxygenated Hg-1201 samples with close T_c values [3]. This comparison is quite correct since oxygenated and fluorinated materials were measured by the same NPD facility and the initial Hg-1201 samples were prepared by the same synthesis technique.

The amount of inserted fluorine, however, was found to be significantly larger than could be expected for the optimally doped phase, assuming an optimal hole number p_{opt}=0.16 (δ_F should be equal to 0.16 instead of 0.24 if V_{Ba}=V_{Hg}= +2, V_O= –2 and V_F= –1). Therefore, we can conclude that the doping mechanism in the Hg-1201 superconductor is more complex than a simple oxidation of the (CuO_2) layers by an inserted fluorine or oxygen. They can oxidize not only the (CuO_2) layers, but, also, possibly, the HgO_2 "dumbbell" as well. The

carrier concentration in the conducting band is a result of the delicate charge balance among these fragments.

Variation of the apical Cu-O2 bond distance caused by the extra anion exchange when $\delta_F \approx 2\delta_O$ is well-pronounced in contrast to the in-plane bonds. Figure 2 shows a practically linear dependence of the Cu-O2 distance vs. δ (oxygen or fluorine). An increase in the amount of the extra anion in the Hg-layer results in a compression of the apical Cu-O2 distance. These distances differ significantly between the fluorinated and oxygenated Hg-1201 phases with close T_c and in-plane Cu-O1 bond lengths. For instance, the difference between these distances in the phases with T_c=97 K is about 0.04 Å, which is much larger than the standard deviation and the difference between the *c*-parameters.

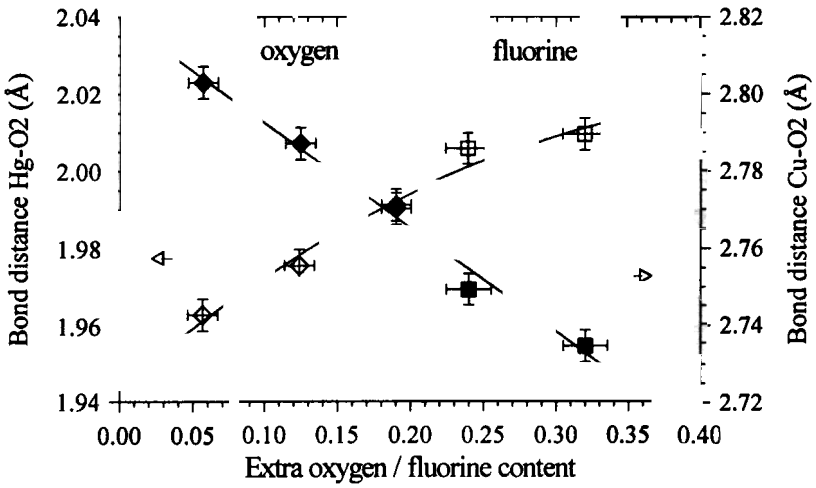

Fig.2. *Bond distances Hg - O2 (left scale, open symbols) and Cu-O2 (right scale, full symbols) as a function of extra oxygen or fluorine content. Data for oxygenated samples (δ=0.057, 0.124, 0.19) are taken from Ref. [3]. Lines through points are guides to the eye.*

The origin of this unusual phenomenon may be explained if we also take into account the variation of the apical Hg-O2 bond distance. The more probable origin of the elongation of the Hg-O2 distance is not a variation of the formal Cu valence, but an interaction between Hg and the extra anions (even located far from the Hg atom). An increase in the coordination number of Hg by the inserted extra anions is accompanied by a shift of the O2 atoms away from the Hg cations towards the Cu atoms, thus elongating the Hg-O2 distance and shortening the Cu-O2 one. We can conclude that the exchange of extra oxygen for double the amount of fluorine causes a variation of the apical distances, predominantly, while the in-plane distance and T_c remain the same. This transformation can be formally considered as an anisotropic compression (along the *c* axis) of the CuO_6 octahedron.

References

Q.Huang, J.W.Lynn, Q.Xiong and C.W.Chu, Phys. Rev. B, **52**, 462 (1995).

2 L.Jansen and R.Block, Physica A, **230**, 467 (1996).

3 V.L.Aksenov, E.V.Antipov, A.M.Balagurov et al., Phys. Rev. B, **55**, 3966 (1997)

4 A.Fukuoka et al., Phys. Rev. B, **55**, 6612 (1997).

5 D.J.Singh and W.E.Pickett, Phys. Rev. Lett., **73**, 476 (1994).

6 A.Hamed et al., Phys. Rev. B, **54**, 682 (1996)

7 V.A.Alyoshin, D.A.Mikhailova and E.V.Antipov, Physica C, **271**, 197 (1996).

Development of the DN-12 diffractometer: new parameters

V.L.Aksenov, A.M.Balagurov, D.P.Kozlenko, S.L.Platonov, B.N.Savenko
JINR, Frank Laboratory of Neutron Physics, Dubna, Russia.
V.P.Glazkov, V.A.Somenkov
Russian Scientific center "Kurchatov Institute", Moscow, Russia
A.P.Bulkin, V.A.Kudryashev, V.A.Trounov
Nuclear Physics Institute, Gatchina, Russia

Two years ago the first stage of creating the new diffractometer DN-12 [1] for neutron scattering experiments using polycrystal samples in high pressure cells based on sapphire or diamond anvils was completed. After the first successful experiments [2-5] development of the DN-12 diffractometer continued during the reported year.

To improve the background conditions and increase the region of available wavelengths, the straight vacuum neutron guide was replaced by a curved supermirror neutron guide. The new design of DN-12 diffractometer on beam N12 of the IBR-2 reactor is shown in fig.1.

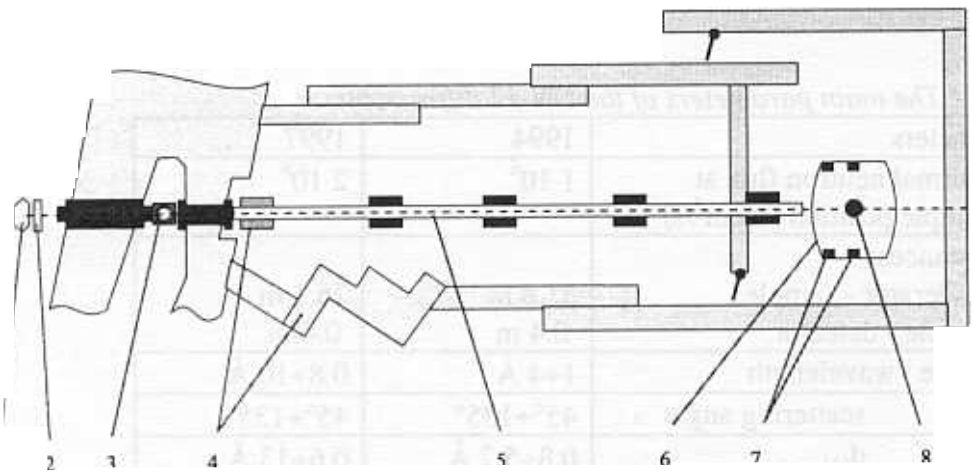

Fig 1. The layout of the DN-12 diffractometer at the IBR-2 pulsed reactor: 1 - active core, 2 - moderator, 3 - background chopper, 4 - fast neutron shield, 5 - curved supermirror guide, 6 - detector shielding, 7 - two-ring detector, 8 - sample position

The wavelength distributions of incident neutrons measured using a vanadium sample before and after the diffractometer was improved are shown in fig.2. As a result, the total neutron flux on the sample increases practically twice and the flux of neutrons with long wavelengths increases several times. The main parameters of DN-12 (before and after improvement) are presented in Table 1.

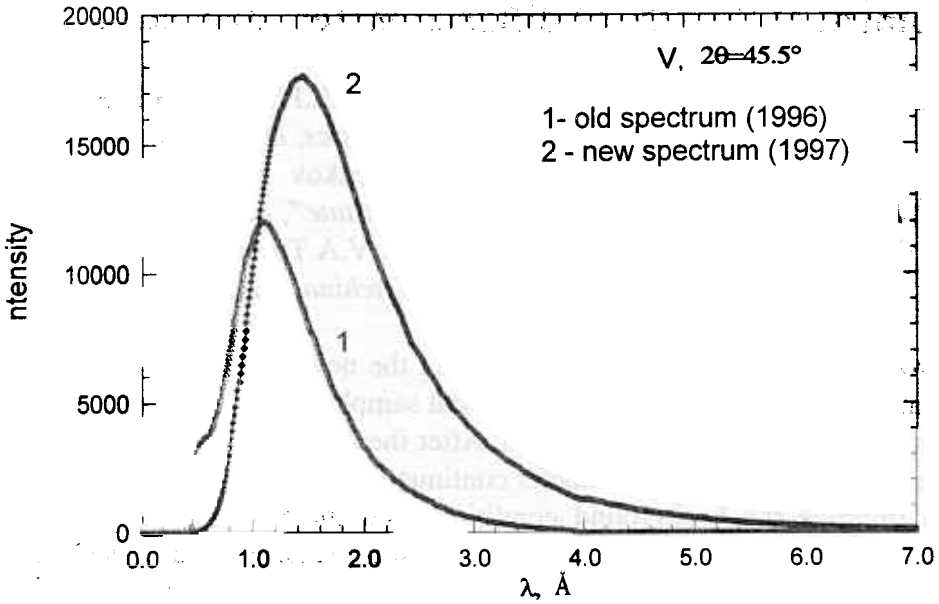

Fig 2. The effective spectra of incident neutrons measured using a vanadium sample with the vacuum tube (1) and the supermirror guide tube (2)

Table 1.The main parameters of the DN-12 diffractometer

Parameters	1994	1997
1. Thermal neutron flux at sample position ($n/cm^2/s$)	$1 \cdot 10^6$	$2 \cdot 10^6$
2. Distances:		
moderator - sample	31.8 m	26.1 m
sample - detector	0.4 m	0.4 m
3. Range : wavelength	1÷4 Å	0.8÷10 Å
scattering angle	45°÷135°	45°÷135°
d_{hkl}	0.8÷5.2 Å	0.6÷13 Å
4. Resolution ($\Delta d/d$ d=2 Å):		
for 2θ=90°	0.022	0.022
for 2θ=135°	0.012	0.012
5 Solid angle of detector system	0.125 sr	0.125 sr
6. Pressure range:		
with sapphire anvils	5 GPa	5-10 GPa
with diamond anvils	10 GPa	15-20 GPa

As the first test experiments, the diffraction patterns of Al_2O_3 (fig.3) and fullerene C_{60} (fig. 4) were measured.

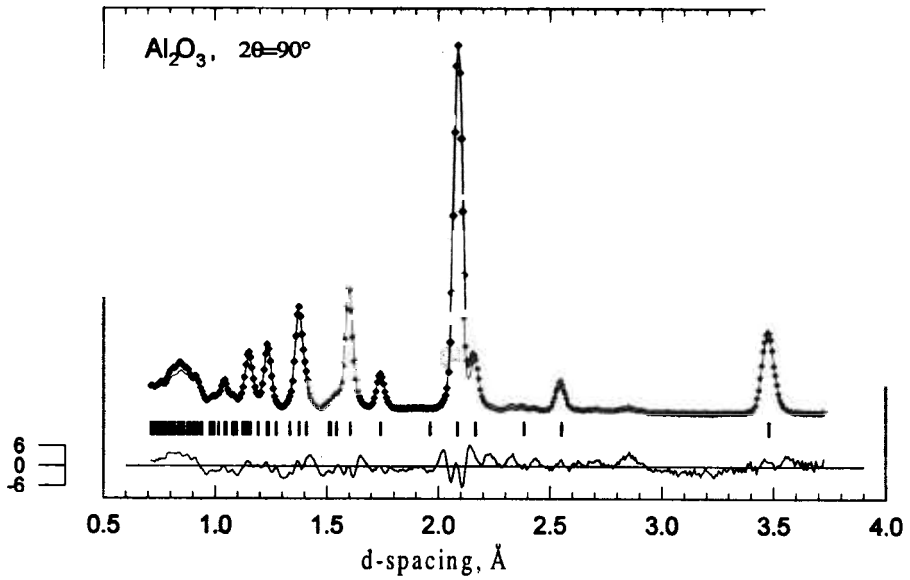

Fig.3 The diffraction pattern of Al_2O_3, measured in normal conditions and processed by the Rietveld method. The scattering angle 2θ=90°. The experimental points, the calculated profile and the difference curve are also shown.

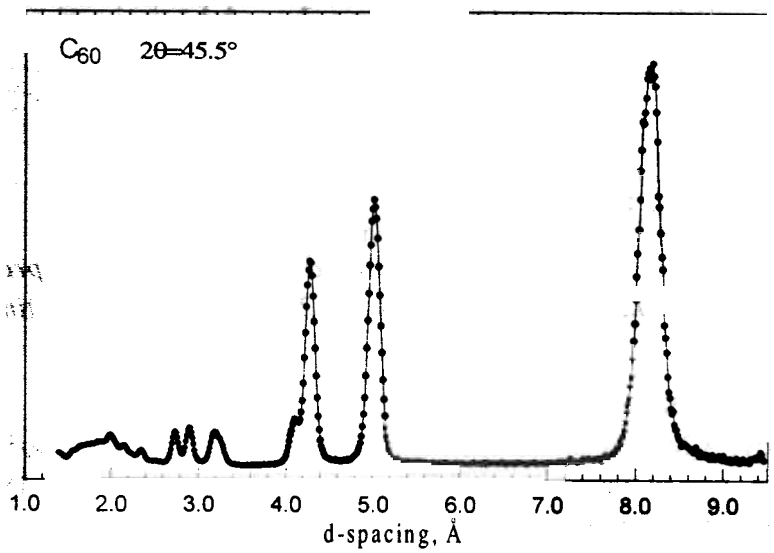

Fig.4. The diffraction pattern of C_{60}, measured in normal conditions. The scattering angle 2θ=45.5°, sample volume V~0.5 cm^3, exposition time t=1 h.

Hematite Fe_2O_3 was studied at pressures up to 3.7 GPa. At the pressure P~2.5 GPa in this system the magnetic phase transition occurs (see fig.5 - the intensities of the magnetic peaks (111) and (100) sharply change under pressure). Due to improvement of the parameters of the diffractometer, more diffraction peaks than in [6] are resolved and the magnetic structure of the new phase can be solved more exactly.

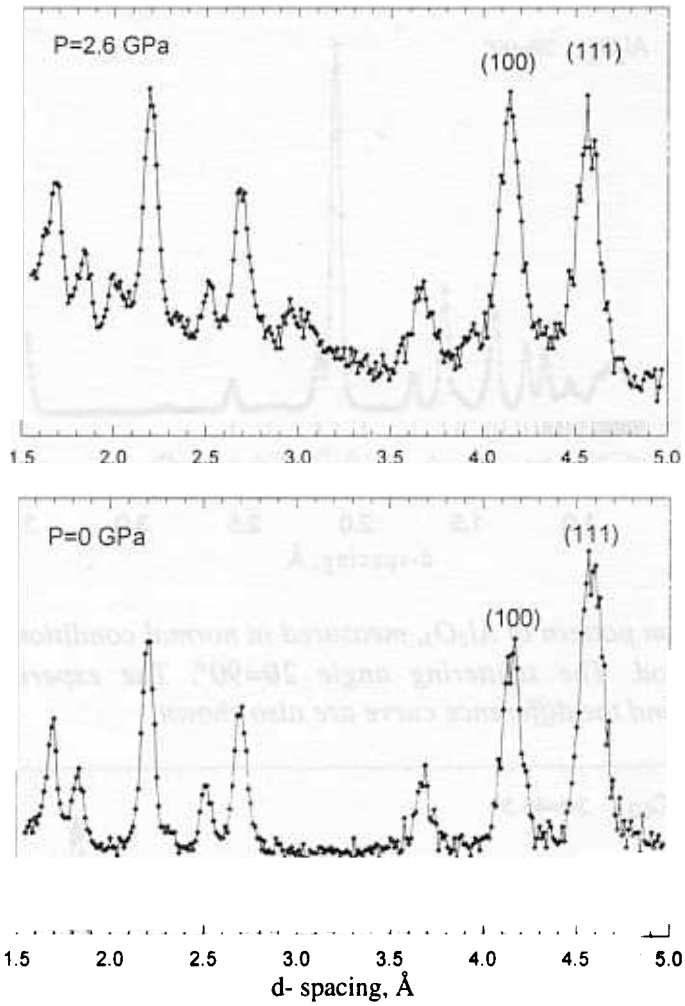

Fig 5. The diffraction patterns of Fe_2O_3, measured at normal and high pressure. The sample volume V=0.5 mm^3, scattering angle 2θ=45.5°, exposition time t=40 h.

References

1. V.L.Aksenov, A.M.Balagurov, S.L.Platonov, B.N.Savenko, V.P.Glazkov, I.V.Naumov, V.A.Somenkov and G.F.Syrykh, High Press. Res., 14, 181 (1995).
2. V.L.Aksenov, A.M.Balagurov, B.N.Savenko, V.P.Glazkov, I.N.Goncharenko, V.A.Somenkov, E.V.Antipov, S.N.Putilin and J-J.Capponi, ibid., 127.
3. A.M.Balagurov, B.N.Savenko, A.V.Borman, V.P.Glazkov, I.N.Goncharenko, V.A.Somenkov, G.F.Syrykh, ibid., 55.
4. V.L.Aksenov, A.M.Balagurov, B.N.Savenko, D.V.Sheptyakov, V.P.Glazkov, V.A.Somenkov, S.Sh.Shilshtein, E.V.Antipov, S.N.Putilin, Physica C 275, 87 (1997).
5. A.M.Balagurov, D.P.Kozlenko, B.N.Savenko, V.P.Glazkov, V.A.Somenkov, Preprint JINR, P14-97-147, Dubna (1997) (in Russian), accepted for publication in Fiz. Tverd. Tela.
6. I.N.Goncharenko, J-M.Mignot, G.Andre, O.A.Lavrova, I.Mirebeau, V.A.Somenkov, High Press. Res., 14, 41 (1995).

Neutron diffraction study of the CMR compound $La_{0.35}Pr_{0.35}Ca_{0.30}MnO_3$

A.M.Balagurov, V.Yu.Pomjakushin, V.L.Aksenov
FLNP JINR, Dubna, Russia
N.A.Babushkina, L.M.Belova
RRC Kurchatov Institute, Moscow, Russia
O.Yu.Gorbenko, A.R.Kaul
Chemistry Department, Moscow State University, Moscow, Russia
N.M.Plakida
BLTP JINR, Dubna, Russia
P.Fischer, M.Gutmann, L.Keller
PSI, Villigen, Switzerland

The $La_{1-x}A'_xMnO_3$ perovskites (A'=Ca, Sr, Ba) are intensively studied now after observation of "colossal" magnetoresistance (CMR) effect in early 90th [1]. This system is characterised by a strong competition between two basic states - insulating and metallic, which depends on the doping level, the temperature or the external magnetic field. Phase transitions between them are usually followed by changing Mn-O bond lengths and oxygen thermal motion. This is the reason of the use of neutron scattering for the investigation of CMR compounds. Total or partial substitution of La for rare earth cation with a smaller ionic radius can be also the reason for changing of the charge or the magnetic state of a compound. The system with Pr was studied especially carefully since both Pr^{3+} and Ca^{2+} ionic radii are rather similar (1.179 Å for Pr^{3+} against 1.180 Å for Ca^{2+}) [2]. A particularly detailed neutron diffraction study of $Pr_{1-x}Ca_xMnO_3$ was performed by Z.Jirak et al. [3].

For $La_{0.35}Pr_{0.35}Ca_{0.30}MnO_3$ (LPCM) which was prepared as a high quality thin film on $LaAlO_3$ substrate, unusual transport properties - the resistivity of the film below 30 K depends on the time and thermal prehistory - was found in [4]. To clarify the possible microscopic background of these effects, we undertook a neutron diffraction study of LPCM. In this report we present the preliminary results of the study.

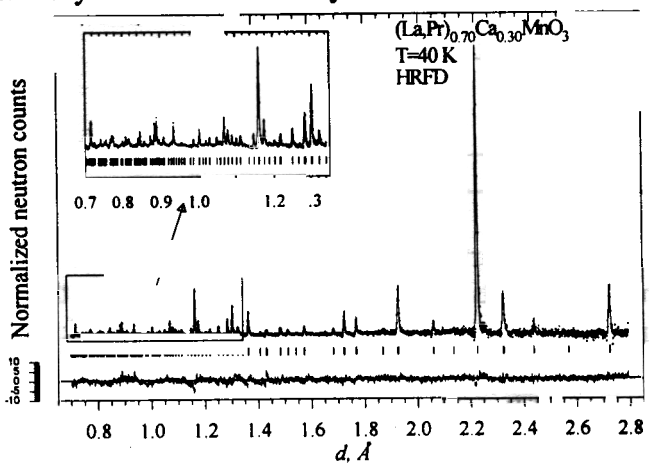

Fig.1. *Diffraction pattern of $La_{0.35}Pr_{0.35}Ca_{0.30}MnO_3$, measured with HRFD at T=40 K and processed by Rietveld method (MRIA programm)*

In the experiments two neutron diffractometers were used: HRFD at the IBR-2 pulsed reactor in FLNP JINR and DMC at the SINQ neutron source in PSI (Villigen). HRFD is a high resolution Fourier diffractometer with the $\Delta d/d$ resolution close to 10^{-3}, which offers the possibility for obtaining precise structural data. DMC is placed at a cold neutron source and is quite suitable for magnetic peak measurements at large d_{hkl}. The typical neutron diffraction patterns measured at these two instruments are shown in figs. 1 and 2.

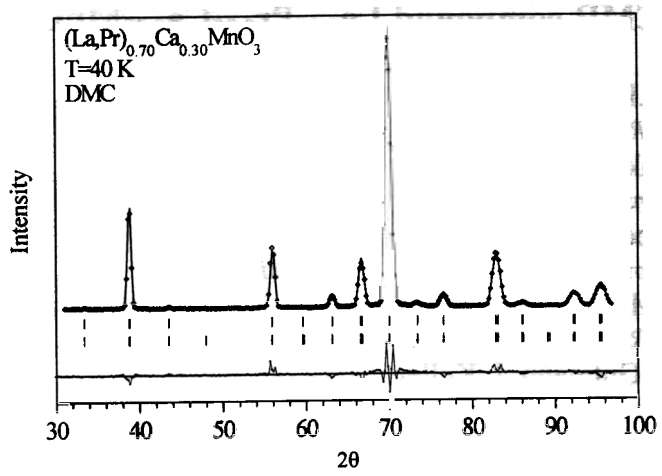

Fig.2. *Diffraction pattern of $La_{0.35}Pr_{0.35}Ca_{0.30}MnO_3$, measured with DMC at T=40 K and processed by Rietveld method (FullProf programm)*

LPCM is crystallised in the Pnma space group, which is conventional for many CMR perovskites. At room temperature the LPCM lattice parameters and atomic co-ordinates (table 1) are very close to the recently published data of $La_{0.525}Pr_{0.175}Ca_{0.30}MnO_3$ [5]. The unusual feature of LPCM is its quasitetragonal metric despite of the orthorhombic atomic structure (fig.3). Probably this LPCM feature is the reason of fast dynamic spatial fluctuations of its structural fragments which cause its unusual transport properties.

A/A′ site		$La_{0.35}Pr_{0.35}Ca_{0.30}$	$La_{0.525}Pr_{0.175}Ca_{0.30}$ [5]
a	(Å)	5.4606	5.4585
b	(Å)	7.7067	7.7146
c	(Å)	5.4603	5.4674
V	(Å^3)	229.79	230.23
A/A′	x	0.0271	0.0236
	y	0.25	0.25
	z	-0.0054	-0.0057
O1	x	0.4934	0.4893
	y	0.25	0.25
	z	0.0682	0.0668
O2	x	0.2818	0.2782
	y	0.0355	0.0342
	z	0.7168	0.7198
Rwp	%	6.88	5.75
$\chi 2$		1.46	1.66

Table 1. The l*attice parameters and the co-ordinates of atoms for: $La_{0.35}Pr_{0.35}Ca_{0.30}$, calculated with HRFD data and $La_{0.525}Pr_{0.175}Ca_{0.30}$, taken from [5].*

The analysis of the LPCM magnetic structure carried out on the basis of the DMC data showed that it is a collinear ferromagnet with Mn magnetic moments ordered parallel to the (a, c)-plane. The temperature dependence of the ordered moment is shown in fig.4. As it is known, in $Pr_{0.7}Ca_{0.3}MnO_3$ together with Mn moments ordering at T≈150 K Pr moments are also ordered at T≈50 K [6]. But for LPCM we did not find any sign of Pr moment ordering.

To study irreversible effects, found in [4], we measured diffraction patterns for both cooling and heating of the sample as well as several patterns at 10 K in the real-time mode. No sign of hysteresis or time dependence effects was found.

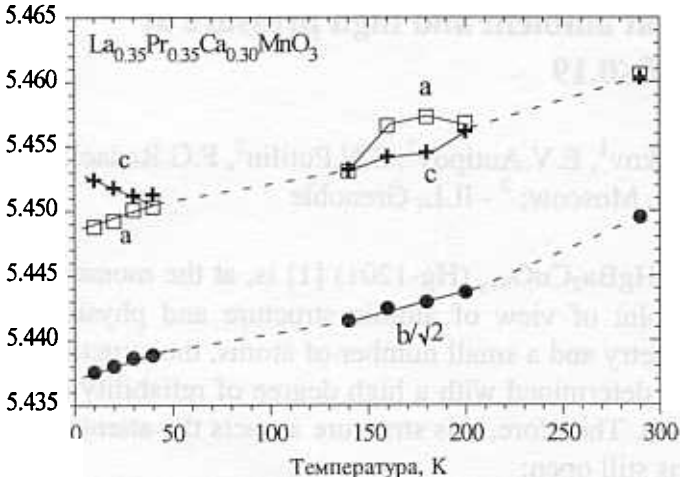

Fig.3. *The temperature dependence of the a, b, and c - lattice parameters of* $La_{0.35}Pr_{0.35}Ca_{0.30}MnO_3$ *(sp. gr. Pnma, a≈c), measured with HRFD. Close to T=140 K the ferromagnetic phase appears. Lines through points are guides to the eye.*

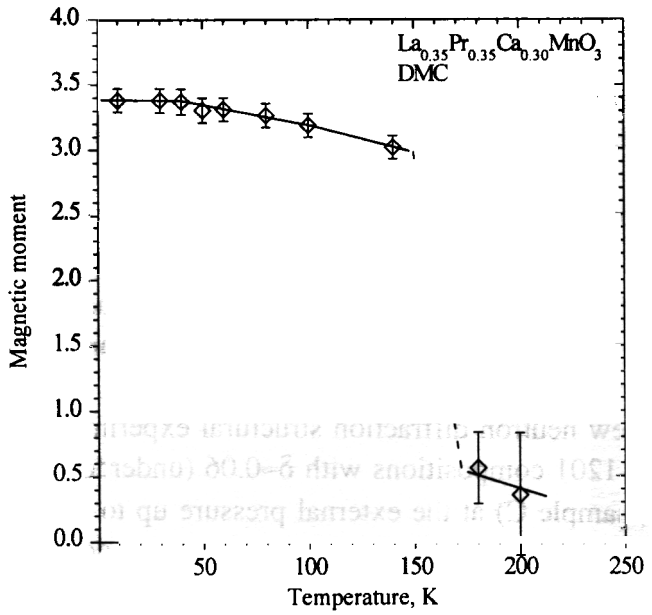

Fig.4. *The ordered magnetic moment of Mn as a function of temperature. The magnetic moments order parallel to the (a,c)-plane. Line through points is guide to the eye.*

This work was supported by RFBR (Grants 96-02-17823 and 97-02-17103) and INTAS-RFBR (Grant 95-639).

References

Von Helmot et al., Phys. Rev. Lett. 71 (1993) 2331.
2. R.D.Shannon, Acta Cryst., A32 (1976) 751.
3. Z.Jirak, S.Kripicka, Z.Simsa, M.Dlouha, S.Vratislav, J. Magn. Magn. Mater., 53 (1985) 153.
4. N.A.Babushkina et al., in press.
5. P.G.Radaelli et al., Phys. Rev. B 56 (1997) 8265.
6. D.E.Cox et. al., Phys. Rev. B, in press.

The structure of $HgBa_2CuO_{4+\delta}$ at ambient and high pressure at $0.06 \leq \delta \leq 0.19$

A.M.Balagurov[1], V.L.Aksenov[1], D.V.Sheptyakov[1], E.V.Antipov[2], S.N.Putilin[2], P.G.Radaelli[3]
[1] - FLNP, JINR, Dubna; [2] - Chem.Dept., MSU, Moscow; [3] - ILL, Grenoble

The high-temperature superconductor $HgBa_2CuO_{4+\delta}$ (Hg-1201) [1] is, at the moment, one of most thoroughly studied from the point of view of atomic structure and physical properties. Due to high crystallographic symmetry and a small number of atoms, the structure has only a few free parameters, which can be determined with a high degree of reliability by structural refinements based on diffraction data. Therefore, this structure attracts the attention of investigators [2,3] to a number of questions still open:

- The relationship between T_c and δ (is it close to the universal parabolic dependence by Presland *et al.* [4] according to which $T_c=T_{c.max}$ [1 - q $(\delta-\delta_{opt})^2$] or is this still the subject for discussion [5]?);
- The value of δ_{opt} corresponding to maximum T_c (different Hg-1201 structure refinements based on neutron diffraction patterns obtained with polycrystal samples, give δ_{opt} from 0.06 to 0.18);
- The reasons why T_c changes as the external pressure increases (see, for example, discussions in [6]).

Until now, the data on the influence of external pressure on the Hg-1201 structure were obtained only for an optimally doped composition ($\delta \approx 0.12$) (in [7] up to 0.6 GPa and in [8] up to 5.1 GPa) and partly for the composition with $\delta \approx 0.19$ (overdoped state) in [8].

In the present work, the results of the new neutron diffraction structural experiments are presented. They were carried out on the Hg-1201 compositions with $\delta \approx 0.06$ (underdoped state, sample A) and $\delta \approx 0.19$ (overdoped state, sample C) at the external pressure up to ~0.8 GPa (structural data at ambient pressure were also obtained for an optimally doped composition, sample B). The results are compared with our earlier published data [8,9] on the effect of external pressure on optimal and overdoped compositions, and analysed from the point of view of δ dependencies of the structure and the T_c.

The neutron diffraction patterns for the A and C samples were measured on the D2B diffractometer in ILL (Grenoble) for several external pressures, while sample B was measured only at ambient pressure. The diffraction pattern from sample A was also obtained with the HRFD diffractometer in Dubna in the range of d-spacing 0.77 – 2.12 Å in order carry out a comparison with previously obtained results and reveal possible systematic errors.

All our refinements of diffraction patterns obtained with different diffractometers on the whole family of samples convinced us that we really dealt with three groups of samples: under-, optimally and overdoped, with the average content of additional oxygen in each group: 0.06, 0.13 and 0.19, respectively, within errors close to ±0.01.

We can conclude that the superconductor $HgBa_2CuO_{4+\delta}$ prepared according to the procedure described in paper [10] is the cation-stoichiometric compound which reaches the highest phase transition temperature at the concentration of oxygen in the Hg-layer $\delta_{opt}=0.13\pm0.01$, oxygen O_δ being situated only in the center of this layer. The value of δ_{opt} was determined in the measurements of seven samples of Hg-1201 with three diffractometers, two of which (D2B and 3T2) are the classical instruments with λ=const and the third (HRFD)

utilises the time-of-flight method. All measured points on the $T_c(\delta)$ dependence lie on one

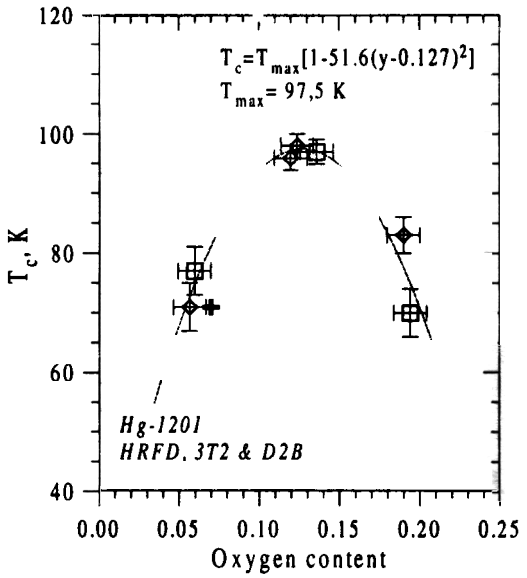

Fig.1. Dependence of T_c for the Hg-1201 compound on the oxygen content δ defined from neutron-diffraction experiments with the HRFD (◊), D2B ( ) and 3T2(+) diffractometers. The solid line is the parabola drawn with the use of the Least Squares Method, its parameters are presented in the right upper corner.

and the same curve (see fig.1) which allows to believe that the δ_{opt} value is realistic.

The compressibilities of the unit cell parameters and the main interatomic distances in the Hg-1201 structure defined from the experimental data as $\kappa_q = -(1/q)\Delta q/\Delta P$ (10^{-3}/GPa), where q - is the generic parameter, are presented in **table 1**. In order to calculate Δq, linear least-squares fits to the experimental points were used, as it is shown in **figs. 2 - 3**

Table 1. Compressibilities of the main parameters in the Hg-1201 structure

Parameter	Sample A	Sample B(data from [8])	Sample C
a	3.73(4)	3.34(16)	3.60(6)
c	5.48(4)	4.58(13)	4.90(6)
V	12.92(7)	11.4	12.07(11)
Hg-O2	3.7(2.2)	0.5(1.4)	0.1(0.3)
Cu-O2	6.7(1.6)	7.6(1.0)	8.3(0.2)
Ba-O2	9(7)	15.9(4.5)	39(10)
Ba-O3	5.4(1.5)	5.4(1.2)	12(2)

The obtained dependencies of the Hg-1201 unit cell parameters on pressure show that the value of the O3 position occupation does not strongly influence the lattice compressibility. For all three studied levels of doping the compressibility anisotropy is quite high reaching $\kappa_c/\kappa_a \approx 1.5$ for sample A. The absolute values of κ_a and κ_c for the optimally doped composition (sample B) are in good agreement with the published data and, in particular, with the data of the X-ray experiment [11] carried out in the range of 5 GPa.

In **figs.2** and **3** the dependencies of the main interatomic distances in Hg-1201 on pressure are presented. For sample B, the point measured at P=0 is shown and the slope of the line is calculated from our data [8]. For sample A, the compressibilities of the Hg-O2 and Cu-O2 apical bonds slightly differ and within errors they do coincide with the compressibility of the unit cell along the *c*-axis (κ_c), i.e. the structure compresses in this direction without significant changes in the coordinates of these atoms (z(O2)≈const). The Ba-O3 distance also shortens as the pressure increases proportionally to the shortening of the *c*-axis. So, for the

underdoped state, homogeneous compression of all structural elements of Hg-1201 takes place as the external pressure increases.

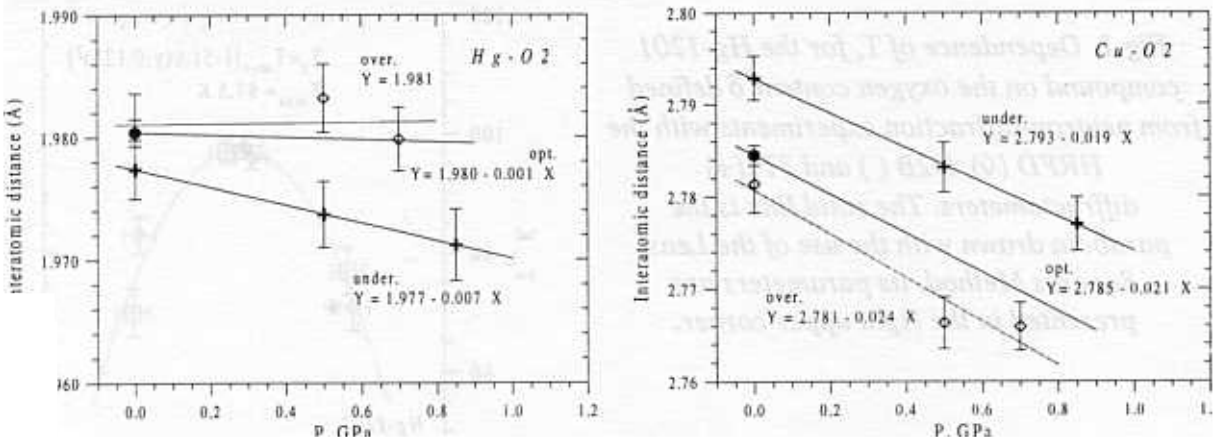

Fig.2. The dependencies of the Hg-O2(a) and the Cu-O2(b) apical distances on pressure.

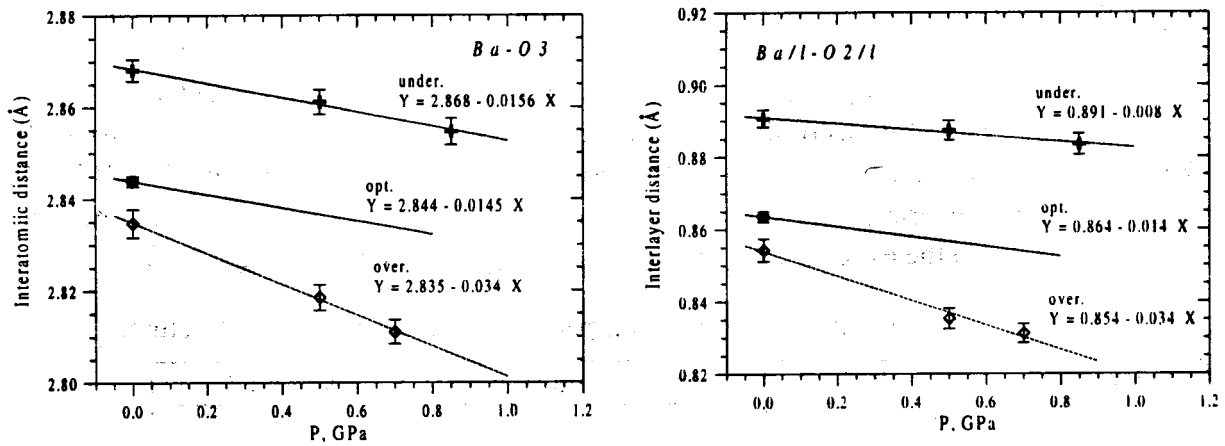

Fig.3. The distances between the Ba-atoms layer and the Hg-1ayer (a) and the O2 oxygen layer (b) as a function of pressure.

As it can be seen from **fig.2a**, the Hg-O2 bond becomes less compressible with an increase of the doping level (B and C samples). It should be mentioned that in [8] this statement was checked over the pressure range up to 5.07 and 2.37 GPa for optimally and overdoped compositions, respectively. The Cu-O2 bond shortens in these samples proportionally to a decrease in the *c* axis length, i.e. the pressure dependence of the apical Cu-O2 bond length for all three types of samples reproduces the dependence of the *c* unit cell parameter on pressure. Different is the behaviour of the distance between the Ba atom and the basal plane - for sample B, the compressibility of this distance is the same as for sample A, i.e. it is approximately corresponding to κ_c, while for the C sample it is almost ~2.5 times higher than κ_c, i.e. the Ba atom in the overdoped sample rapidly approaches the basal plane of the structure as ressure increases.

In the literature on mercury superconducting structures, it is constantly mentioned that the O2-Hg-O2 dumb-bell is a very rigid element of the structure. Our results show, however, that the length of the Hg-O2 bond visibly depends on the oxygen content in the Hg-plane and, besides that, the Hg-O2 bond is really quite strong (hardly tends to shorten under the effect of external pressure), only for the case of the presence of a sufficiently high amount of O_δ oxygen in the Hg-layer. These facts may be connected with possible bending of the O2-Hg-O2 dumb-bell, i.e. with the departure of the mercury atom from a particular position, which

effectively leads to apparent shortening of the bond length. The filling of the O3 position leads to the straightening of the dumb-bell and the bond becomes more rigid.

One of the actively discussed questions in the literature on the mercury superconductors is the charge transfer from the reservoir to the CuO_2 layer with the increase in the doping level or pressure [6,12,13]. Potentially, charge transfer is one of the reasons of a change in T_c following an increase in pressure (another explanation assumes a possible $T_{c,max}$ increase with increasing pressure just due to lowering the volume). A detailed analysis of our results for the volume compressibility, in terms of the model developed in [12], shows that in the optimally doped Hg-1201 the charge transfer induced by a pressure increase is most probably negligible. The same result - the absence of charge transfer under pressure - was obtained in [13] for the compound Hg-1212.

The main conclusions of our investigation are the following:

•At low O_δ concentrations, the Hg-1201 structure compresses homogeneously, i.e. the compressibilities of the main interatomic distances in the Hg-1201 structure correspond to the unit cell compressibility. However at higher O_δ concentrations, the Hg-O2 bond becomes more coarse and the apical distances Hg-O2 and Cu-O2 stop changing homogeneously.

•The analysis shows that in the optimally doped state, charge transfer from the reservoir to the CuO_2 layer is absent, i.e. the effect of increasing T_c is the consequence of a volume change and an increase in $T_{c,max}$. Probably, the conclusion about weak influence of charge transfer on changes in T_c as the pressure increases is also valid for other states of Hg-1201, which is one of the main assumptions of the model developed in [6]

References

1. S.N.Putilin, E.V.Antipov, O.Chmaissem and M.Marezio, Nature (London), **362**, 226 (1993).
2. Q.Huang, J.Lynn, Q.Xiong, C.W.Chu, PR, **52**, 462 (1995).
3. A.Fukuoka, A.Tokowa-Yamamoto, M.Itoh, R.Usami, S.Adachi, H.Yamauchi, K.Tanabe Physica C, 265, 13, (1996).
4. M.R.Presland, J.L.Tallon, R.G.Bukley, R.S.Liu and N.E.Flower, Physica C, **176**, 95 (1991).
5. O.Chmaissem, J.D.Jorgensen, D.G.Hinks, J.L.Wagner, B.Dabrowski, ICNS-97, Toronto, August 1997, Conference abstracts, p.235.
6. L.Jansen, R.Block, Physica A, **230**, 467 (1996).
7. B.A.Hunter, J.D.Jorgensen, J.L.Wagner, P.G.Radaelli et al, Physica C **221**, 1, (1994).
8. V.L.Aksenov, E.V.Antipov, A.M.Balagurov et al, Physica C **275**, 87, (1997).
9. V.L.Aksenov, E.V.Antipov, A.M.Balagurov et al, Phys. Rev. B, **55**, 3966 (1997).
10. V.A.Alyoshin, D.A.Mikhailova, and E.V.Antipov, Physica C **255**, 173 (1995)
11. E.J.Gonzales, W.Wong-Ng, G.J.Piermarini, C.Wolters, J.Schwartz, Powder Diffr., **12**, 106 (1997).
12. E.V.L. de Mello, C.Acha, Phys. Rev. B, 56, 466 (1997).
13. X.Chen, Z. Jiao, Phys. Rev. B, 56, 6302 (1997).

ADVANCED MATERIAL STUDIES ON THE HRFD DIFFRACTOMETER

G.D.Bokuchava[1], J.Rödel[2], J.Schreiber[3], N.R.Shamsutdinov[1], S.Skirl[2], M.Stalder[3]

[1] *Frank Laboratory of Neutron Physics, JINR, 141980 Dubna, Russia*
[2] *Technical University Darmstadt, 64287 Darmstadt, Germany*
[3] *Fraunhofer Institute for Nondestructive Testing, W-6600 Saarbrücken, Germany*

W-Cu gradient materials

Sometimes modern technology requires components with properties that one material alone does not have. Therefore, attempts are made to combine materials with different properties. On their interface, however, significant residual stresses may occur that may cause cracking or failure of the component. Therefore, a comparatively new approach consists of varying materials not abruptly but continuously and thus decrease residual stress discontinuities [1], [2]. For example, a promising material system for future fusion reactor walls is a copper-tungsten gradient material [3]. Copper, an excellent heat conductor, is too soft and is not heat resistant. Tungsten, on the other hand, has the highest melting point of all metals but it is a poor heat conductor (Table 1). Different heat expansion coefficients, however, pose a serious problem of the coexistence of the two phases if one keeps in mind that the intended use of the component is such that it will undergo a temperature change on the order of 1000° C during both manufacturing and operation. W-Cu gradient materials can be produced by different metallurgical procedures, such as sintering of metal powders, hot isostatic pressing and electrochemical processing. In this report, some results of neutron diffraction measurements of residual stresses in W-Cu gradient materials are presented.

Table 1. Some selected properties of component materials

	Copper	*Tungsten*
Heat conductivity [$Wm^{-1}K^{-1}$]	403	174
Yield strength [MPa]	60	550
Young modulus [GPa]	145	411
Melting point [°C]	1083	3410
Thermal expansion coeff. [ppm]	16.6	4.5

With the HRFD structural changes and variation of residual stresses in a W-Cu gradient sample prepared by hot isostatic pressing, were studied. The W-Cu sample was a cylinder (∅11.5×11.3 mm) with a 8-layer structure and a gradient step of W content about 10% in the axial direction. Using a BN-mask a gauge volume of 1 mm width and 11.5 mm diameter is chosen in the sample (fig. 1). The sample is scanned by the neutron beam with the spatial resolution ~1 mm in the gradient direction. Scans are performed in the direction of the gradient for different angles: Ψ=45°,76°,90°,104°,135°. Changes in the tungsten volume fraction (fig. 2) and the lattice parameter for both phases are obtained by Rietveld refinement as a function of the gauge volume axial position. For the investigated 8-layer sample the number of experimental points is sufficient to run the minimization procedure assuming that there is no stress in the axial direction (which is also the gradient direction). So in this case, stresses were determined without knowing the d_0-value. The cylindrical symmetry of the residual stress distribution in the studied sample is assumed. The residual stresses were calculated by Hook's law:

$$\sigma_{ij} = \left(\frac{E}{1+\nu}\right)\varepsilon_{ij} + \left(\frac{\nu E}{(1+\nu)(1-2\nu)}\right)\delta_{ij}\varepsilon_{kk},$$

where E and ν are Young's modulus and Poisson's ratio, respectively The calculated residual stresses for both phases are shown in fig. 3.

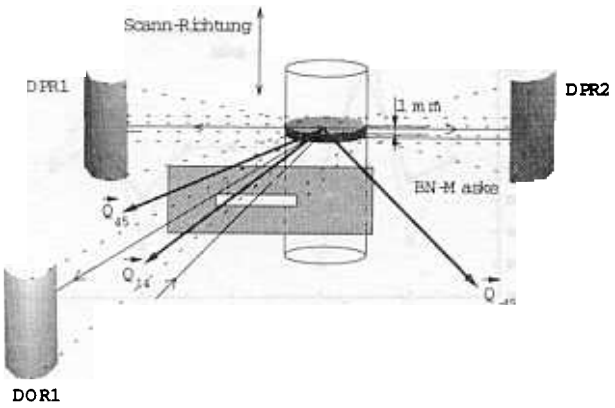

Fig. 1. Strain scanning in the radial direction.

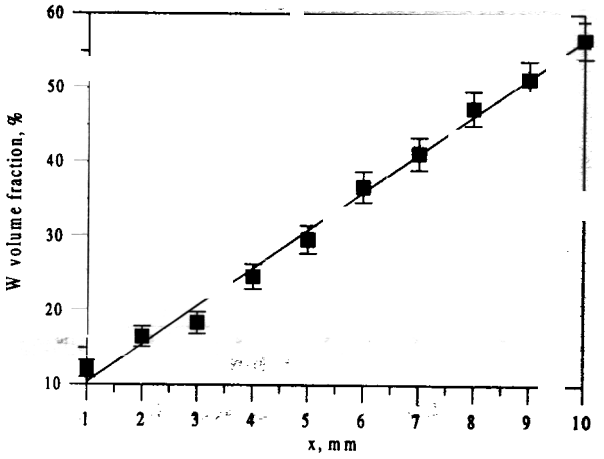

Fig. 2. The tungsten volume fraction distribution along the axial position.

Most obvious two observations are that first, stress in the copper phase barely exceeds 100 MPa whereas in the tungsten phase, it reaches up to 500 MPa and second, stresses in copper are compressive.

The first is possibly due to different yield strengths of two materials which are 60 MPa and 550 MPa, respectively. It should be noted that only a few copper data points exceeds the yield strength limit and only in compression. This again points to the plastic behavior if one compares it with recent calculations [4] which confirm that theoretical residual stresses are lowered to about the yield strength if plasticity is included in the model. The yield strength, however, has no fixed single value but it depends on the microstructure parameters such as the grain size, layer thickness and impurities. Accordingly, different yield strengths of Cu and W can explain the tendency to the maximum measured stress in the two phases. Quantitative estimates ought to be evaluated very carefully, however. Therefore, the linear elastic theory is not sufficient and it describes the experimental results only qualitatively.

At first sight, the second observation seems to be in contradiction with both theory and previous measurements. This disagreement can be resolved to a certain degree if one calculates macrostress ($\sigma_m=x\sigma_w+(1-x)\sigma_{cu}$, where x is the tungsten volume fraction) in both phases and then subtracts them from residual stresses for both phases (see fig. 3) to obtain the microstress distribution (fig. 4). This displays that the actual residual load share of both phases is obviously much more complicated and may even depend on different parameters, such as macrostress.

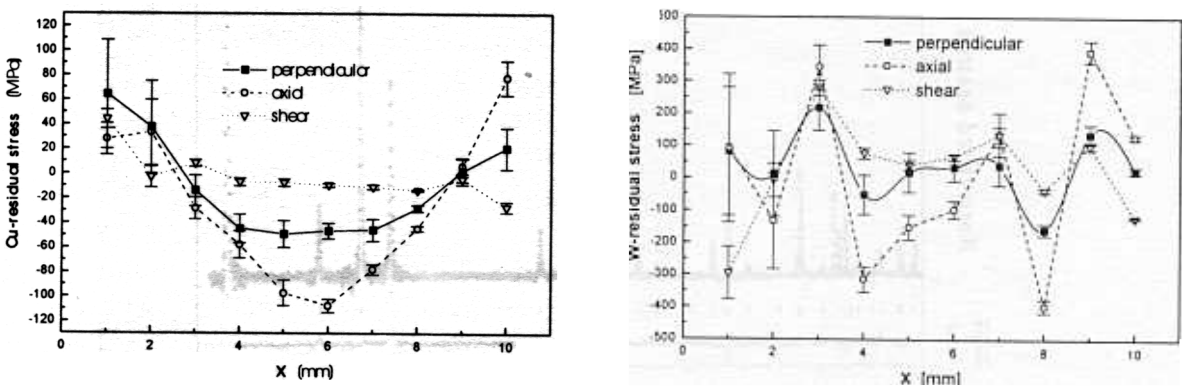

Fig. 3. Residual stresses in the copper and tungsten phase (8-layer sample).

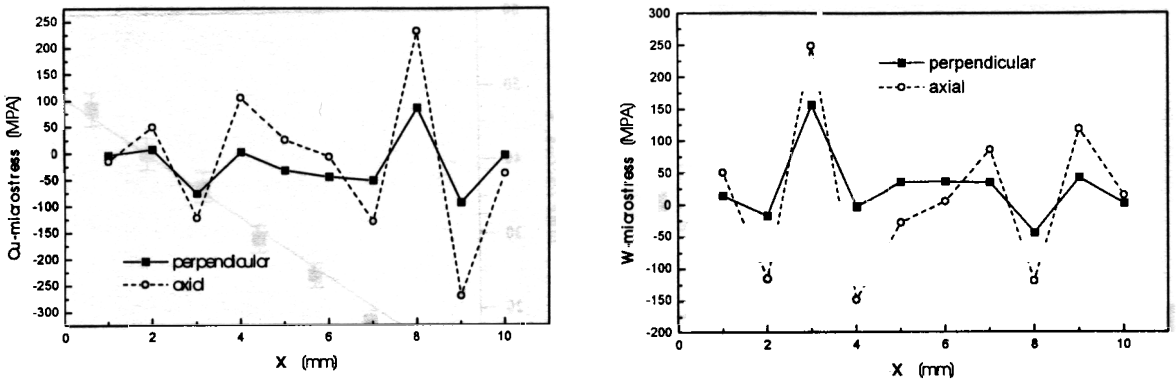

Fig. 4. Microstresses in the copper and tungsten phase (8-layer sample).

Al_2O_3/Al ceramic matrix composites

Another interesting type of materials studied at HRFD is the composites with Al infiltrated into a porous Al_2O_3 matrix. Recent research has led to the development of a material production technique where a metal is infiltrated into a porous ceramic matrix using gas pressure to form an interpenetrating network microstructure [5]. Brittle ceramic materials are reinforced by the inclusion of a ductile phase, usually a metal, to improve toughness, and produce a group of materials known as ductile phase reinforced ceramic matrix composites (CMCs). Infiltration is undertaken at temperatures slightly above the melting point of the metal. The most commonly used ceramic is α-Al_2O_3 infiltrated with Al. There is a large difference in the thermal expansion coefficients of the Al_2O_3 matrix (α=8.3×10^{-6} °C^{-1}) and the infiltrated Al (α=22.5×10^{-6} °C^{-1}). Therefore, because the metal phase contracts stronger than the ceramic one on cooling, one could expect that the tensile residual stress exists in the ductile phase and the compressive residual stress in the ceramic.

Two series of samples with the metal ligament size 0.1 and 1 μm were investigated at HRFD. In each series the matrix porosity and, accordingly, the Al volume fraction were 15%, 25% and 35%. The residual strain for the matrix was estimated from the changes of the lattice parameters *a* and *c* by the Rietveld method which corresponds to averaging over all available (hkl) directions. An analysis of the Al diffraction peak intensities revealed the presence of a sharp texture for the metal phase while in the matrix phase, the preferred orientation was absent (fig. 5).

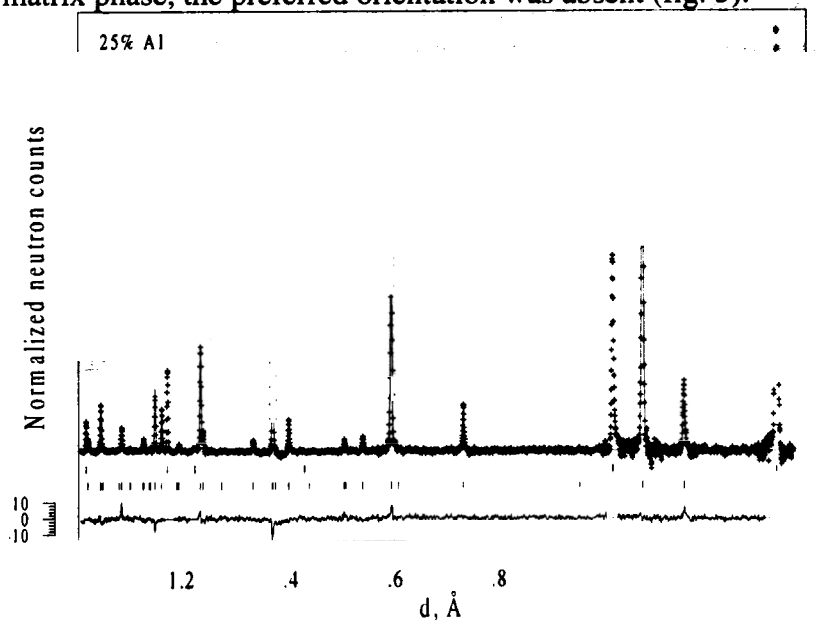

Fig. 5. The part of the neutron diffraction pattern from the Al_2O_3/Al composite with the 25% volume fraction of Al and the average ligament size about 1 μm. The experimental points, the profile calculated by the Rietveld method and the difference curve are shown. The tick marks (from

top down) are the calculated peak positions for Al and α-Al_2O_3, respectively. Textured Al peaks were not included in the profile fitting procedure.

For the textured metal phase, strain was obtained by single diffraction peak processing. In the tested composite samples, the alumina phase is mainly in compression and the aluminum phase in tension, due to thermal expansion mismatch (fig. 6). The average tensile stress of the aluminum phase depends on the microstructure and increases with decreasing metal content and ligament size. The average compressive strain behavior in the ceramic phase is more complicated and essentially differs depending on the microstructure.

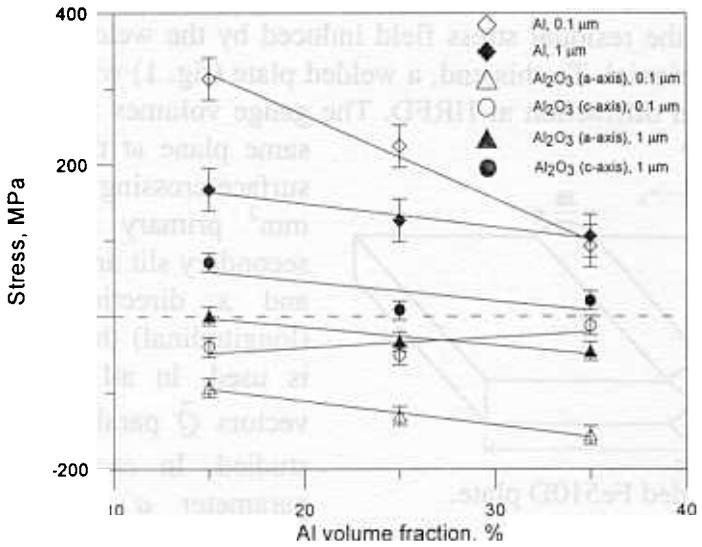

Fig. 6. Residual stresses in the Al_2O_3/Al composites with the fine and coarse microstructure as a function of the Al volume fraction.

REFERENCES

[1] B.Ilschner and N.Cherradi (eds.), Proc. of 3rd Int. Symp. on functionally gradient materials (FGM'94), Presses polytechniques et universitaire romande, Lausanne, Switzerland,1995.

[2] B.H.Rabin and I.Shiota, Functionally gradient materials, MRS Bulletin, Jan.1995.

[3] Y.Itoh, M.Takahashi and H.Takano, *Design of tungsten/copper graded composite for high heat flux components*, Fusion Engineering and Design, **31** (1996), 279-289.

[4] W.Schaller, *Berechnung thermischer Spannungen in einem gradierten Wolfram-Kupfer Verbundwerkstoff*, Report for the Deutsche Forschungsgemeinschaft (DFG), Karlsruhe, 1997.

[5] H.Prielipp, M.Knechtel, N.Claussen, S.K.Streiffer, H.Muellejans, M.Rühle and J.Rödel, *Strength and Fracture Toughness of Aluminum/Alumina Composites with Interpenetrating Networks*, Mat. Sci. & Eng. **A197** (1995), 19.

RESIDUAL STRESS INVESTIGATION IN A WELDED FE510D PLATE

G.D.Bokuchava[1], G.Bruno[2], F.Fiori[2], J.Schreiber[3], N.R.Shamsutdinov[1], Yu.V.Taran

[1] *Frank Laboratory of Neutron Physics, JINR, 141980 Dubna, Russia*
[2] *University of Ancona, 60131 Ancona, Italy*
[3] *Fraunhofer Institute for Nondestructive Testing, W-6600 Saarbrücken, Germany*

Fe510D is a widely used material in electrical and mechanical engineering. The aim of this investigation is to study the residual stress field induced by the welding process in bulk material which is expected to be triaxial. To this end, a welded plate (fig. 1) with a relatively high thickness is investigated by neutron diffraction at HRFD. The gauge volumes are in the points lying in the same plane at the depth of 4 mm from the surface crossing the welded region. The 3x10 mm^2 primary slit and the 3 mm wide secondary slit are used for measuring in the z and x directions, for the y direction (longitudinal) the 3x3x3 mm^3 gauge volume is used. In all positions, three orthogonal vectors $\vec{Q}$ parallel to the x, y and z axes, are studied. In each measurement, the lattice parameter a was obtained by Rietveld refinement and the strain in each spatial direction was evaluated as $\varepsilon=(a-a_0)/a_0$, where a_0, the unstrained lattice parameter, was evaluated as average far from the weld region. Then stresses were calculated by Hook's law and their behavior across the sample is shown in fig. 2.

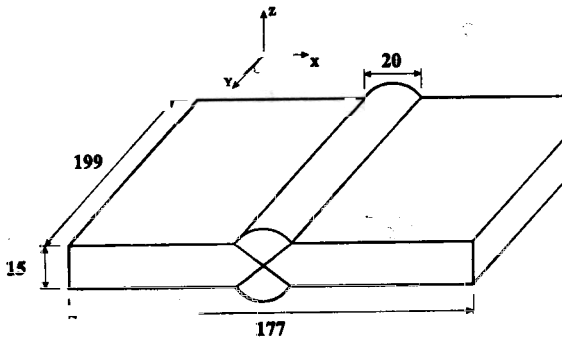

Fig. 1. A welded Fe510D plate.

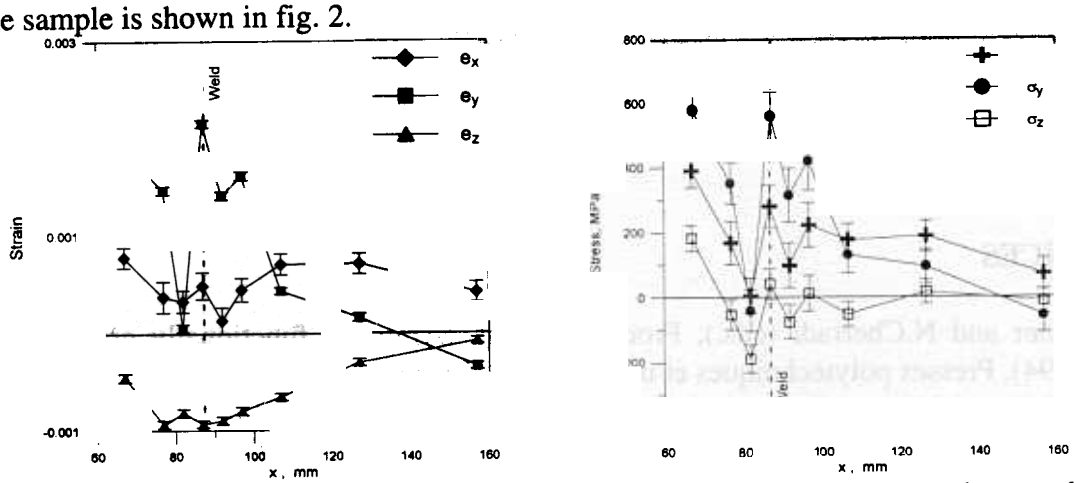

Fig. 2. The dependence of the strain and stress tensor components versus the coordinate x.

In addition to the neutron diffraction experiment, a magnetic measurement based on Barkhausen noise registration was carried out. The aim of this experiment was to compare the obtained results with the neutron diffraction data and perform appropriate calibration of the magnetic method. The welded plate was totally scanned by a magnetic sensor in directions parallel and perpendicular to the weld line and, simultaneously, Barkhausen noise was registered (figs. 3-4). It is assumed that the Barkhausen noise amplitude is related to the stress components σ_x and σ_y as:

$$A_x=C_1\sigma_x+C_2\sigma_y+C_3 \text{ and } A_y=C_4\sigma_x+C_5\sigma_y+C_6,$$

respectively, where A_x and A_y are the magnetic noise amplitudes measured in the directions perpendicular and parallel to the weld line, respectively, C_1 ... C_6 are the constants depending on the properties of the material. The calibration of magnetic data was performed by least square fit of the constants C_1 ... C_6. It should be noted that the neutron diffraction data were measured only near the weld zone while magnetic measurements were conducted over the whole sample area. Therefore, the calibration procedure was carried out only for the sample region for which both neutron diffraction and magnetic data were available. Then, the Barkhausen noise amplitude was recalculated to stresses using fitted constants. In this way the residual stress distribution map was obtained for the studied sample (fig. 5).

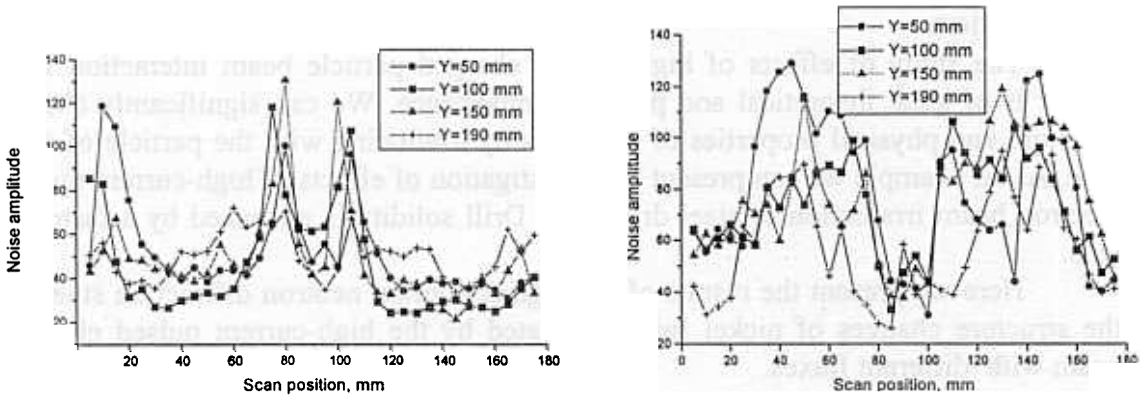

Fig. 3. The distribution of the Barkhausen noise amplitude in the directions perpendicular (left) and parallel (right) to the weld line at different values of the y coordinate.

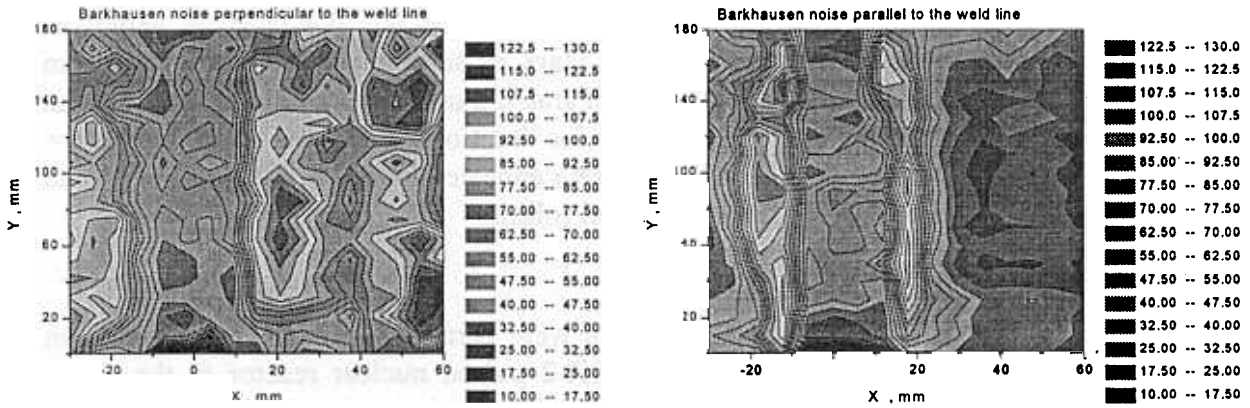

Fig. 4. The distribution map of the Barkhausen noise amplitude in the sample.

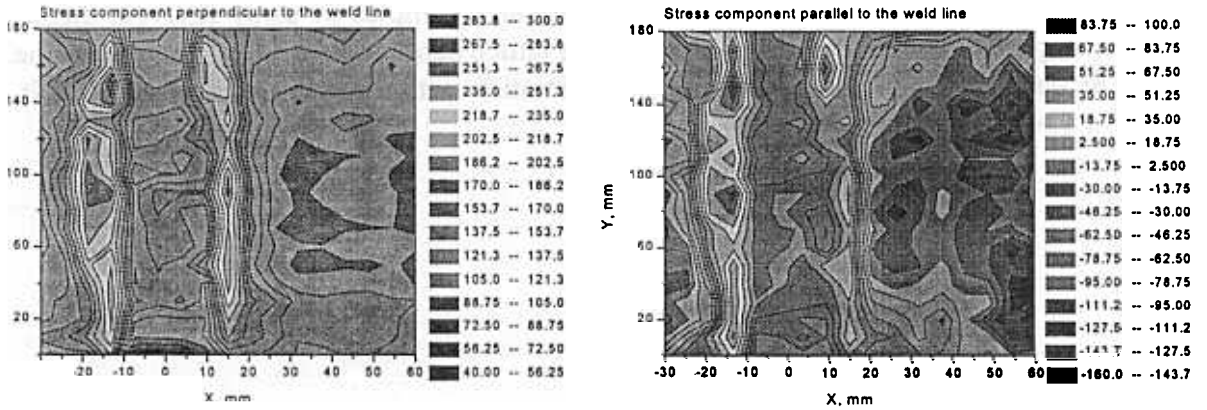

Fig. 5. The residual stress distribution map recalculated from the Barkhausen noise data.

Effects Induced in Nickel Foils by High-Current Pulsed Electron Beam Irradiation

(experimental report on the I.1.47 proposal)

G.D.Bokuchava*, V.V.Sikolenko*, A.V.Kalmikov*
S.A.Korenev+
* - Joint Institute for Nuclear Research, Dubna, Russia
+ - New Jersey Institute of Technology, New Arc, New Jersey

Introduction

The study of effects of high-current charged particle beam interaction with matter is of great theoretical and practical importance. We can significantly change structure and physical properties of materials by irradiating with the particle of such type. As an example we can present the investigation of effects of high-current pulsed electron beam irradiation of steel drills /1/. Drill solidity is enhanced by a factor of tens.

Here we present the results of the high resolution neutron diffraction study of the structure changes of nickel foils, irradiated by the high-current pulsed electron beam with different fluxes.

Experiment

The experiments on foil irradiation were carried out at the ELIONA experimental setup intended to produce electron and ion beams at the Particle Physics Laboratory of the Joint Institute for Nuclear Research /2/. We used an explosive emission vacuum diode with an Arcadyev-Marx pulse voltage generator. The beam current was measured by a Rogovsky LR integrated transformer and by current shunts. The beam parameters were: E = 250 keV, pulse duration t_b = 300 ns, beam current I = 1000 A, pulse repetition 0.2 Hz. All foils were annealed before irradiation in order to escape the influence of texture, arising in foil rolling.

Results

The neutron diffraction experiments were carried out at the high resolution Fourier diffractometer HRFD /3/ at the IBR-2 pulsed nuclear reactor in the Frank Laboratory of Neutron Physics of the Joint Institute for Nuclear Research. Unirradiated, and irradiated for 10 and 20 minutes nickel foils were investigated.

The lattice parameter *a*, and also the widths and positions of the main diffraction peaks were calculated for all measured samples by using Rietveld method /4/. Figure 1 presents the dependence of the lattice parameter *a* on the irradiation time. The dashed curve shows the linear approximation with the parameters $a = 0.00017 t_{irr} + 3.52495$.

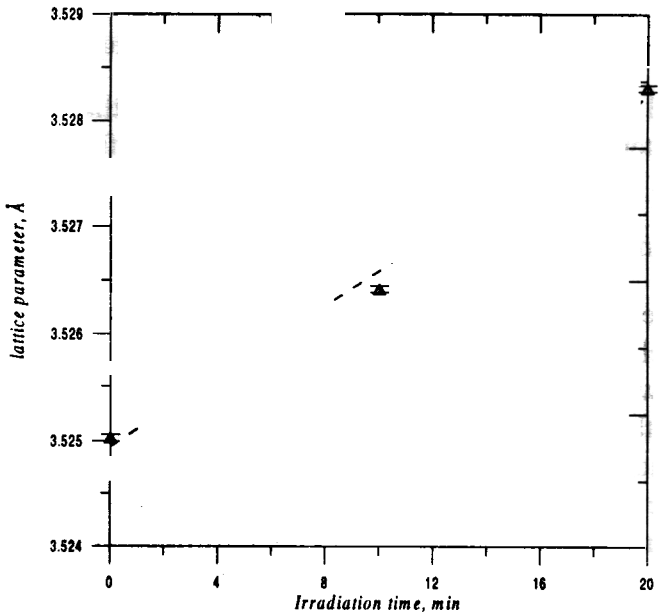

Fig.1. The dependence of the lattice parameter on the irradiation time

Figure 2 shows the dependencies of the main diffraction peaks widths on their positions for all measured foils.

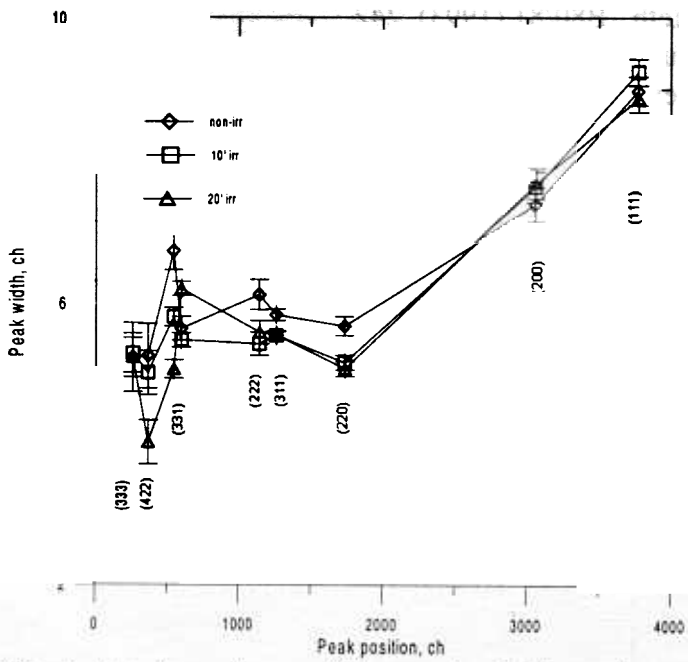

Fig.3. the dependence of the peak width on the peak position. The indexes of the peaks are indicated.

Discussion

The energy of the electron beam is transferred to the electron subsystem of the irradiated matter for a very short time in the course of the interaction of the high-current electron beam with the material. The irradiated material thermal constant τ is defined by the condition when the heat diffusion parameter $w = (b^2t)^{1/2}$ is equal to the electron beam penetration beam h. According to /5/ this parameter is equal to

$\tau = \frac{2h^2 \rho c}{\lambda}$, where ρ is the density, c is the heat capacity, λ is the heat conductivity and b = 2λ/(ρc). In the case of nickel τ = 5.11 μs. This value is much greater than the time of interaction of beam with materia, which is equal to t_b = 300 ns, therefore the condition of adiabatic heating of the local volume is realized. In this case, the local heating temperature at the penetration depth is equal to $T = \frac{2Wt_b}{hS\rho} \sim 9100$ K, where W is the electron beam power density, S is the irradiated surface area. This temperature is greater than the nickel melting point. As a result of high temperature gradient, an elastic deformation wave arises in the irradiated foil. Figure 1 demonstrates linear enhancement of the lattice parameter with an increse of flux as a result of the action of the deformation wave. The recrystallisation from the melted condition takes place in the period between electron beam pulses. This process can be accompanied by partial amorphisation. But the analysis of the main diffraction peaks width dependence on their positions for samples irradiated by different fluxes, shows (see Fig.2) that the amorphisation is absent with the limits of experiment accuracy.

We would like to thank Dr. E.V.Raspopina for the help in sample preparation.

References.

1. I.Vavra, S.A.Korenev, JINR Communication JINR 13-88-60
2. S.A.Korenev, Nucl.Instrum & Meth., B80/81 (1993), 242
3. V.L.Aksenov et.al., JINR Communication E13-92-456
4. V.B.Zlokazov and V.V.Chernishev, J.Appl.Cryst. 25 (1996), 923
5. I.P.Svinjin Calculation of High Voltage Electron Accelerators for Beam Technologies, Moscow, 1989

Investigation of rock anisotropy by neutron diffraction and acoustic sounding

T.I.Ivankina[1], K.Klima[2], T.Lokajicek[2], A.N.Nikitin[1], Z.Pros[2], K.Ullemeyer[1].

[1] *141980 Dubna, JINR, Frank Lab of Neutron Physics, Russia*
[2] *141 31 Prague 4, Geophysical Institute, Czech Academy of Sciences, Czech Republic*

The elastic anisotropy of rocks is controlled by several factors: the phase composition, the single crystal anisotropy of phases, the grain size distribution, the lattice preferred orientation (texture), the contact conditions at grain boundaries, the pore volume and the microcrack orientation.

The method for the experimental investigation of the elastic anisotropy of spherical rock samples was proposed in [1]. The measuring facility at the Geophysical Institute of the Czech Academy of Sciences allows the investigation of the anisotropy of quasi-longitudinal waves (P-waves) by means of ultrasonic sounding at hydrostatic pressure up to 400 MPa. Moreover, even the lattice preferred orientation of large coarse-grained rock samples can be much easier determined due to recent progress in neutron diffraction methods and mathematical methods of data treatment.

The present work was initiated to obtain better insight into the factors which influence the elastic anisotropy of a rock sample at variable hydrostatic pressure. Olivine xenolith (xenolithes originate in the earth mantle) was selected as an example. The olivine texture was determined and correlated with the compressional (P) wave distribution.

A texture analysis of coarse-grained rock samples was performed with the NSHR texture diffractometer at the reactor IBR-2 (JINR, Dubna, Russia [2]). The spherical rock samples are highly polished, the diameter is 50 ± 0.01 mm. They are labelled to allow precise reorientation with respect to the coordinate system of the measuring device and the geographical coordinates. Identical samples were used for ultrasonic measurements.

The time-of-flight (TOF)- spectrum of the olivine sample ZB1 is given in Figure 1. The experimental pole figures were extracted from the spectra by the integration over a predefined channel range and used in a quantitative texture analysis (QTA) by means of the texture component method [3]. From the texture components

all derived pole figures can be recalculated, including even pole figures which cannot be measured directly because of vanishing scattering lengths. Figure 2 shows the recalculated (001), (100) and (010) pole figures. They are important for interpretation, since they correspond to the principal directions of the single crystal P-wave distribution (P_{max} || (100), P_{min} || (010)) , P_{int} || (001)).

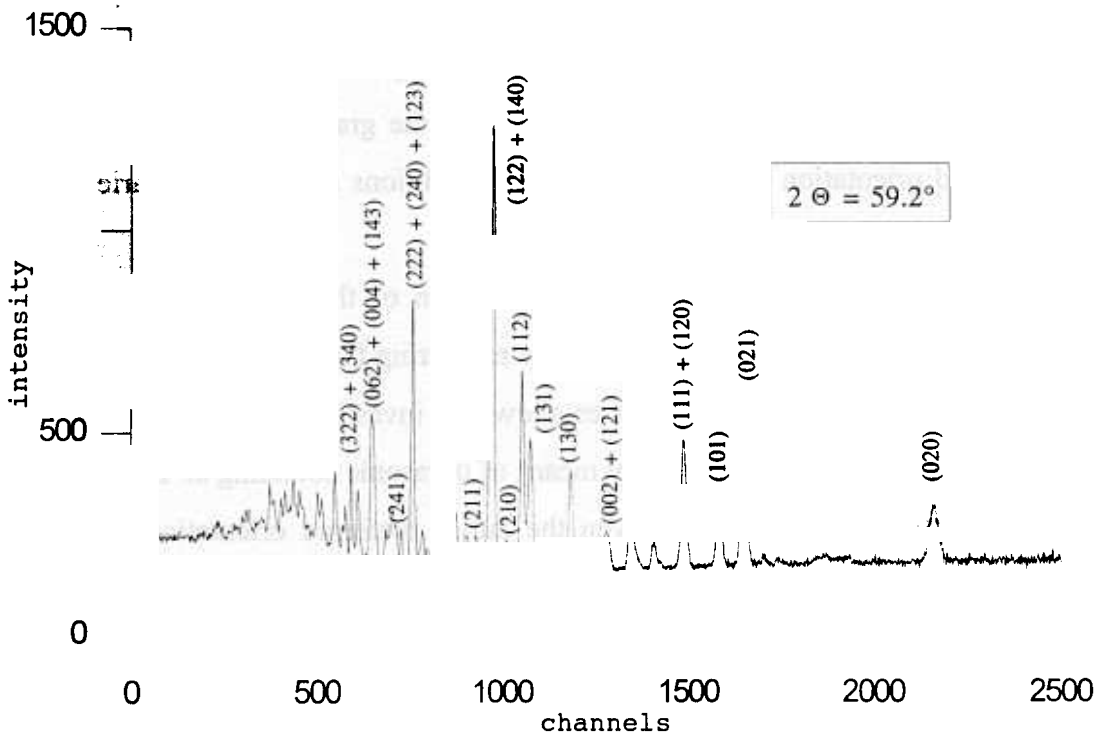

***Fig.1**. The neutron diffraction pattern of olivine. The indicated peaks are used for QTA.*

In Figure 3, the P-wave distribution of the sample ZB1 is given for different pressure levels. The primary data are transformed into the spatial distribution of P-wave velocities and are presented in the stereographic projection to allow a direct comparison correlated with neutron diffraction pole figures.

The most remarkable observation is that the measured P-wave distribution at low pressure levels cannot be explained only by the lattice preferred orientation of olivine. It is concluded that pores and open microcracks have significant influence on the P-wave anisotropy. At a pressure level of approximately 200 MPa, microcracks start to close and the P-wave distribution more and more approximates the one which can be assumed from the texture. Finally, at the maximal pressure the anisotropy of

elastic properties of an olivine sample is controlled only by the crystallographic texture which evidently originates during plastic deformation of xenolith.

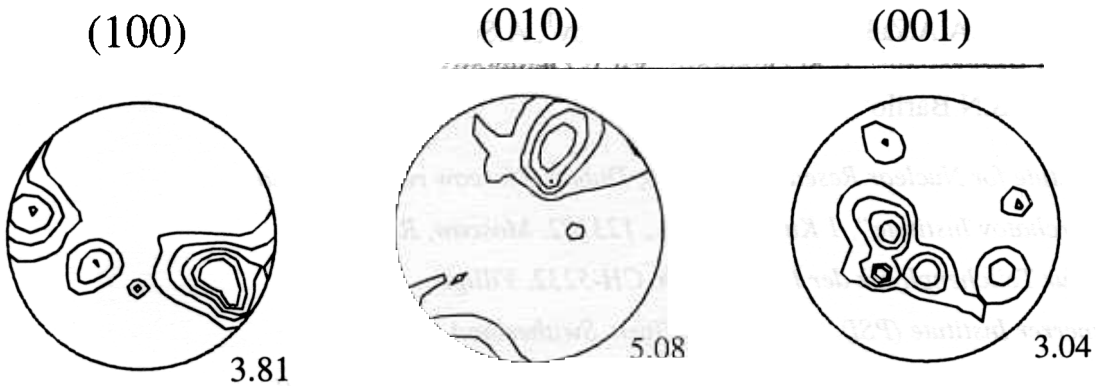

Fig.2 *Pole figures recalculated from the orientation distribution function.*

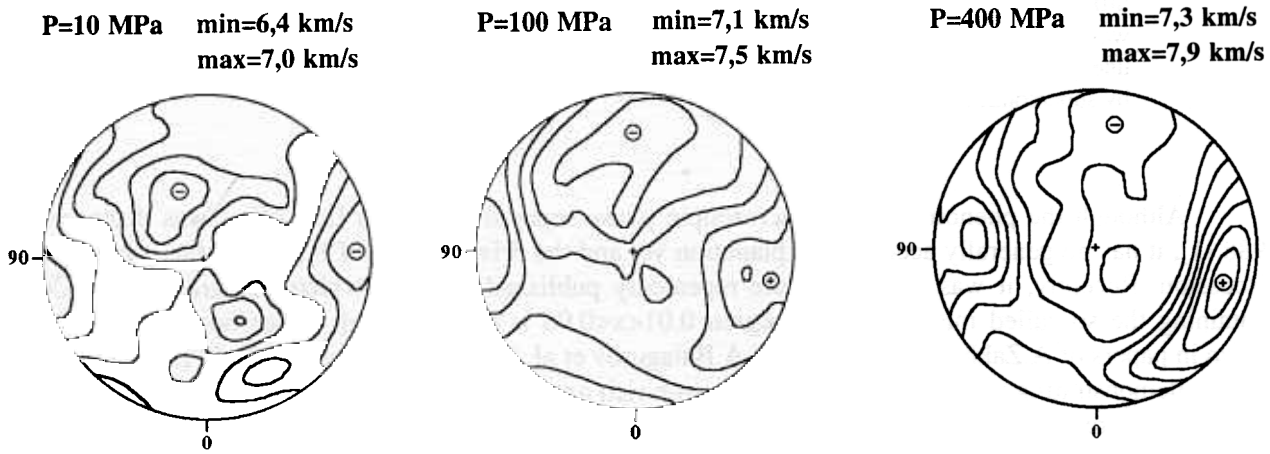

Fig.3*. P-wave distribution at different pressure levels.*

References

[1] Pros Z. Studies of anisotropy in elastic properties of rocks at uniform pressures on spherical samples. In: *High Pressure and Temperature Studies of Physical Properties of Rocks and Minerals*. Kiev, "Naukova Dumka", 1977, p.56-67.

[2] Walther K., Isakov N. N., Nikitin A.N., Ullemeyer K. and Heinitz J. Research on the textured structure of geomaterials by the diffraction method using a high-resolution neutron spectrometer at the I.M.Frank Neutron Physics Laboratory of the Joint Nuclear Research Institute. *Physics of the Solid Earth*, AGU, 1994, **v. 29**, N6, p. 30-37.

[3] Helming K., Eschner T. A new approach to texture analysis of multiphase materials using a texture component method. *Cryst. Res. Technol.*, 1990, **25**, K203- K208.

Microscopic Phase Separation In La_2CuO_{4+x} Induced By The Superconducting Transition

V.Yu.Pomjakushin[1], A.A.Zakharov[2], A.M.Balagurov[1], A.Schenck[3], F.N.Gygax[3], A.Amato[4], D.Herlach[4], A.I.Beskrovny[1], V.N.Duginov[1], Yu.V.Obukhov[1], A.V.Pole[1], V.G.Simkin[1], A.N.Ponomarev[2], S.N.Barilo[5]

[1] *Joint Institute for Nuclear Research, 141980, Dubna, Moscow region, Russia*

[2] *RSC "Kurchatov Institute", 1 Kurchatov sq., 123182, Moscow, Russia*

[3] *Institute fur Teilchenphysik der ETH Zurich, CH-5232, Villigen, PSI*

[4] *Paul Scherrer Institute (PSI), CH-5232 Villigen, Switherland*

[5] *Institute of Solid State Phys. and Semiconductors, 220072,Minsk, Belorussia*

The phase separation (PS) effect in superconducting La_2CuO_{4+x} ($x \leq 0.04$) single crystals with low oxygen mobility was studied via μSR spectroscopy, high resolution neutron diffraction and magnetic susceptibility. Despite the fact that all crystals are inside the miscibility gap ($0.01<x<0.06$), only crystals with a sufficiently large excess oxygen concentration $x>0.04$ show macroscopic phase separation according to the neutron diffraction data. However, in all samples the phase transition to an ordered magnetic state was observed by μSR spectroscopy concomitantly with the onset of superconductivity. This unexpected behavior suggests for the first time that the underlying microscopic PS is driven by superconductivity.

Although the phenomenon of macroscopic phase separation (PS) in La_2CuO_{4+x} was discovered in 1988 [1], it has no generally accepted explanation yet and the driving force of PS is still the subject of the discussion. Recently, it was found that the repeatedly published (e.g., [2]) phase diagram of La_2CuO_{4+x} containing the so called miscibility gap region $0.01<x<0.06$ is not universal. It has been unambiguously shown in papers of A.Zakharov et al. [3] and A.Balagurov et al. [4] that along with "usual" La_2CuO_{4+x} single crystals demonstrating phase separation into oxygen rich and oxygen poor regions, it is possible to prepare crystals that are inside the miscibility gap and possess superconductivity without macroscopical phase separation. A combined analysis of neutron and μSR data has shown that the phase separation phenomenon has an even more complicated character, namely, a macroscopically homogeneous superconducting crystal can be inhomogeneous on the microlevel [5]. Finally, we tentatively assumed in [6] that phase separation occurs on the microscopic scale in La_2CuO_{4+x} at the temperature close to the superconducting transition temperature and hence, can be connected with the formation of the superconducting state.

In this paper, we present new experimental data on La_2CuO_{4+x} single crystals obtained by μSR and neutron diffraction which allow us to clarify the problem. The most intriguing of the results is that in all of the studied crystals, we observed the coexistence of superconductivity and an ordered magnetic state without macroscopic phase separation with coinciding or very close temperatures for the transitions to the AFM and SC states. This is a strong argument in favor of the existence of the so called electronic phase separation in such crystals which is theoretically discussed in [7,8].

Two different kinds of La_2CuO_{4+x} superconducting crystals were studied: macroscopically homogeneous and phase separated. The crystals were prepared by the molten solution method under thermodynamic equilibrium conditions. The details of crystal growth, oxygenating procedure and high-resolution neutron diffraction analysis are presented elsewhere [3,4]. The specific feature of this series of crystals is the low oxygen mobility which results in the absence of macroscopic phase separation connected with oxygen diffusion for crystals in the $x \leq 0.03$ region of the miscibility gap.

Below, we present the experimental data for two representative crystals: x=0.02 for a non-phase separated series of samples (hereinafter, the A crystal) with the superconducting transition temperature T_c=15 K, and x=0.04 for phase separated samples (hereinafter, the B crystal) with T_c=25 K. The B sample was studied before by high resolution neutron diffraction [4]. The data on other crystals from these series differ in specific details but support the main statements of the present work.

Neutron diffraction experiments were performed at the IBR-2 pulsed reactor of JINR (Dubna) with the high resolution Fourier diffractometer (HRFD) [9] and the DN-2 instrument equipped with a 2D position-sensitive detector. μSR measurements were carried out using the General Purpose Spectrometer (GPS) on the πM3 surface muon beam line at PSI (Villigen). Magnetization measurements were performed using a custom-made SQUID magnetometer [10].

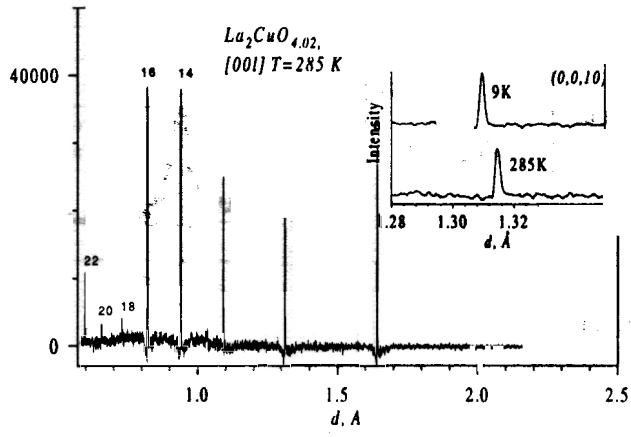

Fig 1: The Diffraction pattern from the [00l] plane in the A crystal. The insert shows fragments of two spectra measured at room and low temperatures.

High resolution neutron diffraction (with $\Delta d/d \approx 0.9 \cdot 10^{-3}$) revealed no trace of phase separation in sample A; neither splitting nor broadening of neutron diffraction peaks was observed giving evidence that on the macroscopic scale, the homogeneous excess oxygen concentration in the crystal is preserved down to the lowest measured temperature 9 K (**Fig 1.**) In the B sample, phase separation into oxygen-rich and oxygen-poor phases was observed clearly at cooling [4]. The relative difference in the elementary lattice parameters of these two phases amounted to about $2 \cdot 10^{-3}$, which is in good agreement with the data obtained for "usual" La_2CuO_{4+x} crystals [1]. In the B crystal, we observed the specific effects of diffraction peak broadening, whose analysis allowed us to conclude that the average dimensions of the coherent regions of coexisting phases coincide and amount to: 100 nm along the c-axis and 150 nm within the plane. The phase separation process starts at T=250 K and is completed at T=200 K.

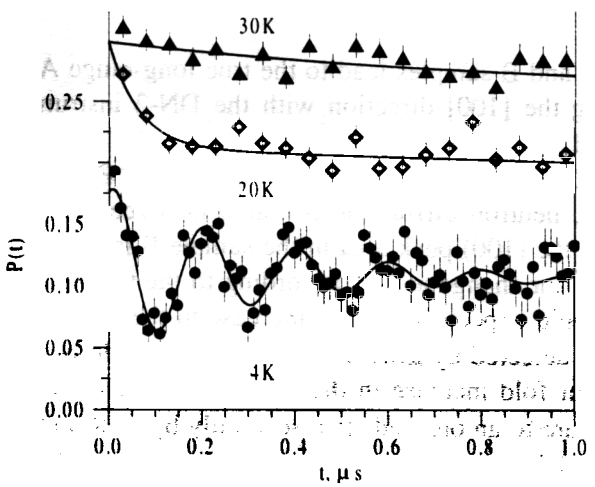

Fig.2: Time dependence of the muon spin polarization P(t) in zero external field above and below the magnetic transition (T_N=15 K) for $La_2CuO_{4.02}$. The data for T=20K and 30K shift upwards along the y-axis.

The magnetic state of the A crystal is identified by the presence of a muon spin precession signal detected in zero external magnetic field (ZF-μSR) below 15 K. Correlated precession of muon spins is possible only if the surrounding Cu moments are ordered on the scale of several coordination spheres. The muon spin precession frequency $f_\mu = \gamma_\mu B_\mu$ is given by the local magnetic field acting on the muon $\mathbf{B}_\mu$ which is proportional to staggered magnetization of copper magnetic moments. Typical ZF-μSR signals observed in the A sample are shown in **Fig. 2** where the difference between the paramagnetic (T=30 and 20 K) and AFM (T=4 K) states of the crystal can be clearly seen. The spontaneous muon spin precession frequency f_μ=5 MHz is typical for the AFM state of stociometric La_2CuO_4 [12] implying that the A sample is ordered in the same AFM structure. No precession signal was observed above 15 K; however, the polarization function possesses a fast decaying component up to 30 K which steadily decreases with

increasing temperature. The origin of this fast depolarization is the slowing down of Cu-spin fluctuations near the phase transition. Thus, the ZF-μSR data unambiguously proves the presence of static antiferromagnetic order in part of the crystal volume. The volume fraction occupied by the AFM phase amounts to ≥50% of the crystal volume.

Unlike the A sample, there are two characteristic magnetic temperatures for the B sample. Below T_{N1}≈230 K, the AFM phase appears only in 10% of the crystal volume. Then, under cooling to T_{N2}≈25 K, a sharp increase in the AFM fraction occurs which reaches 40% at low temperatures (**Fig.3**, the left axis). The spontaneous muon spin precession frequency detected below T_{N1} has, again, typical values of about 5 MHz as expected for AFM La_2CuO_4. The precession frequency smoothly increases with decreasing temperature without any peculiarity at T_{N2}.

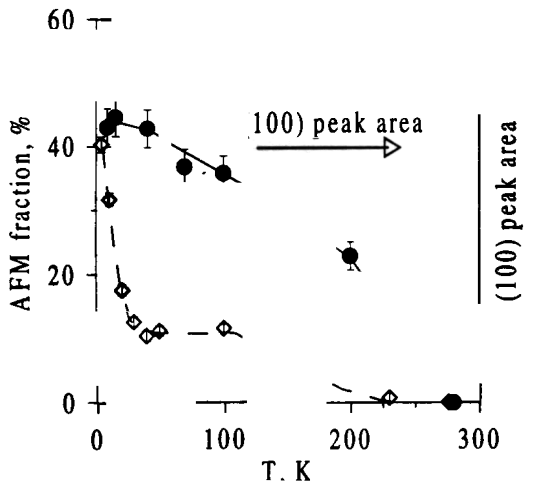

Fig.3: The AFM volume fraction of the $La_2CuO_{4.04}$ crystal seen by μSR (diamonds — left axis). The area of the (100) AFM peak as a function of temperature measured by neutron diffraction (circles, right axis) is also shown.

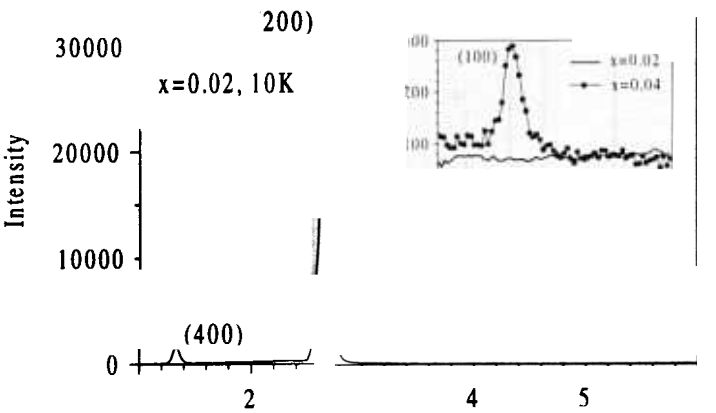

Fig.4: The diffraction pattern from the [100] plane for $La_2CuO_{4.02}$ measured at T=10 K. The insert shows fragments of the diffraction patterns for both $La_2CuO_{4.02}$ and $La_2CuO_{4.04}$ near the (100) AFM peak. The position and intensity of (200) and (400) peaks are the same for both crystals.

To check whether the observed transitions in the A and B samples lead to the true long-range AFM order, we measured the neutron diffraction spectra along the [100] direction with the DN-2 instrument (**Fig.4**). According to the μSR data, we expected to find the (100) magnetic peak below the magnetic transition below T_N=15 K in the A sample and below T_{N1}=230 K in the B sample. Indeed, in the B sample, this peak was well pronounced, whereas in the A sample, neutron diffraction revealed no traces of such reflection (insert in **Fig.4**). The temperature dependence of the (100) peak area in the sample B is shown in **Fig.3** (right axis.) Since the copper magnetic moment does not change at T_{N2}, according to the temperature dependence of the muon spin precession frequency, one would expect to have an increase in the (100) peak area below T_{N2} similar to the increase in the AFM fraction detected by μSR. However, neutrons do not see any peculiarity below T_{N2}=25 K, whereas muons see a four fold increase in the AFM fraction. Similar to sample A, we have a coincidence of the transition temperature to an ordered state seen only by μSR and the temperature where the superconducting transition starts to set on.

We start our discussion of the experimental results with a brief sketch of the "temperature-concentration" phase diagram of La_2CuO_{4+x}. An earlier experimental study showed the presence of the miscibility gap in a rather wide concentration region. However, when a solid solution decomposes into two phases, two routes for the decay are possible: *the nucleation and growth* mechanism and/or the *spinodal* mechanism. Because there is an activation barrier in the former case, the process may be completely quenched in crystals with low mobility of dopants. The spinodal decay does not need an activation process

and, hence, inevitably proceeds to the creation of a spatial fluctuation of the composition in the sample. We believe that the decay mechanism is the main difference in our crystals: the x=0.02 crystal does not have a high enough oxygen index to be in the spinodal region and has to be split via nucleation mechanism — which is not effective at low mobility. The oxygen index in the x=0.04 crystal, on the other hand, situates the sample in the spinodal region and the decay takes place independently of oxygen mobility. We now disscuss two main experimental results of the present work: (i) the appearance (or sharp increase in the volume fraction) of the low temperature AFM phase when the system enters the superconducting state and (ii) why this AFM phase is not seen by neutron diffraction. We should mention that a very similar phenomenon has been observed in the crystal with another oxygen index (x=0.03) [5] where the magnetic transition to the short range spin-glass-like state sets on in the vicinity of the superconducting transition.

One natural explanation for the observed behavior is the suggestion that after cooling, crystals consist of grains of oxygen-rich and oxygen-poor phases of very small size (in the x=0.04 crystal, there are also metallic regions of larger size due to macroscopic PS which produces robust superconductivity at low temperatures). Then the transition at low temperature corresponds to the Neel temperature of the oxygen-poor phase. The absence of AFM neutron reflections at respective temperatures implies that the sizes of the coherent regions of this AFM phase are very small (on the order of several dozen angstroms) and, therefore, they cannot be seen as Bragg reflections because of the size broadening effect.

The coincidence between the temperatures of the magnetic and superconducting transitions in quite different crystals, however, remains surprising. One may have to consider another possibility connected with electronic phase separation which causes a charge concentration wave inside the crystal. From the fact that the appearance of magnetic order for x=0.02, T_N=15 K, in x=0.04, T_{N2}=25 K and in x=0.03 [5], T_f=8 K, is always close to the onset of the superconducting regime in all crystals, independent of their actual microstructure and critical temperatures we may conclude that the magnetic ordering *is induced* by the superconducting transition. It is worth mentioning in this context the relevant theory [8] where the instability of a homogeneous system was found to result from the existence of different insulating correlations characterized by long-range or short-range order. There it was also shown that the stability boundary becomes wider in the presence of superconducting pairing. As a result, the superconducting transition may cause a sample which is homogeneously metallic in its normal phase to split into metallic droplets that are separated from each other by weakly coupled insulating interlayers.

In summary mSR and neutron diffraction studies show that microscopic phase separation (as opposed to macroscopic PS) appears in parallel with superconductivity and is very likely driven by superconducting pairing.

The work was supported by the RFBR (Grants 960217431, 960217823), SNSF (Grant 7SUPJ048473) and by HTSC national program (Grant 96019).

References

1. J.D.Jorgensen, B.Dabrowski, S.Pei, et al. Phys.Rev. **B38** (1988) 11337.
2. F.C.Chou, D.C.Johnston, Phys. Rev., B54 (1996) 572.
3. A.A.Zakharov et al., Physica C, 223 (1994) 157.
4. A.M.Balagurov et al., Physica C, 272 (1996) 277.
5. V.Yu.Pomjakushin et al., Physica C, 272 (1996) 250.
6. V.Yu.Pomjakushin et al., M2S, Beijing, 1997, Proceedings, v.III, p. 1353.
7. V.J.Emery and S.A.Kivelson Physica C**209** (1993) 597.
8. A.A.Gorbatsevich, Yu.V.Kopaev, and I.V.Tokatly, JETP Lett. **52** (1990) 95; Sov.Phys.JETP **74**, 521 (1992); Physica **C 223** (1994) 95.
9. V.L.Aksenov et al., J. Neutron Research, 5 (1997) 181.
10. Yu.V.Obukhov, B.I.Saveliev, and V.V.Khanin, Pribory i Tekhnika Eksperimenta (in Russian) 5, 166 (1991).
11. R.K. Kremer, A.Simon, E.Sigmund, V.Hizhnyakov, JMMM 140-144 (1995) 1285.
12. Y.J.Uemura, et al, Phys Rev Lett 59 (1987) 1045.

Non-lamellar phases in ternary systems POPC/$C_{12}E_2$/H_2O

T. Gutberlet[1], G. Klose[1], A. Islamov[2]

[1] *Institute f. Experimental Physics, University of Leipzig, Linnéstr. 5, D- 04103 Leipzig, Germany*

[2] *FLNP, JINR, 141980 Dubna, Moscow region, Russia*

Mixtures of phospholipids, non-ionic surfactants and water exhibit a wide variety of mesophases dependent on the phospholipid surfactant molar ratio and the amount of water present (1). On reducing the relative hydration or increasing the temperature of the phospholipid surfactant system POPC/$C_{12}E_2$ an unusual lamellar gel (L_b) to inverted hexagonal phase (H_{II}) transition is observed (2). This phase transition occuring at low hydration of RH $\leq$ 75 % and $R_{S/L}$ = 2 is due to mismatch in the alkyl chain lengths of phospholipid and surfactant and relative dehydration of phospholipid by the addition of a surfactant changing the curvature of the mixed membrane. Using neutron powder diffraction the structure and organisation of the ternary system POPC/$C_{12}E_2$/H_2O in the lamellar and hexagonal phases has been studied. At increased relative hydration of RH $\geq$ 80 % and $R_{S/L} \leq 1$ in the lamellar fluid phase (L_a) it has recently been shown, that the surfactant, deuterated at the a-methylene group, is anchored in the phospholipid matrix with the a-methylene group near the hydrophobic-hydrophilic boundary (3).

By using $C_{12}E_2$ with fully deuterated di-oxyethylene moiety or a fully deuterated alkyl chain significant changes in the diffraction patterns measured with the time-of-flight spectrometer DN-2 at the pulsed reactor IBR-2 in JINR of the lamellar gel phase are found in comparison with a non-deuterated mixture of POPC/$C_{12}E_2$ (Fig.1). It demonstrates the incorporation of the surfactant in the L_b phase at the molar surfactant to lipid ratio of $R_{S/L}$ = 2, T = 18 °C, RH = 58 %. Also in D_2O the coexistence of the L_b phase and the hexagonal phase H_{II} is visible due to the shift in the phase transition temperature by presence of D_2O. Different diffraction patterns are also found by changing the contrast between $C_{12}E_2$ with a deuterated alkyl chain (Fig. 2) and POPC with deuterated palmitoyl moiety (not shown). The coexistence of the lamellar and hexagonal phases at T = 18 °C, RH = 58 % in the phospholipid-surfactant mixture of $R_{S/L}$ = 2 is again absolutely evident in the diffraction pattern of the system in D_2O. As the temperature increases the system transforms into the inverted hexagonal phase H_{II}. Only two to three Bragg peaks could be observed in this phase. Nevertheless, significantly different diffraction patterns were obtained on changing the contrast between samples with different molecular parts deuterated or with exchange of H_2O on D_2O. A detailed reconstruction of the obtained diffraction pattern of each investigated POPC/$C_{12}E_2$ system has to be done by model calculations. This will lead to a detailed structural model of all components in the obtained phases of this amphiphilic model system.

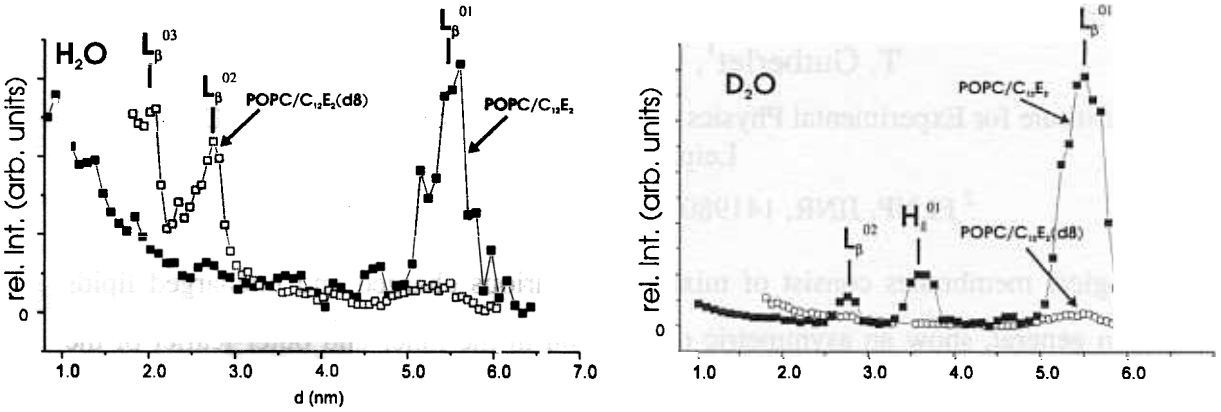

Fig.1. The neutron diffraction pattern of POPC/$C_{12}E_2$ and POPC/$C_{12}E_2$(d8) in H_2O and D_2O at T = 18 °C, RH = 58 %.

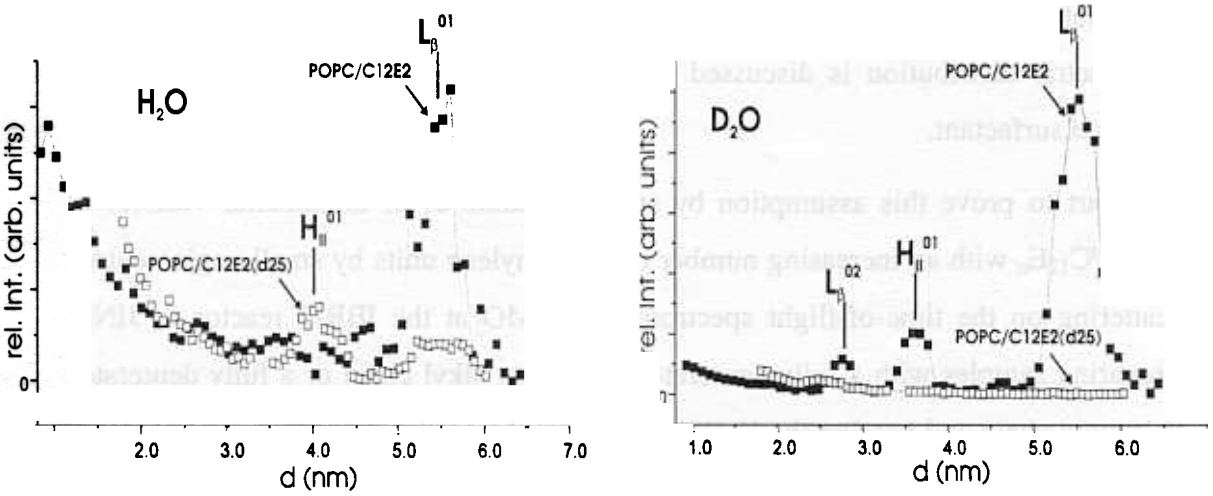

Fig.2. The neutron diffraction pattern of POPC/$C_{12}E_2$ and POPC/$C_{12}E_2$(d25) in H_2O and D_2O at T = 18 °C, RH = 58 %.

S.S. Funari, G. Klose, Chem. Phys. Lipids, 1995, 75, 145

2) T. Gutberlet, U. Dietrich, G. Klose, G. Rapp, J. Colloid Interf. Sci., submitted

3) G. Klose, A. Islamov, B. König, V. Cherezov, Langmuir, 1996, 12, 409

Distribution of surfactant $C_{12}E_n$ in phospholipid membranes

T. Gutberlet[1], G. Klose[1], M. Kiselev[2]

[1] Institute for Experimental Physics, University of Leipzig, Linnéstr. 5, D- 04103 Leipzig, Germany

[2] FLNP, JINR, 141980 Dubna, Moscow region, Russia

Biological membranes consist of mixtures of various charged and uncharged lipids and in general, show an asymmetric distribution in the inner and outer leaflet of the formed bilayer sheet. In model membrane systems only a symmetric distribution of the amphiphiles used is present and an asymmetric distribution is only known in highly curved aggregates, such as small unilamellar vesicles due to difference in sterical requirements for different lipids. In a model membrane system of the phospholipid POPC mixed with the non-ionic surfactant $C_{12}E_n$ the possibility of an asymmetric distribution is discussed on increasing the head group volume of the admixed surfactant.

We start to prove this assumption by studying mixtures of unilamellar vesicles of POPC/$C_{12}E_n$ with an increasing number of oxy-ethylene units by small angle neutron scattering on the time-of-flight spectrometer YuMO at the IBR-2 reactor in JINR. Preparing samples with a fully deuterated surfactant alkyl chain or a fully deuterated palmitoyl chain and varying the H_2O/D_2O content the scattering curves were obtained at 20 and 40 °C in the range Q = 0.06-0.1 $Å^{-1}$. In the Guinier approximation a linear fit reveals the bilayer thickness of POPC/$C_{12}E_2$(d25), $R_{S/L}$ = 1 of 3.84 nm at 25 °C and 3.76 nm at 40 °C. These values are in good agreement with the bilayer thicknesses of DMPC of 3.73 nm (1) or DPPC of 4.06 nm (2) studied under similar conditions using this approach. An asymmetric distribution of the components POPC and $C_{12}E_2$ in the bilayer of a unilamellar vesicle could not be detected in agreement with the model of packing effects of cone-shaped detergents in lipid bilayers (3). Next the surfactant headgroup volume will be increased for an asymmetric distribution to arise as proposed. Measurements of such samples are planned to be carried out within future allocated beam time.

1) D.M. Sadler, F. Reiss-Husson, E. Rivas, Chem. Phys. Lipids, 1990, 52, 41

2) V. I. Gordeliy, L.V. Golubchikova, A. Kuklin, A.G. Syrykh, A. Watts, Prog. Colloid Polymer Sci. 1993, 93, 252

3) H. Heerklotz, H. Binder, G. Lantzsch, G. Klose, A. Blume, J. Phys. Chem., 1997, 101, 639

TEMPERATURE-INDUCED MICELLE TO VESICLE TRANSITION IN THE DMPC/NAC SYSTEM: A SMALL-ANGLE SCATTERING STUDY

M. A. Kiselev[1)], P. Lesieur[2)], A. M. Kisselev[1)], S. Borbely[3)], T.N. Simonova[4)], L. I. Barsukov[4)]

[1)] *FLNP, Joint Institute for Nuclear Research, Dubna 141980, Russia*

[2)] *LURE, Université Paris-sud, F-91405 Orsay, France*

[3)] *Research Institute for Solid State Physics, Budapest, Hungary*

[4)] *Institute of Bioorganic Chemistry, Moscow, Russia*

Introduction

Mixed lipid/detergent systems are currently of great interest because of their wide use in membrane studies and, in particular, for solubilization and reconstitution of membrane proteins. Despite successful reconstitution of a great number of membrane functions, the molecular mechanisms and the thermodynamics of membrane assembly on reconstitution are still debated. The micelle to vesicle transition which represents an essential stage in the transformation of solubilized micellar aggregates into closed bilayer vesicles is of special interest in this respect.

In this work a model system, composed of dimyristoylphosphatidylcholine (DMPC) and sodium cholate (NaC), capable of temperature-induced micelle to vesicle transition has been studied by SANS and SAXS techniques. Data have been treated by using the theoretical frame of Guinier analysis[/1/]. The DMPC/NaC mixed system has been studied earlier via different techniques such as turbidimetry measurements, differential scanning calorimetry, electron microscopy and 31P NMR[/2/]. These studies have demonstrated that a number of various intermediates can be identified when the mixed system is undergoing TI-MVT, but the intermediates have not been characterized yet in sufficient details both structurally and morphologically. SANS measurements have been performed at the YuMO time-of-flight small-angle spectrometer in FLNP and at the small-angle spectrometer in Budapest Institute of Solid State Physics (ISSP). The results obtained at two spectrometers are in good agreement. The X-ray measurements have been carried out at D22 spectrometer (DCI synchrotron radiation source) in LURE, Orsay, France.

Results

The binary system consisting of 15 mM DMPC in H_2O buffer solution has well-known multilamellar structure. Presence of 2 mM NaC is sufficient to disturb regularities in the multilayer arrangement of the mixed lipid/detergent aggregates probably due to electrostatic repulsion induced by incorporation of the negatively charged NaC molecules into adjacent bilayers.

TABLE 1: The influence of NaC molar concentration C_{NaC} on the repeat distance d of the multilamellar structures are created in the system DMPC/detergent/water at T=35°C.

C_{NaC}, mM	0.00	0.25	0.50	0.75	1.00	2.00
d Å,	62.8 ±0.6	63.0 ±0.6	64.1 ±0.7	65.0 ±0.7	69.9 ±1.6	absent

Figure 1 and Figure 2 demonstrate the coincidence of experimental curves with Guinier law for the rod-like micelles at T=20°C and for the vesicles at T=50°C for the transitional system with 6 mM NaC.

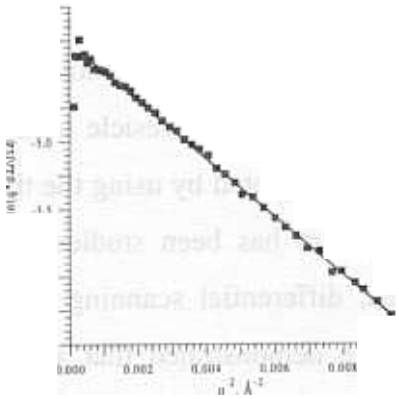

Figure 1. *SANS data (squares) from rod-like micelles: R_C=20.7Å, ellipsoidal cross-section with minor semi-axis 18.8 Å and major semi-axis 36.9 Å. Transitional system 15 mM DMPC and 6 mM NaC in D_2O at T=20°C.*

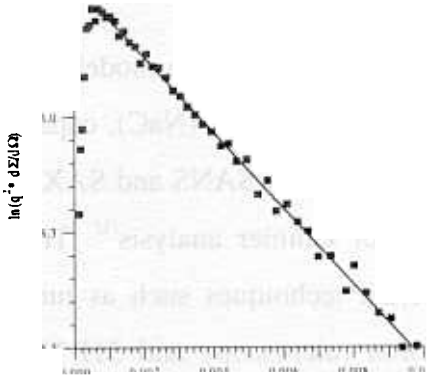

Figure 2. *SANS data (squares) from large unilamellar: R_l=9.1 Å, d_l=31.5 Å. Transitional system 15 mM DMPC and 6 mM NaC in D_2O at T=50°C.*

TABLE 2: Geometry and size of the aggregates for 15 mM DMPC and 6 mM NaC in D_2O. Here, RLM stands for rod-like micelles with a ellipsoidal cross-section and semi-axes a and b, and UV stands for unilamellar vesicles which bilayer has a thickness d_l.

T (C)	20	24	28	30	33 - 40	45	50	60
Type of particle	RLM	RLM	RLM	RLM	not determined	UV	UV	UV
Size, Å a,b	18.9, 36.9	18.2, 34.8	17.4, 34	17.2, 32.5	-			
or d_l						30.5	31.5	32.2

Conclusions

Morphological transformations occurring in the structure of supramolecular aggregates formed in the DMPC/sodium cholate/water have been investigated by neutron and X-ray scattering. The transformation of ellipsoidal micelles to lamellar structures through the formation of rod-like micelles has been established.

At a constant temperature T=20°C when the sodium cholate concentration is increasing, the vesicles observed for a detergent concentration C_d=2 mM are transforming to rod-like micelles for C_d=6 mM and then to ellipsoidal micelles for C_d=12 mM.

When the temperature is increasing with a constant concentration of detergent in the solution C_d=6 mM a transition from rod-like micelles with ellipsoidal cross-section observed below 28°C to unilamellar vesicles observed above 40°C occurs. A change in morphology of the particles occurs in a broad domain of temperatures from 33°C to 40°C that lays essentially higher than the temperature of the main phase transition of DMPC T_{ph}=23.5°C.

The ellipsoidal shape of sphere-like micelles and ellipsoidal cross-section of rod-like micelles have been calculated from SANS measurements as favorable compared with ideal spherical geometry of micelles.

References

(1) Dubnickova, M.; Kiselev, M.; Kutuzov, S.; Devinsky, F.; Gordeliy, V.; Balgavy, P. *Gen. Physiol. Biophys.* **1997**, 16, 175-188.

(2) Polozova, A.I.; Dubachev, G.E.; Simonova, T.N.; Barsukov L. *FEBS Lett.*, **1995**, *385*,

Structural model of the 30S subunit of a ribosome *Thrmus thermophilus* by small-angle scattering

Lixin Fan[1], I. N. Serdyuk[1], D. Svergun[2,3], V.V. Volkov[2], R. Gilles[4], A. Wiedenmann[4] and R. May[5]

[1]*Frank Laboratory of Neutron Physics, JINR, 141980 Dubna, Moscow Region, Russia*
[2]*Institute of Crystallography, Russian Academy of Sciences, Moscow, Russia*[3]
[3]*EMBL, Hamburg Outstation, Notkestraße 85, D-22603 Hamburg, Germany*
[4]*Berlin Neutron Scattering Center, Glienicker Str.100, D-14109 Berlin-Wannsee, Germany*
[5]*Institut Laue-Langevin, Grenoble, France*

The structure of ribosomes which are the nucleoprotein complexes responsible for protein synthesis is of great importance for the understanding of the process of protein synthesis itself. Although the structure of the ribosome has been investigated by various methods over three decades, the problem of determining its structure with a sufficiently high three-dimensional resolution has not been solved yet. Recently, models for the 70S ribosome and its subunits with the resolution about 25Å resulted from creo-electron microscopy and they describe the outer surface of the particle [1,2]. The contrast between the robosomal proteins and the rRNA in these studies is low making it difficult to distinguish between ribosomal components. The new method of SAS data interpretation was applied for studying the 70S ribosomal subunit from E.coli in solution using X-ray and neutron contrast variation. A solid body four-phase model of the 70S ribosome at 35Å resolution was built from the envelope functions of the 30S and 50S subunits and of the corresponding RNA moieties [3]. In this work, neutron scattering experiments were performed applying contrast variation to analyse the structure of the 30S ribosomal from *Th.thermophilus* including the protein-RNA-distribution. Using the new method of SAS data interpretation we derive a tree-dimensional model of the 30S ribosomal subunit from *Th.thermophilus* and its RNA-rich core at the resolution about 35Å.

Two types of ribosomal particles from Th. Th. ware obtained by the technique of methabolic regulation of selective deuterium incorporation into the RNA and the protein components of the ribosome (See table 1) and they were studied by small-angle neutron scattering using contrast variation. The indegnity of partially deutereated particles was controlled by parallel X-ray measurements.

Before SANS measurements the preparations were dialysed against a buffer containing 20 mM Tris-HCl (pH 7.6), 0.5 mM $MgCl_2$, 100 mM KCl. Buffers containing 0, 20, 32,35, 40,72, 80, 98% D_2O were used for contrast variation. The sample with the highest D_2O concentration was prepared by dialysis. The D_2O content was controlled by density and transmission measurements.

SANS measurements were carried out with the YUMO instruments(JINR, Dubna)[4], D11 instruments (ILL, Grenoble)[5] and V4 instruments[6] (HIM, Berlin) at different sample-detector distances and concentrations. 17 neutron scattering curves of different types of ribosomal particles at eight contrasts have been obtained. The radiation X-ray scattering data were collected following standard procedures using the X33 camera of EMBL on the storage ring DORIS III of the Deutsches Elektronen Synchrotron (DESY)[7]

The neutron contrast variation data for the 30S ribosomal subunit of Th. Thermophilus in solution are interpreted in the frame of a two-phase model described by the shapes of the 30S subunit and its RNA-rich core using spherical harmonics. The X-ray and neutron

scattering curves measured at eight different contrasts can be neatly fitted with those evaluated from the two-phase model (see fig.1 a,b,c). The shape of the envelope of the 30S subunit and of the RNA- rich core are evaluated with the resolution 35Å. The final model is presented in Fig 2. A comparison with an analogous model for E.coli [3] shows that the shapes of the RNA component coincide completely in both subunits, whereas the shapes of the protein component are slightly different (See fig. 3).

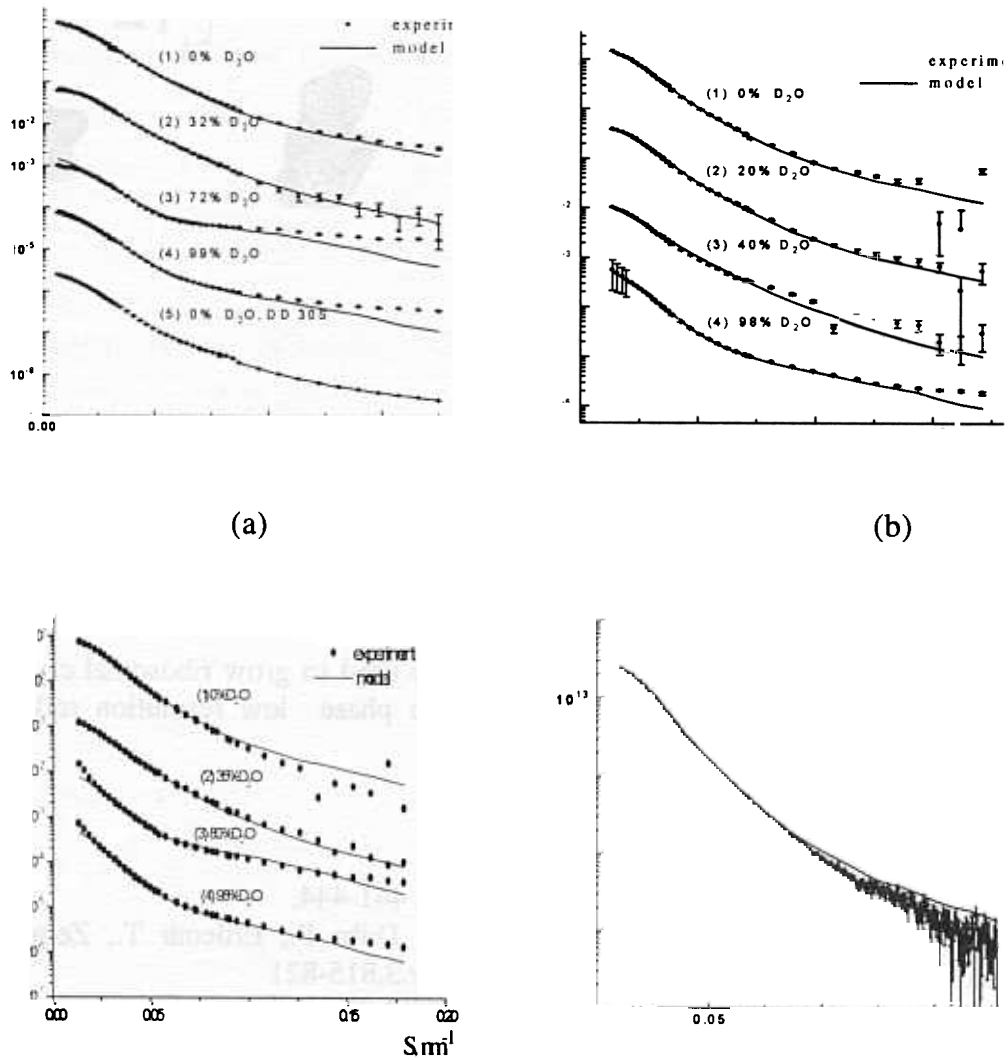

(a) (b)

(c) (d)

Fig.1 Fitting of the neutron((a) to (c)) and X-ray (d) solution scattering data with the two-phase model shown in fig.2

Table Two types of ribosomal particles for neutron and x-ray scattering experiments

Type of particle	Growth medium	Contribution to neutron scattering
30S(I)	H_2O, [^{1}H]-glycerol and [^{1}H]-succinate	both RNA and protein
30S(II)	D_2O, [^{2}H]- glycerol and [^{2}H]- succinate	shape scattering

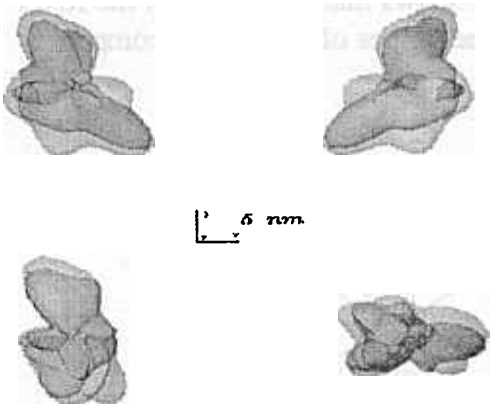

Fig2. Two - phase model with the resolution 3.5 nm for the subunit of the ribosome Th. Th and its RNA (in side). The 30S subunit is displayed in dark yellow and its RNA in dark green.

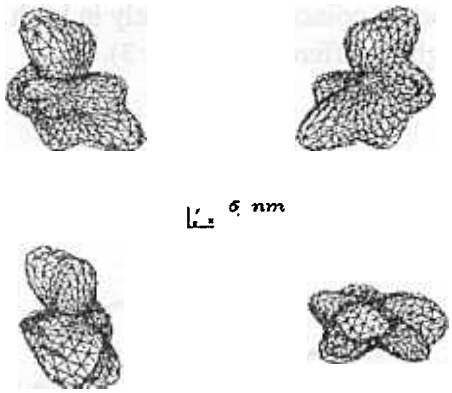

Fig 3. Comparison of the 30S Th. Th and 30S E. coli models. The 30S Th.th is displayed in blue and 30S E.coli is displayed in red.

The *Thermus thermophilus* species are extensively used to grow ribosomal crystals. Our results open the possibility to use this model to phase low resolution reflections in ribosomal crystallography.

Reference

[1]Frank J., Agraval R. K. - Nature, (1995), v.375, 441-444.
[2]Stark H., Mueller F., Orlova V., Schatz M., Dube P., Erdemir T., Zemlin F., Brimacombe R., van Heel M. - Structure, (1995), v.3,815-821
[3]D.I. Svergun, Bukhardt, at al. J. Mol. Biol. (1997) 271, 588-618.
[4]Yu.Ostanevich, Macromol. Chem. Macromol. Symp. (1988), 15, 91-103.
[5]Keiderling, U., Wiedenmann, A. and Wagner, W. Proceedings of Intern. Seminar on Structural Investigation on Pulsed Neutron Source, Dubna, 1-4 September. (1992)
[6]Ibel K. J.Appl. Cryst., (1976), 9, 630-643
[7]Koch, M. H. J. & Bordas, J. . X-ray diffraction and scattering on disordered systems using synchrotron radiation. *Nucl. Instrum. Meth.* (1983), **208**, 461-469.

SANS study of three-layer micelles of an ABC block copolymer

J. Pleštil, H. Pospíšil, M. Steinhart, J. Kříž, B. Masař

Institute of Macromolecular Chemistry, Academy of Sciences the Czech Republic
Heyrovský Sq.2, 162 06 Prague 6, Czech Republic, http://www.imc.cas.cz

This report is the SANS part of the article[1] submitted to Macromolecules.

Introduction

Micelles formed by amphiphilic block copolymers in water have been the object of intensive study both from the point of view of theoretical interest and their potential applicability as surfactants or systems for controled release of drugs or other active substances. For the latter use there is a need of maximum solubilization capacity of the micellar core combined with tailored permeability of the solubilizate across the core-shell interface. In our previous studies[2] of micelles of poly(methyl methacrylate)-*block*-poly(acrylic acid) (PMMA-PAAc) copolymers in water, we showed that both the rate and equilibrium degrees of solubilization are mostly controlled by the interaction parameter of the solubilizate with the polymer block prevailing in the core. Solubilizates with good affinity to the core polymer are thus easily solubilized but, as a rule, they are also easily released from the micelle. Micelles with structured cores containing at least two concentric layers of polymers with different permeability or affinity to the chosen solubilizate are thus of some interest.

One of the possible solutions to this problem are micelles based on ABC triblock copolymers in which all three blocks are mutually incompatible, A and B being hydrophobic and C – hydrophilic. As an example of such system, we examine here poly(2-ethylhexyl acrylate)-*block*-poly(methyl methacrylate)-*block*-poly(acrylic acid) (PEHA-PMMA-PAAc) copolymers and micelles formed by them in water.

Experimental

Block copolymers and micellar solutions

A PEHA-PMMA-PAAc copolymer was prepared by successive group transfer polymerization (GTP). After purification and characterization by size exclusion chromatography (SEC) and NMR the product was transferred into distilled water by dialysis and freeze-dried in the micellar form. For SANS experiments, the freeze-dried product was directly dissolved either in D_2O or distilled water.

SANS measurements

were performed using the time-of-flight small-angle neutron spectrometer YuMO[3]. The solution was placed in an optical quartz cell with a path length of 2 mm. All measurements were corrected for background scattering and normalized using a vanadium standard[4].

The experimental SANS curves were fitted by a scattering curve for homogenous spherical particles with a Schulz-Zimm distribution of radii. The theoretical fitting function was

$$P(q) = \int_0^\infty F(q,R)^2 f_Z(R)\, dR, \tag{1}$$

where the scattering amplitude for a sphere of radius R and scattering contrast $\Delta\varrho$ is

$$F(q,R) = \frac{4}{3}\pi R^3 \;\; \Delta\varrho \cdot \Phi(qR) \quad \text{with} \quad \Phi(qR) \quad 3 \cdot \frac{\sin(qR) - qR\cos(qR)}{(qR)^3}$$

The Schulz-Zimm distribution is a two-parameter function

$$f_Z(R) = \left(\frac{Z+1}{R_m}\right)^{Z+1} \;\; \frac{R^Z}{\Gamma(Z+1)} \cdot \exp\left[\;\; \left(\frac{Z+1}{R_m}\right) R\right],$$

where R_m is the mean radius, Z is the width parameter ($Z > -1$), and $\Gamma(x)$ is the gamma function. The fit was applied to the SANS curves taken under such contrast conditions that the scattering contribution of the micelle corona could be neglected or disregarded.

Results and discussion

The NMR results indicate segregation of the PEHA and PMMA blocks in a micelle. There are two possible structures (Fig.1) compatible with this finding: a) The PEHA blocks form an inner core surrounded by the PMMA layer (three-layer model); b) The PEHA blocks are located in several smaller domains in a PMMA matrice (multi-domain model). In principle, SANS can discriminate between these two models by measuring the size of the whole micellar core (formed by PMMA and PEHA) and of its PEHA constituent.

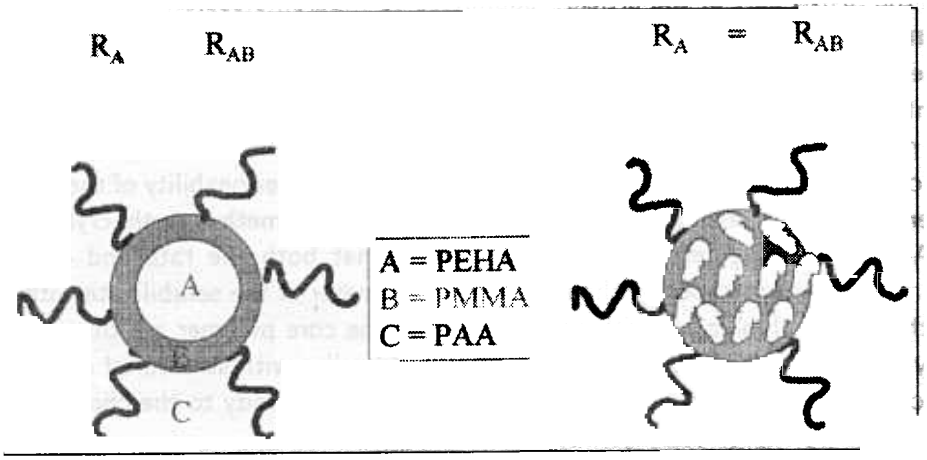

Fig.1: The three-layer model and the multidomain model of micelles.

For the three-layer model, the radius of the PEHA component, R_A, would be smaller than the overall radius of the micelle core, R_{AB}, while for the multidomain model the radii are expected to be very close to each other. The neutron scattering densities were calculated to be $\varrho_A = 0.3 \cdot 10^{10}\,\mathrm{cm}^{-2}$ and $\varrho_B = 1.1 \cdot 10^{10}\,\mathrm{cm}^{-2}$ and for PEHA and PMMA, respectively. This difference in scattering densities enables one to suppress the scattering contribution of one of the components while keeping scattering from the other component still visible. The scattering density of the third component, PAAc, depends on the degree of neutralization and on the H/D ratio in the H_2O/D_2O mixture. Using the partial molar volume of PAAc[5], $\overline{V} = 46.7\,\mathrm{cm}^3/\mathrm{mol}$ and its change upon neutralization[6], $\Delta\overline{V} = -14.6\,\mathrm{cm}^3/\mathrm{mol}$, we estimated the scattering densities of the H_2O/D_2O mixture matching those of PAAc to be $\varrho_0 = 2.8 \cdot 10^{10}\,\mathrm{cm}^{-2}$ and $\varrho_0 = 3.8 \cdot 10^{10}\,\mathrm{cm}^{-2}$ for the acidic and fully ionized forms, respectively. The contribution of condensed Na counterions was not taken into consideration in the latter quantity.

The micelle comprising an ABC triblock copolymer is a three-component particle with constituents differing in scattering density. Therefore, when the scattering density of the solvent is chosen to match the scattering density of one of the blocks there still remain two types of bloks contributing to the scattering. This circumstance complicates interpretation of the SANS curves. Fortunately, in some cases the influence of the second not matched component is either small or limited to a certain part of the scattering curve and the structural parameters related to the investigated component can be estimated.

In this work we attempted to distinguish between the two above given models by measuring the radii R_A and R_{AB}. To this end we used the SANS curves taken for the aqueous solvents with the scattering densities matching the scattering density of PMMA and PAAc, respectively. The corresponding radii were determined using the formulae valid for homogeneous spheres (Eq.1). For the above mentioned reason this approach represents only an approximative way to the structural characteristics of three-component particles.

Fig.2 shows the SANS curves of the micellar solutions in the H_2O/D_2O mixtures matching the scattering density of the PAAc corona (upper curves) or that of PMMA chains in the core (bottom curves). The solid lines are least-square fits by equation 1.

The fits of the curves recorded at zero contrast for the PAAc chains lead to the mean core radii $R_{AB} = 120(2)$ Å for the acidic form and $R_{AB} = 117(2)$ Å for fully neutralized PAAc. A good agreement of these results obtained at different scattering contrasts suggests that the two-component nature of the micelle core does not influence dramatically scattering behaviour at these contrasts.

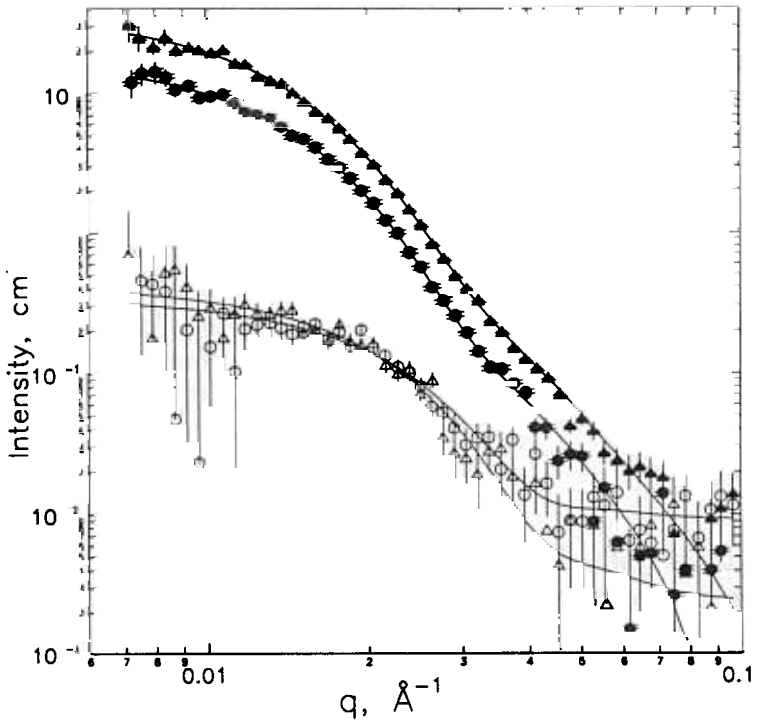

Fig.2: Experimental SANS curves (points with error bars) for the PEHA-PMMA-PAAc micelles in H_2O/D_2O mixtures for acidic (○, •) and sodium neutralized PAAc (△, △). The copolymer concentration c=0.00465 g/ml.
Upper curves: zero contrast of the PAAc corona (acidic form: 49% D_2O (•), neutralized form: 63% D_2O (△)).
Bottom curves: zero contrast for PMMA (24% D_2O, acidic form (○), neutralized form (△)).
Solid lines are least-square fits to Eq.1.

The SANS curves obtained for the matched PMMA scattering density (24% D_2O) do not show any significant difference between the results for acidic and neutralized PAAc. This indicates that the scattering contribution of the PAAc corona is not too large, because its two states examined differ in scattering power. Therefore, the SANS curves reflect mainly the structure of the PEHA component. From the fit to Eq.1 we obtained $R_A = 89(10)$ Å and $R_A = 91(10)$ Å for the sample with acidic and sodium-neutralized PAAc corona, respectively. Low scattering intensities of the SANS (see Fig.2) data lead to great uncertainty in the values of the fitting parameters. Nevertheless, the mean radius of the PEHA component, R_A, seems to be significantly smaller than the overall radius of the micelle core, R_{AB}. Thus the SANS results point to the three-layer model rather than the multidomain one.

In determination of R_{AB} we neglected the difference in the scattering densities of PMMA and PEHA. Similarly, the radius R_A was estimated using the assumption that the relevant part of the SANS curve is not affected by the scattering from the PAAc corona. To assess the influence of these approximations on the resulting radii, we calculated scattering curves of a coated sphere and of a micelle model with Gaussian chains attached to a spherical core. The latter model was recently proposed by Pedersen and Gerstenberg[7]. The model parameters were chosen so as to describe the studied ABC micelles at the particular contrast conditions. The calculations show that the simlifying assumptions do not affect the above conclusions concerning the micelle internal structure.

A more detail discussion of this problem is given in the paper submitted for publication[1].

References

1. Kříž, J.; Masař, B; Pleštil, J; Tuzar, Z.; Pospíšil, H.; Doskočilová, D.; Macromolecules, in press.
2. Kříž, J.; Masař, B; Pospíšil, H; Pleštil, J; Tuzar, Z.; Kiselev, M.A.; Macromolecules 1996, 29, 7853.
3. Ostanevich, Yu.M.; Makromol. Chem., Macromol. Symp. 1988, 15, 91.
4. Pleštil, J.; Ostanevich, Yu.M.; Bezzabotnov, V.Yu.; Hlavatá, D.; Polymer 1986, 27, 1241.
5. Tondre, C.; Zana, R.; J.Phys.Chem. 1972, 76, 3451.
6. Ikegami, A.; Biopolymers 1968, 6, 431.
7. Pedersen, J.S.; Gerstenberg, M.C.; Macromolecules 1996, 29, 1363

Joint use of X-ray diffraction in crystals and small-angle scattering in solutions to determine the three-dimensional structure of the 70S ribosome

I.V.Shcherbakova[1], S.Ch.Agalarov[1], O.M.Selivanova[1], A.S.Spirin[1], V.L.Aksenov[2], L.Fan[2]
I.N.Serdyuk[2], D.I.Svergun[3], V.V.Volkov[3], V.Lyamzin[4], M.Koch[4], K.Wilson[5], R.May[6]

[1]*Institute of Protein Research, RAS, Pushchino, Russia*
[2]*Frank Laboratory of Neutron Physics, JINR, Dubna, Russia*
[3]*Choubnikov Institute of Crystallography, RAS, Moscow, Russia*
[4]*European Molecular Biology Laboratory, Hamburg, Germany*
[5]*University of York, York, UK*
[6]*ILL, Grenoble, France*

Introduction

Ribosome, the site of protein synthesis in the cell, is a huge (molecular weight over 2 x 10^6 Da and size over 20 nm) ribonucleoprotein complex organized in two unequal subunits. Both subunits contain dozens of proteins which comprise about one third of the ribosomal mass; the other two thirds are occupied by the RNA moieties. With recent achievements in cryoelectron microscopy and X-ray crystallography, modern structural ribosomology approached a resolution of 1.5-2 nm in restoring of the ribosomal surface [1, 2]. Unfortunately, the method cannot determine the structure of ribosomal RNA and protein moieties in the ribosome because of small differences in the electron density of RNA and protein. Another way to solve the problem of mutual arrangement of different components of the ribosome is decoding of the diffraction patterns of the ribosome crystal. However, there is no algorithm for solution of phase problem of large complexes. We propose to phase diffraction patterns using four phase model of ribosome obtained from neutron scattering experiments. The neutron scattering curves are to be obtained in a wide interval of scattering vectors and contrasts.

Biosynthetic selective deuteration

Efficient application of the neutron scattering method for the study of the detailed structure of the ribosome strongly depends on the possibility of selective deuteration of its RNA and protein components. The standard way for solving this problem has been to study hybrid isotopic particles obtained by reconstitution from protonated and deuterated components [3]. This approach is time consuming and expensive. Moreover, the reconstitution procedure is well developed only for *E.coli* ribosomal particles, whereas most current structural research is performed on ribosomes from thermophilic and halophilic microorganisms because they are much more stable and crystallize more readily. Growing microbial culture on media with different D_2O content suggests a powerful way for solving the problem of deuterium incorporation. However, it does not lead to a significant change in the relative contrast (ratio of scattering amplitude densities) of the ribosomal RNA and protein components [4]. The only way of contrasting different components is to use a combination of protonated and deuterated substrates during the growth rather than a monosubstrate.

The aim of this part of our study is to develop a general approach to the RNA and protein labelling problem based on metabolic regulation. Applied to ribosomes, this approach has allowed to obtain a set of particles with different ratios of scattering amplitude densities of the RNA and protein components suitable for neutron measurements in 95 - 100 % D_2O where the incoherent background is very low, and good quality data can be obtained for relatively large scattering vector values.

It is known that prokaryotic cells utilise costly substrates (from the point of view of intracellular energetics) as direct precursors of biomacromolecules. However, substrate concentrations play the key

role in the growth. For example, a substrate in excess will be involved by the cell in different catabolic pathway transformations with simultaneous energy release.

Selective [^{2}H] incorporation into the RNA and protein components of the ribosome during cell growth was monitored by [^{1}H]-NMR as a function of the nucleoside concentration and the medium D_2O percentage in the presence of [^{1}H] or [^{2}H]succinate and glycerol. It is demonstrated that for the concentration of nucleosides up to 1.2 mM, nucleoside is essentially incorporated directly into RNA with a negligible crossover into the protein (Fig. 1) as well as a negligible incorporation into RNA of deuterium from either glycerol and succinate substrates (Table 1) or water (Fig.2).

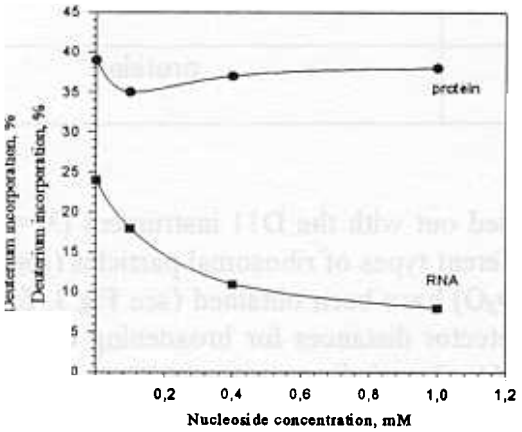

Figure 1. Incorporation of deuterium into different components of the ribosome at various nucleoside concentrations in the growth media containing 65% D_2O, H-glycerol and H-succinate.

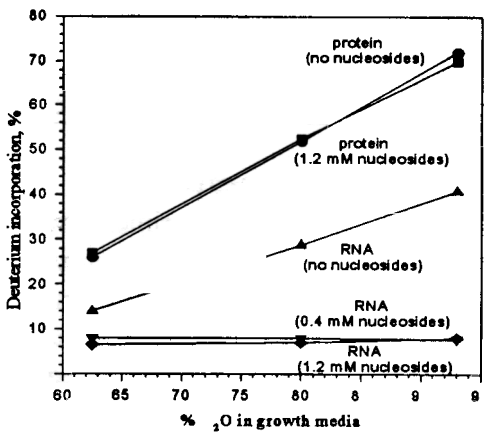

Figure 2. Incorporation of deuterium into the RNA and protein components of the ribosome when *E.coli* is grown in a media containing different percentages of D_2O and different concentrations of H-nucleosides; H-glycerol and H-succinate are used as carbon sources.

Table 1. Ribosomal RNA and protein components with different match points obtained by biosynthetic selective deuteration

Growth media	Deuterium incorporation into nonexchangable residues of proteins		Deuterium incorporation into nonexchangable residues of RNAs	
	% (NMR studies)	calculated match point	% (NMR studies)	calculated match point
10% D_2O, [^{1}H] glycerol, [^{1}H] succinate, 1 mM [^{1}H]nucleosides	2	42	0	70
25% D_2O, [^{1}H] glycerol, [^{1}H] succinate, 1 mM [^{1}H]nucleosides	3	42	2	72
10% D_2O, [^{2}H]glycerol, [^{2}H] succinate, 1 mM [^{1}H]nucleosides	47	82	1	71
25% D_2O, [^{2}H]glycerol, [^{2}H] succinate, 1 mM [^{1}H]nucleosides	60	93	2	72

Table 2 presents the characteristics of the four types of ribosomes and ribosomal subunits obtained in large amounts for neutron scattering experiments by means of biosynthetic deuteration. The percentage of deuterium incorporation in the RNA and protein components varies significantly.

Table 2. Four types of ribosomal particles for neutron scattering experiments

Type of particle	Growth medium	Contribution to neutron scattering in D_2O
I	H_2O, [^{1}H] glycerol and [^{1}H]succinate	both RNA and protein
II	D_2O, [^{2}H] glycerol and [^{2}H]succinate	shape scattering
III	25% D_2O, [^{2}H] glycerol, [^{2}H] succinate and [^{1}H] nucleosides	RNA
IV	25% D_2O, [^{1}H] glycerol, [^{1}H] succinate and [^{2}H] nucleosides	protein

Small–angle neutron experiments

Small–angle neutron scattering experiments were carried out with the D11 instrument (λ = 6 Å) (ILL, Grenoble, France). 28 neutron scattering curves of different types of ribosomal particles (see Table 2) at four contrasts (H_2O, 32% D_2O, 72% D_2O and 98% D_2O) have been obtained (see Fig.3, for example). The curves are measured at three different sample–detector distances for broadening of the scattering vectors interval. For samples with a low concentration (1 - 2 mg/ml) measurements are carried out at the 10 m distance. Samples with high concentrations (20 - 35 mg/ml) are measured at 3.6 m and 1.2 m distances.

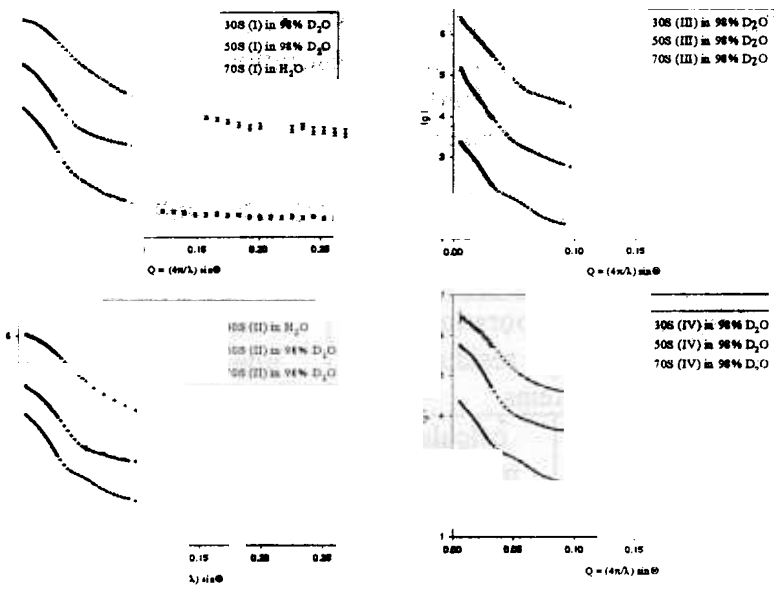

Figure 3. Small–angle scattering curves of different types of the ribosomes and ribosomal subunits at different contrasts.

At the moment the data are used for three–dimensional structure reconstitution to obtain a low resolution model of a bacterial ribosome which will be the basis for further refinement using diffraction patterns of the ribosome crystals.

Crystallographic studies

Stable crystals of appropriate sizes (0.2–0.3 mm) (Fig.4) were obtained. Low and middle resolution diffraction patterns (Fig.5 and Fig.6, correspondingly) were collected on the X11 beam line at EMBL Hamburg outstation using the synchrotron radiation monochromatic wavelength 0.928 Å and a MAR research imaging plate scanner. It is shown that the crystals have a tetragonal space group P43212 or P41212. The cell parameters were 521x521x389 Å. About 2300 reflections were measured.

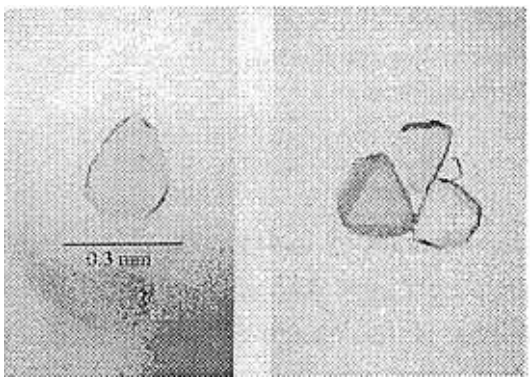

Figure 4. Crystals of *Thermus thermophilus* ribosomes.

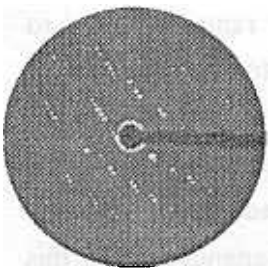

Figure 5. Low resolution diffraction pattern of the *T.thermophilus* ribosomes. Resolution– 150–70 Å

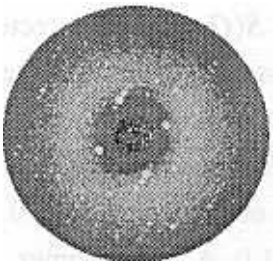

Figure 6. Middle resolution diffraction pattern of the *T.thermophilus* ribosomes. Resolution– 70–23 Å

The obtained diffraction patterns show good agreement with the small–angle X–ray scattering data obtained for solution.

Conclusions

The method of selective deuteration of RNA and protein components of the ribosome in the process of growing has been developed.

Four types of ribosomal particles with a significantly varying percentage of deuterium incorporation into the RNA and protein components are isolated for neutron scattering experiments. The small–angle neutron scattering curves have been measured in a wide interval of scattering vectors and contrasts of particles.

Crystals of *Thermus thermophilus* ribosomes suitable for X–ray diffraction studies are obtained. Low and middle resolution diffraction patterns of the crystals have been collected in the interval of Bragg distances from 150 to 23Å.

References

1. Frank J., Agraval R.K.– Nature, 1995, v.375, 441-444.
2. Stark H., Mueller F., Orlova V., Schatz M., Dube P., Erdemir T., Zemlin F., Brimacombe R., van Heel M. - Structure, 1995, v.3, 815-821.
3. Nierhaus K.H., in *Ribosomes and Protein Synthesis,* IRL Press Oxford, 161-189 (1990)
4. Moore P.B. - Methods in Enzymology, 1979, v.LIX, part G, 639-655.

Study of the phonon-maxon region in the liquid helium excitation spectrum

K.H.Andersen[1], I.V.Bogoyavlenskii[2], V.G.Kolobrodov[2], A.V.Puchkov[3], A.N.Skomorokhov[4]

[1]*Institute Laue-Langevin, Grenoble, France;*
[2]*Kharkov Institute of Physics and Technology, Kharkov, Ukraine;*
[3]*Institute of Physics and Power Engineering, Obninsk, Kaluga Region, Russia,*
[4]*Joint Institute for Nuclear Research, Dubna, Moscow Region, Russia.*

The experiment is a continuation of liquid helium-4 studies by inelastic neutron scattering carried out on the spectrometer DIN-2PI [1,2]. In accordance with the results of the last experiment and the present-day theoretical conception in this range of wave vectors and temperatures, a partite exhibition of modes of quite different nature is possible.

On the basis of the new analysis of our previous ^{4}He neutron scattering data some additional intensities in $S(Q,\omega)$ were detected at $\omega>\omega_0$ over the wavevector range from 0.4 to 1.2 Å^{-1} [2]. This intensity exhibit both the temperature and the wavevector dependence. It increases as the temperature rises to the superfluid transition temperature T_λ. At the same time, this intensity is not observed at small Q but it becomes visible at Q higher than ~0.4 Å^{-1}. The maximum intensity is observed at 0.55-0.62 Å^{-1}. As Q increases this additional intensity decreases, and at Q>1.0 Å^{-1} it becomes indistinguishable. Such Q-T dependence of this intensity would rather be taken to identify the band in our data as a broad remnant zero-sound mode, as expected from the work of Glyde and Griffin [4,5].

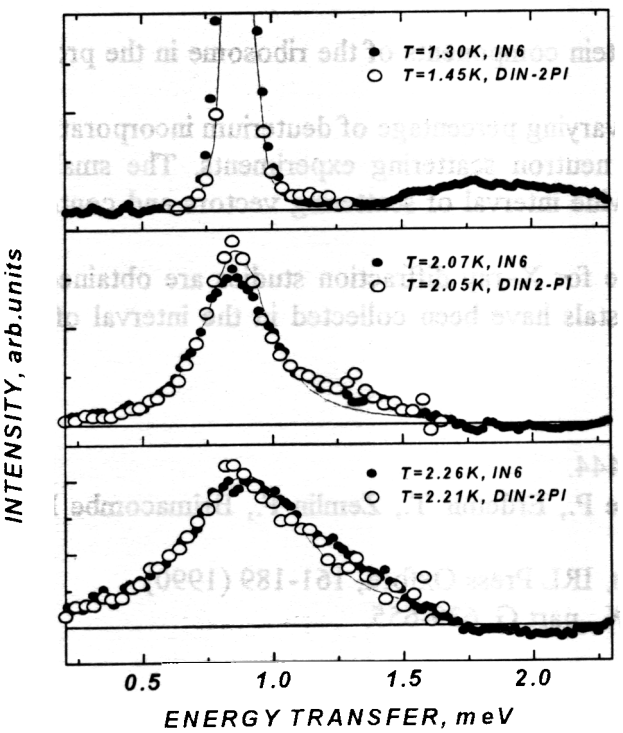

Fig.1. *Comparison of $S_1(Q,\omega)$ obtained on the spectrometer DIN-2PI (Dubna) [2] and IN6 (Grenoble) [3] at Q=0.55 Å^{-1} and closely spaced temperatures. To obtain the one-phonon part of $S(Q,\omega)$ for the IN6 data at T=2.07 and T=2.26 K, the multiphonon part was removed from the experimental spectra according to the simple multiphonon subtraction procedure. The figure shows that after the subtraction of the multiphonon part from total $S(Q,\omega)$, $S_1(Q,\omega)$ of the IN6 data contains some additional intensity which coincides with those observed in the DIN-2PI data.*

Experimental studies of $S(Q,\omega)$ in this Q-ω range by other authors are significantly discrepant [6,7]. Note, that the comparison of the experimental results [3] and our data [2] (fig.1) is the evidence in favor of the assumption that $S_M(Q,\omega)$ contains the intensity which cannot be explained solely as multiphonon scattering. We hope that the study performed will be the experimental test of recent theoretical predictions.

The yielded spectra of the double cross section within the energy transfer range 0.1-2.0 meV and the angular range from 3 to 102 degrees and T=1.53, 1.81, 1.96, 2.1 and 2.22K. Our experiment focused on the measurement at temperatures quite close to the temperature of the superfluid transition and the range of wave vectors between the phonon and maxon regions of the dispersion curve of liquid helium. This experiment was performed at low initial neutron energy (2.37 meV) and decreasing angular uncertainties that provided a high resolution of the experiment. The exposition time for each measured temperature was about 72 hours. The range of scattering angles (3-102 degrees) provides rather a wide range of neutron wave transfer (0.2-1.2 $Å^{-1}$). The raw time of flight experimental data will be transformed into the $S(Q,\omega)$ data for further analysis. The analysis will be carried out using various model of $S(Q,\omega)$ (Glyde-Griffin model, simple subtraction model, Woods-Svensson analysis). To analyze these data, it is necessary to conduct the $S(Q,\omega)$ measurements at low temperature, <1.0K, as well.

References

1.N.M.Blagoveshchenskii, Zh.A.Kozlov et al Phys. Rew. B **50** (1994) 16550

2.N.M.Blagoveshchenskii, I.V.Bogoyavlenskii, L.V.Karnatsevich, A.V.Puchkov, and A.N.Skomorokhov J.Low Temp. Phys. (Sov.), **23** (1997) 374

3.K.H.Andersen, W.G.Stirling, R.Scherm, A.Stunault, B.Fåk, H.Godfrin and A.J. Dianoux, J.Phys.:Condens. Matter **6** (1994) 821

4.H. Glyde, *Excitations in liquid and solid helium*, Clarendon Press., Oxford, (1994), p. 232.

5.H.R.Glyde and A.Griffin, Phys. Rev. Lett. 65 (1990) 1454

6.R.M.Crevcoeur, H.M.Smorenburg, I.M. de Schepper, W.Montfrooij, and E.C.Svensson, *Czech. J. of Phys.* **46** 257 (1996).

7.G.Zsigmond, F.Mesei, C.J.Carlile, Physica B (ECNS'96), in press.

Neutron Scattering Study of Pyridinium Salts

L.Bobrowicz-Sarga[1,2], P. Czarnecki[1], J.Wąsicki[1], T.Sarga[2,3], I. Natkaniec[2,3]

1. Institue of Physics, A. Mickiewicz University, 61-614 Poznań, Poland
2. Frank Laboratory of Neutron Physics, JINR, 141980 Dubna, Russia
3. H.Niewodniczański Institute of Nuclear Physics, 31-342 Kraków, Poland

Pyridine, a strong organic base, easily reacts with many acids to form an interesting family of pyridinium compounds. A number of pyridinium salts reveal solid - solid phase transitions related to a change in the motional behaviour of the cation. Most interesting transitions have been found in the recently discovered new family of ferrelectric crystals formed by pyridinium tetrafluoroborate and pyridinium perchlorate [1,2] only.

We present the results of our neutron scattering studies of pyridinium nitrate $[C_5NH_6]^+[NO_3]^-$, pyridinium perchlorate $[C_5NH_6]^+[ClO]^-$ and pyridinium tetrafluoroborate $[C_5NH_6]^+[BF_4]^-$ (hereafter reffered to as $PyNO_3$, $PyCLO_4$ and $PyBF_4$, respectively). We applied the elastic coherent neutron scattering (ND) method to complement the information on the crystal lattice parameters and inelastic incoherent neutron scattering (IINS) to study the molecular dynamics. ND and IINS spectra were measured as a function of temperature on the NERA time - of - flight spectrometer.

The neutron diffraction spectra for three phases of a polycrystalline $PYClO_4$ sample are given in Fig.1.

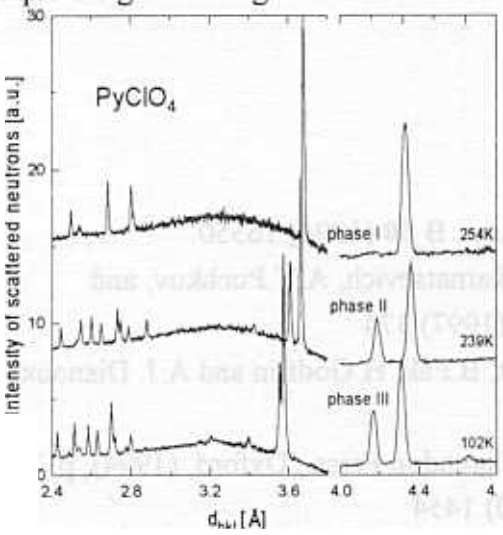

Fig.1.Neutron powder diffraction spectra of three phases of the $PyClO_4$ crystal.

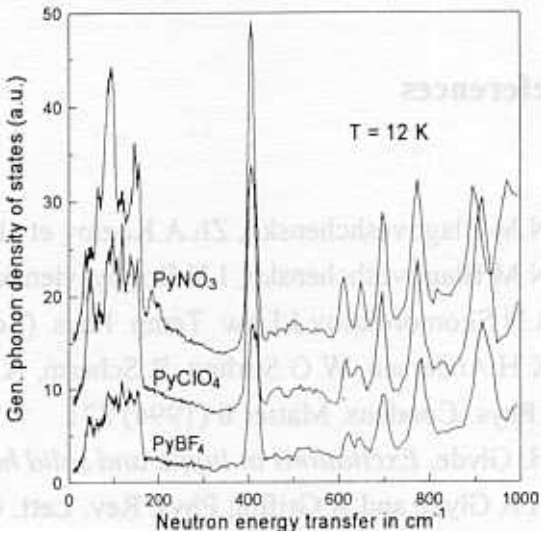

Fig.2. Generalized phonon density of states G (E) for pyridine salts.

Pyridinium perchlorate crystallising at room temperature in the rhombohedral system, space group R3m undergoes two phase transitions at 233 and 245 K [1]. The upper I - II transition is marked by a splitting and shifting of the diffraction peaks. A jump in dielectric permittivity at 245 K indicates that the crystal undergoes a discontinuous ferroelectric transition [2]. The II - III phase transition is probably marked only by a change

in the symmetry of the crystal. The phonon density of states functions G(ω) of $PyBF_4$, $PyClO_4$ and $PyNO_3$ in the energy transfer up to 1000 cm^{-1} are shown in Fig. 2. The spectra may be divided in two regions: the region of the lattice modes 0< E >300 cm^{-1} and the region of the intermolecular modes 300 cm^{-1} < E > 1000 cm^{-1}. The sharp band at about 400 cm^{-1} is associated with the out - of plane vibration of hydrogen in the pyridine ring.

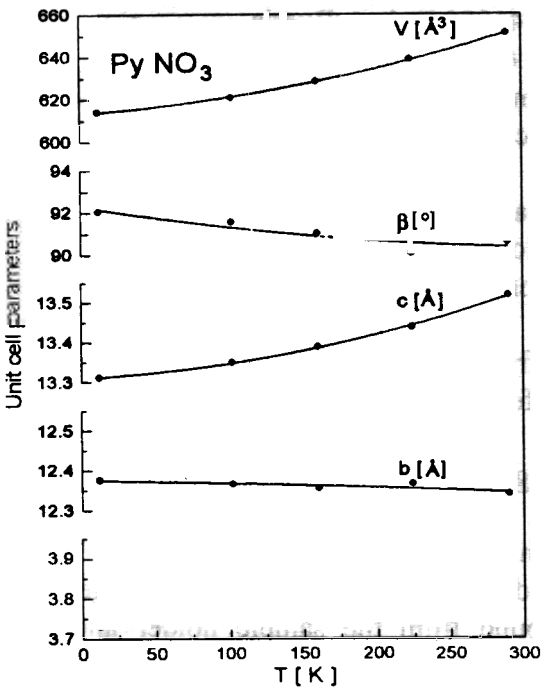

Fig.3 . Temperature dependence of the unit cell parameters of a $PyNO_3$ crystal.

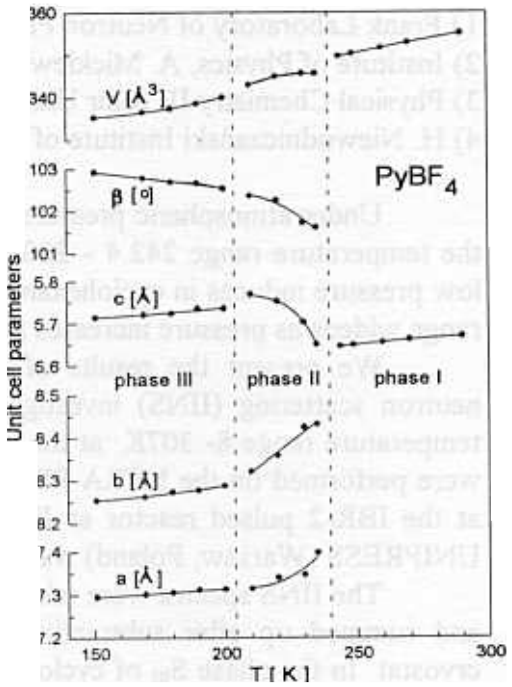

Fig.4. Temperature dependence of the unit cell parameters of a $PyBF_4$ crystal.

Figures 3 and 4 present the temperature dependencies of the unit cell parameters of $PyNO_3$ and $PyBF_4$, respectively. Pyridinium nitrate belongs to the group of salts in which the phase transition was not observed and crystallises in a monoclinic system, space group $P2_1/c$ [3]. As the temperature increases the values of the parameters a, c, and V increase while the values of b and the angle decrease. Pyridinum tetrafluoroborate undergoes two solid-solid transitions at 205 and 240 K. The intermediate phase is ferroelectric as in pyridinium perchlorate. At room temperature the system is trigonal, symmetry R3m. In the ferroelectric phase the system is trigonal, C2. The symmetry of the lowest phase is P2 [4]. The neutron powder diffraction spectra recorded from 140 to 300 K have been used for determining the unit-cell thermal expansion of the $PyBF_4$ crystal. The region of phase transitions was studied with particular care. All phase transitions are clearly seen in the temperature dependencies of the lattice parameters.

References:

1. P.Czarnecki, W. Nawrocik, Z. Pająk and J. Wąsicki, Phys.Rev.B, **49**, 151 (1994)
2. P.Czarnecki, W.Nawrocik, Z.Pająk and J.Wąsicki, J.Phys. Cond.Matter, **6**, 4955 (1994)
3. A.J.Serewicz, B.K. Robertson, E.A. Meyers, J.Phys.Chem., **69**, 1915 (19650
4. P. Czarnecki, J. Wąsicki, A. Katrusiak, C. Ecolivet, A.Girard, A.Belushkin, Physica B, **234-236**,102 (1997)

Neutron Scattering Study of Phase Transitions in Cyclohexanone

L. Bobrowicz-Sarga[1,2], W. Nawrocik[2], A. Würflinger[3], T. Sarga[1,4], S. Bragin[1]

1) Frank Laboratory of Neutron Physics, JINR, 141980 Dubna, Russia
2) Institute of Physics, A. Mickiewicz University, 61-614 Poznań, Poland
3) Physical Chemistry II, Ruhr University Bochum, Germany
4) H. Niewodniczański Institute of Nuclear Physics, 31-342 Kraków, Poland

Under atmospheric pressure two solid phases of cyclohexanone are known: S_I in the temperature range 242.4 - 220.3K and the low temperature phase S_{III}. A relatively low pressure induces in cyclohexanone an additional solid phase, S_{II}, whose temperature range widens as pressure increases [1].

We present the results of neutron diffraction (ND) and inelastic incoherent neutron scattering (IINS) investigations of different phases of cyclohexanone in the temperature range 8- 307K at the pressure 0.1, 130, and 300 MPa. The measurements were performed on the NERA-PR time - of - flight inverted geometry spectrometer [2] at the IBR-2 pulsed reactor at JINR in Dubna. The gas compressor GC-15 made by UNIPRESS (Warsaw, Poland) was used as a high pressure source.

The IINS spectra were taken at fourteen different scattering angles (average 90^0) and summed up after subtracting the background from the sample holder and the cryostat. In the phase S_{III} of cyclohexanone, at the temperature 8K, well resolved bands characteristic of an ordered crystal are clearly seen. At the temperatures 152K and 207K these bands are smeared but quasielastic broadening does not exist (Fig.1).

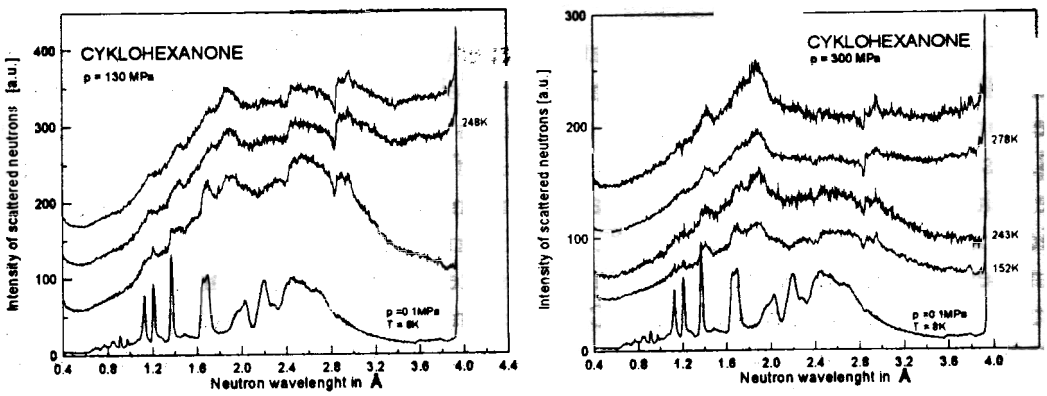

Fig. 1. Temperature dependencies of the IINS spectra of cyclohexanone.

After the phase transition to the phase S_{II} inelastic spectra become more smeared and quasielastic scattering caused by fast reorientation of protons in this phase is well observed. As the temperature increases, inelastic spectra become unresolved and look quite similar in both phases S_{II} and S_I. The measured IINS spectrum at 8K transformed into the function of the phonon state density weighted on the amplitudes of hydrogen atom vibrations is shown in Figure 2. Comprehensive interpretation of phonon

excitation spectra requires model calculations of lattice dynamics. Usually, the optical spectroscopy and crystal structure data are particularly useful for these calculations.Fig. 3 shows the neutron diffraction spectrum of cyclohexanone at 8K and the pressure 0.1 MPa.

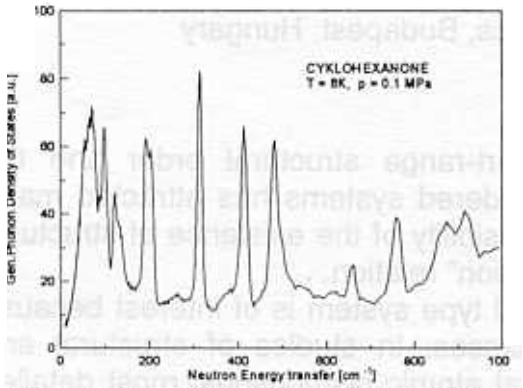

Fig. 2. Generalized phonon density of states of cyclohexanone

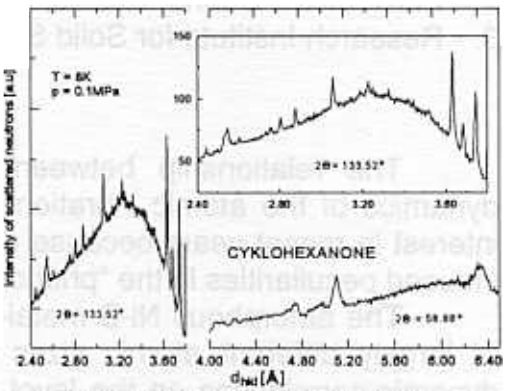

Fig. 3. Neutron diffraction spectrum of cyclohexanone at T=8K and p=0.1MPa

The neutron diffraction spectra of cyclohexanone measured upon heating of the sample are shown in Figures 4 and 5.

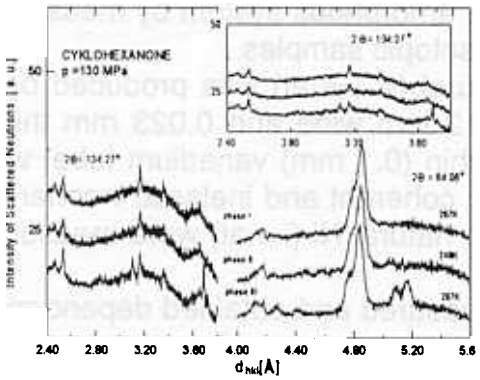

Fig. 4. Neutron diffraction spectra of cyclohexanone at p = 130 MPa

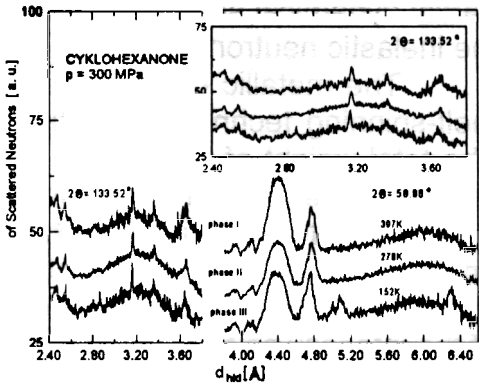

Fig. 5. Neutron diffraction spectra of cyclohexanone at p = 300 MPa.

The ND spectrum of the phase S_{II} at 248K (130 MPa) and 278K (300 MPa) is quite similar to the spectrum of the phase S_I at 267K (130 MPa) and 307K (300 MPa) taking into account the thermal compressibility of the crystal. No change in diffraction spectra is found for the S_{II} - S_I phase transition. Only phase transition S_{III} - S_{II} is clearly seen. The ND spectrum of phase S_{III} at 8K (ambient pressure), 152K (300 MPa) and 207K (130 MPa) is different from analogous spectra of phases S_{II} and S_I. The latter phase transition is marked by a change in the crystal structure and proton dynamics.

References:

1. A. Wurflinger and J. Kreutzenbeck, J. Phys. Chem.Solds.Vol.39, p.193- 196, 1978.
2. I. Natkaniec, S.I. Bragin, J. Brankowski, J. Mayer, Proc. ICANS-XII, Abingdon 1993, RAL Raport 94-025, Vol I.p. 89-96.

Partial dynamic structure factors for amorphous isotopic Ni-B alloys

S.N.Ishmaev[1], Natkaniec[2], E.Svab[3], L.S.Smirnov[2]

1. - RRC Kurchatov Institute, Moscow, Russia,
2. - FLNP JINR, Dubna, Russia,
3. - Research Institute for Solid State Physics, Budapest, Hungary

The relationship between the short-range structural order and the dynamics of the atomic vibrations in disordered systems has attracted major interest in recent years because of the possibility of the existence of structure-induced peculiarities in the "phonon-dispersion" relation.

The amorphous Ni-B metal-metalloid type system is of interest because of largely different atomic sizes and masses. In studies of structural and dynamic correlations on the level of partial atomic distributions, most detailed information can be obtained by neutron scattering methods employing samples with different isotopic contrast contents. Isotopic metallic glasses $^{i}Ni_{65}{}^{11}B_{35}$ (i=nat, 60, <b>=0) were investigated in our previous high-resolution neutron diffraction experiments [1] where the $S_{ab}(Q)$ partial static structure factors and $G_{ab}(r)$ radial distribution functions were determined.

The aim of the proposed experiment is the investigation of the $S_{ab}(Q,E)$ partial dynamical structure factors of the Ni-B amorphous system by measuring the inelastic neutron scattering on the same isotopic samples.

The metallic glass specimen with natural Ni (i=nat) was produced by a melt-spinning technique resulting in ribbons 2 mm wide and 0.023 mm thick. The total weight of the sample, placed in a thin (0.1 mm) vanadium tube, was 26.4 g. In the present experiment, the elastic coherent and inelastic incoherent neutron scattering spectra of the sample with natural Ni (i=nat) were measured on the NERA-PR neutron spectrometer.

The neutron diffraction pattern was measured and obtained dependence of the intensity as function of scattering vector is presented in Fig. 1.

The neutron inelastic cross-section for this sample was rather small. As a result, the satisfactory statistical accuracy was only obtained during the accessible measurement time for the detector with beryllium filter. From these data we determined the generalized vibrational density of states G(E).

Reference:

1. S.N.Ishmaev et al., J. of Non-Cryst.Solids, 94 (1987) 11

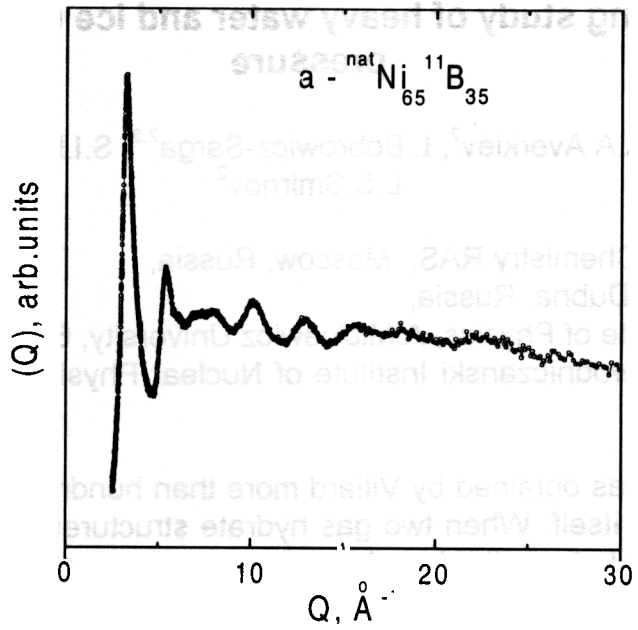

Fig. 1

Fig. 1 shows the neutron diffraction pattern of the metallic glass specimen with natural Ni (i=nat) sample in units of Q. It is in good accordance with the data of [1]. We conclude that structural investigations of disordered systems may be successful on this spectrometer.

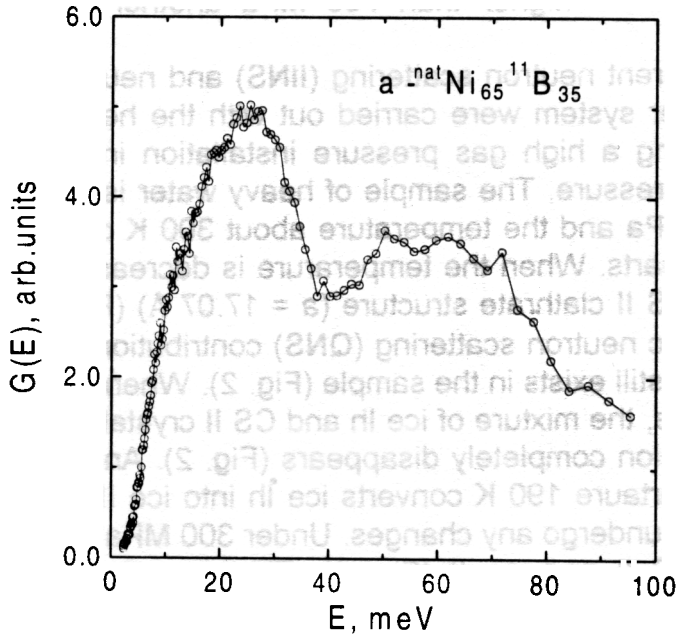

Fig. 2

Fig. 2 shows the generalized vibrational density of states obtained in the incoherent approximation. The density of the vibrations splits into two clearly separate regions: 0-40 and 40-90 meV, corresponding to predominant vibrations of heavy (Ni) and light (B) atoms. We conclude that partial dynamic distributions are very different in this amorphous alloy and must be further investigated over wider regions of energy E and momentum transfer Q.

Neutron scattering study of heavy water and ice under hydrostatic Ar pressure

G.G.Malenkov[1], A.A.Averkiev[2], L.Bobrowicz-Sarga[2,3], S.I.Bragin[2], Natkaniec[2,4], L.S.Smirnov[2]

1-Institute of Physical Chemistry RAS, Moscow, Russia,
2-FLNP JINR, 141980 Dubna, Russia,
3- on leave from Institute of Physics, A.Mickiewicz University, 61-614 Poznan, Poland
4-on leave from H.Niewodniczanski Institute of Nuclear Physics, 31-342 Krakow, Poland,

Argon hydrate was obtained by Villard more than hundred years ago [1] soon after the discovery of argon itself. When two gas hydrate structures were found [2,3,4], argon hydrate was postulated to have the type I structure (sp. gr. *Pm3n, a*=12Å). In 1984, strong evidence of the fact that argon clathrate crystallizes in the type II structure - CS II (sp. gr. *Fd3m, a* =17 Å) was given by D.W.Davidson and co-authors [5,6]. Ar mainly fills small dodecahedral cavities. High solubility of He and Ne in the ice Ih framework was demonstrated [7,8] but the Ar atom with the radius about 1.9 Å is too large to fill the ice Ih cavity. When the ability of He and H_2 to form clathrate hydrates with the ice II framework was discovered [9-11], it became clear that Ar atoms can be placed into ice II cavities.

Phase equilibria in argon - water systems were studied by H.S.Saito et. al. [12] and recently by Yu.Dyadin et al. [13] at pressures up to 15 kbar. The form of the melting curve indicates that at pressure higher than 700 MPa another modification of Ar hydrate appears [13].

Inelastic incoherent neutron scattering (IINS) and neutron diffraction (ND) studies of argon - heavy water system were carried out with the help of the NERA-PR neutron spectrometer [14] using a high gas pressure installation in which argon mediates the transmission of high pressure. The sample of heavy water is saturated with argon at the pressure about 100 MPa and the temperature about 300 K during three days before the recording of spectra starts. When the temperarure is decreased to 283 K, the ND shows the formation of the CS II clathrate structure (*a* = 17.07 Å) (Fig. 1). The IINS exhibites a decreasing quasielastic neutron scattering (QNS) contribution, which indicates that some amount of liquid water still exists in the sample (Fig. 2). When the sample is cooled to 190 K at the same pressure, the mixture of ice Ih and CS II crystals is recorded by ND (Fig. 1) and the QNS contribution completely disappears (Fig. 2). An increase in the pressure to 300 MPa at the tempertaure 190 K converts ice Ih into ice II. The diffraction patterns of CS II, however, do not undergo any changes. Under 300 MPa Ar pressure the sample is a mixture of Ar type CS II and ice II (Fig. 1). The normal isotope deuterium effect is observed in IINS spectra (Fig. 3). The translational energies are only slightly shifted while the librational ones are about 1.4 times less than the corresponding energy obtained for the ^1H_2O-Ar system. The obtained generalized phonon densities of states G(E) for the (Ar+D_2O) system at T=190 K and P=100 and 300 MPa (which is denoted as +) are presented in Fig.4.

References:
1. P.Villard, C.R. Acad. Sci, **123** (1896), 377.
2. M. von Stackelberg, Naturwiss., **36** (1949), 327.
3. W.F.Claussen J.Chem.Phys., **19** (1951), 1425.
4. M. von Stackelberg, H.R.Muller., Z. Electrochem., **58** (1954), 25.

5. D.W.Davidson, Y.P.Handa, C.I.Ratcliffe, J.C.Tse, B.M.Powell. Nature, **311** (1984),5982, 142.
6. D.W.Davidson, S.K.Garg, S.R.Gaugh, Y.P.Handa, C.I.Ratcliff, J.S. Tse, J.A.Reepmeester, J.Incl.Phenom., **2** (1984), 231.
7. A.Kahane, Solid State Commun.,**7** (1969), 1055.
8. A.Yu.Namiot, L.E.Gorodetskaya, Doklady Akademii Nauk, **190** (1970), 604.
9. W.L.Vos, L.W.Finger, R.J.Hemley, Ho-kwang Mao, Phys.Rev.Letters, **71** (1993), 3150.
10. D.Londono, W.F.Kuhs, J.L.Finney, Nature, **332** (1988) 141.
11. D.Londono, J.L.Finney, W.F.Kuhs, J. Chem. Phys., **97** (1992) 547.
12. S.H.Saito, D.R.Marshall, R.Kobayashi, Amer. Inst.Chem.Ing., **10** (1964), 734.
13. Yu.A.Dyadin, E.Larionov, D.S.Mirinskii, T.V.Mikina, L.I.Starostina, Mendeleev. comm., (1997), 32.
14. I.Natkaniec, S.I.Bragin, J.Brankowski, J.Mayer, ICANS-XII.Abingdon. 1993. RAL Report 94-025, v.I, p. 89.

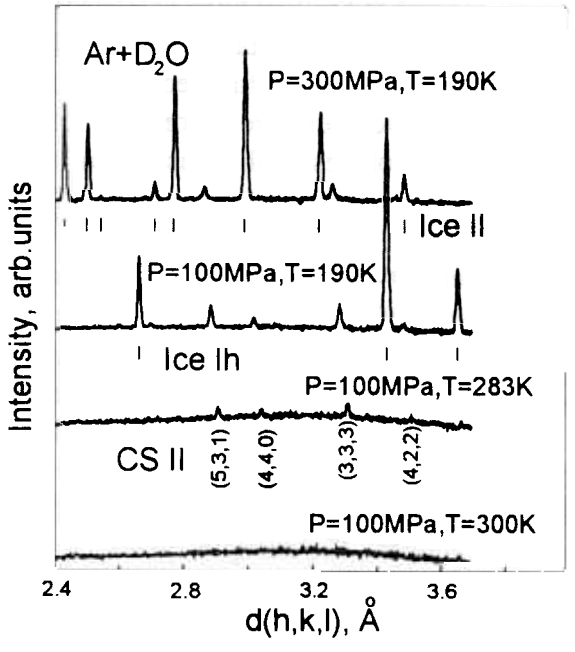

Fig. 1

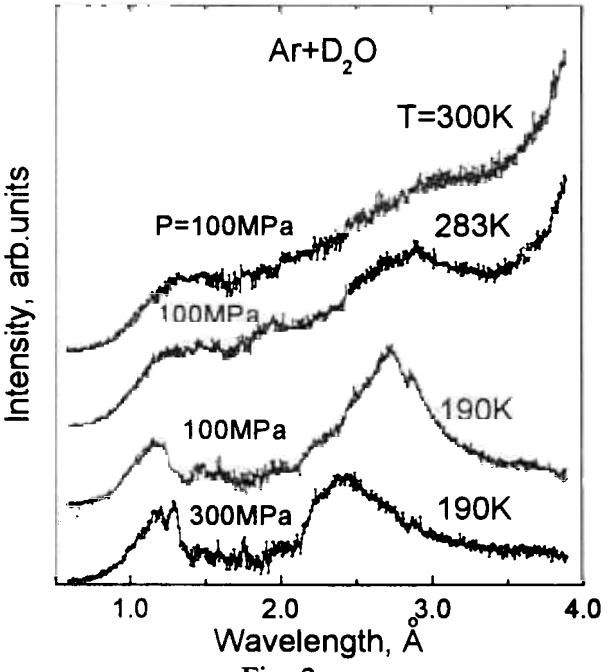

Fig. 2

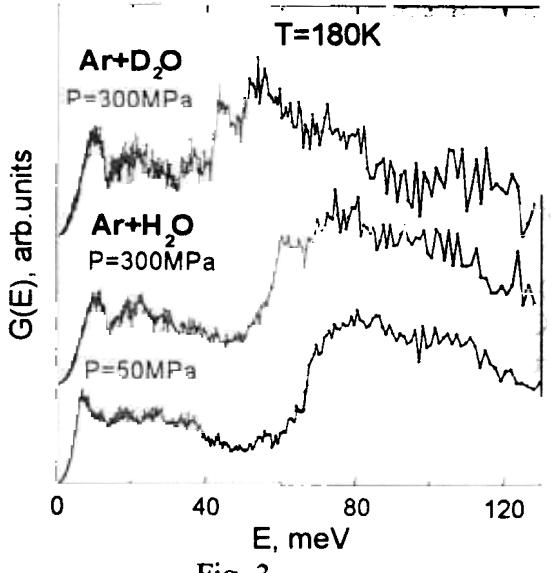

Fig. 3

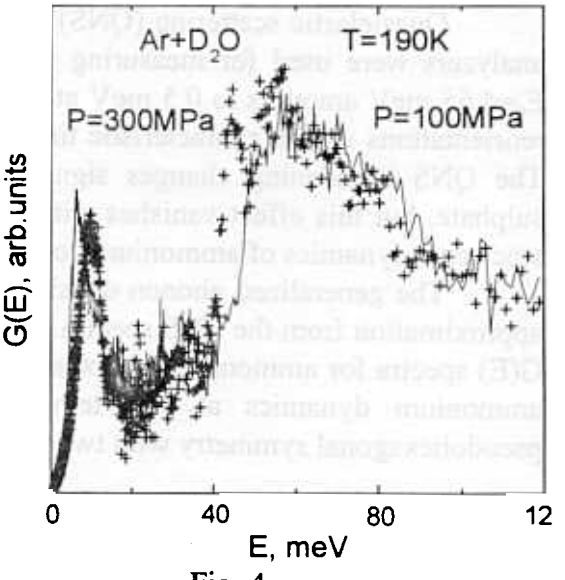

Fig. 4

Neutron Scattering Investigations of Ammonium Dynamics in $(NH_4)_{2-x}Rb_xSO_4$ Mixed Salts

I.Natkaniec[1], M.L. Martinez Sarrion[2], L. Mestres[2], L.S. Smirnov[1], L.A. Shuvalov[3].

[1] *Frank Laboratory of Neutron Physics, JINR, 141980 Dubna, Russia,*
[2] *Dep. of Inorganic Chemistry, University of Barcelona, E-08028 Barcelona, Spain,*
[3] *Institute of Crystallography, RAS, 117333 Moscow, Russia.*

Ammonium sulphate, $(NH_4)_2SO_4$, transforms from the paraelectric Pnam to the ferroelectric $Pna2_1$ phase at 223 K. The unit cells of both phases contain four formula units and consist of two kinds crystalographically independent ammonium ions [1]. No great differences were observed in the IINS spectra of ammonium sulphate above and below the ferroelectric transition [2,3]. These investigations were performed at temperatures above 80K and show broad bands at ca. 335 and 200 cm^{-1} due to torsional and translational motions, respectively. These bands belong to the ammonium ions, as they undergo fast reorientation even in the ferroelectric phase [4]. Crystalline Rb_2SO_4 at room temperature belongs to the space group Pnam. In mixed salts of ammonium-rubidium sulphates both phases can be studied at low temperatures. This allows investigations of harmonic dynamics of the ammonium ions in the paraelectric phase.

Solid solutions of ammonium-rubidium sulphates were prepared by mixing aqueous solutions of $(NH_4)_2SO_4$, and Rb_2SO_4 in various stoichiometric proportions. Crystalline samples were obtained through slow evaporation at 40°C. The composition of the solid solutions, in general, was different from that of the starting mixtures and, therefore, was tested by chemical analysis. Simultaneous investigations by the time-of-flight IINS and neutron diffraction (ND) methods of ten samples of mixed salts $(NH_4)_{2-x}Rb_xSO_4$ for the entire concentration range, $0.0 \leq x \leq 2.0$, were performed on the NERA spectrometer [5] at the IBR-2 pulsed reactor in Dubna. The ND spectra were used to control the sample quality and determine the lattice parameters at different concentrations and temperatures, which is what allowed us to test the x,T phase diagram. The temperature dependence of the IINS spectra of $(NH_4)_2SO_4$ and of ammonium-rich mixed salts measured at temperatures close to the para-ferrroelectric transitions are presented in Fig. 1.

Quasielastic scattering (QNS) is seen above 150 K. Pyrolitic graphite neutron energy analyzers were used for measuring the IINS spectra. The resolution of the elastic line at E_0=4.65 meV amounts to 0.5 meV at FWHM. This means that ammonium ions undergo fast reorientations with a characteristic time in the range of psec even in the ferroelectric phase. The QNS broadening changes significantly at the phase transition for pure ammonium sulphate, but this effect vanishes with increasing rubidium concentration. Above $x>0.4$, the stochastic dynamics of ammonium do not depend on the para-ferroelectric transition.

The generalized phonon density of states G(E) obtained in the one phonon scattering approximation from the IINS spectra measured at 10 K are presented in Fig. 2. Three types of G(E) spectra for ammonium can be seen at different rubidium concentrations. For $x<0.4$, the ammonium dynamics at low temperatures correspond to an ordered crystal of the pseudohexagonal symmetry with two inequivalent NH_4 groups. The four lines in the

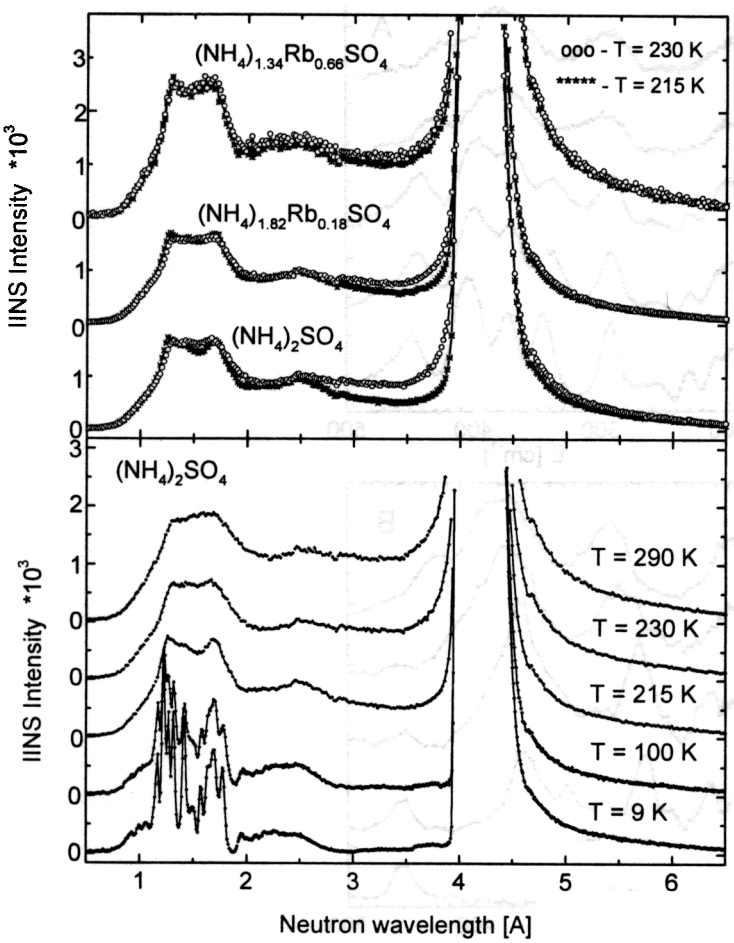

Fig. 1. *The IINS spectra of ammonium sulphate and ammonium-rich mixed salts.*

frequency range of 160-240 cm^{-1} correspond to translational and the four between 280-420 cm^{-1} to torsional vibrations of ammonium ions. In the concentration range $0.4<x>1.2$, the ammonium dynamics form broad bands characteristic of protonic glasses. They correspond to translational vibrations at ca. 200 cm^{-1} and torsional vibrations at ca. 290 and 380 cm^{-1}. Above x=1.2, the mixed salts of $(NH_4)_{2-x}Rb_xSO_4$ remain in the paraelectric phase and, according to structural investigations, ammonium ions predominantly occupy the type II crystallographic position. As one can see in Fig. 2, two translation lines of 190 and
220 cm^{-1} and two torsional vibrations at 270 and 370 cm^{-1}, are due to NH_4 (II) type ammonium ions.

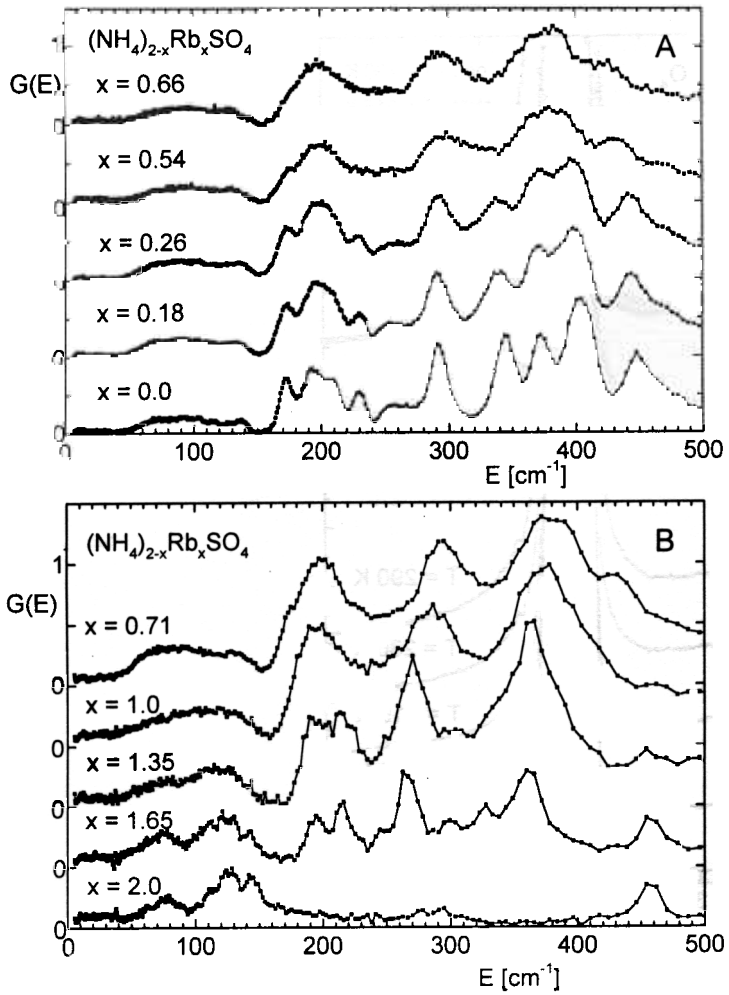

Fig. 2. The generalized phonon density of states G(E) at 10 K of $(NH_4)_{2-x}Rb_xSO_4$ crystals of different concentrations.

References

1. E.O. Schlemper, W.C. Hamilton, J. Phys. Chem., **44** (1966) 4498-4509.
2. A. Bajorek, T. Matchekhina, K. Parlinski, in: Inelastic Neutron Scattering in Solids and Liquids, IAEA Vienna, 1965, Vol. II, p. 355-381.
3. J.J. Rush, T.I. Taylor, in: Inelastic Neutron Scattering in Solids and Liquids, IAEA Vienna, 1965, Vol. II, p. 333-345.
4. P.S. Goyal, R. Chakravarthy, B.A. Dasannacharya, C.J. Carlile, phys. stat. sol. (a), **118** (1990) 425-430.
5. I.Natkaniec, S.I. Bragin, J. Brankowski, J. Mayer, Proc. of the ICANS XII, Abingdon 1993, RAL Report No. 94-025, Vol. I. p. 89-95.

Investigation of Hydrophobic hydration effects by inelastic neutron scattering

A.G.Novikov[1], M.N.Rodnikova[2] , O.V.Sobolev[1]

[1]*Institute of Physics and Power Engineering, Obninsk, Kaluga Region, Russia;*
[2]*Kurnakov Institute of General and Inorganic Chemistry, Russian Academy of Sciences, Moscow, Russia.*

Aqueous solutions of tetraalkylammonium ions are the convenient model systems for investigations of water interactions with apolar particles and effects of hydrophobic hydration which are of significant importance for a number of chemical and biological problems. The influence of apolar molecules on structural properties of water is one of the most actual questions in hydrophobic hydration study. The results of thermodynamics and transport measurements[1], computer simulations [2] lead to the conclusion that the effect of stabilizing the surrounding water hydrogen bond (H-B) network takes place in aqueous solutions of large apolar particles such as tetraalkylammonium ions. It is suggested that hydration water has a more ordered structure ("ice-like") than that of pure water. However, very extensive and accurate structure measurements performed in the last years of aqueous solutions of these ions by the neutron diffraction method [3] did not indicate any changes in the hydration water structure of the studied solutions in comparison to pure water.

The generalized frequency distribution (GFD) of water molecules, which can be obtained from an inelastic neutron scattering experiment, provides some information about structural modifications in the studied solution.

A neutron scattering experiment was carried out on the DIN-2PI double time-of flight spectrometer. The choice of the initial neutron energy E_o=3mev made it possible to have the resolution of elastic neutron scattering ΔE_o=0.13 mev. Neutron scattered spectra were recorded at 15 angles covering the range $16^\circ \leq \vartheta \leq 134^\circ$ which corresponds to the neutron wave vector transfer ($0.33 \leq Q \leq 2.2$)$Å^{-1}$. The sample exposed to the neutron beam was a teflon capillary helix (0.5 i.d. and 1.2o.d) filled with a solution and wound on the thin aluminum framework forming a cylindrical sample with overall dimensions of 160 mm in height and 110 mm in diameter. The total transmission including the solution and a teflon container for neutrons with the initial energy was about 75%.

The measurements were carried out at room temperature and consisted of a number of runs:

- with 0.98m TBACl solution in light water;
- with 0.84m TBACl solution in heavy water;
- with pure light water;
- with pure heavy water;
- with vanadium sample of appropriate geometry.

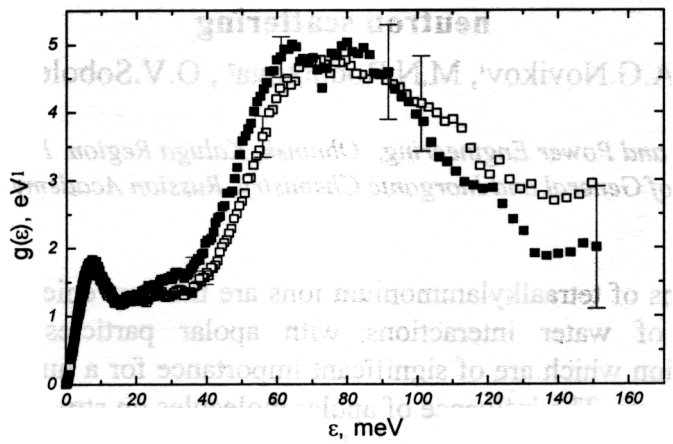

Fig.1. The generalized frequency distribution of pure water(■) and hydration water(□) molecules.

The extracted GFDs of pure water and hydration water in 0.98m TBACl solution are shown in Fig.1. The low frequency peak (with $\varepsilon_0 \approx$ 7meV) of GFD which corresponds to the bending of the O-O-O angle and usually is regarded as evidence of the H-B network existence is of particular interest, because it is very sensitive to changes in the H-B network structure. As it was shown in [4], the intensity of this peak decreases as the temperature grows. It also decreases in the case of ionic hydration[5-7]. Thus, we obtain the reduction of the low frequency mode if the distortion of the H-B network takes place, and we can expect the increase of this mode in an case of "structural promotion of water".

The main feature of hydration waters GFD is a small shift of the libration mode to higher energies in comparison to pure water, which has not been explained yet, but the low frequency mode mentioned above does not change by significant. So, we may conclude that the studied H-B water structure in solution do not have alterations in comparison to pure water. This conclusion is in agreement with the neutron diffraction data[3].

[1] W.-Y.Wen, *Water and Aqueous Solutions*, edited by R.A.Horne (Wiley, New York, 1972)
[2] B.G.Rao and U.C.Singh, J. Am. Chem. Soc. 111, 3125 (1989)
[3] J.Turner and A.K.Soper J.Chem.Phys. 101, 6116 (1994)
[4] A.G.Novikov, A.A.Vankov and L.S.Gosteva, J. Struct. Chem. 31, 77 (1986)
[5] J.Lasseques and D.Savagnat, Mol. Phys. 68, 803 (1989)
[6] A.G.Novikov, M.N.Rodnikova, V.V.Savostin and O.V.Sobolev, Chem. Phys. Letters. 259, 391 (1996)
[7] A.G.Novikov, M.N.Rodnikova, V.V.Savostin and O.V.Sobolev, 234 - 236, 340 (1997).

X-ray and neutron scattering study of the Nb-O solid solutions

H.Wipf[1], S.Danilkin[2], E.Jadrowski[3], H.Fuess[1], T.Wieder[1]

[1] *Darmstadt University of Technology, Germany*
[2] *Institute of Physics and Power Engineering, Obninsk, Russia*
[3] *Joint Institute for Nuclear Research, Dubna, Russia*

Niobium-oxygen solid solutions were studied by X-ray diffraction and inelastic neutron scattering. The samples were niobium rods (diameter 10 mm, length 80 mm) doped with oxygen in a high-vacuum induction furnace in oxygen atmosphere. The oxygen content in two prepared samples was 1.29 and 2.65 at.% determined by the vacuum-fusion method.

X-ray Laue diffraction shows a "bamboo" structure in Nb-O studied samples with single crystal dimensions ranging from 2 mm to 10mm in diameter.

The lattice parameters were measured by X-ray diffraction from powder samples made from the rods. The increase of the lattice parameter due to interstitial oxygen is in agreement with the data of Koch [1]. This shows that all oxygen in the samples is dissolved in the BCC lattice and α-solid solutions are formed by quenching after heat treatment at t≈2240°C.

The vibrational frequency distribution of $NbO_{0.026}$ was measured at room temperature and at t=200°C to increase the intensity of energy gain in neutron scattering in the region of the oxygen vibrations. Further increase of the sample temperature is limited by decomposition of the solid solution. The initial energy of neutrons is E_0=18.4 meV and the range of scattering angles Δϑ=38-133°.

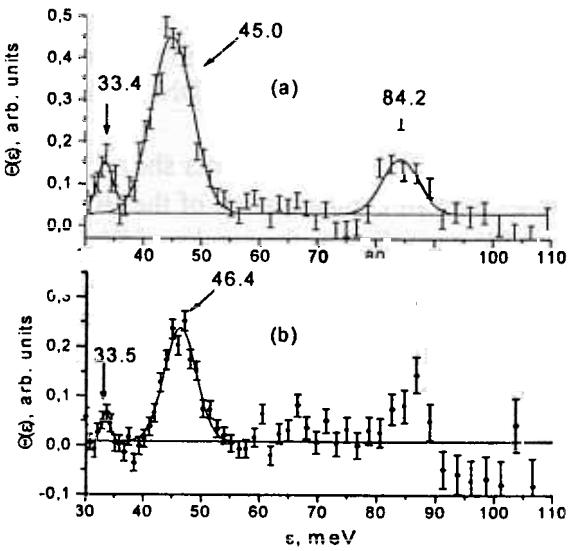

Fig. 1 Frequency spectra of oxygen atoms at t=200°C (a) and at room temperature (b).

Fig. 1 shows the vibrational frequency distributions $\Theta(\varepsilon)$ at ε≥30 meV obtained for $NbO_{0.0265}$ at room temperature and at t=200°C after subtraction of Nb spectra. In the spectrum of $NbO_{0.0265}$ at t=200°C, in addition to the known vibrational mode $\hbar\omega_{1,2} \cong 45$ meV [2], peak at $\hbar\omega = 84.2 \pm 1.2$ meV is observed. It corresponds to oxygen vibrations with the polarization vector along the shorter axes of the octahedral position. The peak at $\hbar\omega \cong 33.5$ meV is possibly connected with vibrations of the metal atoms neighbouring interstitial oxygen. For V-O solid solutions, where the similar peaks were first observed, association of these peaks with vibrations of the metal atoms closest to oxygen was shown by model calculations [3].

[1] Koch C.C., Scarbrough J.O., Kroeger D.M., Phys.Rew.B, 9 (1974) 888.
[2] Danilkin S.A., Zemljanov M.G., et al., Sov. Phys.: Solid State, 29 (1987) 1213
[3] Mazurenko V.G., Danilkin S.A., Fiz. Tverd. Tela, 38 (1996) 229.

Lattice structure and dynamics of the Fe-Cr-Ni-N steel with different Cr content

M.Baeva[1], S.Danilkin[2], A.Beskrovni[3], E.Jadrowski[3]

[1] *Institute of Solid State Physics, Sofia, Bulgaria*
[2] *Institute of Physics and Power Engineering, Obninsk, Russia*
[3] *Joint Institute for Nuclear Research, Dubna, Russia*

High nitrogen austenitic steels are the materials with high strength and corrosion resistance and have structure stability at low temperature and during cold working. The steel properties depend on the interstitial (N) and substitutional (Cr, Ni, Mn) atom contents. The present study concerns the effect of Cr content on the crystalline structure and interatomic bonding in Fe-*x*Cr-12Ni-0.5N (*x*=15; 20; 25; 29 wt.%) alloys. The diffraction measurements were carried out with the Philips-Micro III x-ray diffractometer and with the neutron diffractometer DN-2. The inelastic neutron scattering spectra were measured with the DIN-2PI spectrometer.

The diffraction measurements show the FCC structure for all studied steels. The neutron diffraction discloses a small contamination of the BCC α-phase in all samples. The amount of the α-phase does not exceed 3% according to the results of Rietveld refinement. The linear dependence of the austenite lattice parameter *a* (Å) on the Cr content *x* (wt.%) was observed: $a(x)=3.57178 + 0.00123 \cdot x$. The X-ray data give the same coefficient k_a, but the lattice parameter values are higher by 0.006 Å. However, the accuracy of the neutron lattice parameters seems to be higher because the Rietveld refinement with the NaCl standard was used in the data treatment.

The INS measurements show that the metal frequency spectrum does not depend on the Cr content in the limits of the experimental errors. This demonstrates weak dependence of the Me-Me interatomic bonding on the Cr content.

At the same time, changes in the nitrogen localised vibrations were noted. A small nitrogen frequency increase observed as the Cr content increases contradicts with the lattice dilation caused by Cr atoms (Fig.1). The decrease of the nitrogen peak width with an increase of the Cr content is also nontypical. Such a behaviour is possibly connected with changes in electron screening and in the stress-induced interaction caused by the different Cr contents. These effects could cause ordering of the nitrogen atoms with an increase of the Cr content that manifests itself as a decrease of the nitrogen peak width. This assumption is confirmed by a computer simulation of the ordering in Fe-40Ni-35Cr-*x*N alloys. As it was demonstrated by Owen [1], nitrogen atoms preferentially occupy the octahedral sites where they have a large excess of Cr over Ni atoms in the first coordination shell.

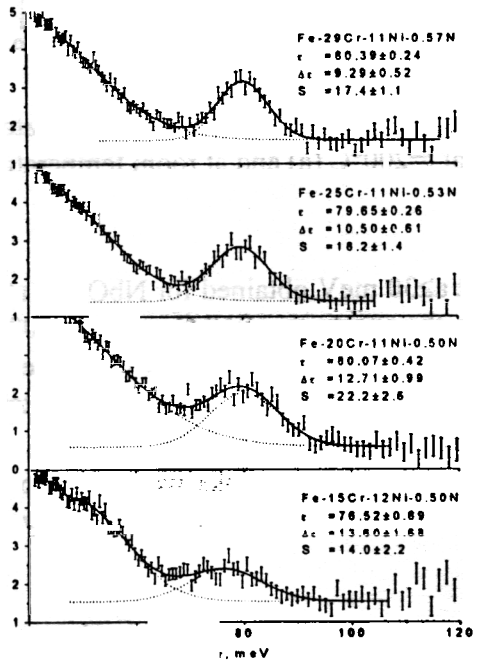

Fig.1. *Nitrogen vibrations in Fe-xCr-12Ni-0.5N alloys*

[1] M.Grujicic, W.S.Owen Nitrogen induced ordering in FCC Fe-Ni-Cr-N solid-solution alloys. High Nitrogen Steels, Proc. of the 3rd Int. Conf., Kiev, Ukraine, Sept. 14-16 1993, part 1, p.686.

Observation of spatial splitting of a polarized neutron beam as it is refracted on the interface of two magnetically non-collinear media

V.L. Aksenov[1], H.Fredrikze[2], S.V. Kozhevnikov[1], Yu.V. Nikitenko[1], M.Th. Rekveldt[2], J. Schreiber[3]

[1] Frank Laboratory of Neutron Physics, Joint Institute for Nuclear Research, 141980 Dubna, Moscow Region
[2] Interfaculty Reactor Institute, Delft University of Technology, Mekelweg 15, 2629JB, Delft, The Netherlands
[3] Fraunhofer Institute for Non-destructive Testing, D-01326 Dresden, Germany

As a rule, investigating the magnetic properties of matter by polarized neutron reflection or refraction samples whose magnetization vector is collinear with the magnetic strength vector of an external magnetic field (collinear magnetic media) are used. If the magnetization vector of the sample is non-collinear with the magnetic strength vector due to the internal or shape anisotropy of the sample (the case of magnetically non-collinear media), in the magnetic field neutrons experience a transition from one spin state (denote "+" or "-") to the other ("-" or "+") as they go through the interface. The total energy of neutrons does not change, which results in a change in the kinetic energy of neutron motion in the direction perpendicular to the interface. As a result, the neutron beam spatially splits into a beam of neutrons which have experienced a thransition to a new spin state (the beams are then denoted as "+-" or "-+") and a beam of neutrons which have not experienced such transition ("++" or "--" beams).

This effect was predicted by Ignatovich in 1978 [1]. In [2,3], expressions for the coefficients of transmission and reflection from an interface of two magnetically non-collinear media are obtained and can be used in experimental data processing. To determine the direction of refracted neutron beams, we use the energy conservation law. For squared glancing angles of refracted neutron beams, we obtain:

$$(\theta^{++})^2=\theta_i^2- \alpha[U + \mu \cdot(B-H)] \cdot\lambda^2 \quad (1)$$

$$(\theta^{--})^2=\theta_i^2- \alpha[U - \mu \cdot(B-H)] \cdot\lambda^2 \quad (2)$$

$$(\theta^{+-})^2=\theta_i^2- \alpha[U - \mu \cdot(B+H)] \cdot\lambda^2 \quad (3)$$

$$(\theta^{-+})^2=\theta_i^2- \alpha[U + \mu \cdot(B+H)] \cdot\lambda^2 \quad (4)$$

where $\alpha=2m/h^2$, θ_i is the glancing angle of the incident neutron beam; U is the potential energy of the nuclear interaction of neutrons and matter; B is the induction in the sample; H is the external magnetic field strength; μ is the magnetic moment of the neutron; m is the mass of the neutron; h is Planck's constant; λ is the neutron wavelength.

A magnetically non-collinear medium can be most simply realized with the help of shape anisotropy in the sample when the strength vector of an external magnetic field is directed at an angle to the surface of the magnetic film.

In [4,5], spatial splitting of a polarized neutron beam reflected from a magnetic film is observed.

In [6,7], spatial splitting of a polarized neutron beam on transmission through a magnetic layer on a nonmagnetic substrate (two interfaces) is investigated. In this case, the neutron beam goes through the magnetic layer and leaves the sample through the edge of the substrate. Because the beams "++" and "--" coincide in direction (in (1) - (2) it is necessary to take B = H), spatial splitting of the polarized neutron beam into two beams and of the nonpolarized neutron beam into three beams is observed.

In the refraction of neutrons as they go through a magnetic layer (two interfaces), the interference between neutron beams takes place due to multiple reflection from the layer boundaries. This leads to a very complicated picture of the dependence of the neutron flux on the wavelength. A simpler picture may possibly be observed in the case of neutron refraction on one interface.

In this article the refraction of a polarized neutron beam on the interface of two magnetically non-collinear media is investigated. The sample is the magnetic film Fe(86%)Al(9,6%)Si(4,4%) with the thickness 20 μm and a Cr 500 Å intermediate nonmagnetic layer. The size of the sample is 5 (along the beam) × 20 (in the vertical direction) mm^2, the thickness of the nonmagnetic substrate $CaTiO_3$ is 1 mm. The glancing angle of the neutron beam θ_i=4.8 mrad, the mean square divergence of the incident neutron beam is ±0.05 mrad, the mean square angular resolution of the spectrometer is ±0.2 mrad, the neutron wavelength varies in the interval λ=1.6 ÷ 4 Å. The external magnetic field strength is H=4.5 kOe, the angle between the sample plane and the magnetic field strength vector is $\beta=70^0$. The neutron beam falls on the surface of the film and leaves the film through the edge.

In the measurements we use a position-sensitive detector and a scheme for complete polarization analysis (a polarizer, two spin-flippers and an analyzer), which makes it possible to register four neutron counts in different measuring modes: I(off,off) – two spin-flippers off; I(on,off) – the first spin-flipper on, the second off; I(off,on) – the first spin-flipper off, the second on; I(on,on) – two spin-flippers on.

With flippers 1 and 2 "on" ("off"), the polarizer - flipper 1 and the flipper 2– polarization analyzer sections predominantly transmit neutrons in the state "-" ("+"). The measurements are conducted with the SPN-1 spectrometer at the IBR-2 pulsed reactor in Dubna.

In Figs. 1a-d the neutron count for four measuring modes over the specified wavelength interval λ=2.02÷2.57 Å (the average wavelength $\langle\lambda\rangle$=2.25 Å) is shown as a function of the angle θ between the sample plane and the direction of the refracted neutron beam. The measuring time in each "off,on" or "on,off" mode is about 6 times larger than in the "off,off" ("on,on") mode and is approximately 15 hours.

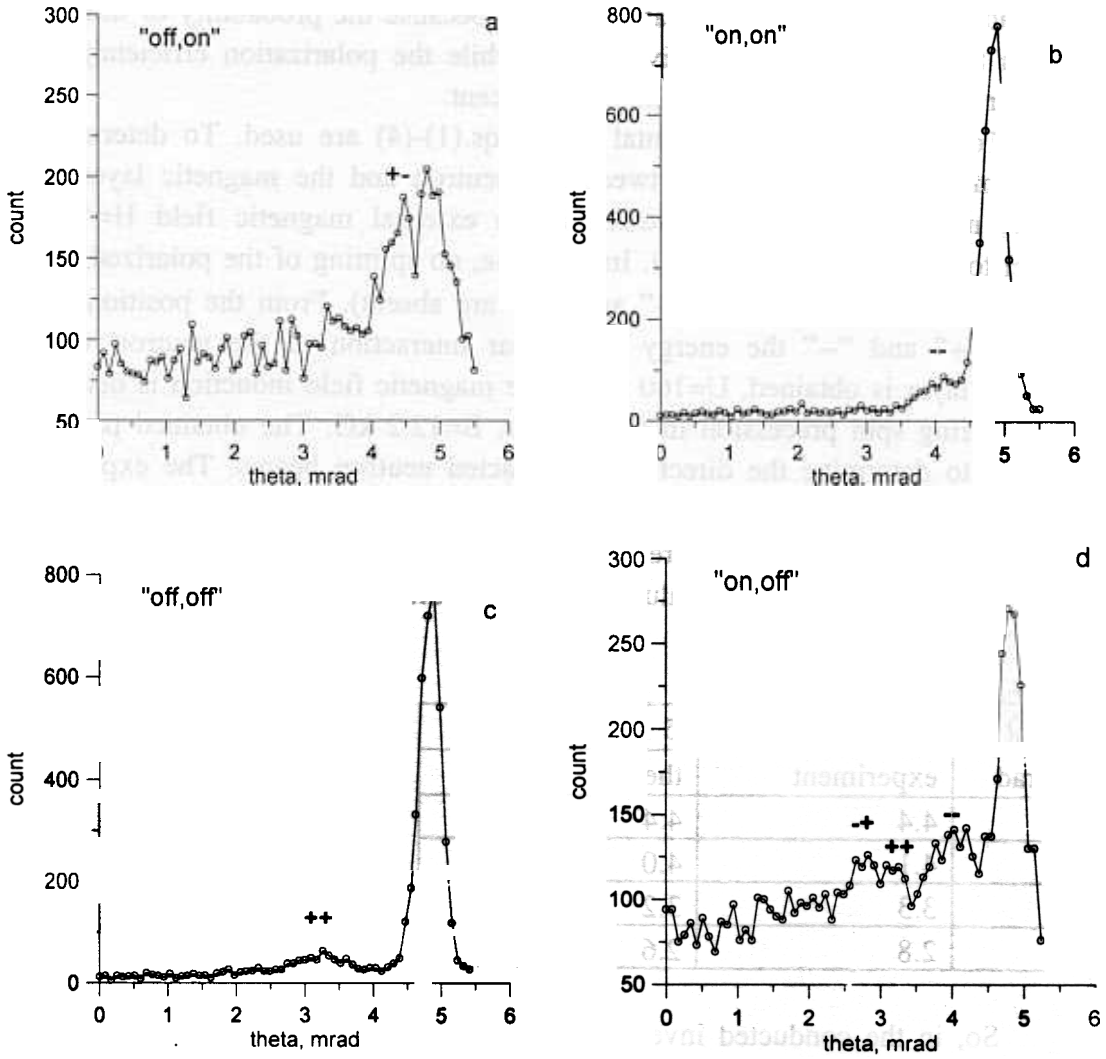

Fig. The dependence of the neutron count on the angle between the plane of the sample and the direction of the refracted neutron beam (the neutron wavelength interval λ=2.02÷2.57 Å, the average wavelength $\langle\lambda\rangle$=2.25 Å) for different measuring modes: a) "off,on" ; b) "on,on" ; c) "off,off" ; d) "on,off" .

The peak at θ=4.8 mrad on the right corresponds to the direct beam (neutrons that missed the magnetic layer). The indices "+-", "--", "++" and "-+" mark the neutron beams refracted on the vacuum-magnetic film interface. The experimental values for the angular positions of these beams are given in Table 1. One can see that the smallest deviation from the direct beam has the beam "+-" (Fig. 1a) and the largest deviation has the beam "-+" (Fig. 1d). It should be noted that the beams "--" (Fig. 1b) and "++" (Fig. 1c) do not coincide in direction in contrast to the case of the refraction on two interfaces. So, one can see that the beam with one initial spin state "+" spatially splits into beams with different final spin states, "-" or "+".

The beam of neutrons with the initial spin state "-" also splits into two beams (Figs. 1b and 1d). In this case, in the measuring mode "on,off" in addition

to the beam "-+" at 2.8 mrad there appear the beams "++" at 3.3 mrad and "--" at 4.1 mrad. The two latter beams are observed because the probability of their going through the sample is comparatively high while the polarization efficiency of the polarizer and the analyzer is not hundred percent.

To analyze the experimental data, Eqs.(1)-(4) are used. To determine the energy of nuclear interaction between the neutron and the magnetic layer of the sample, measurements are conducted in an external magnetic field H=4.5 kOe parallel to the film plane ($\beta=0^0$). In this case, no splitting of the polarized neutron beam takes place (the beams "+-" and "-+" are absent). From the positions of the beams "++" and "--" the energy of nuclear interaction of the neutron with the magnetic layer is obtained, U=160 neV. The magnetic field induction is determined by measuring spin precession in the sample, B=12.2 kG. The obtained parameters are used to determine the direction of refracted neutron beams. The experimental and theoretical values of the angels θ between the plane of the sample and the direction of refracted beams are summarized in Table 1. One can see that the experimental and theoretical values coincide within the angular resolution of the spectrometer ±0.2 mrad.

Table 1

U=160 neV; B=12.2 kG; λ=2.25 Å; θ_i=4.8 mrad		
θ, mrad	experiment	theory
+-	4.4	4.4
--	4.1	4.0
++	3.3	3.2
-+	2.8	2.6

So, in the conducted investigation of neutron refraction on the interface of two magnetically non-collinear media splitting of a polarized neutron beam was observed. The beam of neutrons initially in the spin state "+" or "-" splits into two beams in the states "+" and "-". All split beams have different spatial positions. The reported phenomenon has been observed for the first time.

[1]. V.K. Ignatovich, Letters to JETP **28** (1978) 311.
[2]. V.K. Ignatovich: Physics of ultracold neutrons. Moscow: Nauka 1988.
[3]. N.K. Pleshanov, Z.Phys. **94** (1994) 233.
[4]. G.P. Felcher, S. Adenwalla, V.O. De Haan, A.A. Van Well, Nature **377**(1995)409.
[5]. D.A. Korneev, V.I. Bodnarchuk, V.K. Ignatovich, Letters to JETP **63** (1996) 900.
[6]. V.L. Aksenov, E.B. Dokukin, S.V. Kozhevnikov, Yu.V. Nikitenko, A.V. Petrenko, J. Schreiber "Refraction of polarized neutrons in a magnetically non-collinear layer', Phys.B **234-236** (1997) 513-515.
[7]. V.L. Aksenov, E.B. Dokukin, S.V. Kozhevnikov, Yu.V. Nikitenko, A.V. Petrenko, J. Schreiber "Refraction of polarized neutrons in a magnetically non-collinear medium", Proceedings of the International Workshop "Polarized Neutrons for Condensed Matter Investigations", Dubna, 18-20 June 1996, E3-96-507. Preprint JINR E3-97-10 (1997).

Determination of the magnetic field penetration depth in Nb and $YBa_2Cu_3O_7$ superconducting films by polarized neutron reflectometry

V. Lauter-Pasyuk[a,b], H.J. Lauter[c], V.L. Aksenov[b], E.I. Kornilov[b], A.V. Petrenko[b] and P. Leiderer[a]

[a] *Universität Konstanz, Fakultät für Physik, Postfach 5560, D-78434 Konstanz, Germany*

[b] *Joint Institute for Nuclear Research, 141980 Dubna, Moscow Region, Russia*

[c] *Institut Laue Langevin, B.P.156, F-38042, Grenoble Cedex 9, France*

Polarized neutron reflectometry is used in direct measurements of the magnetic-field penetration depth in a high temperature (HT_c) superconducting film. Two scattering geometries are used. The deduced neutron scattering length density profile gives the exact picture of the composition of the film. The fit to the spin-asymmetry yieldsed a magnetic-penetration depth of 1400 ± 100 Å at a temperature of T = 4.8 K along the c-axis oriented perpendicular to the film surface. The model includs an intrinsic exponential decay of the penetration depth. For the first time the spin-asymmetry is determined with high resolution over an extended Q-range for a HT_c-film. Nb-films are investigated as reference.

Introduction

One of the fundamental parameters of superconductors is the London penetration depth λ_L [1]. Polarized Neutron Reflectometry (PNR) offers a unique possibility of measuring the absolute value of the penetration depth and the shape of the magnetic flux profile. Several studies of Nb-films have already been performed with this technique and the values of λ_L = 410 Å [2] and 900 - 1450 Å [3] for different thicknesses of the film have been obtained. The high difference in the values can be explained by the fact that not the magnetic penetration depth was measured but the screening length $l > \lambda_L$. The screening length takes into account electron scattering by defects in the sample [4]. This effect is discussed in Ref. 5, where the measured value of l was corrected for electron scattering and λ_L = 430Å was obtained, which is the best result today for Nb-films. Also, HT_c-films measured up to date ($YBa_2Cu_3O_7$) [5,6,7,8] have defects as discussed in Ref. 9. In them, the defects or roughnesses do not perturb the penetration depth itself because the correlation length is small in HT_c -films, but do perturb the reflectivity curves so that, e.g., the oscillations of the reflectivity curves are not anymore visible [5].

In order to test the possibilities of PNR and optimize the experimental conditions for HT_c-films studies, first we performed model-calculations and experiments on Nb-films. In particular, care was taken to get HT_c samples showing low or no off-specular scattering as a sign of good quality.

Scattering geometry and Nb/Si experiment

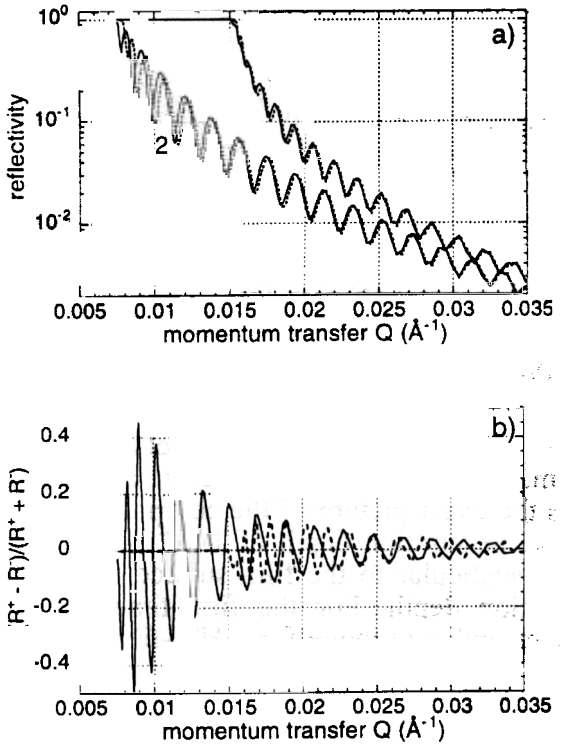

Fig. 1. *In Fig. 1a two theoretical reflectivity curves R^+ (solid line) and R^- (dashed line) for an HT_c-film ($YBa_2Cu_3O_7$ film with the c-axis perpendicular to the surface of the $SrTiO_3$-substrate) are shown for ttwo scattering geometries: 1 - reflection from the air-film side and 2 - reflection from the substrate-film side. Parameters: Film thickness 3000 Å, external field 500 Oe and penetration depth 1400Å.Fig. 1b. The spin-asymmetries for the two scattering geometries.*

Prior to experiments, model calculations were performed to study two variants of the scattering geometry. For all calculations and fits we assumed an exponential law for the intrinsic magnetic profile of the film [10].

In Fig. 1a the reflectivity curves are shown for a HT_c(YBaCuO)-film calculated for the two scattering geometries: reflection from the air-film interface (1) and substrate-film interface (2). For the reflection from the air-film interface (1) the critical Q is given by the NSLD-difference between YBaCuO and air. This difference is larger than the NSLD-difference between YBaCuO and the $SrTiO_3$ substrate. Thus, the Q_c for the reflection from the substrate-film interface (2) is lower compared to (1). In order to get an image of such a NSLD profile look in anticipation at the insert in Fig. 3. Second, the scattering through the substrate (2) shows much higher oscillations because of a high NSLD-difference at the second interface (the film-air interface) compared to the case of the scattering from the air side (1), where the second interface is the film-substrate interface.

The magnetic effect shows up in the difference between R^+ and R^- which is demonstrated on the plot of the Spin-Asymmetry SA = $(R^+-R^-)/(R^++R^-)$ in Fig. 1b. The advantage of scattering through the substrate is obvious. However, the disadvantage is that an intensity factor of 5 is lost when the neutrons traverse the $SrTiO_3$-substrate.

The experiments for the Nb- and HT_c-films were performed on the spectrometers SPN/Dubna [11] and D17/ILL [12].

The results of the measurement of the Nb-film on a Si-substrate at room temperature are depicted in Fig. 2. As predicted in Fig. 1, Q_c shifts to a lower value if the scattering is done from the substrate-side (marked 1 in Fig. 2a). Also, the oscillations are higher compared to the scattering from the air-side. The result of the fit is plotted in the insert in Fig. 2a. The NSLD profile shows a 50 Å thick NbO-layer on the surface and a 100 Å thick interdiffusion region at the substrate interface. The total

film-thickness is 3310 Å. This thickness was chosen in view of HT_c-films for which such high thickness is necessary due to the expected high penetration depth. Also, the surface area of the Nb-film was about 2 cm^2 comparable to the HT_c-film surfaces for which one can expect homogeneous surface properties.

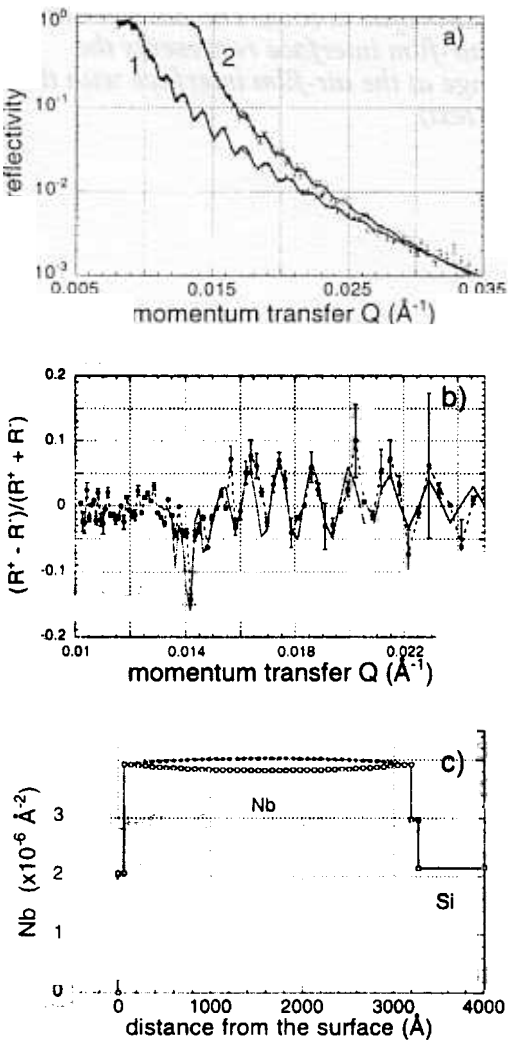

Fig. 2. *The reflectivity curves of the Nb-film on a Si-substrate are shown in Fig. 2a. Reflectivity curve 1 is taken in the reflection geometry from the substrate-film interface and 2 from the air-film interface, respectively. In the insert, the NSLD-profile is shown.*
In Fig. 2b the spin-asymmetry is shown for reflection on the air-film side marked 1 in Fig. 1a. Fig. 2c shows the NSLD-profile including the splitting of the Nb-potential due to the penetrating field.

The reflectivities R^+ and R^- of the Nb-sample at a temperature of 5.8 K were obtained with an applied external field of 556 Oe. The result is shown in Fig. 2b in the SA form. In the fit to the data presented in Fig. 2b the magnetic penetration depth was the only variable. The NSLD profile in Fig. 2c represents the complete result including the surface NbO layer, the interdiffusion layer and the magnetic effect due to the penetrating field. The screening length is determined to be 650 Å in agreement with 550 Å from Ref. 5. It was not the purpose of this study to perform further resistivity measurements to deduce λ_L for the Nb film.

$HT_c/SrTiO_3$ experiment

The HT_c films of $YBa_2Cu_3O_7$ were epitaxially grown on $SrTiO_3$ with a CeO_2 seed-layer. The c-axis is perpendicular to the film surface. The quality of the samples was tested by various methods (AFM, X-ray and electron diffraction). The neutron experiments were performed in two steps: first with reflection from the substrate side and then, from the air side after half a year. In Fig. 3, the two measured reflectivity curves are depicted with the fit to the data. In the obtained NSLD diagram in the inset of Fig. 3, an additional surface layer is visible. This surface layer has grown during this half year from 25 Å to 125 Å and consists presumably of $BaCO_3$ formed through the humidity of air.

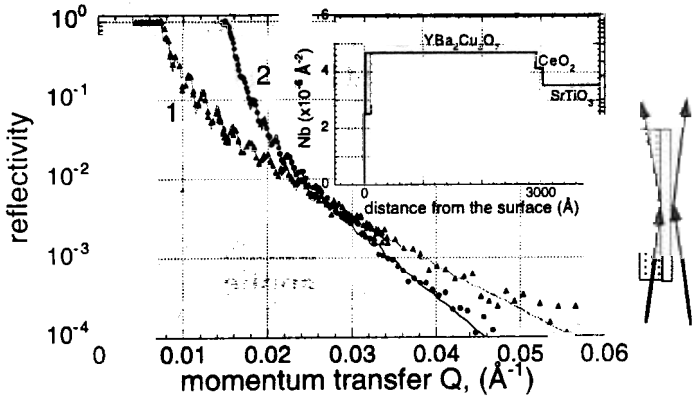

Fig. 3. *The reflectivity curves of the YBaCuO-film on a SrTiO-substrate. 1 is taken in the reflection geometry from the substrate-film interface and 2 from the air-film interface, respectively. The reflection geometries are shown as a sketch on the right. In the insert, the NSLD-profile is seen. The dashed line at the air-film interface represents the change at the air-film interface with time (see text).*

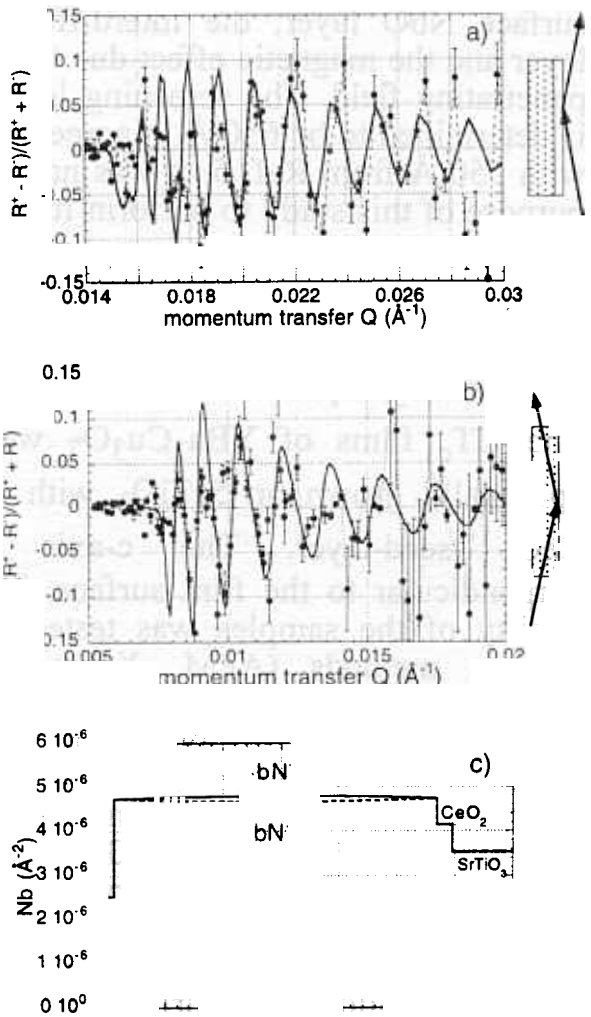

In the case of HT_c films, the penetration depth is measured because the correlation length is very short and thus electron scattering on defects should be negligible. Nevertheless, the defects and the quality of the films can be probed by off-specular scattering. We did not detect any noticeable off-specular scattering in contrast to a rather huge off-specular scattering measured from the film in Ref. 5. This might be the reason why no oscillations were observed on the reflectivity curves [5].

Conclusions

The Nb-films are investigated as a pre-study of HT_c films in order to optimize the parameters of the method . The sample quality, sample size, film thickness, reflection geometries and the film interfaces are investigated. The obtained screening length shows a value already near to the magnetic penetration depth but the difference clearly indicates the influence of the electron scattering on defects. The presented study of HT_c-films shows that the details of the film structure at the interfaces in particular can be obtained. An appreciable Q-range is available to determine the magnetic penetration depth. Nevertheless, the statistics must be further improved to study an eventual non-exponential character of the penetrating magnetic flux.

Acknowledgment

The present work was supported by BMBF under contract Le03Kon and Le04Kon/Dubna.

References

[1] F.London and H.London, Proc. Roy. Soc. (London), A149 (1935) 71
[2] G.P.Felcher, R.T.Kampwirth. K.E.Gray, and Roberto Felici, Phys. Rev. Lett. 52 (1984) 1539
[3] L.P.Chernenko, D.A. Korneev, A.V.Petrenko, N.I.Balalykin, and A.V.Skripnik, Springer Proc. Phys.61 (1992) 209
[4] A.B.Pippard, Proc. Roy. Soc. (London), A216 (1953) 547
[5] H.Zhang, J.W.Lynn, C.F.Majkrzak, S.K.Satija, J.H.Kang, X.D.Wu, PRB 52 (1995) 10395
[6] R.Felici, J.Penfold, R.C.Ward, E.Olsi, and C.Matacotta, Nature 329 (1987) 523)
[7] A.Mansour, R.O.Hilleke, G.P.Felcher, R.B.Laibowitz, P.Chaudhari, and S.S.P.Parkin Physica B 156&157 (1989) 867
[8] S.V.Gaponov, E.B.Dokukin, D.A.Korneev, E.B.Kljuenkov, V.Lebner, V.V.Pasyuk, A.V.Petrenko, H.Rzany, L.P.Chernenko, Pis'ma Zh.Eksp.Teor.Fiz. 49 (1989) 277
[9] G.P.Felcher, Physica B 192 (1993) 137
[10] M.Tinkham, "Introduction to Superconductivity", McGraw-Hill, New-York, 1975
[11] V.V.Pasyuk, D.A. Korneev, A.V.Petrenko and E.B.Dokukin, 2nd International Conference "Surface X-ray and neutron scattering", Bad Honnef, Germany, June 25-28, 1991
[12] Guide to neutron research facilities at the ILL, ILL, Grenoble,pg.74, 1994

MIGRATION OF Ta INTO Si UNDER THE INFLUENCE OF THE FAST HEAVY ION IRRADIATION

A.P.Kobzev, O.A.Nikonov
Frank Laboratory of Neutron Physics, JINR, Dubna, Russia

A.Ju. Didyk, V.A.Skuratov
Flerov Laboratory of Nuclear Reactions, JINR, Dubna, Russia

In recent years, continuous efforts have been undertaken for better understanding of damage production in various materials by swift heavy ions. Oxides are most widely investigated [1]. Recently a phenomenological description of latent track formation in dielectrics and semiconductors was given[2] and in magnetic insulators in [3]. Metals have been thought for a long time as not showing any track formation process. Recently track formation was found in alloys $NiZr_2$ and NiTi [4] at the electronic stopping power, dE/dx , over 40 keV/nm, and in the alloy 12Cr18 Ni10T (dE/dx is about 10 keV/nm) [5]. Even more recently, the obtained experimental evidence of tracks produced in Ti by 845 MeV Pb ions and by 18 MeV ^{60}Co ions [6] demonstrated that metals are , also, susceptible to track formation. Semiconductors, however, seem to have received less attention. Only a few articles present the experimental results on semiconductors irradiated by high energy heavy ions (see, for example refs.[7-9]).

In this report we discuss our new results in the field of radiation stimulated impurity migration in silicon with deposited layers of various impurities (like Pd, Ta and so on). All samples were prepared in VINCA Institute (Belgrade, Yugoslavia).

The samples of silicon single crystals were covered with a thin layer of Ta (the structure of the layer as follows: a silicon substrate with the thickness 300 μm, and 165 nm of Ta). The samples were irradiated by 210 MeV Kr ions with the fluence Ft= $3*10^{13}$ ions/cm^2 and then annealed in vacuum at the temperature 700^{0}C for one hour. A RBS analysis of irradiated and nonirradiated samples was undertaken using a He ion beam generated by the Van de Graaff accelerator of the Frank Laboratory of Neutron Physics of JINR[10].

Figure1 shows the energy spectra for 2.4 MeV $^4He^+$ ions scattered at the angle 170° for both irradiated and nonirradiated samples of silicon covered with a Ta layer. The beam spot width is about 1,5 mm for the incident angle φ=30° and was increases to 4mm for φ=75°. Figure1 shows the spectra for φ=30°. One can see a big difference between the curves. Processing these spectra we obtain the depth profiles of Ta, Si and O (Fig.2). The same depth profiles are obtained by processing the spectra for the incident angle φ=75°. From Fig.2 one can see that the depth of migration of Ta and O atoms is about 500 nm after annealing and irradiation (IA). The depth of migration of Ta and O atoms is 350 nm and 500 nm, respectively, for an annealed but nonirradiated sample (A). The increasing migration of Ta atoms in samples irradiated with Kr ions can be connected with the so called "track structure" (a destructive zone along the projected ranges of Kr ions). The integration of Fick equation for diffusion leads to the following solution for the impurity profile after annealing:

$$C(x,t) = Q/(\pi Dt)^{1/2} * \exp(-x^2/(4Dt)), \qquad 1$$

where Q is the remaining amount of atoms per area unit which was measured after annealing, D is the diffusion coefficient and t is the annealing time. A satisfactory fit of experimental profiles for Ta atoms can be carried out for both A and IA cases. The following values of adjustable parameters for the diffusion of oxygen atoms, Ta atoms, D_{IA}^{Ta}, D_A^{Ta} are found:

$$D_{IA}^{Ta} \cong 6.8*10^{-14} \text{ cm}^2/\text{s} \text{ and } D_A^{Ta} \cong 1.5*10^{-14} \text{ cm}^2/\text{s} \qquad (2)$$

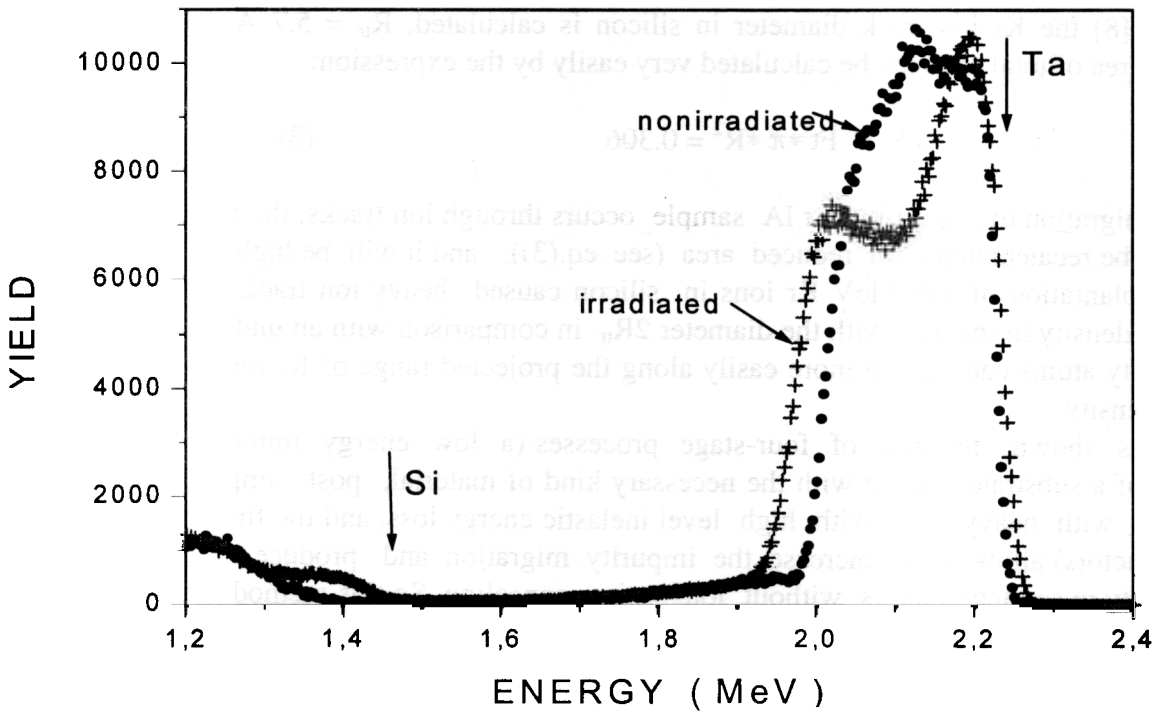

Fig.1. The RBS spectra for irradiated and nonirradiated Ta/Si samples.

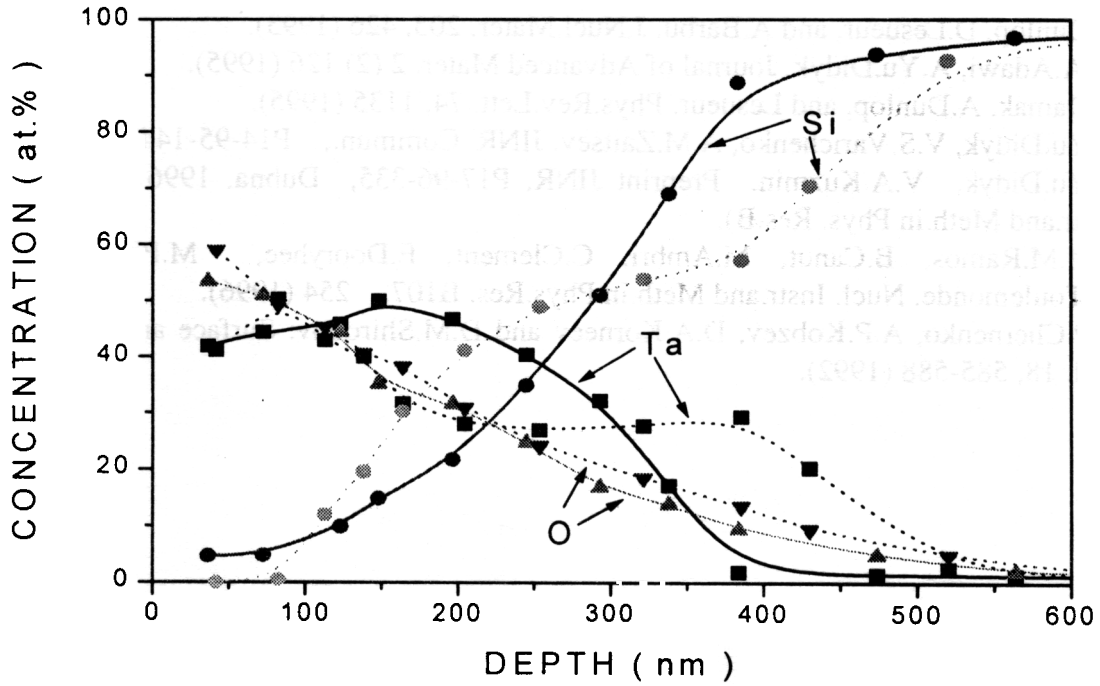

Fig.2. The element depth profiles for Si/Ta samples. Dot lines correspond to the irradiated and annealed sample, solid lines - to the annealed but nonirradiated sample.

In [8] the Kr ion track diameter in silicon is calculated, R_{tr} = 5.7 A. Thus the relative damaged area of total area can be calculated very easily by the expression:

$$\Delta S/S = Ft * \pi * R^2 = 0.306 \qquad (3)$$

If the migration of impurities for IA sample occurs through ion tracks, the migration coefficient D_{IA} has to be recalculated for a reduced area (see eq.(3)), and it will be higher.

The implantation of 210 MeV Kr ions in silicon caused heavy ion track formation with a decreased density in the area with the diameter $2R_{tr}$ in comparison with an undamaged material. So the impurity atoms can diffuse more easily along the projected range of Kr ions in the area with a reduced density.

As it is shown the use of four-stage processes (a low energy impurity implantation or covering of a substrate surface with the necessary kind of material, post implantation annealing, irradiation with heavy ions with high level inelastic energy loss, and the final heat treatment of semiconductors) allows us to increase the impurity migration and produce the necessary type of conductivity in semiconductors without longer time annealing. So this method has good future in the new technology of semiconductor device production.

This study was performed under the support of the International Atomic Energy Agency.

REFERENCES

1. M.Toulemonde, S.Bouffard, and F.Studer. Nucl. Instr.and Meth.in Phys. Res. B91, 108 (1994).
2. A.Yu.Didyk, V.S.Varichenko. Radiation Measurements, 25, No 1-4, 119 (1995).
3. G.Szenes. Phys.Rev. B51, 8096 (1995).
4. A.Dunlop, D.Lesueur, and A.Barbu. J.Nucl.Mater. 205, 426 (1993).
5. M.A.Adawi, A.Yu.Didyk. Journal of Advanced Mater. 2 (2) 126 (1995).
6. H.Damak, A.Dunlop, and Lesueur. Phys.Rev.Lett. 74, 1135 (1995).
7. A.Yu.Didyk, V.S.Varichenko, A.M.Zaitsev. JINR Commun., P14-95-144, Dubna, 1995.
8. A.Yu.Didyk, V.A.Kuzmin. Preprint JINR, P17-96-335, Dubna, 1996 (Submitted to Nucl. Instr.and Meth.in Phys. Res.B).
9. S.M.M.Ramos, B.Canut, M.Ambri, C.Clement, E.Dooryhee, M.Pitaval. P.Thevenard, M.Toulemonde. Nucl. Instr.and Meth.in Phys.Res. B107, 254 (1996).
10. L.P.Chernenko, A.P.Kobzev, D.A.Korneev and D.M.Shirokov. Surface and Interface Analysis. Vol. 18, 585-588 (1992).

A SURVEY OF HEAVY METAL DEPOSITION IN ROMANIA USING MOSSES AS BIOMONITORS

M.V. FRONTASYEVA, C. OPREA, A. LUCACIU*, E. STEINNES**

*Institute of Physics and Nuclear Engineering, Bucharest, Romania
**Norwegian University of Science and Technology, Trondheim, Norway

This is the first systematic study of air pollution with heavy metals and other trace elements in several industrial areas and national parks of the Eastern Romanian Carpathians using a well-established moss biomonitoring technique [1]. Samples of moss *Hylocomium splendens* from 120 sites were analyzed by epithermal neutron activation analysis at the IBR-2 pulsed fast reactor in JINR, Dubna, for a wide range of elements, including some heavy metals and rare earths (*Na, Mg, Al, Cl, K, Ca, Sc, V, Cr, Mn, Fe, Co, Ni* (through the (n, p) reaction), *Zn, As, Se, Br, Rb, Sr, Zr, Mo, Ag, Sn, Sb, I, Cs, Ba, La, Ce, Nd, Sm, Eu, Gd, Tb, Yb, Hf, Ta, W, Au, Th, and U*). Copper, cadmium and lead were determined by flame AAS. Certified reference materials of mosses prepared for the 1995 European moss survey were used to check the quality of the measurements. The results are presented in the form of colored contour maps prepared using GIS (geographic information system) technologies [2].

The regional extent of pollution with some specific metals was studied in particular. In the northern part of the country, the highest concentrations of *Cu, Pb, Zn, As*, and *U* were observed in the area of the Baia Mare mining complex. Moreover, the results show that the polymetallic and manganese mining industries pollute a vast territory with *Mn, Cd, U,* and *Th*. The central part of the Eastern Carpathians is mainly affected by non-ferrous metal industries in Bistrita Nasaud. Gas and oil drilling and refining, as well as thermal power stations, are responsible for *Ni, V, Mo, W, Cu, Cr, As, Sn*, and *Cd* pollution in the Moinesti-Darmanesti and Bacau areas. In the valley of Prahova in the Curvure Carpathians, elevated levels of elements characteristic for gas-oil refinery were observed. However, in these areas of the Eastern Carpathians the particular elemental composition of the bedrock may also have influenced the results by soil particles adhering to the mosses.

This particular study was undertaken as a Romanian-Norwegian-Russian collaboration in order to cover one more "white spot" on the map of Europe for heavy metal atmospheric deposition. Our results are reasonably consistent with those recently reported from similar studies using the moss technique in Germany[3], the Netherlands, Poland [4,5], Bulgaria [6], and other countries on the European continent.

The authors express their gratitude to students of the International University of Nature, Society and Man «Dubna» O.V. Shorenkova and V.M. Komkova for map designing.

REFERENCES

[1] BERG, O., ROYSET, O., and STEINNES, E. Moss used as a biomonitor of atmospheric trace element deposition: Estimation of uptake efficiences. *Atmos.Environ.* 1995, 29 (3), p. 352-360.

[2] LUCACIU, A., FRONTASYEVA, M.V., STEINNES, E., CHEREMISINA, YE.N., OPREA, C., PROGULOVA, T.B., STAICU, L., TIMOFTE, L. Atmospheric deposition of heavy metals in Romania studied by the moss biomonitoring technique employing nuclear and related analytical techniques and GIS technology. *First Int. Symposium on Nucl. and Rel. Tech. in Agr., Ind., Health and Envin.*, (NURT-1997).

[3] MARKERT, B. and al. The German heavy metal survey by means of mosses. *Sci. Total Environ.*, 1996, 182, p. 159-168.

[4] HERPIN, U. and al. The distribution of heavy metals in a transect of the three states the Netherlands, Germany and Poland, determined with the aid of moss monitoring. *Sci. Total Environ.*, 1996, 187, p. 185-198.

[5] MARKERT, B. and al. A comparison of heavy metal deposition in selected Eastern European countries using the moss monitoring method, with special emphasis on the "Black Triangle". *Sci. Total Environ..*, 1996, 193, p. 85-100.

[6] DJINGOVA, R. and al. Heavy metal distribution in Bulgaria using Poplus nigra 'Italica' as a biomonitor. *Sci. Total Environ.*, 1995, 172, p. 151-158.

MEASUREMENTS OF THE THERMAL NEUTRON CROSS SECTION OF THE $^{17}O(n,\alpha)^{14}C$, $^{21}Ne(n,\alpha)^{18}O$, AND $^{36}Ar(n,p)^{33}S$ REACTIONS FOR GASEOUS SAMPLES

Yu.M.Gledenov, V.I.Salatski, P.V.Sedyshev, P.J.Szalanski, J.Andrzejewski*, A.Zak
*University of Lodz, Poland

The new ionization chamber for gaseous samples was designed and tested on the thermal and resonance neutron beams of the FLNP neutron sources. The exposed gas volume serves as the target for neutrons (see Fig.1).

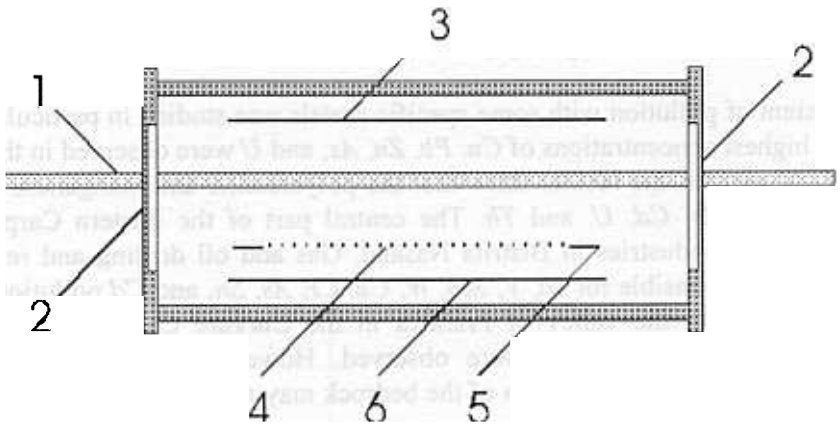

Fig.1. Experimental setup : 1-neutron beam formed by collimators to the split size 60x12 mm, 2-entrance and exit windows made from thin (100-500 μm) aluminium, 3-cathode, 4-grid, 5-grids frame, 6-anode.

The chamber is specifically designed to investigate (n,p) and (n,α) reactions that play the important role in the s-process producing rare ^{36}S isotopes [1]. Until now we measured the thermal cross section for $^{17}O(n,\alpha)^{14}C$, $^{36}Ar(n,\alpha)^{33}S$ (Fig.2) $^{21}Ne(n,\alpha)^{18}O$ (Fig.3) using the relative method where the determined cross section is compared with the cross sections of the $^{3}He(n,p)^{3}H$ (Fig.2) and $^{17}O(n,\alpha)^{14}C$ (Fig.3) reactions. Our results (233±12) mb, (5.43±0.27) mb and (0.18±0.09) mb, respeclively, are in good agreement with the values obtained by other authors for the $^{17}O(n,\alpha)^{14}C$ and $^{36}Ar(n,\alpha)^{33}S$ reactions [2,3] and significantly lower than the estimated upper reported earlier for the $^{21}Ne(n,\alpha)^{18}O$ reaction [4,5]

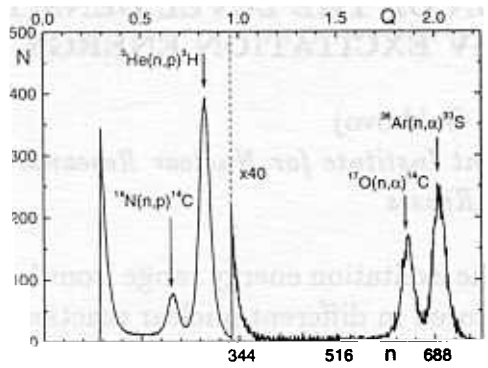

Fig.2. Pulse-height spectra with 93.75%Ar, 6.25%CO_2 and $1.8\cdot10^{-5}$%^{3}He gas mixture at 1.2 atm.

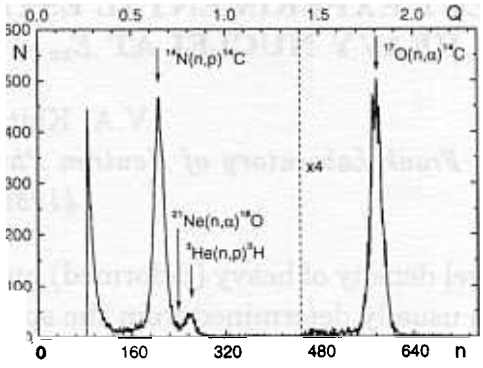

Fig.3. Pulse-height spectra with 95%Ne and 5%CO_2 gas mixture at 1.7 atm.

In the near future we plan to investigate the $^{21}Ne(n,\alpha)^{18}O$ reaction further to decrease our experimental error, which is presently about 50%, and measure the $^{39}Ar(n,\alpha)^{36}S$ cross section for thermal neutrons.

1. H.Beer and R.D.Renzhorn, Astron. Astrophys. **174** (1987), p.323.
2. S.F.Mughabghab et al., Neutron Cross Sections, vol.1, Academic, New York, 1981
3. G.C.Hanna et al., Can. J. Phys. **39** (1961), p.1784.
4. A.I.Abramov, M.G.Yutkin, J. Exp. Theor. Phys. **41** (1961), p.1023.
5. E.F.Bennett, W.C.Redman, P, ANL-7357, 96 (1967).

DIRECT EXPERIMENTAL ESTIMATION OF THE LEVEL DENSITY IN HEAVY NUCLEI AT $E_{ex} < 3 - 5$ MeV EXCITATION ENERGY

V.A. Khitrov, A.M. Sukhovoj
Frank Laboratory of Neutron Physics, Joint Institute for Nuclear Research
141980 Dubna, Russia

The level density of heavy (deformed) nucleus in the excitation energy range from 1-2 to 3-5 MeV is usually determined from the spectra measured in different nuclear reactions in the frame of some model ideas of reaction mechanisms. Therefore, it is extremely important to perform a direct experimental determination of the level density.

Using the sum coincidence technique [1], the positions of levels were established with high confidence level [2] up to the excitation energy of ~ 4 MeV for even-even deformed nuclei and up to ~ 3 MeV for N-odd nuclei. An ordinary detector equipment used for this purpose in FLNP JINR allows us to reveal all such states if only the intensity of cascades populating them exceeds the detection threshold $L_c \simeq 10^{-4}$ events per decay of the compound state excited after thermal neutron capture. Certainly, the presence of the detection threshold permits one to observe only part of nuclear levels.

Nevertheless, using the classical assumption about the shape of the intensity distribution of cascade primary transitions with respect to their mean value [3] (the so-called Porter-Thomas distribution), one can estimate the complete set of nuclear states. For this purpose, the parameters of the Porter-Thomas distribution are fitted to reproduce, as well as possible, the cumulative sum $\sum i_{\gamma\gamma}$ of the experimental cascade intensities (with the summation over their final levels) as a function of its running value for the cascades with $i_{\gamma\gamma} > L_c$. The parameters obtained in such a way are used to extrapolate the $\sum i_{\gamma\gamma}$ dependence into the region $i_{\gamma\gamma} < L_c$.

This procedure was performed for more than 30 nuclei from the mass region $114 \leq A \leq 200$. Most essential results are:

(a) the number of the observed levels in any nucleus below its excitation energy 1-2 MeV is considerably larger than that predicted by models which consider the nucleus as the gas of non-interacting Fermi particles (for example [4]);

(b) at higher excitation energies (at least, in the 2 MeV interval), observed level density is considerably less than the predictions [4]. Also one cannot exclude the possibility that the level density in this interval is almost constant.

Such behaviour of the level density is observed for all studied by us rather far from magic N nuclei. The effect can be interpreted within assumptions about the strong influence of vibrational excitations (phonon energy is some hundred keV) on the nuclear properties below 1-2 MeV and a sharp transition [5] of a nucleus to possible many-quasiparticle excitations at the energy which corresponds to the temperature of the phase transition predicted by the BCS-theory (accounting for a decrease of this temperature for a mixture of Fermi and Bose particles).

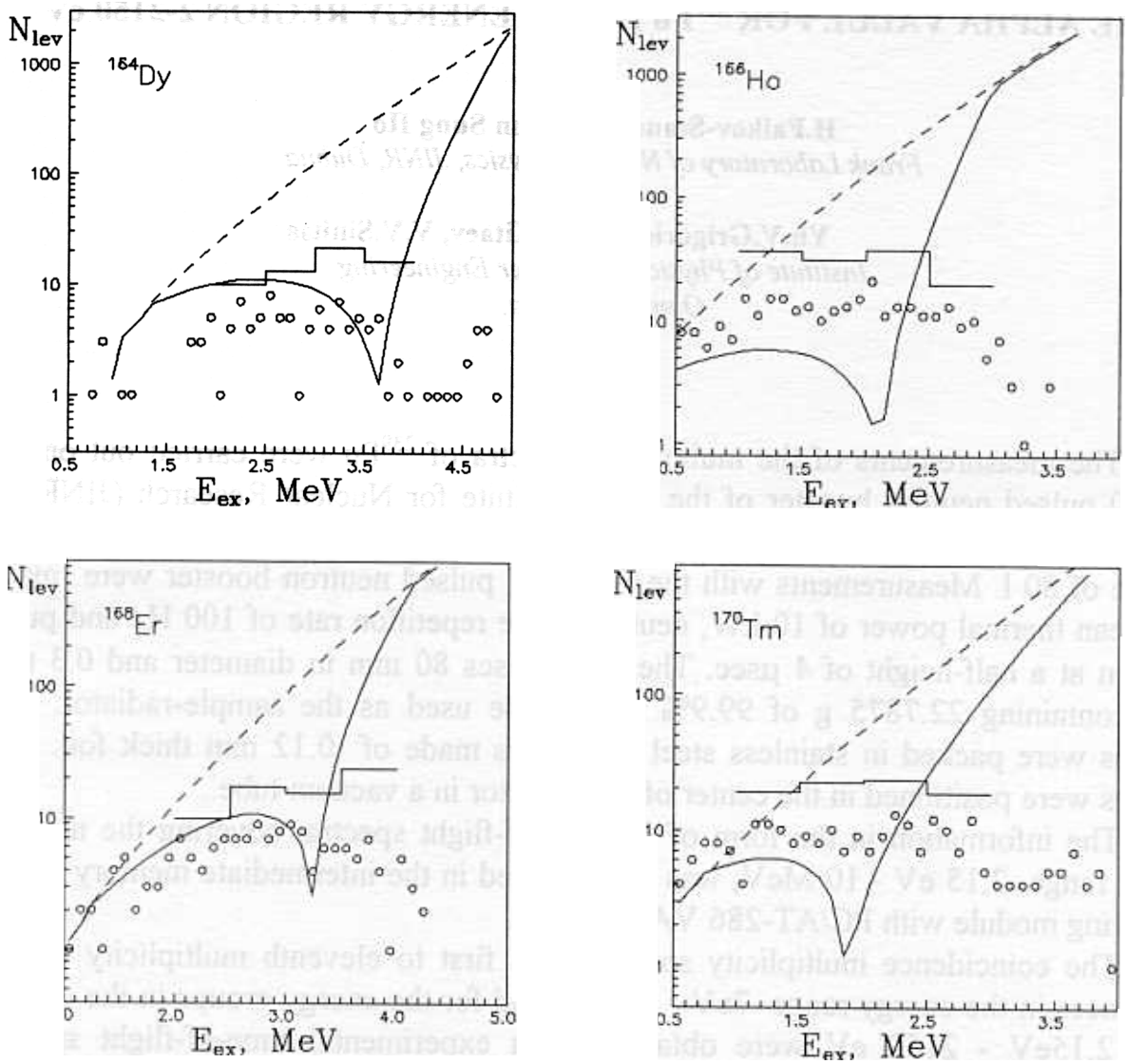

Fig. 1. Comparative level densities for different excitation energies in some investigated nuclei. Dashed lines - extrapolated [4] number of levels, excited by the primary cascade E1- and M1-transitions in the 100 keV interval. Solid lines are the same values calculated in the frame of the hypothesis [5]. Histograms are the estimation of the possible number of intermediate levels at zero detection threshold. Points are the number of the observed cascade intermediate levels at the experimental detection thresholds.

1. S.T.Boneva et al., Sov. J. Part. Nucl. **22(2)** (1991) 232
2. S.T.Boneva et al., Izv. AN SSSR, Ser. Fiz. **51(11)** (1987) 2023
3. C.F.Porter and R.G.Thomas, Phys. Rev. **104(2)** (1956) 483
4. W.Dilg, W.Schantl, H.Vonach and M.Uhl, Nucl. Phys. **A217** (1973) 269
5. S.T.Boneva, V.A.Khitrov, Yu.P.Popov., A.M.Sukhovoj Proc. of IV International Seminar on Interaction of Neutrons with Nuclei "Neutron Spectroscopy, Nuclear Structure, Related Topics, Dubna, April 27-29, 1996, E3-96-336, Dubna,1996, p.183

MEASUREMENT OF THE GAMMA-RAY MULTIPLICITY SPECTRA AND THE ALPHA VALUE FOR ^{239}Pu IN THE ENERGY REGION 2-2150 eV

H.Faikov-Stanczyk, Hyon Sung Ho
Frank Laboratory of Neutron Physics, JINR, Dubna

Yu.V.Grigoriev, V.Ya.Kitaev, V.V.Sinitsa
Institute of Physics and Power Engineering
Obninsk, Russia.

The measurements of the multiplicity spectra of ^{239}Pu were carried out on the IBR-30 pulsed neutron booster of the Joint Institute for Nuclear Research (JINR) in Dubna at 122 m flight paths with a 16-section liquid scintillation detector of a total volume of 80 l. Measurements with the IBR-30 pulsed neutron booster were made at a mean thermal power of 10 kW, neutron pulse repetition rate of 100 Hz and pulse duration at a half-height of 4 μsec. The metal discs 80 mm in diameter and 0.3 mm thick containing 22.7875 g of 99.9% ^{239}Pu were used as the sample-radiator. The samples were packed in stainless steel containers made of 0.12 mm thick foil. The samples were positioned in the center of the detector in a vacuum tube..

The information in the form of 16 time-of-flight spectra, covering the neutron energy range 2,15 eV - 10 MeV, was accumulated in the intermediate memory of the measuring module with PC/AT-286 VANG.

The coincidence multiplicity spectra from first to eleventh multiplicity for 50 resonances in the energy range 7eV - 180 eV and for the energy groups in the energy range 2.15eV - 2150 eV were obtained from experimental time-of-flight spectra following subtraction of the background component. They were normalized to unity and are presented in Fig. 1. The shape of the multiplicity spectra for the resonances with small fission widths is essentially different from the shape of spectra with large fission widths.

So the resonances at 52.52 eV and 164.33 eV with small fission widths $\Gamma_f = 9$ meV and 8 meV, respectively, have the mean multiplicities $K_m = 4.69$ and 4.78, and the resonances, at 47.50 eV and 156.90 eV, with large fission widths $\Gamma_f = 248$ meV and 537 meV have $K_m = 5.89$ and 6.07.

Thus, the first resonances are actually captured, and the second ones are fissionable resonances. These resonances were used to separating the multiplicity spectra of other resonances into the two components of the fission and radiative capture processes. From standard spectra, first the small components of radiative capture and fission were subtracted. To separate the initial multiplicity spectra, as the reference multiplicities for forming the captive spectrum, the first and the second multiplicities were used, where fission does not actually manifest itself. To obtain the fission part of the spectrum the multiplicities higher than sixth were used, where the radiative capture is absent.

Dividing of the total multiplicity spectra into two parts makes it possible to determine the alpha value by the formula:

$$\alpha = \sigma_\gamma/\sigma_f = N_\gamma\,\varepsilon_f / N_f\,\varepsilon_\gamma = \\ = A\,\Sigma K_{i\gamma}\,/\Sigma K_{if}$$

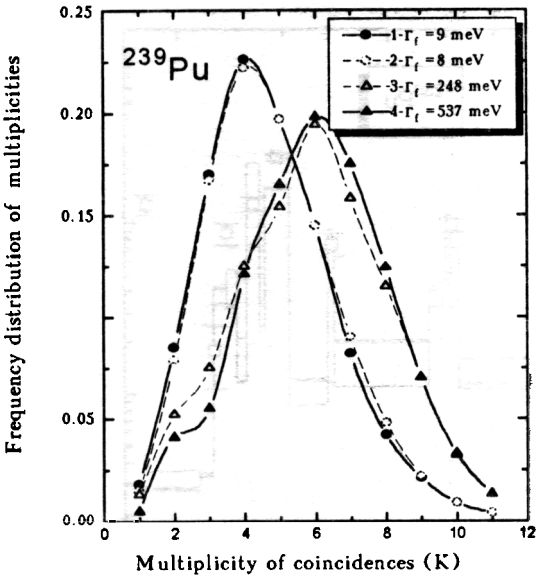

Fig.1 The multiplicity spectra for resonances of ^{239}Pu with different fission widths.

where σ_γ, σ_f are the radiative capture and fission cross-sections; N_γ, N_f are the total number of counts of capture and fission gamma-quanta and $K_{i\gamma}$, K_{if} are the i-st multiplicity radiative capture and fission. Assuming that the efficiencies $(\varepsilon_\gamma, \varepsilon_f)$ of gamma-quantum registration do not depend on energy, one can determine the value $A = \varphi\,(\varepsilon_f/\varepsilon_\gamma)$ by normalizing to the alpha value, obtained in the precision measurements in [2]. The errors in the alpha value are mainly determined by the errors in the decomposition of the total multiplicity spectra into components from the fission events and the radiative capture events. The errors from the uncertainties in the efficiency of gamma-quanta registration are considerably less, because the value A is close to unity. (As a result of the normalization of alpha over 13 resonances from this experiment and from [2], the ratio of the efficiencies is given as equal to unity). The experimental alpha values are shown in Table 1 and in Fig.2.

Table 1.

Experimental and calculated alpha value for ^{239}Pu.

E(eV)	J	<K>	$E_1 - E_2$ (eV)	α(p.w.) (exp)	α ENDF/B-6	α JENDL-3	α BROND-2
7.826	1	4.52	7.30 - 8.28	0.83±0.06	0.824	0.821	0.698
10.92	1	5.07	10.18-11.48	0.31±0.06	0.323	0.282	0.334
11.89	1	4.33	11.48-12.32	1.91±0.20	2.203	2.093	2.251
14.30	1	4.75	13.70-14.50	0.54±0.04	0.519	0.483	0.541
14.65	0	4.48	14.50-15.07	0.87±0.05	1.055	1.001	0.985
15.44	1	5.15	15.07-16.49	0.29±0.05	0.147	0.142	0.164
17.64	1	4.44	17.11-18.19	0.83±0.06	1.071	1.014	1.060

For comparison, the results of evaluation obtained by the GRUCON computer program [3] on the basis of the BROND-2 [4], ENDF/B-6 [5], and JENDL-3 [6] library data are also presented. The experimental and calculated alpha values were obtained in the energy intervals below 50 resonances and in the energy groups (see Tables 2 and 3). As can be seen from Fig.2 and Tab.1 the calculated alpha value of different libraries differ by 5-30%, and in some resonances by 50-100%.

The experimental alpha values differ from the calculated ones most significantly for small and large alpha values, when the contribution of the radiative capture or fission to the total multiplicity spectrum is small and the uncertainty increases greatly

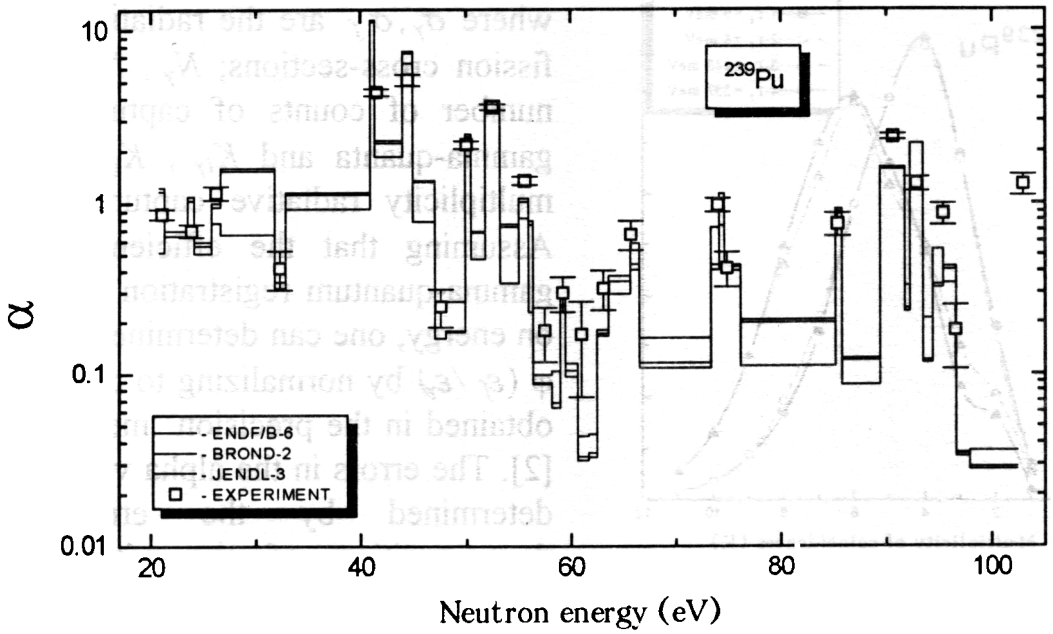

Fig.2 Experimental and calculated alpha values $\alpha = \sigma_\gamma \quad \sigma_f$ *for* ^{239}Pu.

as the spectrum decomposes into its component parts according to accepted standard spectra. These uncertainties decrease when one determines the experimental and calculated alpha values in the wide energy groups (Tables 2 and 3) and using of a large number of resonances. The experimental errors of the alpha values in some resonances amount to 2- 12% for large alpha values; for small alpha values, the errors may achieve to 60%. In the energy groups, the errors are significantly less than 1-5%, but when compared with the experimental data from other papers it is higher than 100% (see Tables 2 and 3).

Table 2.

Experimental and calculated alpha value for ^{239}Pu in the energy groups.

E(eV)	21.5-46.5	46.5-100	100-215	215-465	465-1000	1000-2150
P.work	1.45	0.52	0.80	-	0.80	0.72
BNAB	1.07	0.57	0.87	0.93	0.83	0.89
BROND-2	1.04	0.44	0.61	0.84	0.97	0.97
ENDF/B-6	1.54	0.50	0.71	0.82	0.88	1.00
JENDL-3	1.48	0.48	0.68	0.79	0.87	1.10

In this way, the extensive experimental materials presented in this work give evidence of the great possibilities of the radiation multiplicity spectrometry method for fissionable nuclei. The determination of the alpha value by this method is more precise than in [1,2] because of better resolution. The general view of the obtained results

shows good agreement between experimental data and the evaluated values.

Table 3.

Experimental and calculated alpha value for ^{239}Pu in the energy groups.

E(keV)	0.1--0.2	0.2--0.3	0.3--0.4	0.4--0.5	0.5--0.6	0.6--0.7	0.7--0.8	0.8--0.9	0.9--1.0	1.0--2.0
Gwin (1976)	0.87	0.94	1.16	0.44	0.72	1.54	0.97	0.82	0.70	0.84
Schomb. (1970)	0.96	0.79	1.13	0.44	0.63	1.44	0.94	0.53	0.55	0.69
Czirr (1970)	0.78	0.86	1.11	0.45	0.65	1.60	0.90	0.64	0.70	0.85
Farrell (1970)	0.67	0.67	0.94	0.57	0.64	1.68	0.85	0.79	0.70	1.17
Weston (1972)	0.87	0.93	1.15	0.43	0.72	1.49	0.89	0.71	0.68	0.80
Sowerby (1972)	0.85	0.91	1.15	0.48	0.70	1.67	0.97	0.78	0.93	1.11
Derrien (1989)	0.87	0.93	1.19	0.41	0.71	1.52	0.90	0.75	0.62	-
Belayev (1970)	0.88	1.07	1.23	0.45	0.75	1.72	0.94	0.78	0.71	0.85
Ryabov (1976)	0.85	1.00	1.00	0.88	0.84	1.41	1.31	1.15	1.21	1.04
Bergman (1976)	-	0.74	0.95	0.76	0.95	1.15	0.98	0.88	0.90	1.02
Bolotsky (1977)	0.93	0.92	1.17	0.59	0.75	1.46	1.00	0.78	0.76	0.85
Kononov (1971)	0.71	1.31	1.71	0.48	0.68	0.75	1.03	0.68	0.48	0.65
Muradyan(1986)	0.94	10.1	1.31	0.64	0.93	1.25	1.25	0.87	0.87	1.06
P.work	0.83	0.92	-	0.63	0.69	1.68	1.24	0.72	0.72	0.71
BROND-2[4]	0.62	0.70	1.11	0.55	0.83	1.43	1.09	0.89	0.77	0.90
ENDF/B-6[5]	0.71	0.83	0.82	0.61	0.88	1.21	0.96	0.73	0.88	0.94
JENDL-3 [6]	0.68	0.80	0.79	0.56	0.83	1.98	0.91	0.88	0.87	1.00

Simultaneously, it might be good to point out significant differences in the alpha values from the experiments and calculations made on the basis of the evaluated constants of the last library versions of BROND-2, ENDF/B-6, JENDL-3 for some isolated resonances.

The newly obtained experimental data make it possible to determine the alpha value more precisely in some resolved resonances and in the given energy groups, and permit one to set the problem of the re-estimation of the alpha value in the mentioned libraries. In the future, it would be advisable to continue the investigation in this direction to study the Doppler-effect and the resonance self-shielding in the alpha value.

References

Adamchuk, Yu.V., Voskanyan M.A., Muradyan G.V. et al. *Measurement of the alpha value for the ^{235}U and ^{239}Pu resonances.* Proc. National Conference on Neutron Physics. Kiev, 1983, v.2, p.137.

2. Adamchuk, Yu.V., Voskanyan M.A., Muradyan G.V., et al. *Measurement of the alpha value for the ^{239}Pu resonances,* M: Atom. Energy, v.61, no.3, 1986, p.199.
3 Sinitsa V.V. *Program for calculating the group constants using the library of evaluated neutron data,* VANT, ser. Nuclear Constants, 1984, v.5(59), p.34.
4. Blokhin A.I., Ignatyuk A.V., Kuzminov B.A. et al., In Proc. of Inter. Conf. on Nuclear Data for Science and Technolgy. Julich FRG, 1991, p.800
5 Rose P.F., Dunford C.K., ed. ENDF-102. *Data Formats and Procedures for the Evaluated Nuclear Data File*, ENDF, report BNL, Upton, New York, 11973, USA, 1988.
6. Shibata K. et al. Japanese Evaluated Nuclear Data Library. Version JENDL-3. Rep. JAERI 1319, 1990.

5. PUBLICATIONS

CONDENSED MATTER PHYSICS

Reviews

1. Aksenov V.L. Present-Day Methods of Neutron Diffraction Analysis. Poverkhnost', X-Ray, Synchrotron and Neutron Investigations, 1997, v.7, pp. 20-24 (in Russian).
2. Aksenov V.L., Nikitenko Yu.V. Polarized Neutron Investigations. Ibid., 1997, v.12, p.5 (in Russian).
3. Balagurov A.M. Condensed Matter Studies on IBR-2 Reactor of LNP JINR in 90s. Ibid., 1997, v.7, pp.123-135 (in Russian).
4. Nietz V.V. Neutron Scattering Studies under the Influence of Pulsed Magnetic Field. Ibid., 1997, v.7, pp.72-81 (in Russian).
5. Serdyuk I.N. Novel Development of SANS for Biological Molecules Studies. Ibid., 1997, v.7, pp.39-44 (in Russian).

Diffraction

1. Abakumov A.M. et al. Effect of Fluorination on the Structure and Superconducting Properties of the *Hg-1201* Phase. JINR Communication, E14-97-234, 1997, Dubna; Phys. Rev. Lett., 1998, v.80, pp.385-388.
2. Aksenov V.L. et al. Investigation of the *Hg-1201* Structure under External Pressures up to 5 GPa by Neutron Powder Diffraction. Physica C, 1997, v.275, pp.87-92.
3. Aksenov V.L. et al. Performance of the High Resolution Fourier Diffractometer at the IBR-2 Pulsed Reactor. J. of Neutron Research, 1997, v.5, pp.181-200.
4. Aksenov V.L., Balagurov A.M., Trounov V.A. High-Resolution Fourier Diffractometry for Long Pulse Spallation Sources. J. of Neutron Research, 1997, v.6, pp.135-148.
5. Aksenov V.L., Ossipyan Yu.A., Shakhmatov V.S. Structural Peculiarities of $AC_{60}(A=K, Rb)$ Fullerides. J. Low Temp. Phys., 1997, v.107, p.547.
6. Antipov E.V. et al. Structural Features, Oxygen and Fluorine Doping in *Cu*-Based Superconductors. Physica C, 1997, v.282-287, pp.61-64.
7. Antipov E.V. et al. Synthesis and Neutron Powder Diffraction Study of $HgBa_2CuO_{4+\delta}$. Advances in Superconductivity IX, Eds: S.Nakajima, M.Murakmi, 1997, v.1, pp.427-432.
8. Avdeev M.Yu. et al. Structure Refinement of Two One-Dimentional Solid Electrolytes. Neorganicheskaya Khimiya, 1997 (in Russian) (in press).
9. Balagurov A.M. et al. Influence of Deoxygenation Process on Magnetic Diagram of Iron Doped YBa_2CuO_y Phases: a Neutron Diffraction Study. Physica C, 1997, v.288, pp.10-20.
10. Balagurov A.M. et al. Magnetic Structure of UPd_2Ge_2 Doped by Iron. JETP Lett., 1997, v.66, pp.615-619 (in Russian).
11. Balagurov A.M. et al. Neutron Diffraction Study of Structural Changes in Ammonium Halides ND_4Br and ND_4Cl under High Pressure. JINR Communication, P14-97-147, 1997, Dubna (in Russian), Sov. Phys. of Solid State. 1997 (in press) .
12. Demande P. et al. NMR and Neutron Diffraction Analysis of Oriented Phospholipid Bilayer Interacting with Annexin V. Europ. Biophys. J., 1997, v.26, N 1, p.91.
13. Fedotov V.K. et al. Neutron Diffraction Investigation of γ Manganese Hydride. Z. Phys. Chem., 1997 (in press).
14. Fedotov V.K. et al. Study of the α-*Mn* Solid Solution by Neutron Scattering. Poverchnost', 1997 (in Russian), (in press).
15. Gordeliy V.I., Chernov N.I. Accuracy of Determination of Position and Width of Molecular Groups in Biological and Lipid Membranes *via* Neutron Difraction. Acta Cryst., 1997, D53, pp-377-384.
16. Khvatinskaya D.Ya., Tashmetov M.Yu., Em V.T. Short Range Order in Allows *Ti-Ta-C*. Neorganic Materials, 1997, v.33, N 3, pp.320-323.
17. Luzin V. Optimization of the Texture Measurements I: Method. Textures and Microstructures 1997 (in press).

18. Luzin V. Optimization of the Texture Measurements II: Further Applications. Textures and Microstructures, 1997 (in press).
19. Lychagina T.A., Nikolayev D.I. Influence of the Texture on *Al-6%Mg* Alloy Deformation. Textures and Microstructures (in press).
20. Mestres L. et al. *X*-Ray and Neutron Powder Diffraction Study of the $Rb_{2-x}(NH_4)_xSO_4$ System. J. Phys. Soc. Jpn., 1997 (in press).
21. Nevriva M. et al. Single Crystal Growth and the Structure of $Bi_2Sr_2Ca_{1-x}Y_xCu_2O_{8+y}$. Electrochemical Society Proceedings, 1997, v.39, pp.480-486.
22. Nikolayev D.I. Numerical Computations of the Physical Property Averages. Textures and Microstructures, 1997 (in press).
23. Nikolayev D.I., Schaeben H. Calculus of the Pole Density Function. Textures and Microstructures, 1997 (in press).
24. Nikolayev D.I., Savyolova T.I. Normal Distribution on the Rotation Group *SO(3).* Textures and Microstructures, 1997, v.29, pp.201-233.
25. Plyasova L.M. et al. Neutron Diffraction Study of Structure of Reducted Cuprous Chromate. Poverchnoct', 1997 (in Russian), (in press).
26. Pomjakushin V.Yu. et al. Microscopic Phase Separation in La_2CuO_{4+y} Induced by the Superconducting Transition. Phys Rev Lett., 1997 (in press).
27. Pomjakushin V.Yu. et al. Phase Separation in La_2CuO_{4+y} Single Crystals Studied by μSR and Neutron Diffraction. Physica C, 1997, v.282-287, pp.1353-1354.
28. Prokert F., Savenko B.N., Balagurov A.M. Neutron Diffraction Study of Phase Transitions in Mixed Crystal $Sr_{0.7}Ba_{0.3}Nb_2O_6$ between 20 and 300 K. Ferroelectrics, 1997, v.188, pp.187-199.
29. Schaeben H., Nikolayev D.I. A Note on the Notion of the Central Limit Theorem in the Component Fit Method. Acta Applicandae Mathematicae, 1997 (in press).
30. Scheffzyek Ch. Intracrystalline Strain Measurements of Quartz Samples from the Elbe-Zone by Means of a Double Bent-Crystal Neutron Diffractometer. Textures and Microstructures, 1997 (in press).
31. Scheffzyek Ch. Texture Investigation of Natural and Experimentally Deformed Halite from the Zielitz and Merkers Mine by Neutron Diffraction. Textures and Microstructures, 1997 (in press).
32. Siegesmund S. et al. Application of Geological Fabric Analysis to Characterize Natural Building Stones - Case Study: Kauffung marble. Internationale Zeitschrift fur Bauinstandsetzen , 1997, N 3, pp.1-15 (in German).
33. Skirl S. et al. Analysis of Residual Stresses in Al_2O_3/Al Composites with Interpenetrating Networks. Part I: Neutron Diffraction. Acta Materialia, 1997 (in press).
34. Tashmetov M.Yu., Em V.T., Savenko B.N. Influence of Monmetal Atoms on the Ordered Structures of Titanium Carbide. Sov. Phys. of Solid State, 1997 (in press).
35. Tashmetov M.Yu., Myhtarova N.N., Em V.T. Investigation Ordered Structures in the Titanium Oxycarbides. Fizika Metallov I Metalovedenie, 1997, v.83, N 3, pp. 117-121 (in Russian).
36. Ullemeyer K., Weber K. Texture Analysis of Rocks: Lattice Preferred Orientation as an Indicator of a Complicated Deformation History. Textures and Microstructures, 1997 (in press).
37. Yakovlev V.B., Nikitin A.N. Microstress Modelling on Crystallite Surfaces in Textured Polycrystalline Quartz. J. Earthquake Pred. Res. 1997, v.6, pp.235-243.

Small-Angle Scattering

1. Avdeev M.V. et al. Multi-Ring Position-Sensitive Detector for Registering Small-Angle Neutron Scattering. Nucl. Instr. Meth. A. 1997, v. 392, pp.18-22.
2. Balasoin M. Et al. Temperature Dependent Structure of the $CoFe_2O_4$ Colloidal Solutions Investigated with SANS. JINR Communication, E14-97-121, 1997, Dubna; Rom. Rep. Physics, 1997, v.49, pp.9-10.
3. Bulavin L.A. et al. Measurements of the Structural, Electrostatic Parameters and Surface Tension of Micelles of an Ionic Surfactant versus Concentration, Ionic Strength of Solution and Temperature by SANS. Colloids and Surfaces, 1997, v.2080 (in press).
4. Bulavin L.A. et al. Structure of Micellar Aggregates of Non-Ionic Surfactants in Salt-Water Solutions by SANS. Colloid J. Russ. Acad. Sci.-Engl., 1997, v. 59, pp. 13-18.
5. Dubnickova M. et al. Effect of N-Lauryl-N,N-Dimethylamin N-Oxide on Dimyristoyl Phosphatidylcholine Bilayer Thickness: A Small-Angle Neutron Scattering Study. Gen. Physiol. Biophys, 1997, v.16, pp.175-188.
6. Garamus V.M., Pedersen J.S. Carbon Black Dispersion in Non-Ionic Surfactant Water Solutions. Colloids and Surfaces, 1997, v.2415 (in press).

7. Garamus V.M.. The Study of Mixed Micelles Varying Temperature by Small-Angle Neutron Scattering. Langmuir, 1997, v.13, pp.6388-6392.
8. Gorski N. et al. A SANS Investigation of the TDMAO Micelle System at High Hydrostatic Pressure. J. Appl. Cryst., 1997 (in press).
9. Gorski N. et al. The Shape of *Se*-Precipitates in a CdS_xSe_{1-x} - Doped Glass. Ber. Bunsenges. Phys. Chem., 1997, v.101, pp.1552-1554.
10. Gorski N., Kalus J. Determination of the Structure of Tetradecyldimethylaminoxide Micelles in Water by Small-Angle Neutron Scattering. J. Phys. Chem. B, 1997, v.101, pp.4390-4393.
11. Islamov A. et al. Small-Angle Neutron Scattering Studies of Aqueous Phospholipid/nonionic Surfactant Mixtures. J. of Colloid & Interface Sci., 1997 (in press).
12. Kriz J. et al. NMR and SANS Study of Poly(methylmethacrylate)-block-poly(acrylic acid) Micelles and Their Solubilization Interactions with Organic Solubilizates in D_2O. Macromolecules, 1996, v.29, pp.7853-7858.
13. Lixin Fan et al. Determination of Deuterium Incorporation in a Two-Component Particle by Small-Angle Neutron Scattering. Physica B, 1997, v.234-236, pp.196-198.
14. Lixin Fan et al. Determination of Deuterium Incorporation in to RNA and Protein Components of the E.coli Ribosome at Biosynthetic Deuteration by Small-Angle Neutron Scattering. J. Appl. Cryst., 1997, v.30, pp.59-64.
15. Mischenko N. et al. Interaction Betwen the Micellar Knots of the Physical Network in Triblock Copolymer Gels. Colloid and Polymer Science, 1997 (in press).
16. Serdyuk I.N. Neutron Scattering in the Ribosome Structure. Physica B, 1997, v.234-236, pp.188-192.
17. Serdyuk I.N., Galzitskaya O.V., Timchenko A.A. On the Nature of Roughness of the Globular Proteins. Biofizika, 1997, v.42, pp.1197-1207 (in Russian).
18. Serdyuk I.N., Zaccai G. Triple Isotopic Substitution in Small-Angle Neutron Scattering: Application to Some Problems of Structural Biology. J. Appl. Cryst., 1997, v.30, pp.1-5.
19. Shcherbakova I.V. et al. Metabolic Regulation of Selective Deuterium Incorporation into RNA and Protein Components of the Ribosome. Biological Macromolecular Dynamics. Proceedings of a Workshope on Inelastic and Quasielastic Neutron Scattering in Biology (Ed. S.Cusack), Adenine Press, 1997, pp.165-169.
20. Timchenko A.A., Galevskkaya O.V., Serdyuk I.N. Roughness of the Globular Protein Surface: Analysis of High Resolution *X*-Ray Data. Proteins, 1997, v.28, pp.194-201.
21. Ulitin A.B., Agarov S.Ch., Serdyuk I.N. Preparation of a "Beheaded" Derivative of the 30S Ribosomal Subunit. Biochimie, 1997, v.79, pp.523-526.

Reflectometry, Polarized Neutrons

1. Aksenov V.L. et al. Polarized Neutron Reflectometry Method for Direct Measurement of the Magnetic Field Penetration Depth in *Nb* and *YBa2Cu3O7* Superconducting Films. Poverkhnost', 1997 (in Russian), (in press).
2. Aksenov V.L. et al. Refraction of Polarized Neutrons in a Magnetically Non-Collinear Layer. Physica B, 1997, v.234-236, pp.513-515.
3. Davtyan L.S. Geometry of Adiabatic Changes. International Journal of Theoretical Physics, 1997, v.36, N 3, pp.673-680.
4. Hope S. et al. Thickness Dependence of the Total Magnetic Moment per Atom in the *Cu/Ni/Cu/Si(001)* System. Phys. Rev. 1997, B55, pp.11422-11431.
5. Lauter H.J. et al. Determination of the Magnetic Field Penetration Depth in *YBa2Cu3O7* Superconducting Films by Polarised Neutron Reflectometry. Physica B, 1997 (in press).
6. Lauter-Pasyuk V. et al. Direct Measurement of the Magnetic Field Penetration Depth in *YBa2Cu3O7* and *Nb* Superconducting Films by Polarised Neutron Reflection. Physica B, 1997 (in press).
7. Lauter-Pasyuk V. et al. Effect of Nanoparticle Size on the Internal Structure of Copolymer-Nanoparticles Composite thin Films Studied by Neutron Reflection. Physica B, 1997 (in press).
8. Lauter-Pasyuk V. et al. Neutron Reflectivity Studies of Composite Nanoparticle-Copolymer Thin Films. Physica B, 1997 (in press).

Inelastic Neutron Scattering

Balagurov A.M. et al. Spectrometer for Neutron Inelastic Scattering Investigations of Microsamples. JINR Communication, P13-97-312, 1997, Dubna (in Russian).

2. Barthell J. et al. Quasielastic Neutron Scattering on the 0.94m Tetrabutylammonium Chloride Aqueous Solution. J. Mol. Liquids (in press).
3. Blagoveschenskii N.M. et al. The Investigation of Liquid Helium by Neutron Scattering. New Data Analysis. Fiz. Niz. Temp, 1997, v.23, N 5-6, pp.509-514 (in Russian).
4. Bogoyavlenskii I.V. et al. Neutron Scattering Study of *4He S(Q,w)* at the Phonon-Maxon Region. Physica B, 1997, v.234-236, pp.324.
5. Bogoyavlenskii I.V., Puchkov A.V., Skomorokhov A.N. Analysis of Liquid He^4 Neutron Scattering Data on Basis of the Glyde-Griffin Model. Physica B, Condensed Matter, 1997 (in press).
6. Danilkin S.A., Jadrowski E.L. Phonon Dispersion in *Nb* on Time-of-Flight Spectrometer DIN-2PI on IBR-2 Reactor. JINR Communication, D14-97-64, 1997, Dubna (in Russian).
7. Danilkin S.A., Jadrowski E.L. Phonon Dispersion in *Fe-18Cr-10Mn-15Ni* FCC Steel. Physica B, 1997, v. 234-236, pp. 900-902.
8. Danilkin S. et al. X-Ray and Neutron Scattering Study of the α-NbO_x Solid Solutions. J of Alloys and Compounds, 1997 (in press).
9. Morozov S.I. Site Occupation and Local Modes of Hydrogen in V_2N and Ta_2N. Physica B, 1997, v.234-236, p.32.
10. Novikov A.G. et al. The Study of Hydration Effects in Aqueous Solution of *LiCl* and *CsCl* by Inelastic Neutron Scattering. J. Chemical Physics, 1997 (in press).
11. Novikov A.G. et al. Study of *Li+* Ion Hydration by Inelastic Neutron Scattering. Physica B, 1997, v.234-236, p.340.
12. Novikov A.G. et al. The Effects of Positive and Negative Hydration in Quasielastic Cold Neutron Scattering. Zh. Neorg. Khimii, 1997, v.42, N 9, pp.1580-1586 (in Russian).
13. Novikov A.G. et al. Collective Dynamics of Liquid Potassium Studied by Inelastic Neutron Scattering. Physica B, 1997, v.234-236, pp.359.
14. Parshin P.P., Zemlyanov M.G., Sumin V.V. The Structure and the Lattice Dynamics of Hydrogen Amorphized $PrNi_2H(D)_{3.6}$. Sov. Phys. of Solid State, 1997 (in Russian), (in press).
15. Semenov V.A. Inelastic Neutron Scattering Investigation of Cr_2O_3. Sov. Phys. of Solid State, 1997 (in Russian), (in press).
16. Sumin V.V. Local Modes of Interstitial Atoms in Transition Metals. Sov. Phys. of Solid State, 1997, v.39, N 1, pp.23-27 (in Russian).
17. Sumin V.V., Gantulga Ch. Study of Hydrogen Capture by Oxygen or Nitrogen in Transition Metals Using the Inelastic Neutron Scattering Method. Fizika Metallov I Metallovedeniya, 1997, v.8, N 5, pp.115-125 (in Russian).
18. Sumin V.V., Gantulga Ch. The Interaction of Oxygen (Nitrogen) with Hydrogen in *Ti, V* and *Ta*. J. of Alloys and Compounds, 1997, v.253-254, pp.275-278.
19. Zajezhev M.V. et al. Problems of Slow-Neutron Scattering of Liquid Alkali Metals. Physica B, 1997, v.234-236, p.919.

Accelerated Ions and μSR

1. Duginov V.N. et al. μSR Study of Intermediate Heavy Fermion Compound $CeRuSi_2$. Phys. Rev. B, 1997, v.55, N 18.
2. Duvanov S.M., Kabyshev A.V., Kobzev A.P. Ion Beam and Electrical Conductivity Analysis of Nanocrystalline α-Al_2O_3 Ceramics Implanted with *Ti+n* Ions and Annealed. Materials Science Forum, 1997, v.248-249, pp.271-277.
3. Jaworska D., Kobzev A.P. The Backside Gettering of *Au* in Silicon. Electron Technology (Warszawa), 1997, v.30, N 2, pp. 149-155.
4. Kobzev A.P. et al. Element Depth Profiles of Porous Silicon. JINR Communication, E14-97-184, 1997, Dubna (in Russian).
5. Krivosheev I.A. et al. Magnetic Structure of Holmium Studied by μSR. JETP Lett., 1997, v.65, N 1, p.81 (in Russian).
6. Krivosheev I.A. et al. Heavy Fermion Compound $CeRuSi_2$ Studied by μSR. Hyperfine Interactions, 1997, v.105, p.187.
7. Mamedov T.N. et al. Anomalous Frequency Shift of Negative Muon Precession in *n*-Type Silicon. Hyperfine Interactions, 1997, v.105, pp. 345.

8. Pomjakushin V.Yu. et al. Spin Freezing in Superconducting $La_2CuO_{4.03}$ Single Crystal. Hyperfine Interactions, 1997, v.105, pp.83-88.
9. Povarova R.B. et al. Study of the *NiAl* Structure Alloyed by Titanium. Izvestiya RAS, Metalls, 1997, N 1, pp.118-122 (in Russian).
10. Zastavenko L.G., Chernenko L.P., Chernenko A.G. Photon Localiszation Limit or On Film Thickness Measurements by the X-Ray Emission Technique. JINR Communication, P14-97-230, 1997, Dubna (in Russian).

Conferences

1. Aksenov V.L. et al. Investigation of the *Hg-1201* Structure under External Pressure up to 5 GPa by Neutron Powder Diffraction. ECNS'96, October 6-7, 1996; Physica B , 1997, v.234-236, pp.940-941.
2. Avdeev M.V., Garamus V.M. Study of Nonionic Surfactants in the Water-Salt Solution by SANS. 1st Open Conference of USC, JINR, February 24-27, 1997, Dubna, Russia.
3. Avdeev M.V. State of the Project "Multi-Ring PSD for the YuMO SANS Spectrometer". XV IWANSSSP, March 17-23, 1997, Zarechny, Russia.
4. Avdeev M.Yu. et al. The Cation Distribution in Non- Stoichiometric Titanes Found by X-Ray Single Crystal and Neutron Powder Diffraction and Bond Valence Calculations. RSNE-97, May 26-29, 1997, Dubna (in Russian).
5. Avdeev M.Yu. et al. X-Ray and Neutron Diffraction if New Family of Solid Electrolytes, RSNE-97, May 26-29, 1997, Dubna.
6. Baeva M. et al. Investigation of Nitrogen *Fe-Cr-Ni* Steels by Inelastic Neutron Scattering, Neutron and X-Ray Diffraction. XV IWANSSSP, March 17-23, 1997, Zarechny, Russia,
7. Balagurov A.M. et al. Single-Crystal Diffraction Study of Phase Separation *in* La_2CuO_{4+y}. ECNS'96, October 6-7, 1996; Physica B, 1997, v.234-36, pp.797-799.
8. Bodnarchuk V.I., Korneev D.A. Neutron Reflection from Magnetic Films with Nondiagonal Reflectivity Matrices. XV IWANSSSP, March 17-23, 1997, Zarechny, Russia
9. Bokuchava G.D. et al. Residual Stress Investigations in Austenitic Steel Samples with Different Degree of Low Cycle Fatigue. Neutron Texture and Stress Analysis (NTSA), June 23-26, 1997, Dubna.
10. Bokuchava G.D. et al. Determination of Residual Stresses in *WCu* Gradient Materials. NTSA, June 23-26, 1997, Dubna.
11. Bokuchava G.D., Sikolenko V.V., Korenev S.A. Neutron Diffraction Investigation of Effects, Induced in Materials by High Current Pulsed Electron Beam Irradiation. EPDIC-V, May 25-28, 1997, Parma, Italy.
12. Borovik A.S., Kobzev A.P., Kovaleva E.A. Investigation of the $YBa_2Cu_3O_7$ Oxygen Subsell. XX International Meeting on Interaction of the Charged Particles with the Crystals, May 26-28, 1997, Moscow.
13. Bulavin L.A., Garamus V.M., Karmazina T.V. Mixed Micelles Varying Temperature by Small-Angle Neutron Scattering. American Crystallographic Association Annual Meeting, July 19-25, 1997, St. Louis, USA.
14. Bulavin L.A., Garamus V.M., Karmazina T.V. Parameters of Mixed Micelles Varying Temperature by Small-Angle Neutron Scattering. 11th Conference of the European Colloid and Interface Society, September 14-19, 1997, Lunteren, The Netherlands.
15. Efimova G.A.. et al. A High-Temperature Apparatus for the Investigation of Physical Properties of Geological Materials by Means of Neutron Diffraction. NTSA, June 23-26, 1997, Dubna, Rissia.
16. Efimova G.A., Kireenkova S.M., Nikitin A.N. The Influence of the Loading Conditions on the Physical Parameters Values of Rocks at the Phase Transformations under High Pressure. EGS-97, April 21-25, Vienna, Austria.
17. Efimova G.A. et al. Modelling of Processes in Rocks and Minerals of Seismological Zones at High Pressures and High Temperatures and Comparison with Neutron Diffraction Data. NTSA, June 23-26, 1997, Dubna, Russia.
18. Chromik S. et al. Properties of YBCO/PBCO/YBCO Trilayer Structures. Third European Conference on Applied Superconductivity, June 30 - July 3, 1997, Koningshof, The Netherlands.
19. Grigorieva N.B. et al. Structure Defects of Anion Excessive Fluorite $Ca_{1-x}R_xF_{2+x}$ Phases. Symposium on Structure and Properties of Crystalline Materials, March 4-6, 1997, Dubna.
20. Kiselev M.A. et al. Investigation of the Temperature Induced Micelle to Lamellar Transition via Small Angle Neutron Scattering. XV Intern. Workshop on the Applications of Neutron Scattering to Solid State Physics, March 17-23, 1997, Zarechny, Russia.
21. Kiselev M.A., Lesieur P., Kisselev A.M. Investigation of Dimethyl-sulfoxide Influence on the Structure and Properties of the Phospholipid Membranes. National Conference for Application of *X*-Ray, Synchrotron Radiation, Neutrons and Electrons for Materials Study, May 25-29, 1997, Dubna, Russia (in Russian).

22. Kisselev A.M. et al. Temperature Induced Micelle to Vesicle Transition as Studied by Neutron and *X*-Ray Small Angle Scattering. NATO ASI "Dynamical Properties of Unconventional Magnetic Systems", April 2-12, 1997, Gielo, Norway.
23. Kiselev M.A. et al. The Dimethyl-Sulfoxide Influence on the Phase Transitions of Phospholipid Membranes: SAXS, SANS and DSC Study. International Workshop "Instrumentation and Methods of Synchrotron Radiation Investigations in Condensed Matter", September 4-9, 1997, Belovezskaya Puscha, Republic of Belarus.
24. Kobzev A.P. The Major Topics of the Investigation at the EG-5 Accelerator JINR. XII Conference on Electrostatic Accelerators, November 25-27, 1997, Obninsk, Russia.
25. Kockelmann H. Neutron and *X*-Ray Diffraction Measurements of Residual Stresses in a Shape Welded Steel Tube. NTSA, June 23-26, 1997, Dubna, Russia.
26. Levashvili V.L. et al. Neutron Bragg and Diffuse Scattering Investigation of Defect in Single Crystals of ZrO_2-Y_2O_3 Cubic Stabilized Zirconia. SCD, March 1997, Dubna.
27. Luzin V. Optimization of the Texture Measurements III: Statistical Relevance of ODF Represented by Individual Orientations. International Conference on Texture and Anisotropy of Polycrystals, Materials Science Forum, September 22-25, 1997, Clausthal, Germany.
28. Martinez-Sarrion M.L. et al. *X*-Ray and Neutron Powder Diffraction Study of $RB_{2-X}(NH_4)_XSO_4$. System. National Conference for Application of *X*-Ray, Synchrotron Radiation, Neutrons and Electrons for Materials Study, May 25-29, 1997, Dubna, Russia (in Russian).
29. Martinez-Sarrion M.L. et al. Phase Diagram and Ammonium Ion Role in the Paraelectric-Ferroelectric Phase Transition in $Rb_{2-x}(NH_4)_xSO_4$. 3-rd Baltic Ferromagnetics Seminar, June 1-7, 1997, Bozeman, Montana, USA.
30. Martinez-Sarrion M.L. et al. Phase Diagram And Ammonium Ion Role. 3-rd Baltic Ferromagnetics Seminar June 1-7, 1997, Bozeman, Montana, USA.
31. Martinez-Sarrion M.L. et al. X-Ray and Neutron Powder Diffraction Study of $RB_{2-X}(NH_4)_XSO_4$. System, ESM-17, August 24-28, 1997, Lisbon.
32. Mironova G.M. On the Mechanism of Superconductivity. M2S-HTSC-V, March, 1997, p.857, Beijing, China.
33. Mironova G.M. Angle-Resolved Time-of Flight Neutron Scattering as a New Method for Condensed Matter Investigations. 4-th Int. Sem. on Neutron Scattering Investigations, April 10-12, 1997, Poznan, Poland.
34. Mironova G.M. Critical Role of Secondary Structure in Radiation Propagation through Matter. SSCD, March 4-6, 1997, Dubna, Russia.
35. Mironova G.M. Alternative Approach to Radiation Interaction with Matter. EPDIC-5, May 25-28, 1997, Parma, Italy.
36. Mironova G.M. Lasting Effect in Neutron Scattering. EPDIC-5, May 25-28, 1997, Parma, Italy.
37. Mironova G.M. Real Time Diffraction, Transmition, Small Angle and Inelastic Neutron Scattering. EPDIC-5, May 25-28, 1997, Parma, Italy.
38. Mironova G.M. Caustics in Scattering Spectra. National Conference for Application of *X*-Ray, Synchrotron Radiation, Neutrons and Electrons for Materials Study, May 25-29, 1997, Dubna, Russia (in Russian).
39. Mironova G.M. Time of Flight Neutron Transmission and Scattering in Mutually Perpendicular Planes - a New Method for Studying Orientation Effects in Solids. NTSA, June 23-26, 1997, Dubna, Russia.
40. Morozov S.I. et al. Site Location and Dynamics of Hydrogen in Ternary Interstitial Phases. International Conference on Neutron Scattering, August 17-21, 1997, Toronto, Canada.
41. Natkaniec I. Et al. Neutron Diagram and Ammonium Ion Role In the $RB_{2-X}(NH_4)_XSO_4$ Mixed Crystals. XV IWANSSSP, March 17-23, 1997, Zarechny, Russia
42. Nikitin A.N., Ivankina T.I. Formation of Texturized Rocks with Piezoelectric Properties. EGS-97, April 21-25, Vienna, Austria.
43. Popov Yu.P. et al. New Method of Analysis of Intermediate Energy Neutron Spectra (3 keV< E_n <100 keV). International Seminar on Interaction of Neutrons with Nuclei, May 14-17, 1997, Dubna, Russia.
44. Popov Yu.P. et al. New Method of Analysis of Intermediate Energy Neutron Spectra (3 keV< E_n <100 keV). XLVII Meeting on Nuclear Spectroscopy and Structure of Atomic Nucleus, June 10-13, 1997, Obninsk, Russia.
45. Pros Z. Et al. Investigation of Texturized Solid Bodies by Ultrasonic Waves and Neutron Diffraction. EGS-97, April 21-25, Vienna, Austria.
46. Pros Z. et al. Investigation of Texturized Solid Bodies by Ultrasonic Waves and Neutron Diffraction. NTSA, June 23-26, 1997, Dubna, Russia.
47. Ullemeyer K. et al. Neutron Time-of-Flight Pole-Figure Measurements of Geological Samples at the SKAT Multidetector System. Conference on Deformation Mechanisms in Nature and Experiment, March 17-19, 1997, Basel, Switzerland.

NEUTRON NUCLEAR PHYSICS

Experiment

1. Aleksejevs A. et al. Evaluation of Neutron Fundamental Parameters from the Total Cross-Section Data., Physica Scripta, v. 56, pp. 20-25, 1997.
2. Alexandrov Yu.A. Investigation of the Electromagnetic Properties of the Neutron and the Neutron Charge Radius. JINR, E3-96-336, p.365, ISINN-4.
3. Alfimenkov V.P. et al. Energy and Orientation Dependence of Neutron Depolarization in a Large Single Crystal of Ferromagnetic Holmium. J. Appl. Phys., v. 81, p.1358, 1997.
4. Alfimenkov V.P. et al. Experimental Set-Up and the Results of Left-Right Asymmetry Measurement in ^{235}U Fission Fragment Angular Distributions as a Function of Polarized Neutron Energy. ISINN-4, JINR, E3-96-336, Dubna, p.120, 1996.
5. Alfimenkov V.P. et al. Investigation of the Parity Violation and Interference Effects in ^{235}U Fission Induced by Resonance Neutrons. JINR Comm., E3-97-106, Dubna, 1997.
6. Alfimenkov V.P. et al. Polarized Epithermal Neutron Studies of Magnetic Domains. In: Application of Accel. in Research and Industry, Ed. J.L. Duggan and I.L. Morgan., AIP Press, N.Y., p.345, 1997.
7. Alfimenkov V.P. et al. Study of Parity Violation Effect in Interaction of Neutrons with Polarized La Nuclei. Yad. Fiz., ,v. 59, p. 1929, 1996 (in Russian).
8. Ali M.A. et al. A Semi-Phenomenological Approach to Describing Heavy Nuclei Neutron resonance Cascade Gamma-Decay. In: "Nuclear structure and related topics", Contributions, Dubna, E4-97-218, 1997, p.13.
9. Ali M.A. et al. Cascade Gamma Decay of the ^{182}Ta Compound State. Izv. RAN, Ser. Fiz., v.61, p. 2082, 1997 (in Russian).
10. Ali M.A. et al. Two-Step Gamma-Cascades After Thermal Neutron Capture in ^{127}I. Ibid, p.2093.
11. Ali M.A., Khitrov V.A., Sukhovoj A.M. A Search for the Strong Vibrational Excitations in Heavy Nuclei Below E_{ex}<3-5 MeV, In: "Nuclear structure and related topics", JINR, Dubna, E4-97-218, 1997, p.14.
12. Andreyev A. et al. Alpha-Decay Characteristics of Neutron-Deficient ^{190}Po, ^{189}Bi and ^{186}Pb Isotopes. Z.Phys. A358, (1997), p.63-68.
13. Bagryanov B.V. et al. First Results on Testing of the Ultracold Neutrons Pulsed Source at BIGR Reactor (Sarov, VNIIEF). V International Seminar on the Interaction of Neutrons with Nuclei, ISINN-5, Dubna, 14-17 May 1997, JINR.
14. Beer H. et al. Stellar Neutron Capture Rates of Nuclei Near Magic Neutron and Proton Shells, ISINN-5, Neutron Spectroscopy, Nuclear Structure, Related Topics (Abstracts), Dubna, 1997, p.64.
15. Belyaev V.B. et al. Triple Collisions in the Star Plasma. Proceedings of XVth Int. Conf. on Few-Body Problems in Physics, Groningen, The Netherlands, 22-26 July 1997, p.392.
16. Bogdzel A.A. et al. Analysis of Energy Dependence of Fission Fragment Angular Distribution in Resonance Neutron Induced Fission of ^{235}U Aligned Target. ISINN-5, Abstracts, p.82, Dubna, May 14-17, 1997, JINR E3-97-93, Dubna, 1997.
17. Bondarenko I.V. et al. Proposed Fundamental Investigations Using Interference Filters and Gravity Spectrometry. Proceeding of the International Symposium on Neutron Optics and Related Research Facilities, Kumatory, 1996. J.Phys. Soc. Jap. 1996, v.65, Suppl.A, pp.29-32.
18. Boneva S.T.et al. On Improving the Accuracy of Describing the Parameters of Neutron Resonance Cascade Gamma-Decay Using the Idea of Nuclear Phase Transition. In: International Conference on Nuclear Data for Science and Technology, May 19-24, 1997, Trieste, Italy, Abstract Book, p.90.
19. Brudanin V.B. et al. General Purpose Supercompact Compton Suppression Gamma Spectrometer. International Conference on Nuclear Data for Science and Technology Abstract book, p.63, Trieste, May 19-24, 1997.
20. Budnik A.D. et al. Calculation of the Thermal Neutron Background in a Planned Experiment of Measuring the *N-N* Scattering Cross Section at the BIGR Pulsed Reactor. JINR, P3-97-20, Dubna, 1997 (in Russian).
21. Bulgakov et al. Measurements of $d + d \rightarrow {}^3He + n$ Cross-Section at ultra low Energies. Yad. Fiz. , v. 60, p.1349, 1997.
22. Bunatyan G.G. et al. On the Neutron Charge Radius and the New Experiments Proposed for the Precise *(n,e)* - Scattering Length Measurement. Z.Phys A (in Press).
23. Chen Zemin et al. Angular Distribution and Cross Section Measurements of $^{64}Zn(n,\alpha)^{61}Ni$ Reaction for Neutron Energy 5 MeV. Proceedings of the International Conference on Nuclear Data for Science and Technology, Trieste, May 19-24, 1997, p.42.

24. Crawford B.E. et al. Neutron Capture Parity Violation Study in $^{106,108}Pd$. Bull. of the Am. Phys. Soc., 42, 1071 (1997).
25. Crawford B.E. et al. Parity Nonconservation in ^{238}U neutron Resonances. Bull. of the Am. Phys. Soc., 42, 1667 (1997).
26. Enik E. et al. First Investigations on UGRA Spectrometer., ISINN-5, Abstracts , JINR, E3-97-95., Dubna, p. 72, 1997.
27. Fajkow-Stanczyk H. et al. Gamma-Ray Multiplicity Spectra and the Alpha Value for ^{239}Pu in Groups and Resolved Resonances. Preprint JINR, E3-97-212, Dubna, 1997 (submitted to Journal of Physics G).
28. Fajkow-Stanczyk H. et al. The Gamma-Ray Multiplicity Spectra and the Alpha Value for ^{239}Pu in Groups and Resolved Resonances. International Conference on Nuclear Data for Science and Technology, Trieste, 19-24 May 1997.
29. Fotiades N. et al. Spectroscopy of ^{192}Po. Phys.Rev. C., vol.55, (1997), p.1724-1729.
30. Fotiades N. et al. Spectroscopy of $^{193,195,197}Po$. Phys.Rev. C., vol.56, (1997), p.729.
31. Furman W.I. et al. Anticompton *HpGe-BGO* Gamma Spectrometer for Nuclear Physics Experiments at Pulsed Neutron Sources. International Conference on Nuclear Data for Science and Technology, Abstract book, p.64, Trieste, May 19-24, 1997.
32. Furman W.I. et al. Energy Dependence of Fission Fragment Angular Anisotropy in Slow Neutron Induced Fission of ^{235}U Aligned Target. Int .Conf. on Nuclear Data for Science and Technology. Trieste, May 19-24, 1997, Abstract book, p.56.
33. Furman W.I. et al. Energy Dependence of Fission Fragment Angular Anisotropy in Resonance Neutron Induced Fission of ^{235}U. Dynamical Aspects of Nuclear Fission. Proceedings of 3-rd Int. Conf. Casta Papiernicka, Aug. 30-Sep. 4, 1996, JINR E6,7-97-49, p.356, Dubna, 1997.
34. Georgiev G.P. et al. Study of Gamma-Ray Multiplicity Spectra for Radiative Capture of Neutrons in $^{113,115}In$. INDC (CCP) - 405, IAEA Nuclear Data Section, Vienna, 1997.
35. Gledenov Yu.M. et al. Measurements of the Cross Sections for the $^{17}O(n,\alpha)^{14}N$, $^{36}Ar(n,\alpha)^{33}S$ and $^{21}Ne(n,\alpha)^{18}O$ Reactions Induced by Thermal Neutrons. JINR Comm., P3-97-239, Dubna, 1997 (in Russian).
36. Gledenov Yu.M. et al. Measurements of the Thermal Cross Section of the $^{17}O(n,\alpha)^{14}C$, $^{21}Ne(n,\alpha)^{18}O$ and $^{36}Ar(n,\alpha)^{33}S$ Reactions on Gaseous Samples, ISINN-5, Neutron Spectroscopy, Nuclear Structure, Related Topics (Abstracts), Dubna 1997, p.80.
37. Gledenov Yu.M. et al. Study of the Fast Neutron Induced (n,α) Reaction for Middle-Mass Nuclei. Proceedings of the International Conference on Nuclear Data for Science and Technology, Trieste, May 19-24, 1997, p.41.
38. Gledenov Yu.M.et al. The (n_{th},p) and (n_{th},α) Cross Section Measurements. Proceedings of the International Conference on Nuclear Data for Science and Technology, Trieste, May 19-24, 1997, p.41.
39. Grigoriev Yu.V. et al. Measurements of γ-Multiplicity Spectra and the α-Value for Plutonium-239. Preprint FEI, 2586, Obninsk, 1997 (in Russian).
40. Grigoriev Yu.V. et al. The Measurement of the Gamma-Ray Multiplicity Spectra and the Alpha Value for Uranium-235 and Plutonium-239. IV International Seminar on the Interaction of Neutrons with Nuclei, Dubna, 27-30 April 1996, JINR, E3-96-336, p.318-323, Dubna, 1996.
41. Gunsing F. et al. The Spins of Resonances in Reactions of Neutrons with ^{238}U and ^{113}Cd. Phys. Rev.C, 56, 1641 (1997).
42. Ignatovich V.K., Utsuro M., Ignatovich Ph.V. Forbidden Reflections in Laue Geometry. Phys. Rev.B. (1997). v.55, No.2, p.14039-14042.
43. Ignatovich V.K., Utsuro M. Optical Potential and Dispersion Law for Long-Wave-Length Neutrons. Phys. Rev.B. (1997), v.55, No.22, p.14774-14783.
44. Ignatovich V.K., Utsuro M. Tentative Solution of UCN Problem. PL A 255 (4-6) p. 195-202 1997.
45. Kazarnovski M.V. et al. The New Method for Measurements of the Neutron-Capture Cross Sections for the Maxwellian Neutron Spectra at the Stellar Temperatures. Proceedings of the International Conference on Nuclear Data for Science and Technology, Trieste, May 19-24, 1997, p.265.
46. Keith C.D. et al. Precision Measurement of the Neutron Total Cross Section of ^{3}He in the Energy Range 0.1-500 eV. Bull. of the Am. Phys. Soc., 42, 1686 (1997).
47. Khitrov V.A., Sukhovoj A.M. States of Heavy Nuclei Strongly Excited in the *(n,gamma)* Reaction: Possible Dominant Component at E_{ex}<3-5 MeV. In: International Conference on Nuclear Data for Science and Technology, May 19-24, 1997, Trieste, Italy, Abstract Book, p.89.
48. Khuukhenkhuu G. et al. Systematic of the Fast Neutron Induced *(n,p), (n,α)* Reaction Cross Sections, ISINN-5, Neutron Spectroscopy, Nuclear Structure, Related Topics (Abstracts), Dubna 1997, p.98.

49. Khuukhenkhuu G. et al. Systematical Analysis of (n,α) Reaction Cross Sections in The Wide Energy Range. Proceedings of the International Conference on Nuclear Data for Science and Technology, Trieste, May 19-24, 1997, p.126.
50. Khuukhenkhuu G. et al. Systematics of The Fast Neutron Induced *(n,p)* Reaction Cross Sections. Proceedings of the International Conference on Nuclear Data for Science and Technology, Trieste, May 19-24, 1997, p.127-128.
51. Lowie L.Y. et al. Neutron Resonance Spectroscopy of ^{107}Ag and ^{109}Ag. Phys. Rev.C, 56, 90 (1997).
52. Masalovich S.V., Frank A.I.. Neutron Microscopy with Phase Contrast. Proceeding of the International Symposium on Neutron Optics and Related Research Facilities, Kumatory, 1996. J. Phys. Soc. Jap. 1996, v.65, Suppl.A, pp.159-162.
53. Mayerhofer U. et al. The Nucleus ^{198}Au Investigated with Neutron Capture and Transfer Reactions: II. Construction of the Level Scheme and Calculation of Level Density. Fizika (Zagreb) B5 (1996), p.229-253.
54. Mohr P. et al. Direct Neutron Capture of ^{48}Ca at kT=52 keV. Phys.Rev. C56, p.1154-1156.
55. Mutterer M. et al. Recent Results on the Energetics of the Ternary Fission of ^{252}Cf. DANF-96, JINR E6,7-97-49, p.250, Dubna, 1997.
56. Nosov V.G., Frank A.I. Dynamic Neutron Optics. Proceeding of the International Symposium on Neutron Optics and Related Research Facillities, Kumatory, 1996. J.Phys. Soc. Jap. 1996, v.65, Suppl. A, pp.13-18.
57. Pokoilovski Yu.N. On the Question of Possible Experimental Observation of Anderson Localization of Neutron. JINR, E3-97-117, Dubna, 1997. Z.Phys B (in press).
58. Pokotilovski Yu.N., Rogov A.D. Optimization Study of Ultracold Neutron Sources at TRIGA Reactors Using MCNP. JINR, E3-97-127, Dubna, 1997.
59. Popov Yu.P. et al. New Method of Analysis of Intermediate Energy Neutron Spectra (3 keV<E_N<100 keV), International Workshop «Properties of Nuclei Far from the Stability Valley». Obninsk, 10-13 June, 1997, p.299.
60. Popov Yu.P. et al. New Method of Analysis of Intermediate Energy Neutron Spectra (3 keV ≤E_n≤ 100 keV). ISINN-5, Neutron Spectroscopy, Nuclear Structure, Related Topics (Abstracts), Dubna 1997, p.96.
61. Popov Yu.P. et al. Analysis of Neutron Spectra in the Energy Range from 2 to 100 keV Using High Resolution γ-Spectrometry. XLVII Workshop on Nuclear Spectroscopy and Atomic Structure. Book of Abstracts, p.229. Obninsk, 10-13 June 1997. Submitted to Izv. Akad. Nauk.
62. Popov Yu.P., Sedyshev P.V., Sedysheva M.V. New Method of Analysis of Intermediate Energy Neutron Spectra (1 keV<E_n<100 keV). Proceedings of the International Conference on Nuclear Data for Science and Technology, Trieste, May 19-24, 1997, p.40.
63. Prokofjevs P. et al. Level Scheme of ^{166}Ho. In: "Nuclear structure and related topics", JINR, Dubna, E4-97-218, 1997, p. 76.
64. Rakityansky S.A. et al. Nonradiative pd Fusion in Stellar Plasma. Proceedings of XVth Int. Conf. on Few-Body Problems in Physics, Groningen, The Netherlands, 22-26 July 1997, p.526.
65. Rakityansky S.A. et al. Nonradiative Proton-Deuteron Fusion in Stellar Plasma. Nucl. Phys., vol. A 613, p.132, 1997.
66. Sigel P. et al. High-Energy γ-Ray in α-Accompanied Spontaneous Fission of ^{252}Cf. Z.Phys., A359, p.41, 1997.
67. Sigel P. et al. New Results on γ-Emission in Binary and Ternary Fission of ^{252}Cf. DANF-96, E6,7-97-49, p.262, Dubna, 1997.
68. Sigel P. et al. Ternary Fission Process. Jaresbericht MPI Heidelberg, p.4, 1996.
69. Smith D.A. et al. Parity Violating Asymmetries in ^{117}Sn. Bull. of the Am. Phys. Soc., 42, 1071 (1997).
70. Smith D.A. et al. Parity Violating Asymmetries in the Neutron Resonances of Palladium. Bull. of the Am. Phys. Soc., 42, 1667 (1997).
71. Sofianos S.A. et al. Faddeev Calculations for eta d Scattering. Proceedings of XVth Int. Conf. on Few-Body Problems in Physics, Groningen, The Netherlands, 22-26 July 1997, p.445.
72. Sofianos S.A., Rakityansky S.A. and Vermaak G.P. Sub-Threshold Resonances in Few-Neutron Systems. Journal of Phys. G, vol.23 (1997).
73. Sofianos S.A., Rakityansky S.A. Exact Method for Locating Potential Resonances and Regge Trajectories. Journal of Phys. A, vol. 30, p.3725, 1997.
74. Sofianos S.A., Rakityansky S.A. On the Possibility of η-Mesic Nucleus Formation. Invited talk at European Conference on Advances in Nuclear Physics and Related Areas, Thessaloniki-Greece 8-12 July 1997.
75. Sofianos S.A., Rakityansky S.A., Braun M. Eta-Meson Light Nucleus Scattering and Charge Symmetry Breaking. Invited Talk at the International Workshop on Exciting Physics with New Accelerators Facilities (EXPAF97), SPring8, Aioi, Japan, March 1997.
76. Stephenson S.L. et al. Parity Violation in ^{232}Th Neutron Resonances and Confirmation of the 'Sign Effect'. Bull. of the Am. Phys. Soc., 42, 1667 (1997).

77. Sukhovoj A.M. and Khitrov V.A. Cascade Gamma-Decay of Heavy Nucleus Compound-States. Izv. RAN, Ser. Fiz., v.61, p. 2068, 1997 (in Russian).
78. Sukhovoj A.M. and Khitrov V.A.. Experimental Estimation of Level Density of Heavy Nucleus Really Excited in the *(n,gamma)* Reaction at E_{ex}<3-4 MeV. JINR, P3-97-223, Dubna, 1997 (in Russian).
79. Tambovtsev D.I. et al. Experimental Investigations of the Energy Dependence of the Angular Anisotropy of Fragments from the Resonance Neutrons Induced Fission of Oriented ^{235}U Nuclei.. Yad. Fiz., v.60, issue 6, p.981, 1997 (in Russian).
80. Tang Guoyou et al. Test of the Gic and Measurement of Double Differential Cross Sections for $^{58}Ni(n,p)^{58}Fe$ Reaction at 4.1 MeV. ISINN-5, Neutron Spectroscopy, Nuclear Structure, Related Topics (Abstracts), Dubna 1997, p.78.
81. Varlamov V.E. et al. The Discovery of Penetration of Subbarrier Ultracold Neutrons through Beryllium Foils and Covering Layers. JETP Lett., v. 66, issue 5, pp.317-322 (in Russian).
82. Voronov B.I. et al. Neutron Spectrometer UGRA: Arrangement and Main Characteristics, JINR Comm., P13-97-36, Dubna ,1997.
83. Wilburn W.S. et al. Low Noise Photocathode Preamplifiers for Measuring A_γ in $\vec{n}+p=d+\gamma$. Bull. of the Am. Phys. Soc., 42, 1667 (1997).
84. Zeinalov Sh.S. et al. Fast Detector of Fission Fragments. JINR Comm., P13-97-222, Dubna, 1997 (in Russian).

Theory

1. Barabanov A.L. and Furman W.I. Formal Theory of Neutron Induced Fission., Z.Phys. A, v.357, 1997.
2. Frank A., Gaehler R. Neutron Time Focusing. IV International Seminar on Interaction of Neutrons with Nuclei ISSIN-4 (Dubna, April 27-30, 1996). JINR, E3-96-336, Dubna, 1996.
3. Lamoreaux S.K., Ignatovich V.K. Tidal Pressure Induced Neutrino Emission as an Energy Dissipation Mechanism in Binary Pulsar Systems. J.Phys. Soc. Jap. (1997), v.66, No.4. p.1225-1228.
4. Nosov V.G., Frank A.I. Superlow Neutrons and the Dispersion Law for Neutron Waves in Matter. Physical Review, 1997, v.55,.p.1129-1139.
5. Tretyakova T.Yu., Lanskoy D.E. Λ Hypernuclei with Neutron halo. VI Inter. School-Seminar on Heavy-Ion Physics. Dubna, Sept. 22-27, 1997, Abstracts, p.106.
6. Tretyakova T.Yu., Lanskoy D.E. Structure and Production of Λ Hypernuclei with Neutron halo. Genshikaku Kenkyu, 41, p 49, 1997.
7. Tretyakova T.Yu., Lanskoy D.E. Structure and Production of Λ Hypernuclei with Neutron halo. European Conference on Advances in Nuclear Physics and Related Areas. Thessaloniki, Greece, 8-12 July, 1997. Abstracts, p. 155.

NEUTRON SOURCES

Pepyolyshev Y.N., Vinogradov A.V., Dzvinel W. On a Surveillance Method for Operative Production Quality Using Multivariate Data Classification Application, 30th ISAT, Florence, Italy, 16th-19th June 1997.
2. Pokotilovski Yu.N., Rogov A.D. Optimization Study of Ultracold Neutron Sources at TRIGA Reactors Using MCNP. JINR Comm., E3-97-127, Dubna, 1997.
3. Popov A.K. An Analysis of a Long Power Oscillation Process in the IBR-2 Pulsed Reactor. JINR Comm., P12-97-361, Dubna, 1997 (in Russian).

APPLIED RESEARCH

1. Alekseev I.V. Heterotransitions in Semiconductors with a *TlSe-TlInSe$_2$* Chain Structure. Physics and Technology of Semiconductors (in print).
2. Alekseev I.V., Abdinova S.G. The Spectral Distribution of Response of $TlInSe_2$ Non-Linear Gamma-Ray Detector. Nuclear Instruments and Methods (in print); Preprint JINR P14-97-115, Dubna 1997.
3. Alpatov V.G. et al. Excitation of Isomeric States of $Ag^{107,109}$ Nuclei in Inelastic Scattering of Fast Neutrons from the IBR-2 Reactor of JINR. Preprint ITEP, No.6-97, Moscow, 1997; Yad. Fiz, 1997.
4. Barenboim G.M et al. Elaboration of the Experimental Inter-Republican System for Ecological Biomonitoring of the Terek Basin. International Workshop of the Problems of Pollution of the Caspian Sea with Heavy Metals, 29 Oct.- 3 Nov., 1997, Makhachkala, Russia.

5. Frontasyeva M.V. Epithermal Neutron Activation Analysis at the IBR-2 Pulsed Fast Reactor in Dubna for Studying the Environment. Book of Abstracts, Asia-Pacific Symposium on Radiochemistry-97, October 6-9, 1997, Kumamoto University, Japan.
6. Frontasyeva M.V. et al. A Survey of Heavy Metal Deposition in Romania Using Mosses as Biomonitors, Advanced Research Workshop "Air Pollution in the Ural Mountains", May 25-30, 1997, Magnitogorsk; Russia, p. 39-40.
7. Frontasyeva M.V., Ignatenko O.V. Epithermal Neutron Activation Analysis of Mosses for Monitoring Environmental Pollution Around the Baikal Paper and Pulp Plant, International Forum "Safe Development of the Region", 2-6 July 1997, Irkutsk.
8. Frontasyeva M.V., Steinnes E. A Comparison of NAA and ICP-MS for the Determination of Trace Elements in Ombrotrophic Peat Bog. Book of Abstracts, Asia-Pacific Symposium on Radiochemistry '97, October 6-9, 1997, Kumamoto University, Japan.
9. Frontasyeva M.V., Steinnes E. Epithermal NAA for Studying the Environment. Book of Abstracts, Advanced Research Workshop "Air Pollution in the Ural Mountains", May 25-30, 1997; Magnitogorsk; Russia, p. 35-36; JINR Preprint, E14-97-136, Dubna, 1997; Annual Report for 1996 FLNP JINR, Dubna, 1997, p. 67.
10. Frontasyeva M.V., Steinnes E. Epithermal Neutron Activation Analysis of Mosses Used to Monitor Heavy Metal Deposition Around an Iron Smelter Complex. Advanced Research Workshop "Air Pollution in the Ural Mountains". May 25-30, 1997, Magnitogorsk; Russia, p. 38-39.
11. Galinskaya T.E. et al. Neutron and X-ray Investigation of Tetragonal Single Crystal of Yttria Stabilized Zirconia (YSZ). Structure and Properties of Crystalline Materials, Dubna, March 4-6, 1997, abstracts, p.43.
12. Gorshkova O.M., Frontasyeva M.V. Distribution of *Fe, Mn, Co* and *Ni* in Organic Colloids in Sea and Pore Water from the Pacific Ocean Fe-Mn Nodule Province. VIII Pacific Science INTER-CONGRESS, Suva, Fiji Islands, July13-19, 1997.
13. Kutsenogii K.P. et al. Multielement Composition Determination of Atmospheric Aerosols in Siberia by the Neutron Activation Analaysis "The Optics of the Atmosphere and the Ocean", 106 N 6 (1997) 664-672.
14. Levashvili V.L. et al. Neutron Bragg and Diffuse Scattering Investigations of Defects in Single Crystals of ZrO_2-Y_2O_3 Cubic Stabilized Zirconia. Structure and Properties of Crystalline Materials, Dubna, March 4-6, 1997, abstracts, p.47.
15. Lucaciu A. et al. Atmospheric Deposition of Heavy Metals in Romania Studied by the Moss Biomonitoring Technique Employing Nuclear and Related Analytical Techniques and GIS-technology. BioMAP, International Workshop on Biomonitoring of Atmospheric Pollution (with emphasis on trace elements). BioMAP, International Workshop on Biomonitoring of Atmospheric Pollution (with emphasis on trace elements), Lisboa, Portugal, September 21-24,1997.
16. Nikonov V., Lukina N., Frontasyeva M. Pollution-Induced Changes in the Properties of Podzol *Al-Fe*-Humus Soils. Proceedings of International Conference "Problems of Anthropogenic Soil Formation", June 16-21, 1997, Moscow. M: V. Dokuchaev, Soil Institute, 1997, 4,192-195.
17. Nikonov V.V., Lukina N.V., Frontasyeva M.V. Scattered Elements in *Al-Fe*-humus Podzol Formation. Pchvovedenie, 12, 1997.
18. Nikonov V.V., Lukina N.V., Frontasyeva M.V. Technogenic Transformation of Podzol *Al-Fe*-humus soil. Proceedings of the International Conference "Problems of Antropogenic Soil Formation", 1, 293-296, 1997, Moscow, Russia.
19. Oprea C., Frontasyeva M.V. Improved Methodology for the Determination of Halogens in Environmental Samples Using Epithermal Neutron Activation Analysis, First Open Conference of Young Scientists of JINR, February, 24-26, 1997, Dubna, Russia.
20. Peresedov V.F. Atmospheric Aerosols and Possibilities of their Analysis at the IBR-2 Reactor for Study of Elemental Content. JINR Rapid Communications, No.4,97, Dubna, 1997; Journ. of Rad. Anal. and Nucl. Chem.(1997), Vol.226.
21. Peresedov V.F., Gundorina S.F., Ostrovnaya T.M. Rare-Earth Elements in Soil and Pine-Needle from Northern Terrestrial Ecosystems. Journ. of Rad. Anal. and Nucl. Chem., Vol.219, No.1 (1997), 105-110; JINR Rapid Communications, No.2, [82]-97, p. 63-70, Dubna, 1997.
22. Rieder E.E. et al. Nonstoihiometry Defect Structure of $KBiO_3$ Single Crystal. Neutron Structure Investigation. Structure and Properties of Crystalline Materials, Dubna, March 4-6, 1997, abstracts, p. 53.
23. Sarin V.A. et al. *X*-Ray and Neutron Diffraction Studies of Defects in the Structure of ZrO_2- Y_2O_3 Monocrystals in the tetragonal and Cubic Phases. National Conference on the Application of X-Ray and Synchrotron Radiation and Neutrons and Electrons to Investigation of Materials, Moscow-Dubna, 25-29 May 1997, p.136.
24. Sarin V.A. The Opportunity of the Neutron Structure Analysis to Study the Defects in Single Crystals. Structure and Properties of Crystalline Materials, Dubna, March 4-6, 1997, abstracts, p.24.

MEASUREMENT AND COMPUTATION COMPLEX

1. Astakhov Yu. et al. Current State and Prospects for Developing the FLNP Measurement and Computation Complex. Proceedings of the International Workshop on Data Acquisition Systems for Neutron Experimental Facilities, June 2-4, 1997, Dubna, pp.153-162.
2. Astakhov Yu. et al. Distributed Information System for IBR-2 Status Presentation on the Web, ibid., pp.259-264.
3. Astakhov Yu. et al. The Unified Software for the Data Acquisition and Control Systems of the IBR-2 Spectrometers, Proceedings of the International Workshop on Data Acquisition Systems for Neutron Experimental Facilities, June 2-4, 1997, Dubna, pp.295-304.
4. Astakhov Yu.A. et al. FLNP Local Computing Network. Proceedings of the XVII International Symposium on Nuclear Electronics, September 15-21, 1997, Varna, Bulgaria (to be published).
5. Belkovetz V.A. et al. The Thermal Stabilization System of LUE with a Programmed Controller. JINR Comm., P9-97-143, Dubna, 1997 (in Russian).
6. Bogdzel A.A. et al. Experimental Investigations of the Energy Dependence of Angular Anisotropy of Fragments in the Fission of Oriented Nuclei of ^{235}U Induced by Resonance Neutrons. Nuclear Physics, 1997, v.60, No.6, pp.981-987.
7. Drozdov V. et al. The Multi-Processor DSP-Based System for Multi-Element Detectors on a High-Resolution Neutron Fourier-Diffractometer, Proceedings of the International Workshop on Data Acquisition Systems for Neutron Experimental Facilities, June 2-4, 1997, Dubna, pp.172-181.
8. Kirilov A. et al. Using X11 to Create VME-Based Neutron Spectrometer Accumulation, Control and Supervising System (Features and Experience), ibid., pp.313-320.
9. Kirilov A.S. et al. A VME-Based Accumulation, Control and Supervising System for Neutron Texture Measurement, JINR Comm., E13-97-220, Dubna, 1997.
10. Kirilov A.S. et al. Control over Exposure, the Writing of Spectra and Texture Goniometer in the Program Complex of the Data Acquisition and Control Systems of the NSVR and SKAT Spectrometers. JINR Comm., P13-97-163, Dubna, 1997 (in Russian).
11. Kirilov A.S. The Informing of the User on the Progress of Measurements at the NSVR and SKAT Spectrometers via Local Network. JINR Comm., P13-97-162, Dubna, 1997 (in Russian).
12. Kirilov A.S., Heinits J. Instrument Control System Features Created on the Basis of the X11/OS-9 Package. Proceedings of the International Workshop NOBUGS'97, December 10-12, 1997, Argonne, IL USA (to be published).
13. Kirilov A.S., Heinits J. Visual Approximate Analysis of Experimental Data in the Process of Measurements at the NSVR and SKAT Spectrometers. JINR Comm., P13-97-219, Dubna, 1997 (in Russian).
14. Kirilov. A.S., Heinits J. Interpretation of the Procedure of Experiments in the Program Complex of the Data Acquisition and Control Systems of the NSVR and SKAT Spectrometers. JINR Comm., P13-97-161, Dubna, 1997 (in Russian).
15. Korobchenko M. et al. Unified VME-Based Data Acquisition Systems for the Spectrometers at the IBR-2 Pulsed Reactor - Interface Module with PSD Detectors, Proceedings of the International Workshop on Data Acquisition Systems for Neutron Experimental Facilities, June 2-4, 1997, Dubna, pp.102-104.
16. Korobchenko M. et al. Unified VME-Based Data Acquisition Systems for the Spectrometers at the IBR-2 Pulsed Reactor - Processor Module, ibid., pp.163-171.
17. Korobchenko M. et al. VME Spectrometric Memory Unit, ibid., pp. 213-217.
18. Korobchenko M.L. et al. Architecture of the Unified Data Acquisition Systems in VME Standard for Neutron Spectrometers at the IBR-2 Pulsed Reactor. Proceedings of the XVII International Symposium on Nuclear Electronics, September 15-21, 1997, Varna, Bulgaria (to be published).
19. Korobchenko M.L., Levchanovsky F.V. Method of Encoding the Point Detector Number in Neutron Time-of-Flight Spectrometers. Proceedings of the XVII International Symposium on Nuclear Electronics, September 15-21, 1997, Varna, Bulgaria (to be published).
20. Litvinenko E. et al. PV-WAVE Based Tools for Visual Analysis of Neutron Scattering Data in FLNP, Proceedings of the International Workshop on Data Acquisition Systems for Neutron Experimental Facilities, June 2-4, 1997, Dubna, pp.248-258.
21. Litvinenko E.I. Current State and Prospects of PV-Wave Based Application. Proceedings of the International Workshop on New Opportunities for Better User Group Software (NOBUGS'97), December 10-12, 1997, Argonne, IL USA (to be published).
22. Ostrovnoi A. et al. Design of Sample Environment Systems for Controlling and Operating Experiment Conditions at the Spectrometers of the IBR-2 Reactor, Proceedings of the International Workshop on

Data Acquisition Systems for Neutron Experimental Facilities, June 2-4, 1997, Dubna, pp.68-72.
23. Tishin V.G. Two-Fold Time-to-Digital Converter for Two-Dimensional Detectors with Delay Line for Measuring Slow Neutron Fields at the IBR-2 Reactor, ibid., pp.65-67.
24. Tulaev A.B. et al. The POWER-Automated System for Monitoring Noises of the IBR-2 Pulsed Reactor. Proceedings of the XVII International Symposium on Nuclear Electronics, September 15-21, 1997, Varna, Bulgaria (to be published).
25. Voronov B.I. et al. Neutron Spectrometer UGRA: Design and Some Characteristics. JINR Comm., P13-97-36, Dubna, 1997 (in Russian).

6. PRIZES

JINR Prizes:

In Experimental Physics:

Second Prize:

V.P.Alfimenkov. L.Lason, Yu.D.Mareev, V.V.Novitsky, L.B.Pikelner, V.R.Skoy, M.I.Tsulaya, A.N.Chernikov. «Parity Violation in the Interaction of Neutrons with Polarized Lanthan and the Spin Structure of the Cross Section for Polarized Neutrons and Lanthan»

FLNP Prizes:

In Nuclear Physics:

First Prize:

V.E.Varlamov, P.Geltenbort, V.V.Nesvizhevsky, M.Pendelbury, A.P.Serebrov, A.V.Strelkov, R.R.Tal'daev, A.G.Kharitonov, V.N.Shvetsov, K.Schreckenbach. «The Discovery of Penetraion of Subbarier UCN through Beryllium Foils and Covering Layers»

Second Prize:

YU.M.Gledenov, V.I.Salatskii, P.V.Sedyshev, P.Shalanski. «Measurement of the Neutron-Alpha Reaction Cross Section of ^{17}O, ^{17}Ne, ^{36}Ar»

Third Prize:

A.M.Sukhovoj, V.A.Khitrov. «Experimental Estimation at E<<3-4 MeV of the Level Density of Nuclei Excited in the (n,γ) Reaction»

In Condensed Matter Physics:

First Prize:

A.M.Abakumov, V.L.Aksenov, V.A.Alyoshin, E.V.Antipov, A.M.Balagurov, D.A.Mikhailova, S.N.Putilin, M.G.Rozova. «Effect of Fluorination on the Structure and Superconducting Properties of the Hg-1201 Phase»

Second Prize:

V.V.Sumin. «Local Modes of Interstitial Atoms in Transition Metals»

V.L.Aksenov, A.M.Balagurov, B.N.Savenko, D.V.Sheptyakov, V.P.Glazkov, V.A.Somenkov, S.Sh.Shilstein, E.V.Antipov, S.N.Putilin. «Investigation of the $HgBa_2CuO_{4+\delta}$ Structure under External Pressures up to 5 Gpa by Neutron Powder Diffraction»

A.M.Balagurov, V.V.Sikolenko, I.S.Lyubutin, G.Andre, F.Bouree, H.M.Du. «The Magnetic Structure Upd_2Ge_2, Doped with Iron»

In Applied Physics:

Second Prize:

Yu.A.Astakhov, E.I.Litvinenko, Yu.N.Pepyolyshev, A.B.Tulaev. «The POWER - System for the Investigation of Noises in the IBR-2 Pulsed Reactor». «The Dustributed Information System for Neutron Reactor Status Presentation on the Web»

The JINR young scientists contest in condensed matter and nuclear physics with neutrons:

First Prize:

G.D.Bokuchava. «Neutron Diffraction Investigation of Internal Stresses in Austenite Steel with Cyclic Fatique»

Second Prize:

Yu.A.Astakhov. «FLNP Computing Infrastructure»

T.L.Enik. «Neutron Electrical Polarization Studies»

Encouraging Prize:

D.B.Kozlenko. «Neutron Diffraction Investigations of Structural Changes in Ammonium Halides Nd_4Br and NdCl at High Pressure»

A.V.Kozlov. «Dynamic Refraction and Transmission of Neutrons»

7. SEMINARS

Date	Authors	Title
6.02.97	A.V.Belushkin (FLNP JINR)	Neutron scattering investigations of systems with disordered hydrogen bonds
13.02.97	F.A.Gareev (BLTP JINR)	Geometrical quantization of micro- and macrosystems. The planetary-wave structure of elementary particles
13.03.97	A.V.Murzin (INR, Kiev)	Nonstatistical effects in the primary γ-transitions in the $(\overline{n},\gamma)$ reaction
30.04.97	V.K.Ignatovich	About Japan in short. Life, science, impressions
10.06.97	T.Imanaka (Kyoto University, Japan)	Radiation doses after the nuclear bombardment of Hiroshima and Nagasaki . Investigations of the consequences of the Chernobyl accident
20.06.97	Yu.A.Ossipyan (Ins. for Solid State Physics, Chernogolovka) N.M.Plakida (BLTP JINR) V.L.Aksenov (FLNP JINR)	The physics of fullerenes High temperature superconductivity Neutron investigations of condensed matter
21.07.97	K.Sumita (Science Council of Japan)	Recent Accidents at Nuclear Reactors in Japan and at the Reactor in Monjou
23.10.97	A.V.Strelkov (FLNP JINR) A.I.Frank (FLNP JINR)	The discovery of ultracold neutrons New aspects in two optics of long wave neutrons
6.11.97	E.P.Shabalin (FLNP JINR)	Workshop on cold neutron moderators (Argonne National Laboratory, USA, 29.09-2.10.97)
20.11.97	V.V.Nesvizhevsky (ILL, Grenoble, France)	Recent results of investigations with slow neutrons in ILL
4.12.97	V.D.Ananiev A.V.Belushkin (FLNP JINR)	Physical startup of the IBR-2 reactor. Twenties anniversary
18.12.97	W.I.Furman V.I.Luschikov Yu.P.Popov L.B.Pikelner A.M.Balagurov V.I.Prikhodko V.A.Sariv A.V.Belushkin (FLNP JINR)	Realization of research themes in 1997

8.1. STRUCTURE OF LABORATORY AND SCIENTIFIC DEPARTMENTS

Directorate:
Director:
V.L.Aksenov
Deputy Directors:
A.V.Belushkin
W.I.Furman
Scientific Secretary:
V.V.Sikolenko

Reactor and Technical Departments
Chief engineer: V.D.Ananiev
IBR-2 reactor
Chief engineer: A.V.Vinogradov
IBR-30 booster + LUE-40
Head: S.A.Kvasnikov
Nuclear physics and pulsed neutron sources sector
Head: V.L.Lomidze
Mechanical maintenance division
Head: A.A.Belyakov
Electrical engineering department
Head: V.P.Popov
Design office
Head: V.I.Konstantinov
Construction
Head: A.N.Kuznetsov

Scientific Departments and Sectors
Condensed matter department
Head: A.M.Balagurov
Nuclear physics department
Head: V.N.Shvetsov
Department of electronics, computers and networks
Head: V.I.Prikhodko
Department of IREN
Head: A.P.Sumbaev
Activation analysis and radiation research sector
Head: V.A.Sarin
Applied research sector
Head: V.I.Luschikov

Administrative Services
Deputy Director: S.V.Kozenkov
Secretariat
Finances
Personnel

Scientific Secretary Group
Translation
Graphics
Photography
Artwork

THE CONDENSED MATTER DEPARTMENT

Sub-Division	Title	Head
Group No.1	HRFD	V.Yu.Pomjakushin
Group No.2	DN-2	A.I.Beskrovnyi
Group No.3	DN-12	B.N.Savenko
Group No.4	NSVR	K.Ullemeyer
Group No.5	YUMO	M.A.Kiselev
Group No.6	SPN-1	Yu.V.Nikitenko
Group No.7	REFLEX	D.A.Korneev
Group No.8	NERA-PR	I.Natkaniec
Group No.9	KDSOG	E.A.Goremychkin
Group No.10	EG-5	A.P.Kobzev
Group No.11	Automatization	E.S.Kuzmin

THE NUCLEAR PHYSICS DEPARTMENT

Sub-Division	Title	Head
Group No.1	Polarized neutrons and nuclei	V.P.Alfimenkov
Group No.1	Neutron spectroscopy	A.B.Popov
Group No.3	Nuclear reactions	Yu.S.Zamyatnin
Group No.4	Properties of the neutron	Yu.A.Alexandrov
Group No.5	Proton and α-decay	Yu.M.Gledenov
Group No.6	Properties of γ-quanta	A.M.Sukhovoy
Group No.7	Radiation capture of neutrons	G.P. Georgiev
Group No.8	Ultra-cold neutrons	V.N.Shvetsov
Group No.9	Neutron structure	G.S.Samosvat
Group No.10	Rare reactions	Yu.N.Pokotilovsky

8.2. USER POLICY

The IBR-2 reactor usually operates 10 cycles a year (2500 hrs. total) to serve the experimental programme. A cycle is established as of 2 weeks of operation for users, followed by a one week period for maintenance and machine development. There is a long shut-down period between the end of June and the middle of October.

All experimental facilities of IBR-2 are open to the general scientific community. The User Guide for neutron experimental facilities at FLNP is available by request from the Laboratory's Scientific Secretary.

Condensed matter studies at IBR-2 have undergone some changes in accordance with the experience gained during the last several years. It was found to be necessary to establish specialized selection committees formed of independent experts in their corresponding fields of scientific activities. The following four committees were organized:

1. Diffraction *Chairman* - V.A.Somenkov - Russia	3. Neutron optics *Chairman* - A.I.Okorokov - Russia
2. Inelastic scattering *Chairman* - J.Janik - Poland	4. Small angle scattering *Chairman* - L.Cser - Hungary

Dr. Vadim V. Sikolenko, Scientific Secretary of FLNP, is responsible for the user policy. Two deadlines for proposal submission are: May 16 - for the experimental period from October through February; and October 16 - for the period from March through June.

Scientific Secretary is responsible for:

- distribution of "Application for Beam Time" forms to potential users;
- registration of submitted proposals;
- reviewing of the proposals by instrument scientists to estimate the technical feasibility of the proposed experiment;
- sending of the approved proposals to Members of Selection Committees and registration of their comments and recommendations.

The IBR-2 beam schedules are drawn up by the head of the Condensed Matter Department together with instruments responsibles on the basis of experts recommendations and are approved by the FLNP Director or Deputy Director for condensed matter physics. The schedules are sent to Chairmen of Selection Committees.

After the completion of experiments, "Experimental Report" forms are filled out by experimenter(s) and submitted to the Scientific Secretary.

The Application Form and other information about FLNP are available by WWW: http://nfdfn.jinr.ru/~sikolen/usepol.html

Contact address:
***Dr. V.Sikolenko**, Frank Laboratory of Neutron Physics*
Joint Institute for Nuclear Research
141980 Dubna, Moscow region, Russia
Tel.: (+7)-095-926-22-53, (+7)-09621-65096, Fax: (+7)-09621-65085; (+7)-09621-65882,
E-mail: sikolen@nf.jinr.ru

8.3. MEETINGS AND CONFERENCES

In 1997, FLNP organized the following meetings:

1.	International Seminar "Structure and Properties of Crystalline Materials" SPCM	March 4-7	Dubna
2.	V International Seminar on Interaction of Neutrons with Nuclei (ISINN-5)	May 13-16	Dubna
3.	National Conference on X-ray, Synchrotron, and Neutron Investigations (RSN-97)	May 26-29	Dubna-Moscow
4.	International Workshop on Data Acquisition Systems for Neutron Experimental Facilities (DANEF'97)	June 2-4	Dubna
5.	International Seminar "Neutron Analysis of Textures and Stresses NTSA	June 23-27	Dubna

In 1998, FLNP will organize the following meetings:

1.	International Seminar «Collective Effects in Condensed Matter»	March 7-15	Pamporovo, Bulgaria
2.	VI International Seminar on Interaction of Neutrons with Nuclei (ISINN-6)	May 13-16	Dubna
3.	International Workshop on Deuteration of Biological Molecules for Structural and Dynamic Studies	May 19-25	Dubna
4.	II International Seminar «Ferroelectrics-Relaxors»	June 23-26	Dubna
5.	VIII School on Neutron Physics	August 30 - September 5	Dubna

8.4. COOPERATION

List of Visitors from Non-Member States of JINR in 1997

Name	Organization	Country	Dates
M.A.Ali	NRC, AEA, Cairo	Egypt	01/01-02/01
B.E.Gebauer	HMI, Berlin	Germany	15/01-19/01
M.Hempel	Fraunhofer Inst. for Nondestructuve Testing, Dresden	Germany	19/01-03/02
G.Fioni	DSM/DAPNIA/SPHN, CEA, Saclay	France	19/01-22/01
V.Lauter-Pasyuk	ILL, Grenoble	France	19/01-03/02

H.-J. Lauter	ILL, Grenoble	France	19/01-03/02
E.Steinness	Univ. of Trondheim	Norway	31/01-03/02
R.Zamoun	URGN, Draria	Algiers	17/02-15/04
M.Hedibel	URGN, Draria	Algiers	17/02-15/04
B.Meftah	URGN, Draria	Algiers	17/02-22/04
A.Makkar	URGN, Draria	Algiers	17/02-15/04
H.-G.Brockmeier	TU Clausthal	Germany	22/02-26/02
R.F.Koontz	SLAC, Stanford	USA	01/03-07/03
S.L.Gold	SLAC, Stanford	USA	01/03-07/03
M.Stalder	Fraunhofer Inst. for Nondestructive Testing, Dresden	Germany	13/03-25/03
J.Schreiber	Fraunhofer Inst. for Nondestructive Testing, Dresden	Germany	13/03-21/03
P.Hoghoj	ILL, Grenoble	France	17/03-24/03
M.Niffenegger	PSI, Villigen	Switzerland	18/03-25/03
M.Rudalics	Johannes Kepler University	Austria	19/03-08/04
V.Lauter-Pasyuk	ILL, Grenoble	France	19/03-28/03
H.-J.Lauter	ILL, Grenoble	France	19/03-28/03
G.Pepy	LLB, Saclay	France	24/03-25/03
M.Carta	ENEA CRE CASACCIA	Italy	05/04-08/04
A. D'Angelo	ENEA CRE CASACCIA	Italy	05/04-08/04
A.Filip	CEA, Saclay	France	05/04-08/04
G.Bruno	University of Ancona	Italy	06/04-19/04
J.Rowlands	LANL	USA	07/04-08/04
S.Akajima	JAERI	Japan	07/04-08/04
G.Spriggs	LANL, Los Alamos	USA	07/04-08/04
T.Parish	LANL, Los Alamos	USA	07/04-08/04
J.Campbell	LANL, Los Alamos	USA	07/04-08/04
D.Loaiza	LANL, Los Alamos	USA	07/04-08/04
K.Turjan	National Renewable Energy Lab.	USA	23/04-24/04
Ch.Scheffzuek	GeoFRZ, Potsdam	Germany	12/05-18/05
S.Ahmad	Plevsound Ltd., London	UK	12/05-14/05
P.Bordet	CNRS, Grenoble	France	15/05-16/05
H.-J. Lauter	ILL, Grenoble	France	17/05-31/05
V.Lauter-Pasyuk	ILL, Grenoble	France	17/05-31/05
M.L.Mestres Vila	University of Barcelona	Spain	25/05-08/06
A.Wiedenmann	HMI, Berlin	Germany	26/05-01/06
He Jian	China Inst. of Atomic Energy, Beijing	China	27/05-04/06
Ye Chuntang	China Inst. of Atomic Energy, Beijing	China	27/05-04/06
Yang Tonghua	China Inst. of Atomic	China	27/05-04/06

	Energy, Beijing		
M.A.Kilany	NRC, AEA, Cairo	Egypt	02/06-02/06.98
T.Gutberlet	Univ. Leipzig	Germany	07/06-14/06
O.Steinsvoll	Inst. for Energiteknikk, Kieller	Norway	09/06-22/06
M.Stalder	Fraunhofer Inst. for Nondestructive Testing, Dresden	Germany	15/06-15/07
H.H.G.Braun	Univ. Kiel	Germany	16/06-29/06
C.-H. De Novion	LLB, Saclay	France	22/06-27/06
B.Leiss	Univ. Goettiingen	Germany	22/06-02/07
A.Frischbutter	GeoFRZ, Potsdam	Germany	26/06-02/07
B.Leiss	Univ. Goettiingen	Germany	22/06-02/07
A.Frischbutter	GeoFRZ, Potsdam	Germany	26/06-02/07
P.Spalthoff	FRZ, Geesthacht	Germany	27/06-17/07
I.Goldmints	MIT, Cambridge	USA	09/07-09/07
G.Fioni	DSM/DAPNIA/SPHN, CEA, Saclay	France	12/07-15/07
B.Frois	DSM/SPP/CE, Saclay	France	14/07-15/07
M.Utsuro	Kyoto University	Japan	20/07-21/07
K.Sumita	Science Council of Japan	Japan	20/07-21/07
H.Hironobu	University of Tsukuba	Japan	22/07-22/07
J.Schreiber	Fraunhofer Inst. for Nondestructive Testing, Dresden	Germany	31/07-03/08
C.Heater	NIST, Gaithersburg	USA	20/08-21/08
D.Mildner	NIST, Gaithersburg	USA	20/08-21/08
R.Machrafi	University Mohamed V.Rabat	Morocco	25/08-25/08.98
Zhang Guohui	Peking University	China	09/09-24/09
Tang Guoyou	Peking University	China	09/09-24/09
Shi Zhaomin	Peking University	China	09/09-24/09
Chen Jinxiang	Peking University	China	09/09-24/09
P.Lesieur	LURE, Orsay	France	10/09-14/09
K.J.Touryan	NREL, Golden	USA	28/09-29/09
A.C.Touryan	NREL, Golden	USA	28/09-29/09
M.Dahlborg	CReN, Strasbourg	Sweden	08/10-09/10
U.C.A.Dahlborg	CReN, Strasbourg	Sweden	08/10-09/10
R.Huber	"HUBER"	Germany	13/10-17/10
K.Walther	GeoFRZ, Potsdam	Germany	13/10-17/10
H.-J.Lauter	ILL, Grenoble	France	19/11-28/11
F.I.A.Asfour	NRC, AEA, Cairo	Egypt	27/11-25/12
V.Lauter-Pasyuk	ILL, Grenoble	France	19/11-28/11
M.Stadler	Fraunhofer Inst. for Nondestructive Testing,	Germany	02/12-24/12

	Dresden		
R. Van De Kruijs	University of Technology, Delft	The Netherlands	08/12-15/12
M.T.Rekveldt	University of Technology, Delft	The Netherlands	08/12-15/12
J.Schreiber	Fraunhofer Inst. for Nondestructive Testing, Dresden	Germany	11/12-17/12
V. Renugopalakrishnan	UNAM, Mexico	Mexico	14/12-17/12
A.J.Eilert	KTU, Utrecht	The Netherlands	24/12-25/12
R.H.Eilert	KTU, Utrecht	The Netherlands	24/12-25/12

8.5. EDUCATION

The University Centre (UC) affiliated with the Joint Institute for Nuclear Research and based on the faculties of the Moscow State University and Moscow Engineering Physics Institute admits, for continuation studies, undergraduate students of the last two years of study in higher education institutions who have attended introductory specialized courses or lectures in the following topics: particle physics, nuclear physics, investigation of condensed matter at nuclear reactors and accelerators, radiation biology. The second and third specializations are in line with research performed at FLNP, which has at its disposal a good experimental base for both sectors comprising the IBR-2 reactor and the IBR-30 booster pulsed neutron sources.

The education courses and practical training for the students affiliated with FLNP have been organized, to a large extent, to prepare specialists in neutron physics for both the Laboratory and for other Russian neutron centres.

As an example illustrating this aim, we present the list of courses taught by lecturers of the Condensed Matter Physics Chair of the UC (Head: Prof.V.L.Aksenov):

- theoretical methods in condensed matter physics
- methods of investigation of condensed matter at nuclear reactors and accelerators
- fundamentals of neutron physics and neutron sources
- methods for structure analysis of ideal and real crystals
- synchrotron radiation spectroscopy of solid matter
- influence of radiation on solid-state properties
- methods of experimental data processing.

A number of leading FLNP scientists take part in delivering these courses. Each student is allowed access to the Laboratory's computer network. An obligatory condition for successful completion of the 4th year is the capability to use modern personal computers. Earlier, students were included in the research groups led by their instructors, which made it possible for undergraduate students working on their theses to take part in preparing or performing experiments.

In 1997, the teaching process at UC continued successfully. Twelve students who had their UC training course at FLNP were employed by JINR or other scientific centers in Russia.

The Condensed Matter Physics Chair gave graduation certificates to its fifth group of students in the reported year. This group had 6 students, making the total number of students who have graduated from the Chair, 45. One of them have been employed by FLNP and who have renewed the staff of the FLNP Scientific Department of Condensed Matter Physics to a noticeable degree.

8.6. PERSONNEL

Distribution of the Main Staff Personnel per Department as of 01.01.98

Departments	Permanent personnel			Contracts			Trainees
	S.	E. & T.	St.	S.	E. & T	St.	
1. Nuclear Physics Department			3	37.5	15	6.5	4
Personnel of the Directorate				13	2		1
2. Condensed Matter Physics Department	4	1		36.5	9	6	4
Personnel of the Directorate				26	3		2
Physical and Technical Research Sector	5	2		2		1	
Personnel of the Directorate				1			
Department of Electronics, Computers and Networks				16	23.5	9	
Personnel of the Directorate				1			
IREN Department	4			3	5	3	
Personnel of the Directorate				2			
IBR-30 Department					15	3	
Nuclear Safety Sector				6	1	1	
Personnel of the Directorate							1
IBR-2 Department					40	7	
Personnel of the Directorate					1		
Technical services:							
Mechanical and Technical Department					11	49	
Electric and Technical Department		1	2		11	25	
Central Experimental Workshops			5		6	33	
Design Bureau		3			9		
Tool and Cleaning Services			9		1	15	
Management Services			1		18	5	
	13	7	20	144	170.5	163.5	12
	40 (7.5%)			490 (92.5%)			
Total	**530 (100%)**						

Comment: S. - Scientists, E. & T. - Engineers & Technicians, St. - Staff

Personnel of the Directorate as of 01.01.98

Country	People
Azerbaijan	4
Armenia	1
Bulgaria	3
China	1
Egypt	1
Germany	4
Georgia	2
Iraq	1
Kazakhstan	1
Mongolia	3
Moldavia	1
Morocco	1
Poland	11
Romania	5
Russia	12
Slovakia	1
Ukraine	1
TOTAL	**53**

8.7. FINANCE

Financing of the FLNP Scientific Research Plan in 1997

No.	Theme	Financing plan, $ th.	Expenditures for 12 months, $ th.	In % of FLNP budget
I	**Condensed matter physics**	**4017.4**	**2554.8**	**63.6**
	-0864-	1909.9	1850.9	96.9
	-0851-	1592.4	383.5	24.1
	-1012-	446.1	256.8	57.6
	-0975-	69.0	63.6	92.2
II	**Neutron nuclear physics**	**1113.2**	**938.7**	**84.3**
	-0974-	677.7	722.5	106.6
	-0993-	435.5	216.2	49.6
III	**Elementary particle physics**			
	-1007-	**6.1**	**40.8**	**668.9**
IV	**Relativistic nuclear physics**			
	-1008-	**41.3**	**13.0**	**31.5**
V	**TOTAL:**	**5178.0**	**3547.3**	**68.5**

In 1997 a series of works to repair and adjust the fast emergency system of the IBR-2 pulsed reactor were conducted.

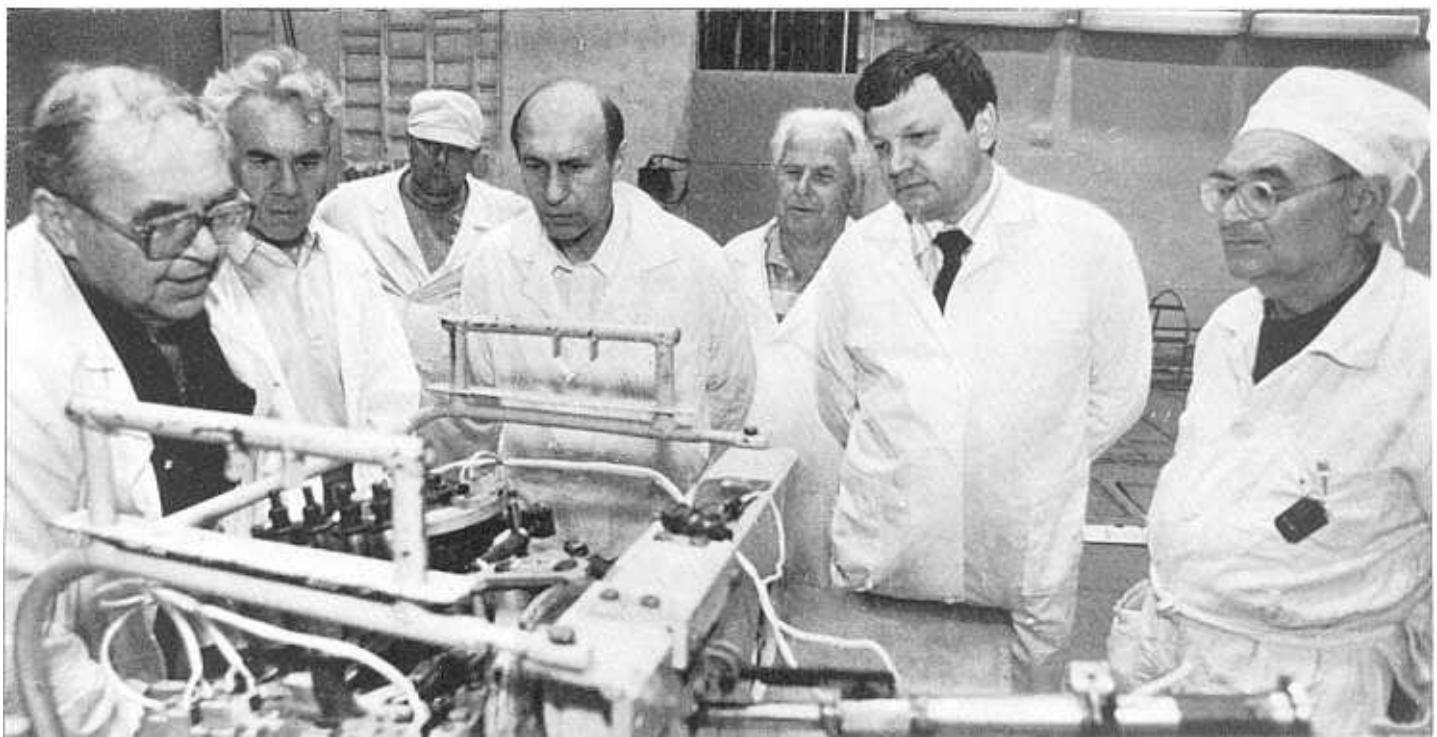

JINR Directorate are shown around and are introduced to the state of art at the new water moderator.

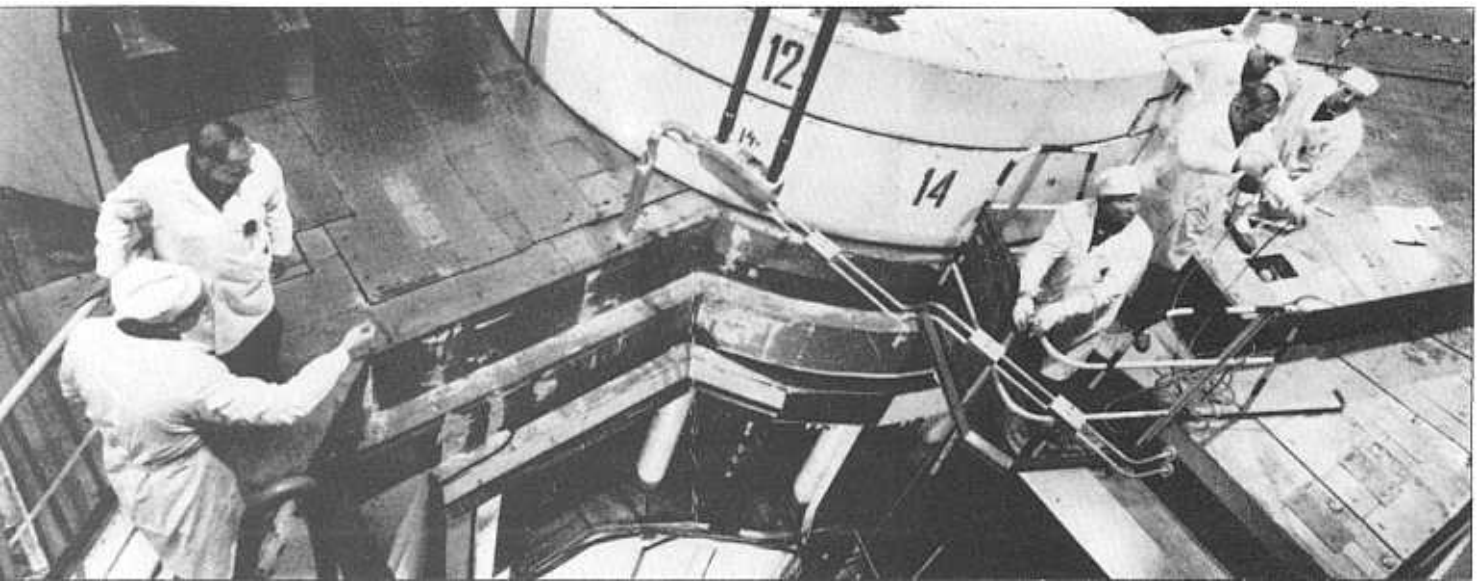

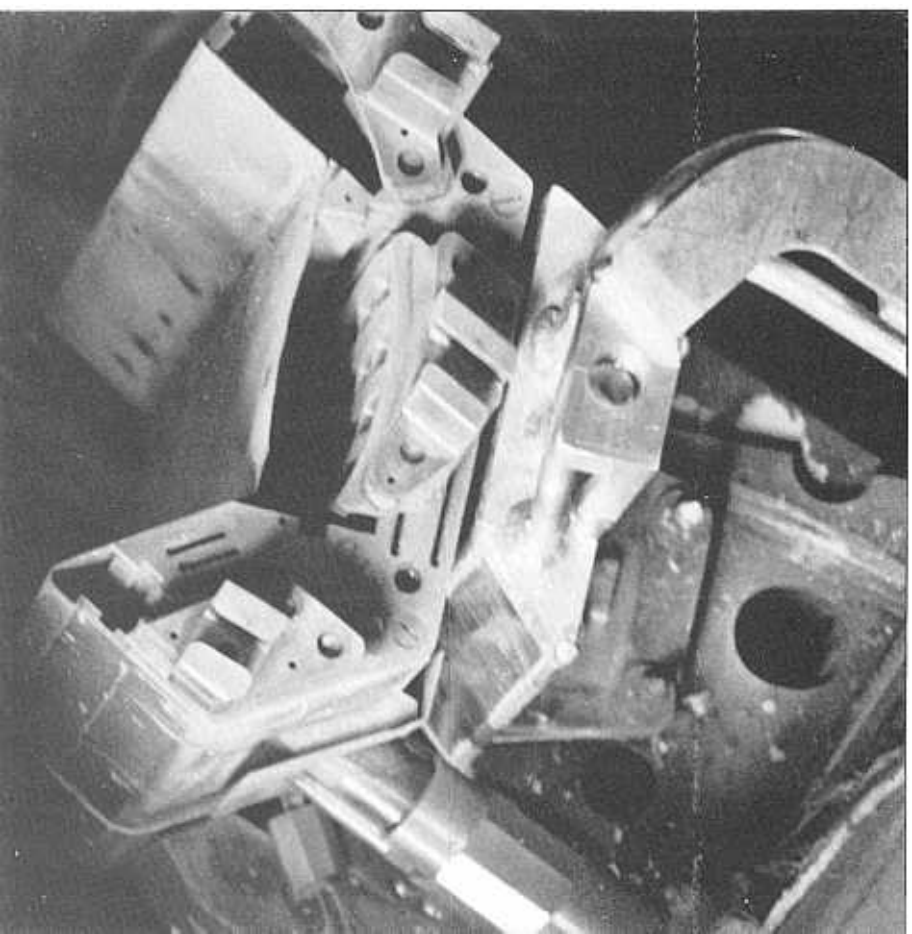

New water moderator.

Prof. J.Janik at the NERA-PR instrument site.

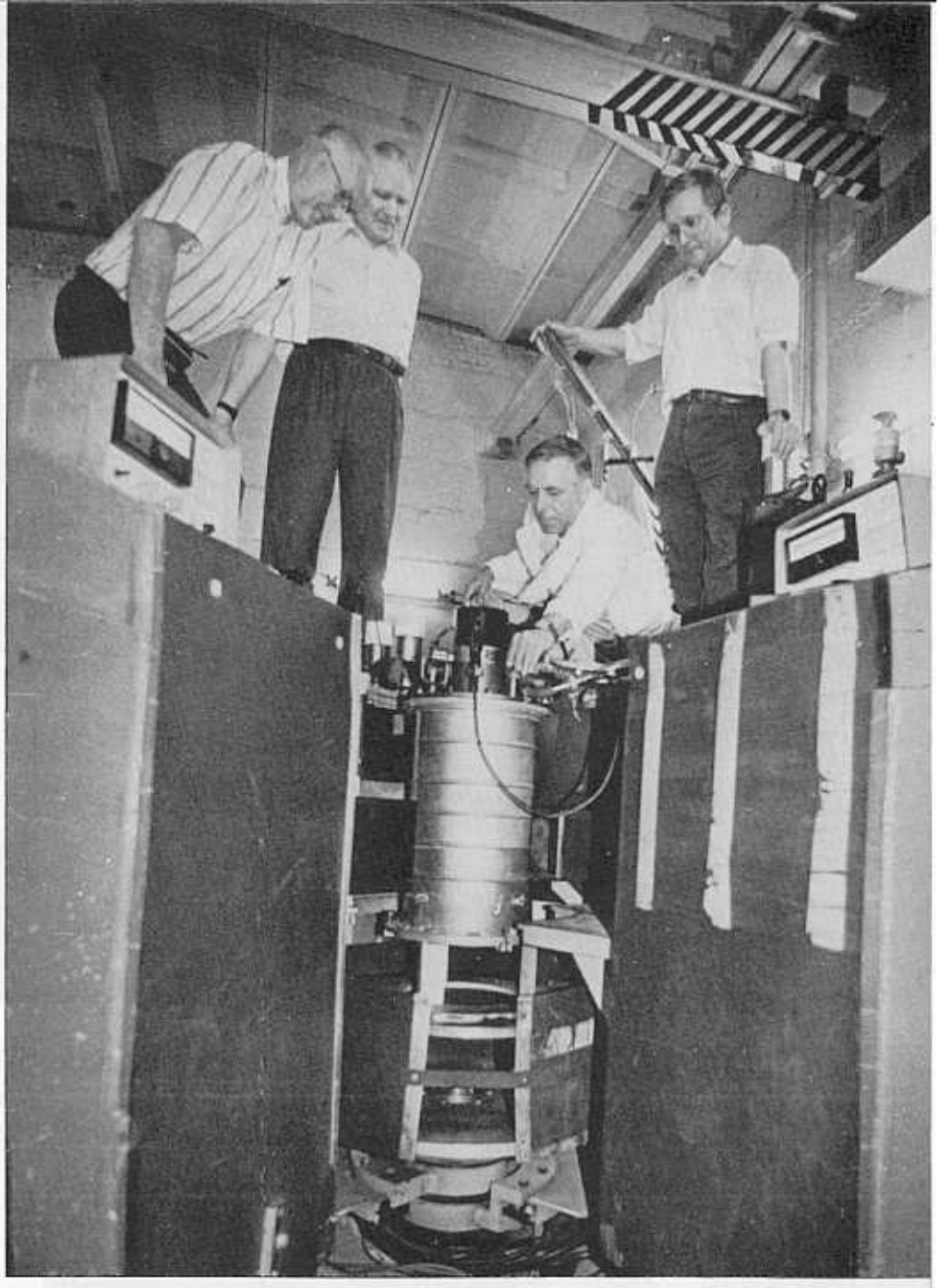

Academician V.E.Fortov, the Vice-Premier Minister of the Russian Federation and RF Plenipotentiary in JINR (left), visits the Frank Laboratory of Neutron Physics.

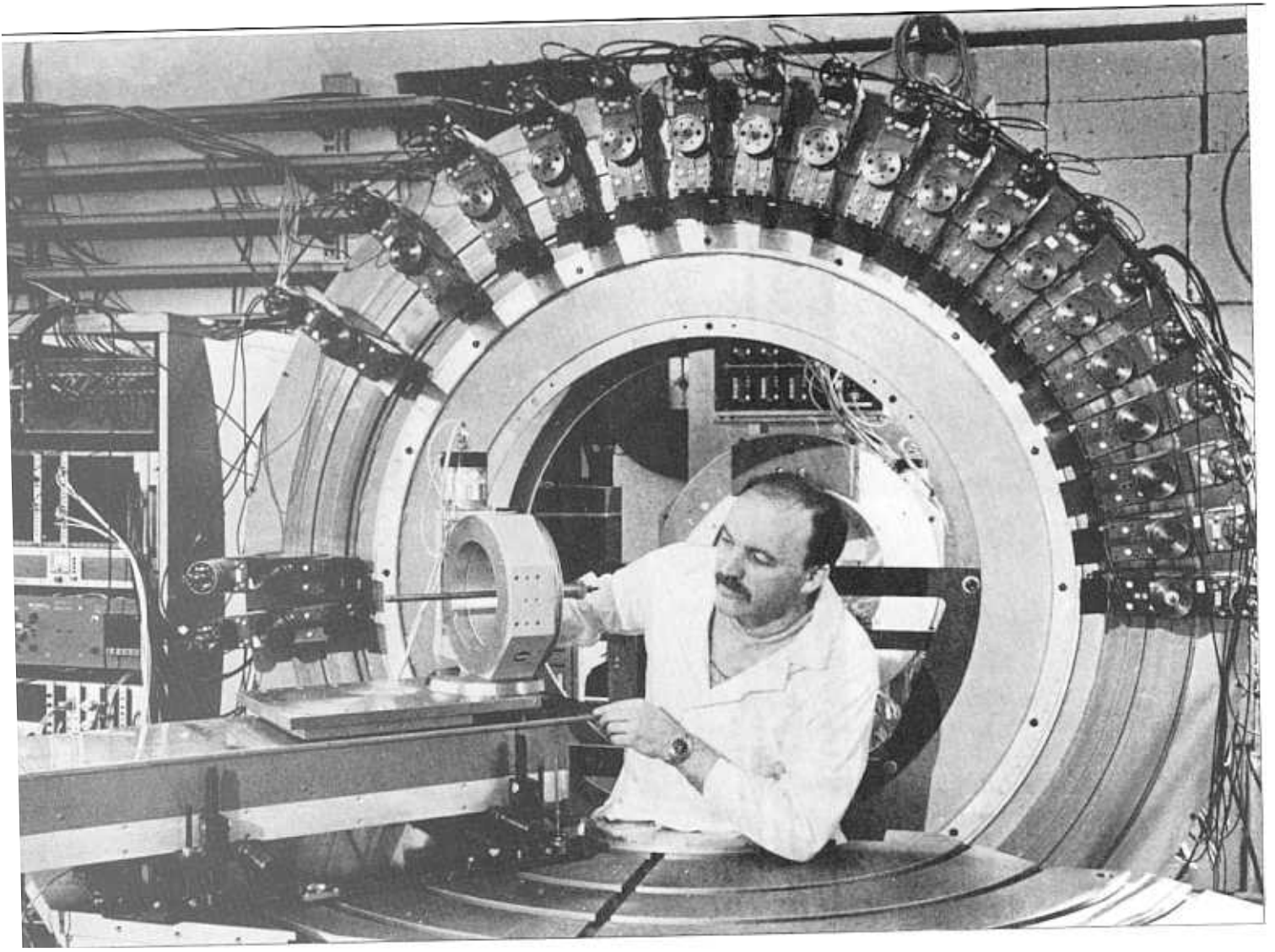

K.Ullemeyer assembles equipment on the new spectrometer SKAT.

C.Scheffzuek adjusts the Huber goniometer for the SKAT setup.

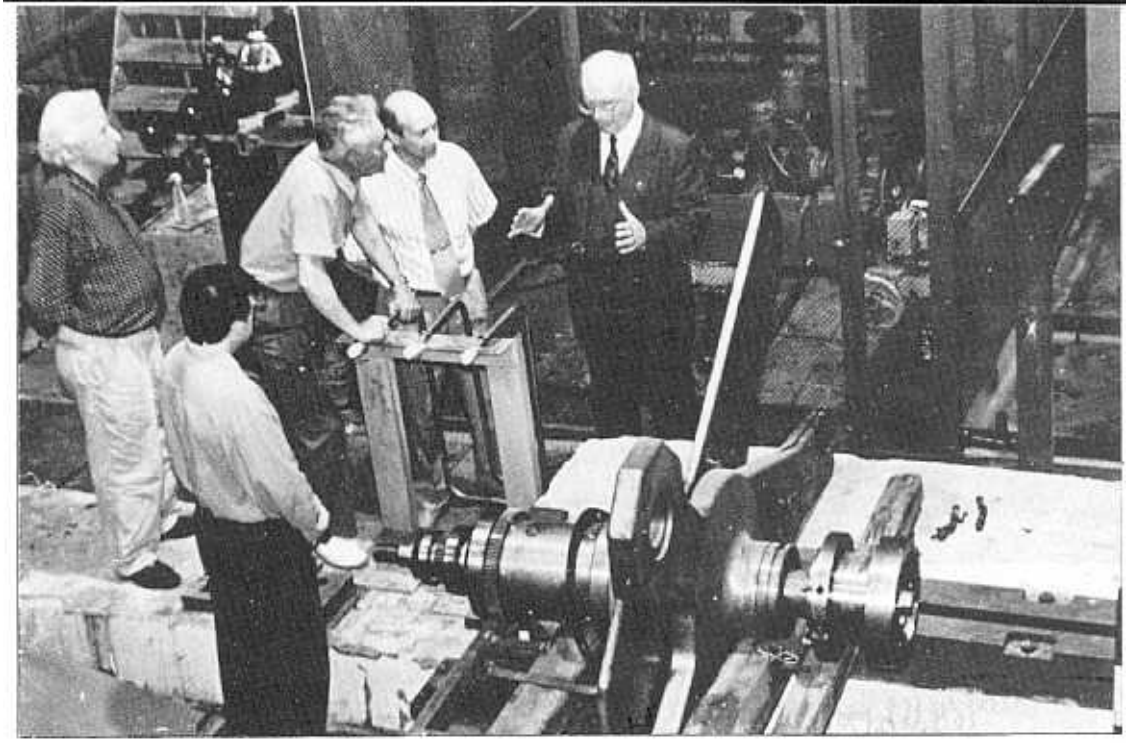

Prof. L.D.Ryabev near the moving reflector prototype.

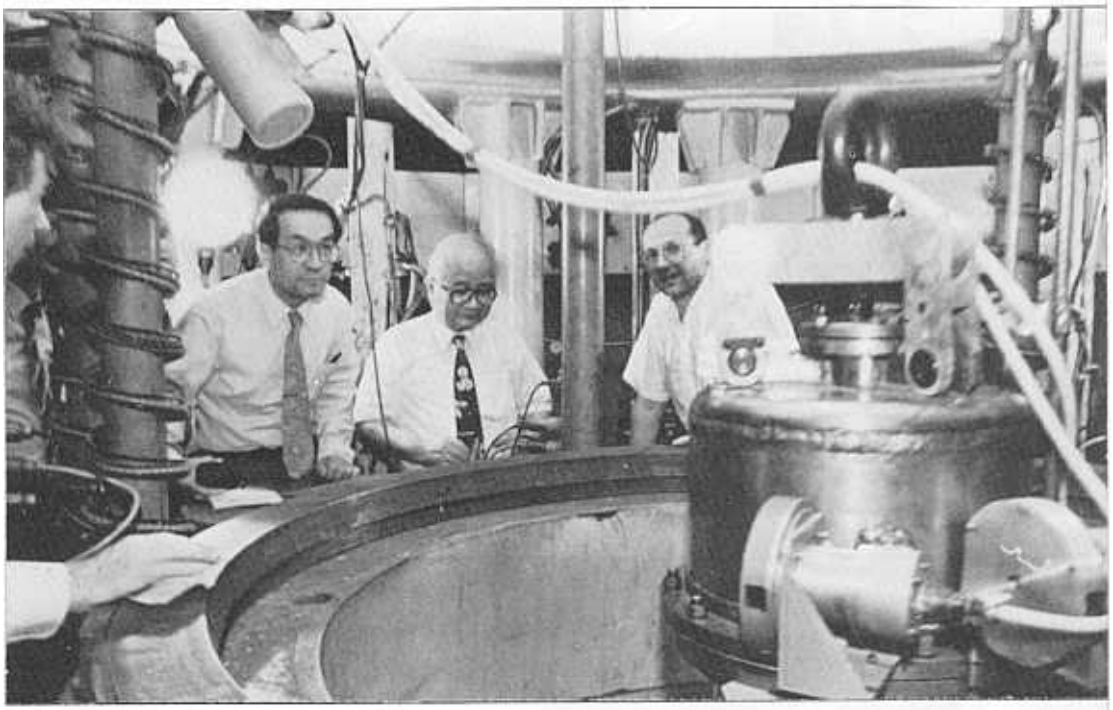

Prof. K.Sumita in the IBR-2 reactor hall.

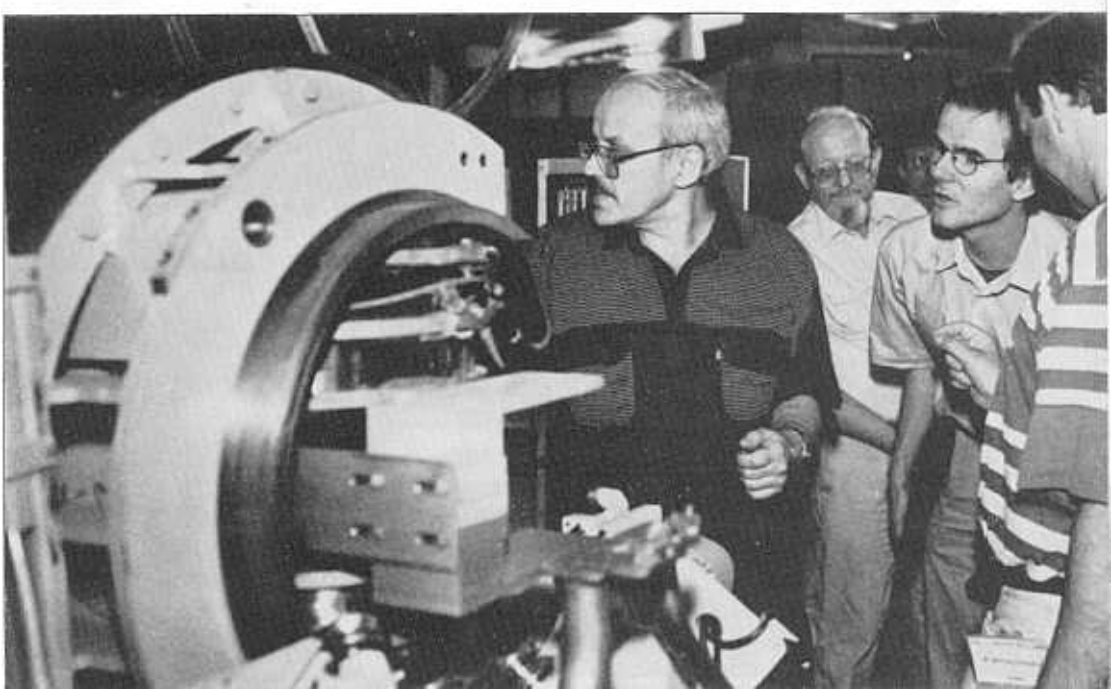

Prof. D.A.Korneev disassembles the new spectrometer REFLEX.

Participants of the National Conference on the Interaction of Synchrotron, X-Ray, Neutron and Electron Radiation with Matter.

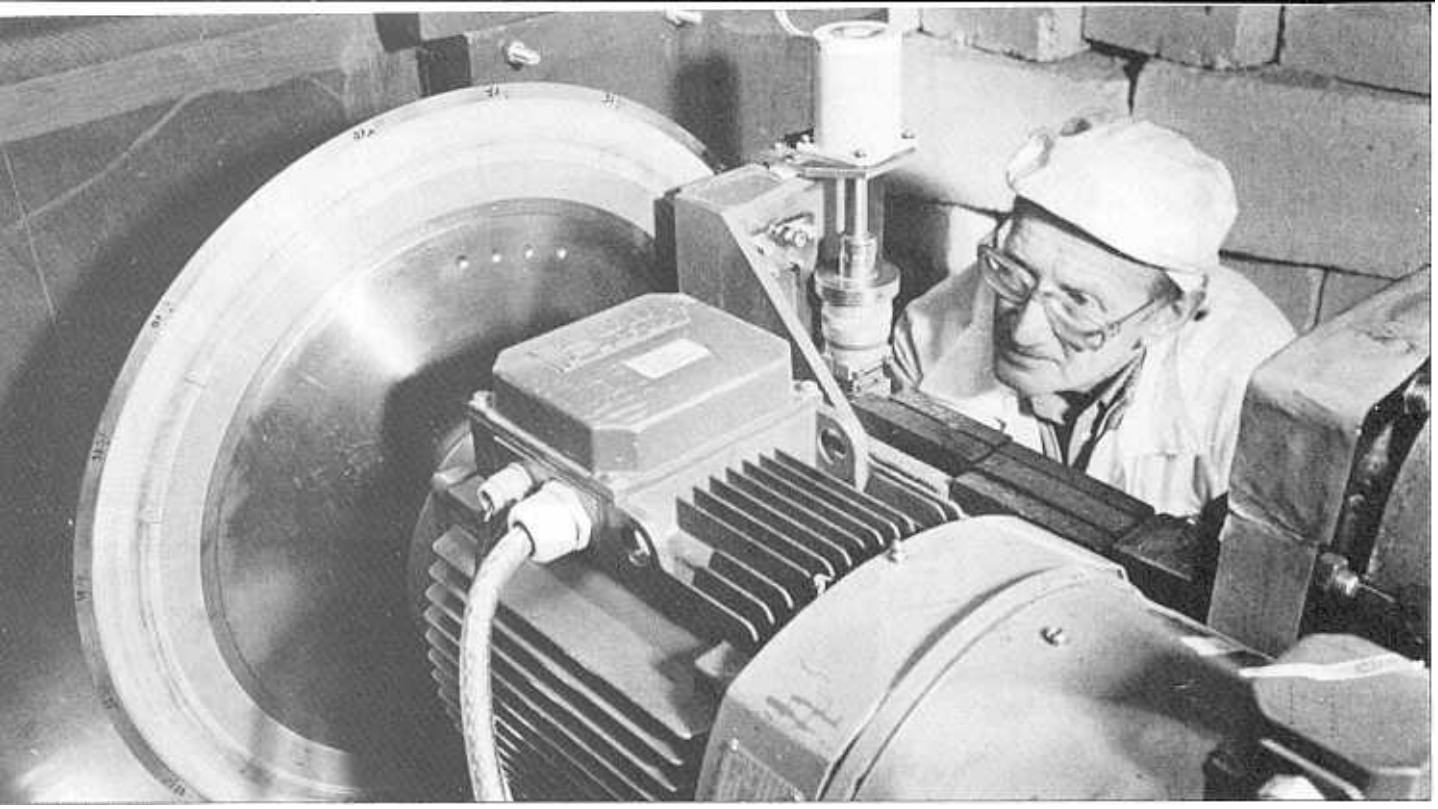

V.G.Simkin tunes the control system of the Fourier chopper.

Ch.de Novion, Director of LLB, V.L.Aksenov, Director of FLNP, and A.V.Belushkin, Deputy Director of FLNP, discuss the beginning of joint experiments.

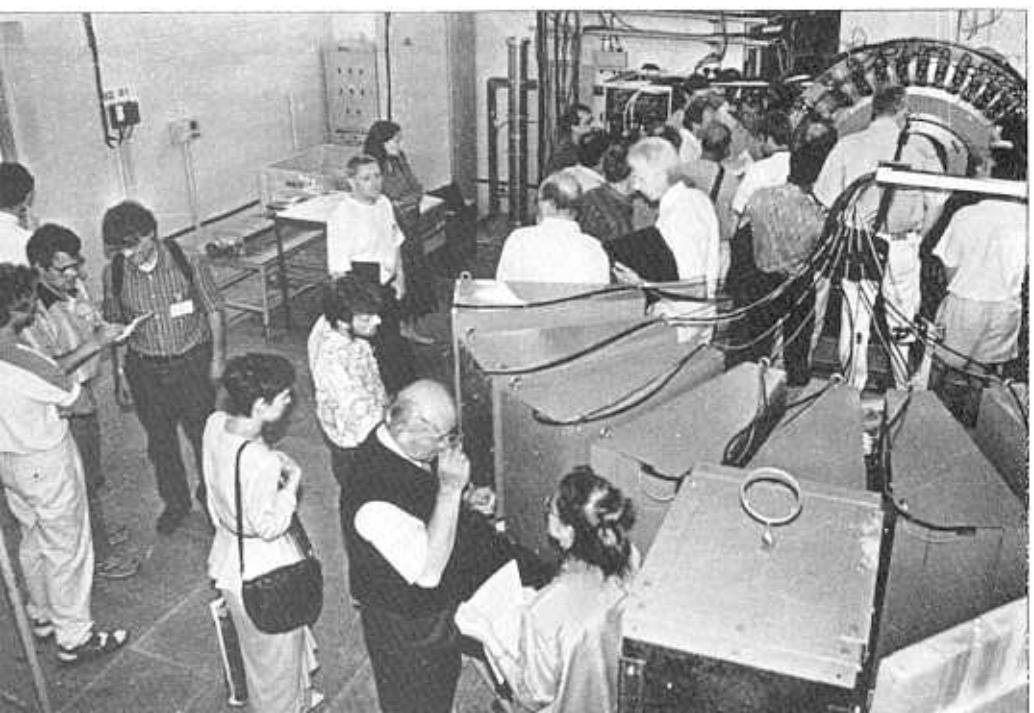

Participants of the DANEF meeting at the SKAT site.

Opening of the memorial plaques in honor of Prof. I.M.Frank and Prof. F.L.Shapiro in the Frank Laboratory of Neutron Physics.

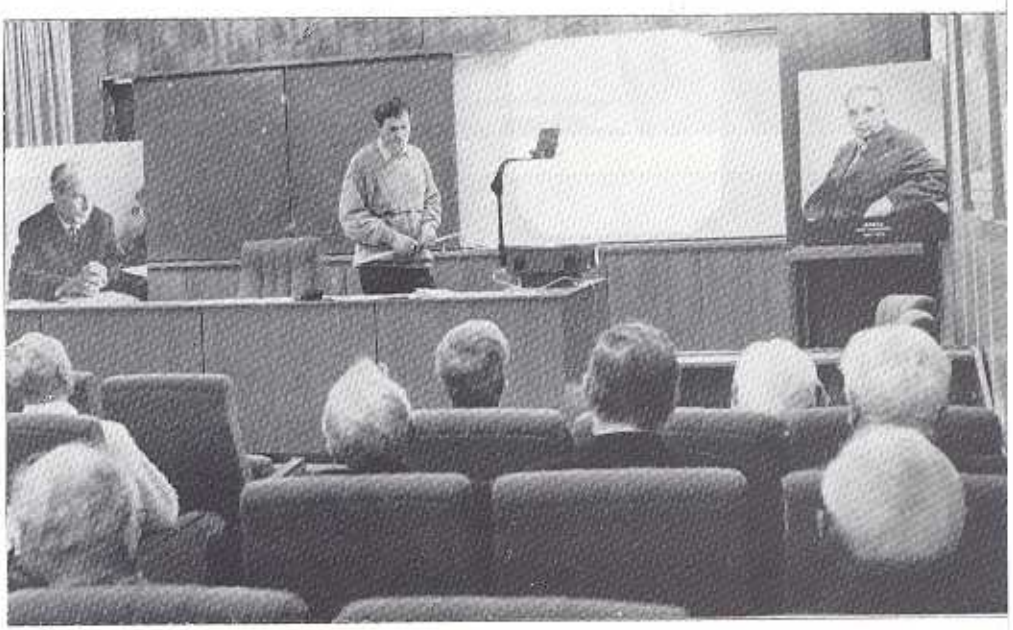

A.V.Strelkov makes a report at the seminar devoted to the opening of the memorial plaques in honor of Prof. I.M.Frank and Prof. F.L.Shapiro in the Frank Laboratory of Neutron Physics.

Celebration of the 20-year anniversary of the IBR-2 physical startup.

Warsaw. JINR exhibition in the House of Science. The ASPECT stand.

The portal monitor manufactured by the ASPECT center for detecting nuclear materials at customs posts.

Chess competition in FLNP.